# Copper-Mediated Oxygenation and Amination of Phenols

Mohammad Sharif Askari

A Thesis
In the Department
Of
Chemistry and Biochemistry

Presented in Partial Fulfillment of the Requirements
For the Degree of
Doctor of Philosophy (Chemistry) at
Concordia University
Montreal, Quebec, Canada

July 2015

**CONCORDIA UNIVERSITY**
**SCHOOL OF GRADUATE STUDIES**

This is to certify that the thesis prepared

By: Mohammad Sharif Askari

Entitled: Copper-Mediated Oxygenation and Amination of Phenols

and submitted in partial fulfillment of the requirements for the degree of

Doctor of Philosophy (Chemistry)

complies with the regulations of the University and meets the accepted standards with respect to originality and quality.

Signed by the final examining committee:

| | |
|---|---|
| Uri Shalev | Chair |
| Bruce Arndtsen | External Examiner |
| Valter Zazubovits | External to Program |
| Pat Forgione | Examiner |
| Gilles Peslherbe | Examiner |
| Xavier Ottenwaelder | Thesis Supervisor |

Approved by

Chair of Department or Graduate Program Director

Dean of Faculty

# Abstract

### Copper-Mediated Oxygenation and Amination of Phenols

**Mohammad Sharif Askari, Ph.D.**
**Concordia University, 2015**

Phenols are abundant feedstock chemicals and their functionalization constitutes an attractive method for the synthesis of fine chemicals and materials. In biological systems, the copper-containing enzyme tyrosinase catalyzes the *ortho*-oxygenation of tyrosine into L-dopaquinone in the first step of the melanogenesis process. The copper centres in the enzyme activate $O_2$ through the formation of $\mu$-$\eta^2$:$\eta^2$-peroxodicopper(II) ($^{\mathbf{S}}\mathbf{P}$) and subsequent electrophilic aromatic substitution on tyrosine provides L-dopaquinone. Despite many efforts for the past 50 years to develop a synthetic mimic for the aerobic oxygenation of phenols, a truly catalytic system for the selective *ortho*-oxygenation of phenols was only recently reported. The copper(I) complex of *N,N'*-di-*tert*-butylethylenediamine (DBED) is used as the precatalyst that activates oxygen and catalyzes the *ortho*-oxygenation of phenols. Investigating the mechanism of this catalytic process is the first objective of this research, whereby spectroscopic techniques are used to identify intermediates in this reaction and perform kinetic studies. The second objective of the research is the development of analogous phenol *ortho*-amination using nitrosoarenes as substitutes for oxygen.

The mechanistic studies were performed by spectroscopic characterization of intermediates and comparison with independently prepared complexes or literature spectra. In situ UV-vis spectroscopy of the reaction at 25 ºC demonstrated the formation of a copper(II)-semiquinone complex that persists during the oxygenation process. In order to identify the preceding intermediates, UV-vis spectroscopy at temperatures as low as -120 ºC was used, and the intermediates were characterized spectroscopically through comparison with similar reported species. Based on the observed intermediates a mechanism is proposed whereby the copper complex activates oxygen to forming $^{\mathbf{S}}\mathbf{P}$; an oxygen atom is then transferred to a bound phenolate through electrophilic aromatic substitution. Kinetic studies using low-temperature stopped-flow techniques provides evidence for a binuclear mechanism of $O_2$ activation and that the reaction rate is independent on phenol concentration. The mechanistic investigation suggests that oxygen activation and phenol functionalization proceed through the same pathway as the one observed with tyrosinase, thus substantiating the bio-mimetic nature of this catalytic reaction.

Nitrosoarenes (ArNO) are isoelectronic with singlet oxygen, therefore copper-ArNO complexes are structural and electronic mimics of copper-$O_2$ complexes, and are expected to react in a similar way with external substrates. The redox lability of nitrosoarenes was proved by preparing and characterizing a copper(II)-nitrosoarene radical-anion complex. Structural and computational investigation confirmed its similarity to end-on copper(II)-superoxo species. Two-electron reduction of nitrosoarene was performed using the copper(I) complex of diamine ligand, and results in a complex that mimics the side-on copper(II)-peroxo ($^{S}\mathbf{P}$) structure. This complex undergoes stoichiometric reaction with phenolates to form aminophenols after reductive work-up, thus demonstrating similar reactivity to tyrosinase models.

# Acknowledgments

First of all I would like to thank my supervisor Dr. Xavier Ottenwaelder for guiding me throughout my graduate studies. His help, guidance, and most importantly patience are greatly appreciated. Thanks for taking me to all the conferences and introducing me to chemists from all over the world. Without your motivation I would not have made it through the Ph.D. program!

I would like to thank my supervisory committee members Dr. Pat Forgione and Dr. Gilles Peslherbe for their valuable advice and guidance throughout my undergraduate and graduate studies. I thank Dr. Guillaume Lamoureux for providing me access to his computational cluster. I had the occasion to carry out an internship in the lab of Prof. Dr. Siegfried Schindler at the Justus-Liebig Universität Giessen. I am grateful to him for his mentorship and his group for the fun times.

All the undergraduate and graduate professors who taught me chemistry – just to name few Drs. Cerrie Rogers, Sébastien Robidoux, Louis Cuccia, Yves Gélinas, Christine DeWolf, and John Capobianco – have contributed indirectly to the research. I gratefully acknowledge their efforts, teachings, and guidance.

I would like to thank previous and current XoRG members especially Laura Chaloner, Maryam Habibian, Badr Benassila, David de Bellefeuille, Laura Andrea Rodríguez-Solano, and Yuxuan Li. You all provided a great place to work and discuss pretty much everything! I am grateful to the undergraduate trainees who worked on my projects: Brigitte Girard, Fawn McIntyre, Carlos Leung, Seungguk Kim, Frédéric Rouseeau, Anastasia Kazakova, Klervi Dalle, Maëlle Mosser, Andrew Proppe, Andrew Dalton, Pierre-Etienne Rouet, Layla Halabi, Bryony McAllister, and Michael Glazerman. Special mention to the late Brad Sabat who made significant contributions to the lab's research and will be remembered forever.

Much of the research presented in this thesis would not have been possible without our collaborators at McGill university: Dr. Jean-Philip Lumb, Kenn Esguerra, and Zheng Huang. Special thanks go to Dr. Maylis Orio from France for performing several of the computational studies reported here. Dr. Muralee Murugesu and his students Fatima Habib and Po-Heng Lin carried out the magnetic measurement experiments and are acknowledge for their contribution.

I would like to thank the Department of Chemistry and Biochemistry for providing such a professional and friendly place to conduct research. Special thanks go to the graduate program director Dr. Heidi Muchall for always improving the quality of education provided in the Chemistry and Biochemistry department. The countless help of the facility technicians, Dr. Alexey Denisov, and Franco Nudo is greatly appreciated. I would like to thank my friends in the department – just to name some Diana Rodriguez, Ana María Ibarra, Paola Rojas, Derek O'Flaherty, and Fei Chen – you all made my stay at Concordia University a memorable experience!

This work would not have been possible with funding from external agencies NSERC, FRQNT and CFI, as well as the FRQNT Centre for Green Chemistry and Catalysis. I would like to especially acknowledge NSERC for funding most of my graduate studies and for the Michael-Smith Foreign Supplement Award for the internship in Germany.

Last but not the least, it has always been the encouragement of my parents and family members that motivated me to pursue higher education. They have always supported me in the best and the worst of times. Without their continuous motivation I would not have made it this far. I dedicate this thesis to my parents. Thank you!

## Contribution from Authors

### Manuscript 1: A Biomimetic Mechanism for the Copper-Catalyzed Aerobic Oxygenation of 4-tert-Butylphenol

Mohammad S. Askari: Experimental work, manuscript writing.
Jean-Philip Lumb: Manuscript writing and editing.
Xavier Ottenwaelder: Research supervision, manuscript writing and editing.

### Manuscript 2: Catalytic Aerobic Oxidation of Phenols to *Ortho*-Quinones with Air-Stable Copper Precatalysts

Mohammad S. Askari: Experimental work, manuscript writing.
Laura Andrea Rodríguez-Solano: Screening of some conditions and UV-vis experiments.
Andrew Proppe: Solvent screening.
Bryony McAllister: Initial copper screening.
Jean-Philip Lumb: Manuscript editing.
Xavier Ottenwaelder: Research supervision, manuscript writing and editing.

### Manuscript 3: The Two Spin States of an End-on Copper(II)-Superoxide Mimic

Mohammad S. Askari: Experimental work, computational studies, manuscript writing.
Brigitte Girard: Initial synthesis and crystallization of $[(\mathrm{Me_6tren})\mathrm{Cu}(\mathrm{PhNO}^{\bullet-})](\mathrm{TfO})$.
Muralee Murugesu: SQUID experiments.
Xavier Ottenwaelder: Research supervision, manuscript writing and editing.

### Manuscript 4: Controlled Nitrene Transfer from a Tyrosinase-Like Arylnitroso-Copper Complex

Mohammad S. Askari: Experimental work, initial computational studies, manuscript writing.
Maylis Orio: Computational studies.
Xavier Ottenwaelder: Research supervision, manuscript writing and editing.

# Table of Contents

## List of Figures

**List of Schemes**

## List of Tables

**List of Abbreviations**

| | |
|---|---|
| acac | Acetylacetonate |
| AcO | Acetate |
| ArNO | Nitrosoarene |
| BPh$_4$ | Tetraphenylborate |
| DβM | Dopamine-β-monooxygenase |
| DBED | *N,N'*-di-*tert*-butylethylenediamine |
| DFT | Density Functional Theory |
| DTBC | 3,5-di-*tert*-butylcatechol |
| DTBPNa | Sodium 2,4-di-*tert*-butylphenolate |
| DTBP | 2,4-di-*tert*-butylphenol |
| DTBQ | 3,5-di-*tert*-butylquinone |
| EAS | Electrophilic Aromatic Substitution |
| ESI-MS | Electrospray Ionization-Mass Spectrometry |
| IR | Infrared |
| KIE | Kinetic Isotope Effect |
| L | Ligand |
| Me$_6$tren | Hexamethyltris(2-aminoethyl)amine |
| **O** | bis($\mu$-oxo)dicopper(III) |
| OAT | Oxygen-Atom Transfer |
| *oxy*Hc | Oxygenated Hemocyanin |
| PHM | Peptidylglycine α-hydroxylating monooxygenase |
| $^{\mathbf{S}}$**P** | Side-on peroxodicopper(II) |
| $^{\mathbf{T}}$**P** | Trans-$\mu$-1,2-peroxodicopper(II) |
| $^{\mathbf{E}}$**S** | End-on superoxocopper(II) |
| $^{\mathbf{S}}$**S** | Side-on superoxocopper(II) |
| SQUID | Superconducting Quantum Interference Device |
| TfO | Triflate |
| Tol | Tolyl |
| (TMG)$_3$tren | Tris((1-methylimidazol-2-yl)methyl)amine |
| tmpa | Tris((2-pyridyl)methyl)amine |
| Tp | Tris(pyrazolyl)borate |
| Uv-vis | Ultraviolet-visible |
| MsO | Mesylate |
| TMPD | *N,N,N'N'*-tetramethylpropylenediamine |

# 1. Introduction

## 1.1. Goals and Motivation

One of the major challenges in synthetic chemistry is the conversion of abundant and inexpensive raw materials into functional molecules. One important functionalization is the selective oxidation and oxygenation of aromatic compounds. As such, reactions that involve oxygen-atom transfer and nitrogen group transfer have been studied extensively and development of such methods still continues today with the ultimate goal of environmentally-friendly reactions employing, if needed, inexpensive metal catalysts.[1-3] Phenols are ubiquitous feedstock materials that through oxygenation form synthetically versatile catechols (or quinones)[4] or through amination form aminophenols (or iminoquinones) that are useful synthetically or as fine chemicals (Scheme 1-1).[5] In biological organisms, tyrosinase catalyzes the *ortho*-oxygenation of tyrosine into dopaquinone using $O_2$ as the oxygen-atom source and copper ions to catalyze and direct the reaction.[6] The efficiency and the benign nature of this reaction (water is the only by-product) has inspired more than 50 years of research into understanding the mechanism of this transformation and, more importantly, in developing aerobic copper-catalyzed reactions for the oxygenation of phenols.[7] Even though the mechanism of phenol oxygenation by tyrosinase is known to some detail,[8] a synthetically useful aerobic catalytic reaction based on copper for the oxygenation of phenols was only recently developed and reported by the Lumb group at McGill.[9]

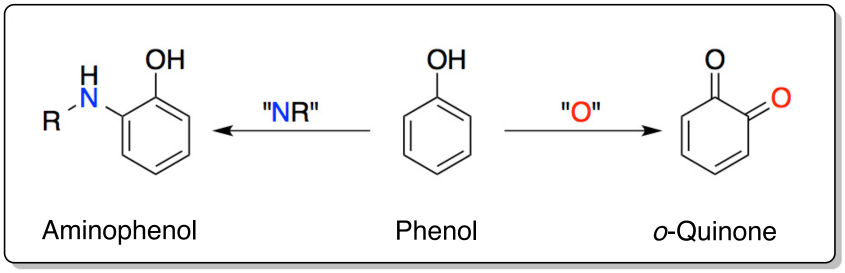

Scheme 1-1: The *ortho*-oxygenation and amination of phenols.

In order to improve the applicability of the reported catalytic reaction and expanding the concept into other useful methodologies, an understanding of the reaction mechanism is required.

For this purpose the goals of the research presented in this thesis can be summarized in two points:

1) Determining the mechanism of the copper-catalyzed aerobic oxygenation of phenols under Lumb conditions.[9]
2) Developing a similar method for the *ortho*-amination of phenols (or phenolates) using nitrosoarenes as the nitrogen group source.

For the first objective, in order to justify the biomimetic nature of the catalytic aerobic oxygenation, the $Cu/O_2$ intermediates involved and the mechanism by which oxygen-atom transfer occurs must be the same as in tyrosinase. Furthermore, the mechanism must justify the high selectivity observed for oxygen-atom transfer as opposed to competing radical formation pathways.[10] The second objective builds on what is known in $Cu/O_2$ chemistry as nitrosoarenes are isoelectronic with singlet oxygen and are expected to interact with copper complexes in a similar way forming structural and electronic mimics of $Cu/O_2$ complexes.[11] This structural similarity implies similar reactivity and in principle by choosing the proper ligand, nitrosoarene, and reaction conditions it should be possible to perform the *ortho*-amination of phenols.[12] As the feasibility of a stoichiometric reaction is a prerequisite to developing the catalytic version, the focus was placed on understanding the electronic structure of the Cu/nitrosoarene complexes and performing the stoichiometric *ortho*-amination of phenolates. This model reaction stands as a proof of concept for the similarities of $Cu/O_2$ and Cu/nitrosoarene chemistries and demonstrates the importance of mechanistic studies in developing novel reactions.

## 1.2. Aerobic Copper-Mediated Reactions in Synthesis

Copper-mediated reactions, catalytic and stoichiometric, have attracted a great amount of attention in recent years.[2] The interest in employing copper salts in organic reactions, especially in oxidation and oxygenation is in part due to the abundance of the metal, hence its low price, the stability of the metal sources in different oxidation states i.e. Cu(0), Cu(I), and Cu(II), and the coordination and redox lability of copper. The redox lability is especially important in bond-forming reactions and activation of small molecules as such reactions require a change in the oxidation state of the metal centre. Of particular interest in green chemistry is the functionalization of organic compounds using abundant oxidants either as terminal electron acceptors in oxidation reactions or as oxygen-atom source in oxygenation reactions. Many established protocols for oxygen-atom transfer reactions in organic synthesis utilize stoichiometric amount of synthetic oxidants such as periodates[13-14] or persulfates.[15] The main drawback in using these reagents is the formation of stoichiometric amounts of various potentially hazardous organic and inorganic waste as side-products that have to be separated. Therefore, methods employing $O_2$ are highly desirable as the side-product of the oxidation/oxygenation is water.[16] However, even though oxygenation is thermodynamically favourable, it is kinetically challenging due to the triplet state of $O_2$. In the ground state the $O_2$ molecule contains two unpaired electrons in the two degenerate $\pi^*$ orbitals. As most organic compounds are in the singlet state direct reaction of $O_2$ with organic substrates is spin-forbidden. To circumvent the kinetic barrier a metal catalyst is often required to reduce $O_2$ and activate it for further reactions.[17] Since oxygen binding is now coupled with its reduction, the metal catalyst must be able to undergo redox processes. Of the various metals reported in the literature capable of activating oxygen, copper[2] and iron[18] have received the most attention due to the ease by which they undergo redox processes and the stability of the metal centres in different oxidation states.

The occurrence of these metals in biological systems initiated investigations into the role of metals in oxygen transport and activation. In some biological organisms, the heme protein hemoglobin and myoglobin as well as the the non-heme protein hemerythrin, are responsible for the storage and transport of oxygen and heme enzymes such as Cytochrome P450 perform the oxidation of substrates in the mitochondria.[19] In arthropods and molluscs, the oxygen carrier protein, hemocyanin, contains copper atoms that can reversibly bind and release oxygen. Similarly, the copper-containing enzyme tyrosinase catalyzes the oxygenation of tyrosine in the first step of the melanogenesis process that produces melanin pigments (Scheme 1-2).[6] These natural systems have inspired significant amount of research in this field and many model systems have been developed to study the role of the metal centres in these metalloenzymes and develop synthetically useful methods for the oxidation of organic substrates. Iron enzymes and their model systems are beyond the scope of this thesis, and only copper enzymes and their models will be further discussed.

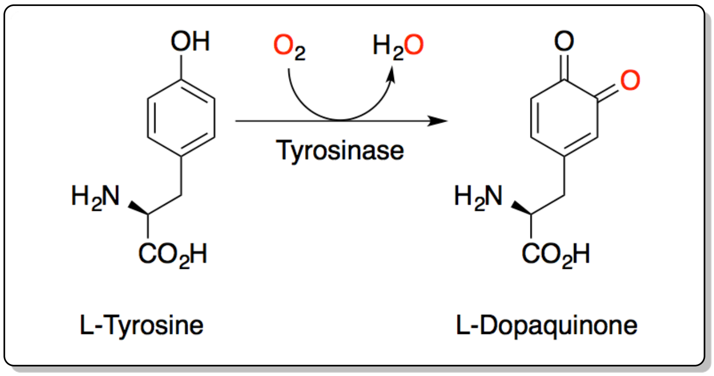

Scheme 1-2: Oxygenation of L-tyrosine to L-dopaquinone by tyrosinase.

A particular class of biologically inspired reactions is the selective *ortho*-oxygenation of phenols using molecular oxygen. The product of this reaction, depending on the reaction conditions, is either the *ortho*-catechol or the *ortho*-quinone, both of which are synthetically versatile. As phenols are naturally occurring and ubiquitous compounds, using them as the starting material for the production of highly functionalized compound is desirable. Several protocols to perform this reaction employing synthetic oxidants, especially periodate compounds, have been developed and reported in the literature.[4,13,15] The obvious shortcomings of these reactions include the necessity to prepare the oxidants and the generation of stoichiometric amount of salts or iodine-containing organic waste. Since the overall reaction is the transfer of one oxygen atom, this reaction in principle could be performed using molecular oxygen, in which case the only byproduct would be water. The difficulty, however, resides in the lack of selectivity of aerobic reactions of phenols due to the prevalence of C-C bond-forming reaction pathways upon formation of phenoxyl radicals by hydrogen atom abstraction.[10]

Another potentially useful functionalization of phenols would be the *ortho*-amination to provide aminophenols that are important on their own or as intermediates in various industries including photographic and dye manufacturing.[5] Typically C(aromatic)-N bond forming reactions involves the coupling of nucleophilic amines with aromatic halides (Scheme 1-3).[20] Another possible retrosynthetic disconnection provides electrophilic amine source and nucleophilic carbon centre on the aromatic ring. The synthetic equivalents for the nucleophilic carbon can be the phenolate that places a negative charge at the *ortho*-carbon by resonance, and the equivalent for the electrophilic amines could be nitrosoarenes.

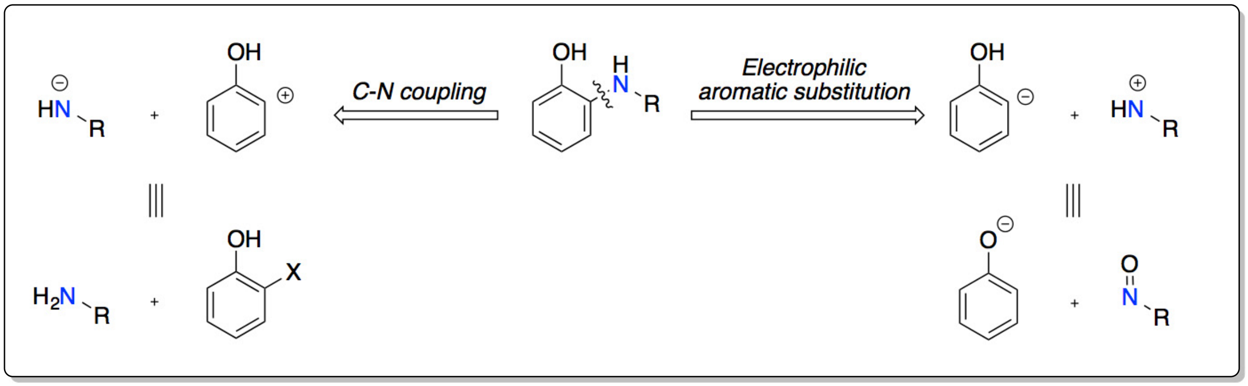

Scheme 1-3: Restrosynthetic analysis for *ortho*-amination of phenol (X = halide or pseudohalide).

Nitrosoarenes are isoelectronic with singlet oxygen and as such they are expected to interact with metal complexes in a similar way, forming structural and electronic analogues of metal/$O_2$ species. If structural mimics of Cu/$O_2$ intermediates can be formed with nitrosoarenes, then *ortho*-amination of phenols should in principle proceed through a similar pathway as the biomimetic *ortho*-oxygenation performed by tyrosinase. Contrary to the field of Cu/$O_2$ chemistry that has seen rapid development over the past 50 years,[21] using nitrosoarenes as mimics of molecular oxygen, their interaction with copper centres, and the reactivity of the resulting complexes have been little studied. Chapter 4 and 5 of this thesis will describe the feasibility of this approach in stoichiometric *ortho*-amination of phenolates.

## 1.3. Copper-Containing Enzymes

Proteins containing copper are involved in electron transfer and oxygen binding/activation in biological processes.[6,8] Two types of copper enzymes involved in $O_2$ activation will be described in this section: 1) non-coupled binuclear Cu enzymes, e.g. Dopamine-β-monooxygenase (DβM) and peptidylglycine α-hydroxylating monooxygenase (PHM); and 2) coupled binuclear Cu enzyme, e.g. tyrosinase. Both of these enzymes perform the oxygenation of organic compounds utilizing one oxygen atom from $O_2$, hence the name monooxygenase, while the other oxygen is incorporated into a water molecule. Even though the active site of both types of enzymes contain two copper centres and the overall reaction is a net oxygen-atom transfer, the mechanism by which this process occurs and the intermediates involved are different. The terms coupled and non-coupled refer to the presence and absence of magnetic coupling between the copper ions, respectively. This interaction depends on the distance between the two copper atoms and the presence or the nature of bridging units.[8]

### 1.3.1. Non-coupled binuclear copper enzymes

Dopamine-β-monooxygenase (DβM) and peptidylglycine α-hydroxylating monooxygenase (PHM) activate oxygen at copper centres and transfer a hydroxyl radical to relatively reactive aliphatic carbons (Scheme 1-4). The active site of these enzymes contains two copper atoms $Cu_M$ and $Cu_H$ at an approximately 11 Å distance from each other.[22-23] The long distance between the two copper centres indicates that $O_2$ binds to only one copper centre. The coordination environment around $Cu_M$ consists of two histidines and one methionine while for $Cu_H$ all the coordinating moieties are histidine residues. $Cu_M$ is responsible for oxygen binding and catalytic activity while $Cu_H$ supplies the extra electron needed in the process of oxygen reduction. Based on spectroscopic studies, it is proposed that one electron reduction of a bound $O_2$ at the $Cu_M$ site results in the formation of a copper(II)-superoxo species which performs the H-atom abstraction from the substrate forming copper(II)-hydroperoxo and a radical species.[24] Direct –OH transfer hydroxylates the substrate and produces a copper(II)-oxyl, $Cu^{II}$-($O^{\bullet -}$), formally a copper(III)-oxo, $Cu^{III}$-($O^{2-}$), which in turn is reduced to Cu(II)-OH by electron transfer from the $Cu_M$ centre.[25]

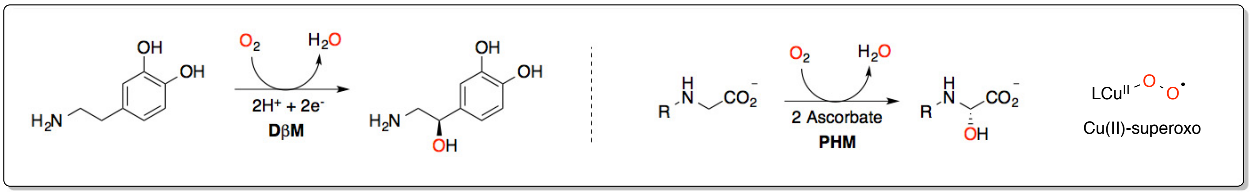

Scheme 1-4: Oxygen-atom transfer reactions catalyzed by DβM and PHM and the active oxygenating species.

### 1.3.2. Coupled binuclear copper enzymes

Tyrosinase catalyzes the first step of the melanogenesis process by oxygenating tyrosine to dopaquinone (Scheme 1-2).[2,6-8] The activation of oxygen in this enzyme is mechanistically different than in the non-coupled enzymes (Section 1.3.1). The active site contains two copper atoms ~4.6 Å apart, each coordinated to three histidine residues. In the deoxy form the copper centres are both in the +1 oxidation state.[26-27] Dioxygen binds to the two copper atoms in a side-on fashion. Electron transfer from each copper(I) atom to the dioxygen reduces the $O_2$ bond order, forming the peroxo species and two copper(II) centers. Contrary to the superoxo intermediate – formed in DβM and PHM – that is efficient at hydrogen-atom abstraction and formation of radicals, the peroxo intermediate is electrophilic and reacts preferentially by adding to nucleophilic species such as the aromatic ring of a coordinated tyrosine.

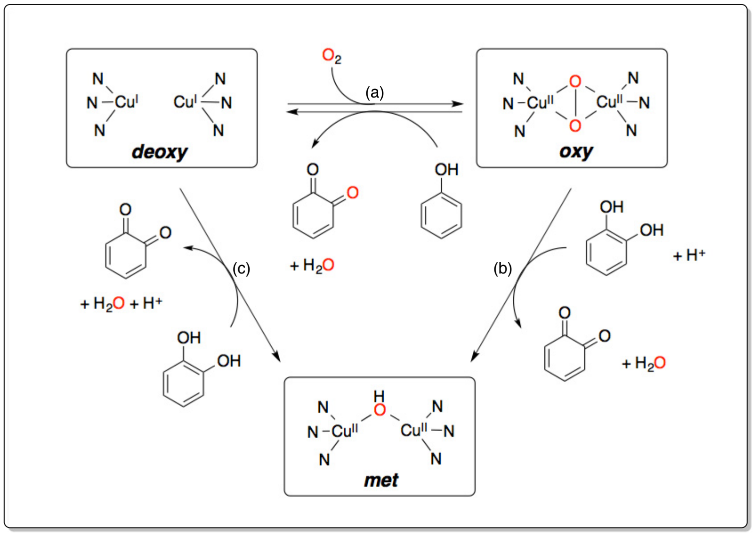

Scheme 1-5: The three states of the active site of tyrosinase. (a) The *deoxy* form binds $O_2$ in side-on fashion to form the side-on peroxo ($^S$**P**) species (*oxy*). The peroxo performs (a) oxygen atom transfer to phenol or (b) oxidation of the catechol. (c) The resting state of tyrosinase is the *met* state that is activated by reduction of the Cu(II) centres with catechol.[6,8]

Based on spectroscopic and kinetic studies, a mechanism for the oxygenation of tyrosine has been proposed.[28] The copper(I) centres in the active site bind $O_2$ in side-on fashion to form the peroxo intermediate. The substrate binds to one of the copper atoms in *oxy*-tyrosinase and oxygen-atom transfer occurs through electrophilic aromatic substitution (EAS) reaction. The measured Hammett parameter of $\rho$ = -2.4 when using *para*-substituted phenol substrates is consistent with EAS where oxygen atom transfer is the rate-limiting step.[29]

As the above examples of copper-containing enzymes demonstrate, the mechanism of oxygen-atom transfer depends on the nature of the Cu/$O_2$ intermediate formed that in turn depends on the Cu-Cu distance.[21] This dependence of $O_2$ activation and reactivity on geometric and electronic properties of the copper complexes has inspired great amount of research on model systems.

## 1.4. Model Systems for $Cu/O_2$ Species

Over the past 50 years, many researchers have sought to develop catalytic reactions for oxygen-atom transfer based on the reactivity of copper-enzymes.[2] However, outside of the protecting pocket of a protein, $Cu/O_2$ intermediates are more susceptible to degradation and pose several challenges in the development of bio-inspired catalysts. Many copper complexes with tailored ligands have been designed to mimic the active site of copper-enzymes and several reviews have been published in recent years describing the structure and spectroscopy of the $Cu/O_2$ intermediates formed with such compounds.[7,21,30] In this section, only models of the $Cu/O_2$ adducts in DβH, PHM, and tyrosinase will be discussed. It is worth noting that even though enzymes function at ambient temperatures, the majority of synthetic $Cu/O_2$ intermediates are only stable at temperatures below -50 °C. This kinetic instability limits the available methods for structural characterization of these species. Typically, $Cu/O_2$ species are characterized by electronic and vibrational spectroscopies and in only a few cases have X-ray crystal structures been obtained. The various $Cu/O_2$ intermediates show characteristic charge-transfer bands in the ultraviolet and visible regions that allow for the identification and quantification of the intermediates. In addition, reduction of the $O_2$ bond order causes a major shift in the vibrational frequency of the O-O and the Cu-O bonds that can serve as a characteristic method for determining the binding mode and the degree of bond reduction.

Interaction of Cu(I) complexes with oxygen can result in different types of $O_2$ bonding and geometries. The different known $Cu/O_2$ adducts are shown in Scheme 1-6. The type of intermediate that forms depends largely on the electronic and steric properties of the supporting ligand and to lesser extent on the counter-ion and solvent.[21] Unless prevented by steric factors or kinetic trapping, the 1:1 $Cu/O_2$ intermediates ($^{\mathbf{S/E}}\mathbf{S}$) rapidly react with another equivalent of the starting Cu(I) complex to form the 2:1 $Cu/O_2$ species ($^{\mathbf{S/T}}\mathbf{P}$ and **O**).

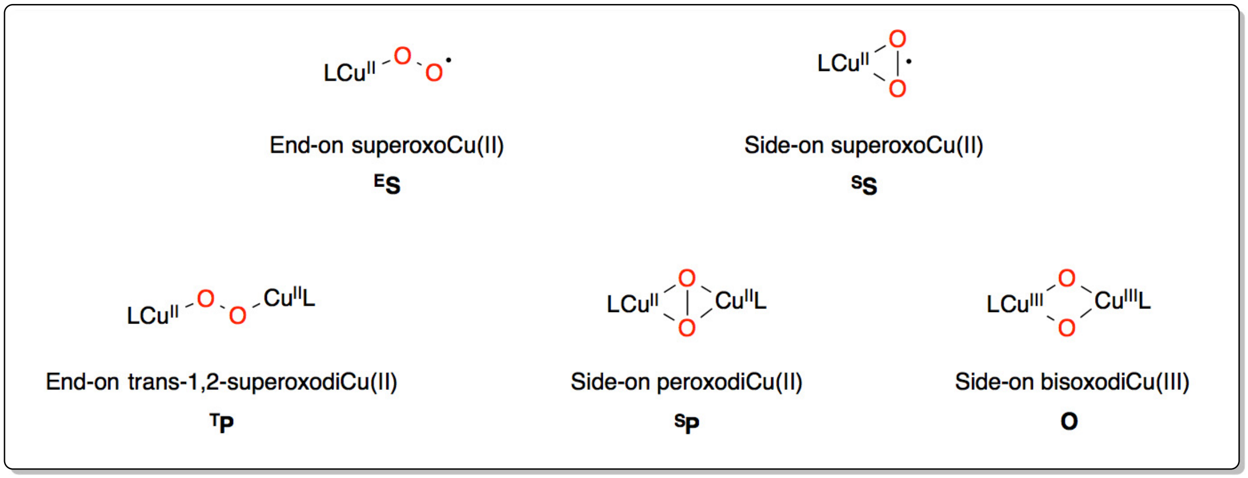

Scheme 1-6: Mononuclear and binuclear Cu/$O_2$ species.

### 1.4.1. Mononuclear Cu/$O_2$ intermediates: $^{S/E}$**S**

Two different binding modes of $O_2$ to copper centres are possible in the 1:1 stoichiometry: End-on superoxocopper(II) ($^{E}$**S**) and side-on superoxocopper(II) ($^{S}$**S**). In the superoxo intermediates, oxygen is reduced by one electron from the copper(I) center forming formally a superoxide radical anion $O_2^{\bullet -}$ and a copper(II) centre. This intermediate is proposed to perform hydrogen atom abstraction in enzymes such as DβH and PHM.[25] Superoxo species are usually very reactive even at low temperatures and they react with another equivalent of the parent copper(I) complex to form the binuclear peroxo $(O_2)^{2-}$ $^{T}$**P** and $^{S}$**P** or bisoxo $(O^{2-})_2$ **O**. This high reactivity limits their characterization to fast spectroscopic techniques and only few X-ray structures have been reported. [31-32]

#### 1.4.1.1. End-on superoxocopper(II): $^{E}$S

The end-on superoxo ($^{E}$**S**) intermediates are obtained by using tertradentate ligands. This type of intermediate was first characterized by exposure of Cu(I) complex with pyridine-based tmpa and tren-based $Me_6$tren supporting ligands (Scheme 1-7).[33] Oxygenation of the $[(tmpa)Cu(MeCN)]^+$ complex in EtCN at -90 °C forms the $^{E}$**S** species that reacts with another equivalent of $[(tmpa)Cu(MeCN)]^+$ to form the $^{T}$**P** species rapidly.[34] The end-on superoxcopper(II) was characterized by its UV-vis spectroscopic signature showing charge-transfer bands at ca. 410 nm (4,000 $M^{-1}cm^{-1}$) and ca. 580 nm (1,100 $M^{-1}cm^{-1}$). The $Me_6$tren ligands forms an electron-rich copper(I) complex owing to the stronger donor ability of amines in comparison to pyridines. Interestingly, oxygenation of this complex forms $^{\mathbf{E}}\mathbf{S}$ with very similar UV-vis signature as the tmpa complex, indicating that the $Cu_2O_2$ core is responsible for the electronic transitions observed. Similar to the tmpa ligand case, the $[(Me_6tren)Cu(O_2^{\bullet-})]^+$ complex rapidly forms the more thermodynamically stable $^{\mathbf{T}}\mathbf{P}$ at -90 °C.[33]

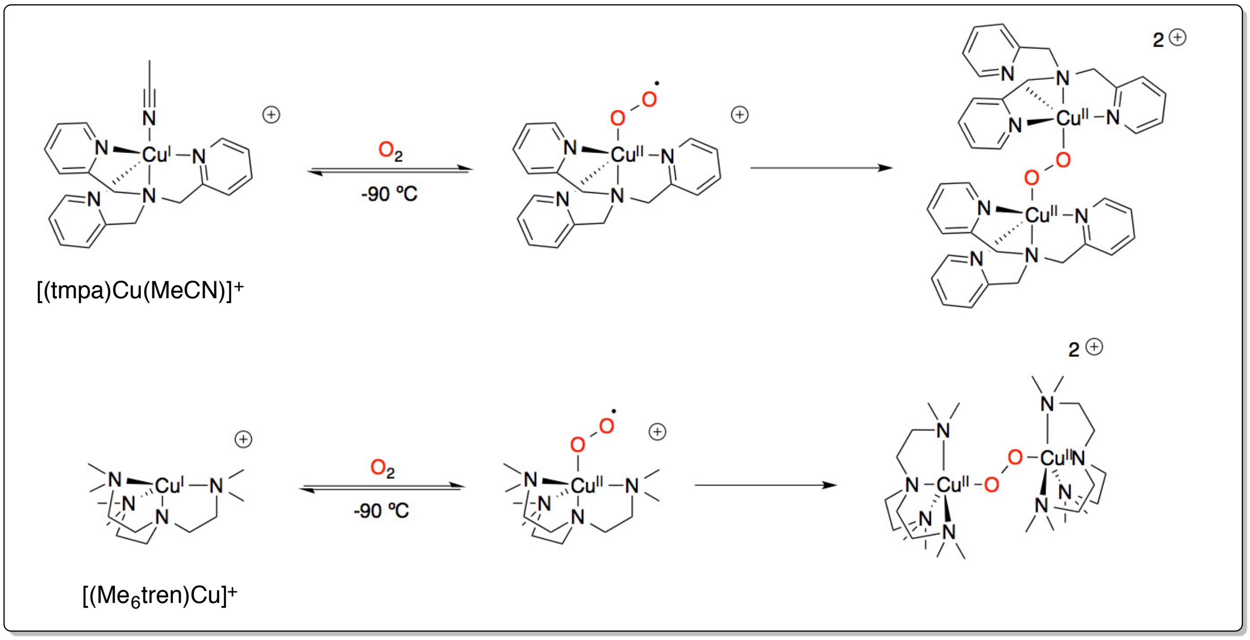

Scheme 1-7: Oxygenation products of $[(tmpa)Cu(MeCN)]^+$ and $[(Me_6tren)Cu]^+$ complexes at -90 ºC.[33]

Schindler and Sundermeyer in 2006 reported the electron-rich $[(TMG)_3trenCu]^+$ complex (Scheme 1-8) that forms the $^{\mathbf{E}}\mathbf{S}$ species and is stable for a sufficient amount of time at -80 °C for crystallization.[31,35] The crystal structure of $[(TMG)_3trenCu(O_2^{\bullet-})]^+$ represents the first structurally characterized end-on superoxocopper(II) intermediate and confirms the end-on binding nature of $O_2$ in these complexes. The highly basic guanidine groups coupled with the high steric demand of the ligand promotes the fast formation of the $[(TMG)_3trenCu(O_2^{\bullet-})]^+$, thereby depleting the starting copper(I)-complex and avoiding the formation of $^{\mathbf{T}}\mathbf{P}$. The UV-vis spectrum of this complex displays absorption bands at 412 nm (4, 800 $M^{-1}cm^{-1}$) and 580 nm (1,500 $M^{-1}cm^{-1}$).[35] The O-O stretching frequency at 1120 $cm^{-1}$ ($\Delta[^{18}O_2] = 63\ cm^{-1}$)[35] is in the expected range for copper(II)-superoxide species.[21]

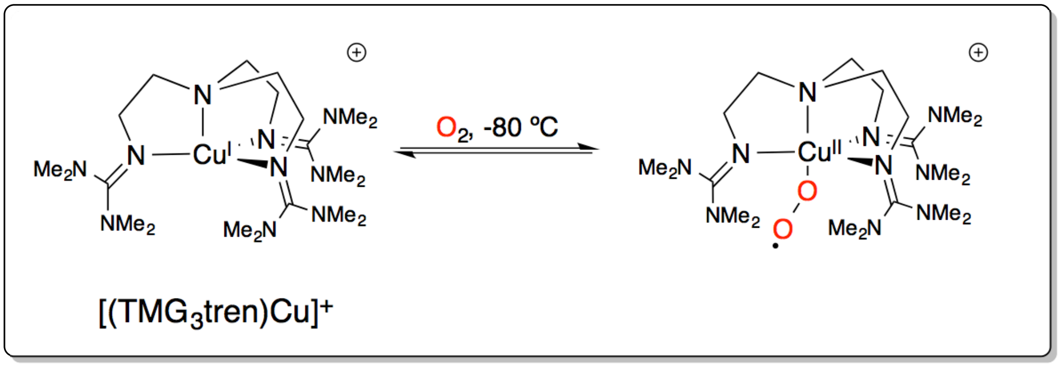

Scheme 1-8: The [(TMG$_3$tren)Cu]$^+$ complex and its reversible oxygenation to [(TMG)$_3$trenCu(O$_2^{\bullet-}$)]$^+$.[31]

### 1.4.1.2. Side-on superoxocopper(II): $^{S}$S

Modification of the denticity and basicity of the ligand can result in the side-on binding of O$_2$ to copper centres. Tridentate and bidentate ligands most often form side-on Cu/O$_2$ intermediates. The first crystallographically characterized side-on superoxocopper(II) ($^{S}$**S**) complex was reported by Kitajima.[32] By employing tris(pyrazolyl)borate ligand (Tp)[36] functionalized with bulky alkyl group (Tp$^{t\mathrm{Bu},i\mathrm{Pr}}$) the $^{S}$**S** species was obtained and was sufficiently stable for crystallization (Scheme 1-9). The geometry of the copper(II) center is distorted square-pyramidal with the oxygen binding side-on in the equatorial plane and O-O bond distance of 1.22 Å. The resonance Raman spectra of the superoxo complexes display O-O stretching vibration band at 1112 cm$^{-1}$ ($\Delta$[$^{18}$O$_2$] = 50 cm$^{-1}$). The $^{S}$**S** intermediates display weak absorption bands at ca. 500 nm (200 M$^{-1}$cm$^{-1}$) and ca. 700 nm (40 M$^{-1}$cm$^{-1}$).[21]

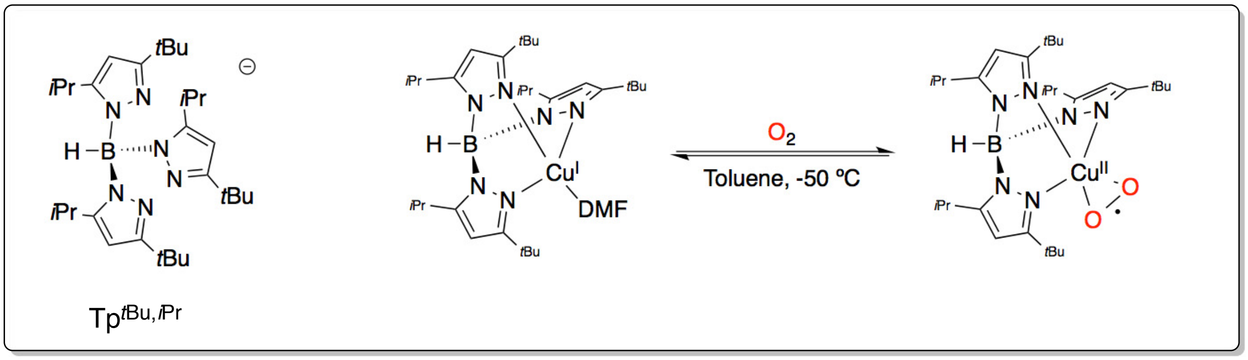

Scheme 1-9: The bulky anionic ligand employed by Kitajima and its reversible activation of O$_2$.[32]

### 1.4.2. Binuclear Cu/$O_2$ intermediates: $^{S/T}$P, O

Binuclear Cu/$O_2$ complexes are involved in important biological processes such as oxygen transport and melanogenesis.[6] Contrary to side-on binuclear complexes ($^{S}$**P**), the end-on binuclear complexes ($^{T}$**P**) arising from end-on superoxo species ($^{E}$**S**) have not been observed in biological systems. In molluscs and arthropods the oxygen carrier copper protein is hemocyanin. The X-ray structure of *oxy*-hemocyanin reveals side-on binding of $O_2$ to two copper centers each coordinated to three histidine residues.[37-39] The related copper enzyme tyrosinase, that catalyzes the oxygenation of tyrosine, possesses the same active site albeit with different structural features allowing for substrate binding.[40-41] This section describes the structure and the spectroscopic features of three binuclear Cu/$O_2$ intermediates.

#### 1.4.2.1. End-on *trans*-1,2-peroxodicopper(II): $^{T}$P

As mentioned in section 1.4.1, the initially formed copper(II)-superoxo intermediate usually reacts with another equivalent of the starting copper(I) complex to form binuclear Cu/$O_2$ adducts. The end-on superoxocopper(II) complexes, typically formed with higher denticity ligands (see section 1.4.1.1) form 1,2-*trans*-peroxodicopper(II) complexes. The first structurally characterized example of this type was reported by Karlin and is based on the tmpa ligand.[34] This complex with pyridine-based donors forms the $^{E}$**S** intermediate, $[(\mathrm{tmpa})\mathrm{Cu}(O_2^{\bullet-})]^+$, at low temperatures and rapidly forms the 1,2-*trans*-peroxo complex, $\{[(\mathrm{tmpa})\mathrm{Cu}]_2(O_2^{2-})\}^{2+}$ (Scheme 1-7).[33] The crystal structure of the intermediate confirmed the end-on binding of peroxide with O-O bond length of 1.43 Å. This complex served as the prototypical $^{T}$**P** and its spectroscopic features were used as criteria for the detection and quantification of 1,2-*trans*-peroxo intermediates.

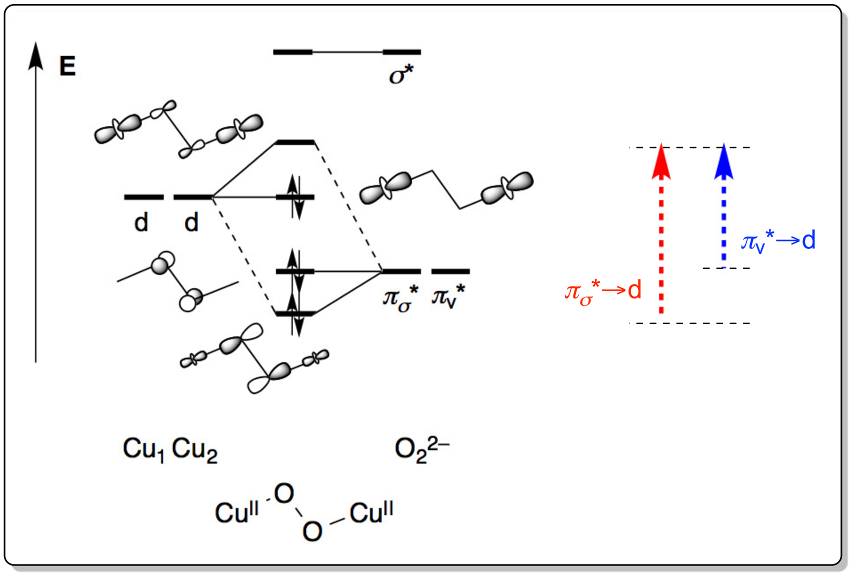

Figure 1-1: Simplified molecular orbital diagram for the 1,2-*trans*-peroxodicopper(II).[21] The electronic transitions are displayed on the right.

The deep purple-coloured 1,2-*trans*-peroxo intermediate shows strong absorptions at 525 nm (11,500 $M^{-1}cm^{-1}$) and 590 nm (7,000 $M^{-1}cm^{-1}$). These absorptions are assigned to charge transfer bands from the $\pi_\sigma$* and $\pi_v$* to Cu(II) d-orbitals, respectively (Figure 1-1).[42-43] Interestingly, modification of the coordinating moiety in the ligand does not change the UV-vis spectrum significantly. For example, $[(Me_6tren)Cu]^+$ complex forms the 1,2-*trans*-peroxo intermediate at -90 °C with spectral bands at 552 nm (13,500 $M^{-1}cm^{-1}$) and 600 nm (10,000 $M^{-1}cm^{-1}$).[33] Typically, the 1,2-*trans*-peroxocopper(II) intermediates are thermally unstable and decompose at higher temperatures by ligand or solvent oxidation. Schindler et *al.* reported the $\{[(Me_6tren)Cu]_2(O_2^{2-})\}^{2+}$ complex with $BPh_4$ counter-ions that shows remarkable stability at ambient temperature in the solid state.[44] The higher stability was attributed to the formation of a "protecting pocket" formed by the $BPh_4^-$ counterions around the $^{\mathbf{T}}\mathbf{P}$ molecule. The crystal structure of this complex gives an O-O bond length of 1.368(9) Å similar to the intermediate formed with $[(tmpa)Cu(MeCN)]^+$ complex.[34] Resonance Raman data of the $^{\mathbf{T}}\mathbf{P}$ complexes show isotope-sensitive O-O stretching frequency at 832 $cm^{-1}$ ($\Delta[^{18}O_2]$ = 44 $cm^{-1}$) for tmpa[42] and 825 $cm^{-1}$ ($\Delta[^{18}O_2]$ = 48 $cm^{-1}$) for the $Me_6$tren complex ($\Delta[^{18}O_2] = \nu(^{16}O_2) - \nu(^{18}O_2)$)[33] These values are significantly lower than the end-on superoxo complexes at ca. 1112 $cm^{-1}$ ($\Delta[^{18}O_2]$ = 50 $cm^{-1}$) indicating lower O-O bond order as expected for a peroxo anion.

### 1.4.2.2. Side-on peroxodicopper(II): $^{S}\mathbf{P}$

The interest in side-on peroxodicopper(II) ($^{S}\mathbf{P}$) intermediates stems from the prevalence of this species in copper-containing proteins responsible for oxygen transport and activation.[6,8] The active sites of tyrosinase, catechol oxidase, and hemocyanin all contain two copper atoms coordinated to three histidine residues.[26,40-41] Upon oxygenation, $O_2$ binds to the two metal centers in the side-on fashion and is reduced to the peroxo state by electron transfer from the two copper atoms. Even though these three proteins contain the same active site they perform different functions. Tyrosinase catalyzes the oxygenation of tyrosine to dopaquinone. Catechol oxidase on the other hand only catalyzes the oxidation of catechol to quinone and hemocyanin is involved in reversible oxygen binding and release.[8] The structural difference that eliminates the catalytic activity from hemocyanin is the presence of the active site deep in the protein manifold, thereby preventing substrate access.[41] The prevalence of $^{S}\mathbf{P}$ intermediate in these proteins and its ability to transfer oxygen atom to aromatic compound, i.e. tyrosine, inspired substantial amount of research in the formation and characterization of such intermediates using model copper complexes.[21]

In general, bidentate and tridentate ligands favour the formation of side-on Cu/$O_2$ species. The first examples of a side-on peroxodicopper(II) intermediate ($^{S}\mathbf{P}$) were reported by Kitajima who used a variety of substituted anionic tris(pyrazolyl)borate, $Tp^{R,R'}$ (R = Me, *i*Pr, Ph; R' = Me, *i*Pr) as the supporting ligand (the $Tp^{iPr,iPr}$ is shown in Scheme 1-10). [45-48] As Kitajima's work preceded the crystallographic characterization of *oxy*Hc, the nature of the Cu/$O_2$ intermediate in the enzyme was assigned based solely on spectroscopic features. The $Tp^{R,R'}$Cu(I) complexes form intermediates with spectroscopic parameters that closely resemble the *oxy*Hc. The relative stability of these complexes allowed for structural characterization by X-ray crystallography that showed the side-on binding mode of $O_2$ to the two copper centres.[46,48] The elucidation of the structure of *oxy*Hc, later confirmed the side-on binding mode in the protein. [37-39,49]

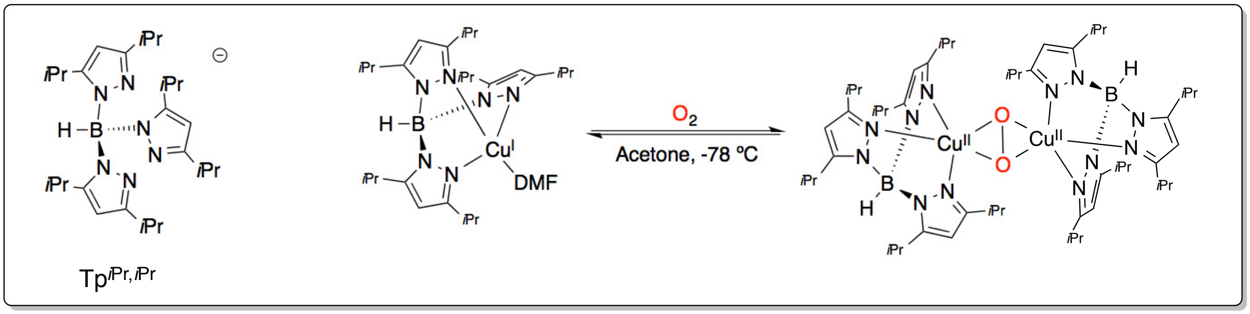

Scheme 1-10: The Tp$^{i\mathrm{Pr},i\mathrm{Pr}}$ ligand and the $^{S}$**P** species from oxygenation of the Cu(I) complex.[46,48]

As with other Cu/$O_2$ intermediates $^{S}$**P** shows characteristic spectroscopic features that remain within a narrow range with different supporting ligands. The UV-vis spectrum typically shows an intense band at 340-380 nm (18,000 – 25,000 $M^{-1}cm^{-1}$) and another less intense feature around 510-550 nm (~1,000 $M^{-1}cm^{-1}$).[21] Based on computational investigation by Solomon, the transitions responsible for the observed bands have been assigned to $\pi_\sigma* \rightarrow d$ (~350 nm) and $\pi_v* \rightarrow d$ (~530 nm) charge-transfer transitions (Figure 1-2).[43,50-52] The higher intensity of the $\pi_\sigma* \rightarrow d$ is due to the better overlap of orbitals on the same plane. Resonance Raman spectroscopy on the oxygenated complexes display isotope sensitive band at ca. 750 $cm^{-1}$ ($\Delta[^{18}O_2]$ ~ 40 $cm^{-1}$) that is assigned to the O-O stretching vibration.[21] The free peroxide displays O-O stretching frequency at ca. 850 $cm^{-1}$; back-donation from Cu(II) d orbitals into the σ* of O-O weakens the peroxide bond and shifts the stretching frequency towards lower wavenumbers.[53]

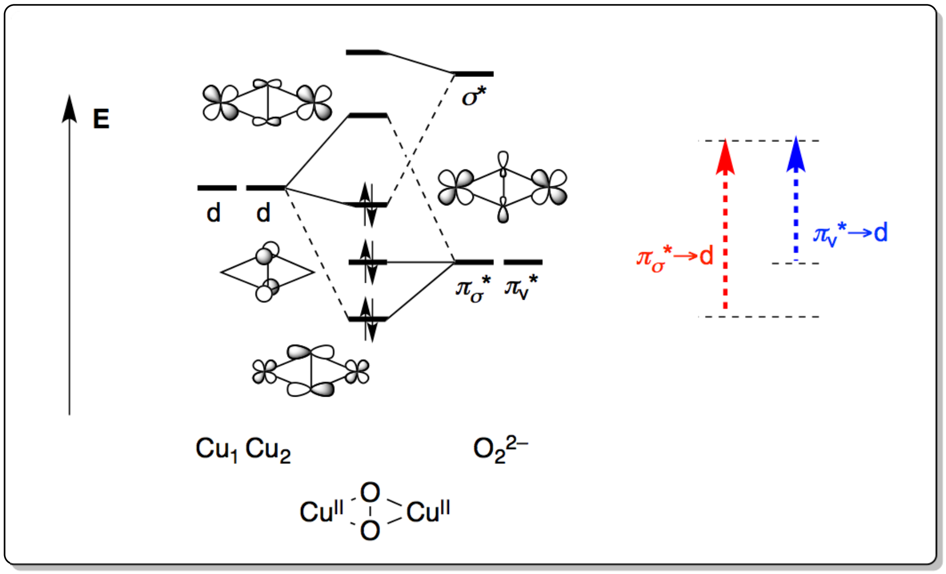

Figure 1-2: Simplified molecular orbital diagram for the side-on peroxodicopper(II).[21] The electronic transitions are displayed on the right.

Of particular importance in understanding the structure and reactivity of $^{S}\mathbf{P}$ species is the simple bidentate ligand *N,N'*-di-*tert*-butylethylenediamine (DBED) that forms a trigonal complex with Cu(I) and with an acetonitrile molecule occupying the third coordination site.[54-55] Oxygenation of the $[(DBED)Cu(MeCN)]^+$ complex in THF at -80 °C affords the $^{S}\mathbf{P}$ intermediate, $\{[(DBED)Cu]_2(O_2^{2-})\}^{2+}$ (Scheme 1-11), which is stable for relatively long time ($t_{1/2} \approx 20$ days, THF, -80 °C); this relatively high stability allowed for detailed analysis of the $^{S}\mathbf{P}$ electronic structure by various spectroscopic techniques. The UV-vis spectrum of the $^{S}\mathbf{P}$ intermediate displays the usual charge transfer bands at 350 nm (36,000 $M^{-1}cm^{-1}$), 485 nm (1,200 $M^{-1}cm^{-1}$), and 605 nm (900 $M^{-1}cm^{-1}$).[54-57]

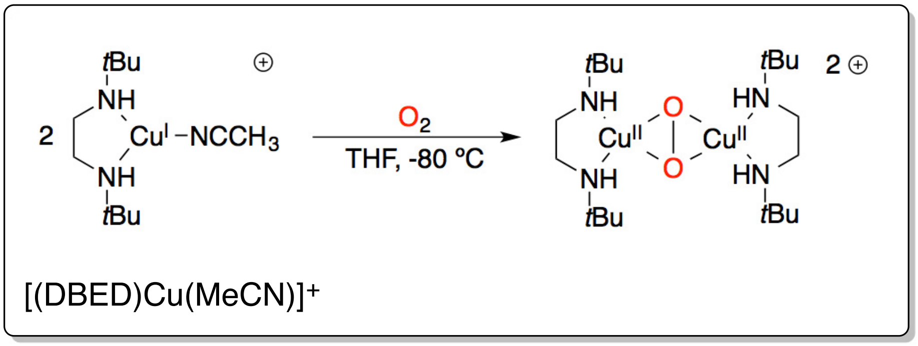

Scheme 1-11: $[(DBED)Cu(MeCN)]^+$ complex and the product of its oxygenation.[54]

To conclude, tridentate nitrogen heteroaromatic (pyrazole and pyridine) ligands have been used frequently to stabilize the $^{S}$**P** intermediate, however, bidentate aliphatic amine ligands have been shown to support this species too.[58] The stability of the $^{S}$**P** species formed depends mainly on the ligand and to some extent solvent and counterion. Many of the side-on peroxodicopper(II) species exist in equilibrium with the bis(oxo)dicopper(III) species where the O-O bond is completely cleaved by four electron reduction.[58-59]

### 1.4.2.3. Bis(*μ*-oxo)dicopper(III): O

The bis(*μ*-oxo) complex forms through the complete reduction of $O_2$ into two $O^{2-}$ (oxides) and the oxidation of two Cu(I) to Cu(III). The preferred geometry for $d^8$ Cu(III) ion is square-planar; therefore ligands that provide square-planar coordination geometry tend to stabilize the **O** species over its $^{S}$**P** isomer. Many bidentate ligands and some tridentate ligands have been used to form the **O** species.[21] Usually, the **O** species is in equilibrium with the $^{S}$**P** species. Structural data and computational investigations have shown that the $Cu_2O_2$ core in the **O** species is more compact than in the $^{S}$**P** species with Cu-Cu distance in **O** being 2.8 Å and in $^{S}$**P** is 3.6 Å (Scheme 1-12).[59] As a result, increasing the steric demand of the ligand keeping all other factors constant will favour formation of the $^{S}$**P** species.

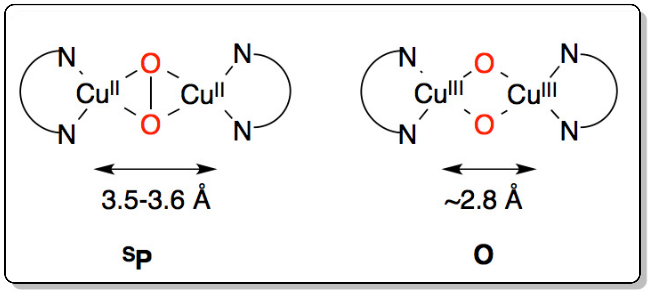

Scheme 1-12: Distance between the copper centres in $^{S}$**P** and **O**.[59]

Other factors that influence the $^{S}$**P**/**O** equilibrium are temperature, solvent and counterion. Lowering the temperature favours stronger bonds and less flexible structure, thus higher oxidation state of the copper centre, i.e. **O** species.[60] More coordinating counterions such as triflate ($CF_3SO_3^-$) and mesylate ($CH_3SO_3^-$) bind to the copper centres through the axial position forming square pyramidal geometry about the copper atoms, thus favouring the +2 oxidation state and consequently $^{S}$**P**. In comparison, **O** species are preferentially obtained with counterions such as $BF_4^-$ and $PF_6^-$ where there is minimal coordination to the copper(III) centers in accord with their preference for square planar geometry.[58-59] The effect of solvent is coupled with the state of the ionic species in the solution. In more polar solvents (2-MeTHF, THF, acetone) where less ion pairs between the copper complex and the counterion are formed the **O** species is favoured while in less polar solvents ion pairing promotes formation of $^{\mathbf{S}}\mathbf{P}$.[60]

As with other Cu/$O_2$ species, **O** complexes display characteristic spectroscopic features. In the UV-vis region, they display two intense charge-transfer bands at ca. 300 nm (~20,000 $M^{-1}cm^{-1}$) and 400 nm (~25,000 $M^{-1}cm^{-1}$).[21] The strong absorption in the visible region is responsible for the intense orange-brown colour of the **O** species. Based on computational studies the bands at ca. 300 nm and 400 nm have been assigned to the $\pi_\sigma^*\rightarrow d$ and $\sigma^*\rightarrow d$ transitions, respectively.[61] The $\sigma^*\rightarrow d_{xy}$ transition is unique to the bisoxo complex as only by full reduction of $O_2$ is the $\sigma^*$ populated. The prominent resonance Raman band in the **O** species is at 600 $cm^{-1}$ ($\Delta[^{18}O_2]$ ~ 25 $cm^{-1}$) that is assigned as the $Cu_2$-$O_2$ breathing mode.[61-62]

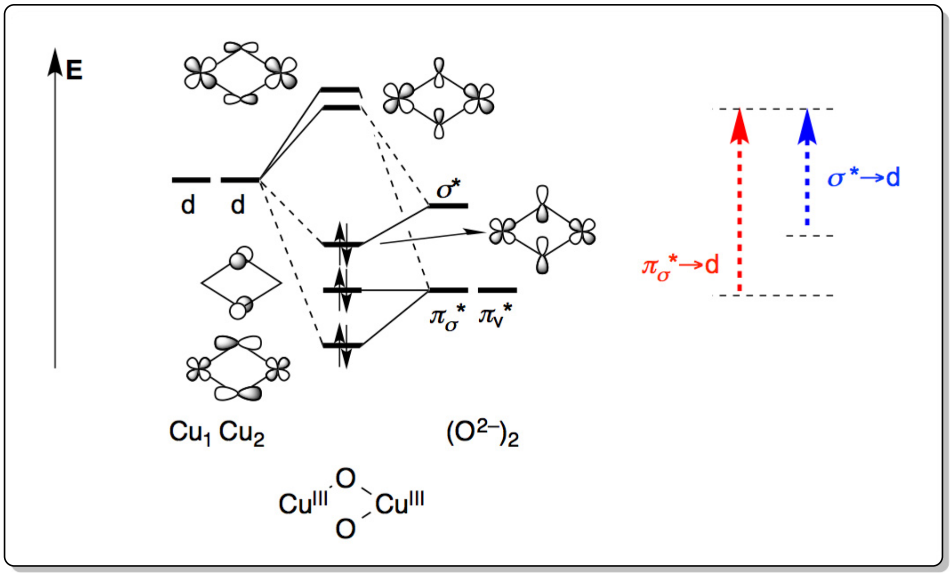

Figure 1-3: Simplified molecular orbital diagram for the bis(oxo)dicopper(III).[21] The electronic transitions are displayed on the right.

In summary, with bidentate ligands it is not uncommon to observe an equilibrium between the $^{\mathbf{S}}\mathbf{P}$ and the **O** species. The quantity of each can be determined from the characteristic UV-vis absorptions of the intermediates. The bis(*μ*-oxo)dicopper(III) intermediate has not yet been observed in biological systems.

### 1.4.2.5. Summary of the $Cu/O_2$ intermediates

The following table summarizes the various types of $Cu/O_2$ species and their major spectroscopic features (Table 1-1).

Table 1-1: Summary of approximate characteristic UV-vis absorption and stretching frequencies (O-O or Cu-O) for the $Cu/O_2$ intermediates.

| $Cu/O_2$ species | UV-vis absorption $\lambda$ / nm ($\varepsilon$ / $M^{-1}cm^{-1}$) | Resonance Raman $\nu$ / $cm^{-1}$ ($\Delta[^{18}O_2]$ / $cm^{-1}$) |
|---|---|---|
| $^{E}$**S** | 412 (4,800)<br>580 (1,500) | 1120 (63) |
| $^{S}$**S** | 500 (200)<br>700 (40) | 1112 (50) |
| $^{T}$**P** | 525 (11,500)<br>590 (7,000) | 830 (45) |
| $^{S}$**P** | 360 (22,000)<br>530 (1,000) | 750 (40) |
| **O** | 300 (20,000)<br>400 (22,000) | 600 (25) |

Superoxo ($^{E/S}$**S**) and bis($\mu$-oxo) (**O**) intermediates are efficient at hydrogen-atom abstraction from O-H and C-H bonds of organic substrates forming radical species. On the other hand, peroxo complexes, with the exception of 1,2-*trans*-peroxodicopper(II) ($^{T}$**P**), perform oxygen-atom transfer to C-H bonds.[8] The focus of this thesis is oxygen-atom / nitrogen-group transfer reactions inspired by peroxo intermediates. Therefore, only $^{S}$**P** reactivity will be further discussed.

### 1.4.3. Reactivity of $^{S}$P

In addition to studying the geometric and electronic structure of metals in metalloenzymes, the role of metals in catalyzing the enzymatic reaction is of interest to the bioinorganic chemist. Enzymes have evolved over millions of years to catalyze difficult reactions efficiently and with high selectivity. The catalytic properties of metalloenzymes is not only a function of the metal and its first coordination sphere but also depends on the protein's three-dimensional structure.

Achieving the same efficiency and selectivity in synthetic procedures would require either using enzymes as catalysts or developing catalytic systems based on the reactivity of metalloenzymes. The high substrate-specificity and the aqueous medium required for optimal enzymatic efficiency limits the utility of enzymes in synthetic laboratories. Therefore, it is highly desirable to develop catalytic reactions using model metal complexes as the (pre-)catalysts. From the various metlloenzymes, the ones that are involved in oxidation or oxygenation have received significant attention because of the involvement of $O_2$ as the oxygen-atom source or as the terminal oxidant. The abundance of $O_2$ and the benign side-product, i.e. water, makes these reactions particularly attractive. However, as it will be shown in the following discussion, harnessing the oxidative power of $O_2$ for chemo- and regio-selective functionalization without the protective pocket of an enzyme is particularly challenging and most of the efforts have been directed towards the development of structurally complex ligands to improve the selectivity of the reactions.

A particular enzyme related to the research work presented in this thesis is the copper-containing enzyme tyrosinase. The first step, and the rate limiting one, in the melanogenesis pathway is the *ortho*-oxygenation of L-tyrosine to L-dopaquinone (Scheme 1-2).[7] As described previously (see section 1.3.2), the active site of this enzyme contains two copper(I) atoms at a distance of ~4.6 Å from each other with each coordinated to three histidine residues. Activation of $O_2$ occurs by side-on binding to the two copper centres to form the side-on peroxodicopper(II) ($^{S}$**P**) intermediate (Scheme 1-5), which is proposed to be the active oxidant in the transformation. Thus, many researchers focused their attention on the synthesis of model $^{S}$**P** complexes to understand the mechanism of oxygen-atom transfer in tyrosinase and eventually developing a catalytic method for the *ortho*-oxygenation of phenols. The substrate of choice has been 2,4-di-*tert*-butylphenol (DTBP) that by having two blocked positions at C2 and C4 by *tert*-butyl groups will preferentially react at the *ortho* (C6) position. To further eliminate side reactions, including C-C coupling, the sodium phenolate salt (DTBPNa) is used under stoichiometric conditions (Scheme 1-13).[10]

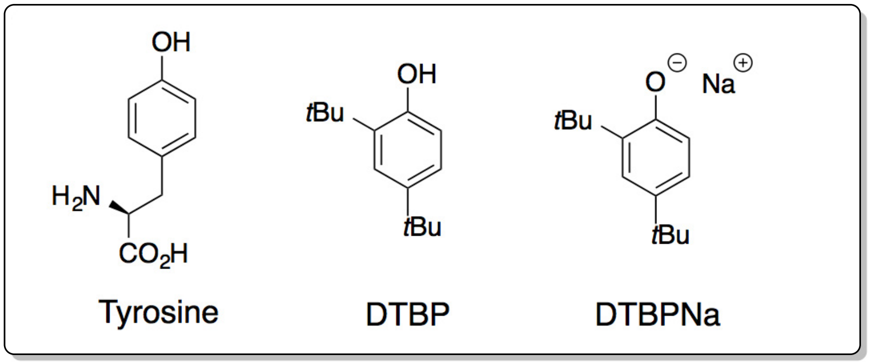

Scheme 1-13: Structures of tyrosine, 2,4-di-*tert*-butylphenol (DTBP), and sodium 2,4-di-*tert*-butylphenolate (DTBNa).

#### 1.4.3.1. Stoichiometric *ortho*-oxygenation of phenolates

Aerobic oxidation of phenols poses several challenges of which $O_2$ activation and selectivity are the major ones. Activation of dioxygen by metal centres, especially copper, has been well studied and often it is possible to predict the type of intermediate formed from the structure and electronic properties of the supporting ligand (see section 1.4.1 and 1.4.2).[21] The selectivity on the other hand is more difficult to control. Being electron-rich aromatics, phenols are easy to oxidize and, in the presence of oxidants such as a $Cu/O_2$ species, phenoxyl radicals readily form by hydrogen-atom abstraction.[10] The resonance forms of the phenoxyl radical places the unpaired electron on either the oxygen or on C2 or C4. Carbon-based radicals typically perform C-C coupling reactions that lead to bisphenols (Scheme 1-14). Even though radical-based aromatic C-C coupling reactions, especially with naphthols, are extensively studied and find application in the synthesis of natural products[63] and fine chemicals,[64] in the context of phenol oxygenation, bisphenols are considered undesired side-products. In order to avoid free-radical type reactivity, phenolates can be used. Because of their higher basicity and coordination ability, they bind to the metal centre and confine the reactivity to the first coordination sphere of the metal, preventing propagation of free radicals and formation of C-C coupled products.[10] This strategy has been used to study the mechanism of phenolate oxygenation however, by using the phenolate salts, it is not possible to achieve turnover and perform the reaction with catalytic amounts of a copper complex.

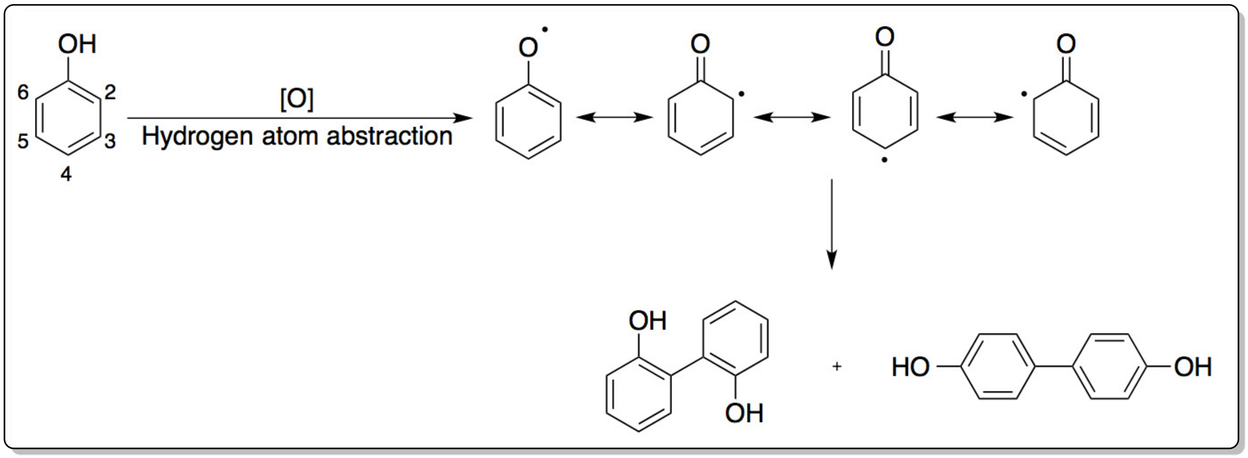

Scheme 1-14: Formation of phenoxyl radical by hydrogen-atom abstraction and C-C bond formation.

While many examples of phenolate *ortho*-oxygenation by $^{S}\mathbf{P}$ species of copper(I) complexes with specially tailored ligands have been reported in the literature, [65-73] the most detailed mechanistic study, where the various intermediates were characterized by spectroscopic and computational methods, was reported by Stack and Solomon using DBED as the supporting ligand (Scheme 1-15).[57]

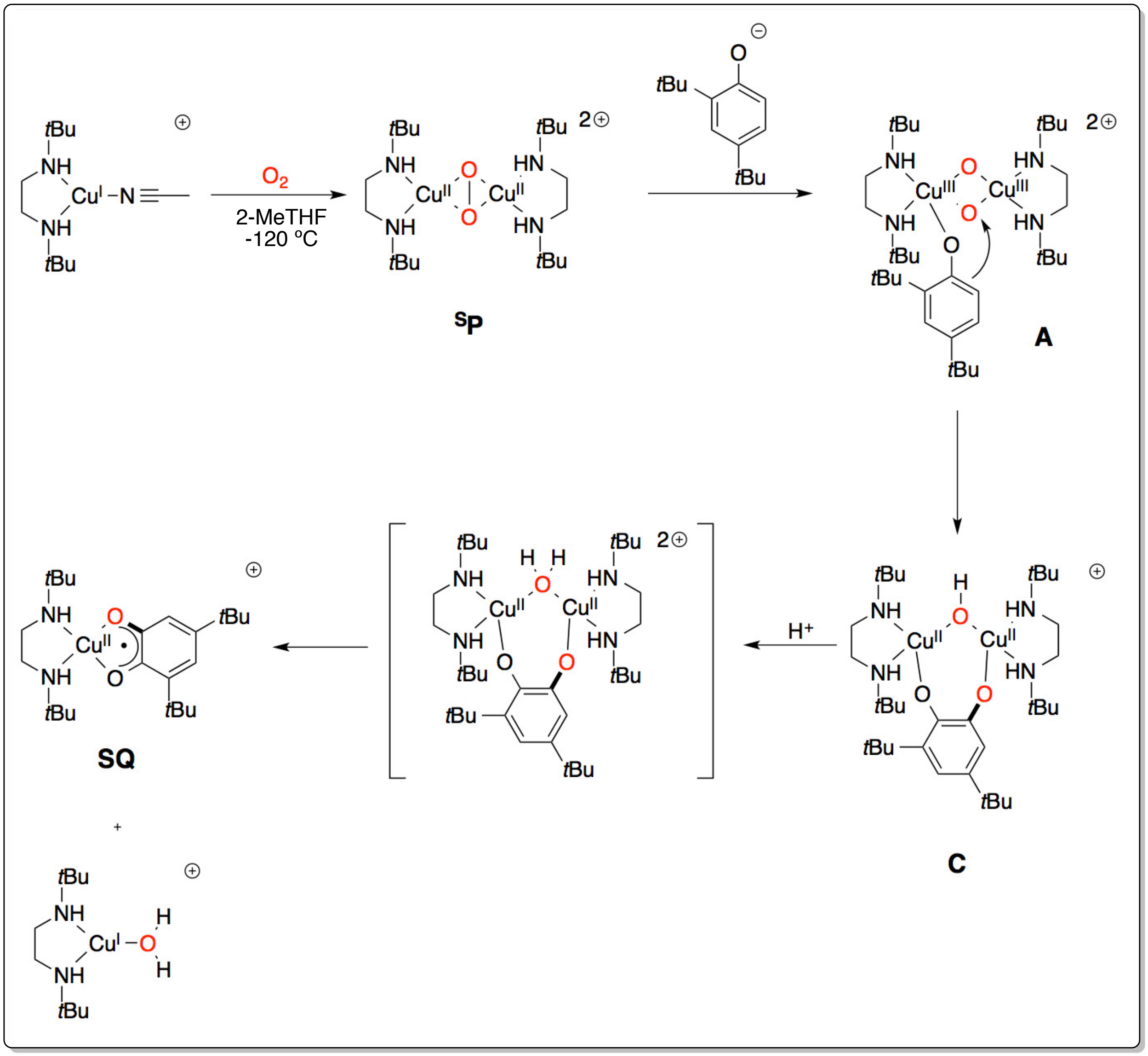

Scheme 1-15: Proposed mechanism for the oxygenation of DTBPNa with [(DBED)Cu]$^+$ complex.[57]

The reaction and the intermediates are shown in Scheme 1-15. The $^{\mathbf{S}}$**P** species was first preformed through oxygenation of [(DBED)Cu(MeCN)]TfO in 2-methyltetrahydrofuran (2-MeTHF) at -120 ºC. Addition of a solution of DTBPNa (two to three equivalents with respect to $^{\mathbf{S}}$**P**) induces the coordination of phenolate to the copper centres. Phenolate binding is accompanied by electron transfer from the copper(II) centres to the bound peroxide, breaking the O-O bond and forming the bis(oxo)phenolatodicopper(III) (**A**) complex. These geometric and electronic changes upon addition of phenolate cause significant alteration in the UV-vis spectrum of the Cu/O$_2$ species allowing for their identification and quantification (see Table 1-1). Due to the preference of copper(III) for square-planar geometry, the phenolate moves into the equatorial plane of the $Cu_2O_2$ core and one of the DBED nitrogen coordinates in the axial position. Within a few hours at -120 ºC, species **A** decays to an intermediate without major absorption features in the visible region. Based on computational modeling, the structure of this intermediate is assigned to the catecholatocopper(II) complex **C**. In the transition from **A** to **C**, one oxygen atom is transferred to the aromatic ring and under stoichiometric conditions it is the rate-limiting step in the overall *ortho*-oxygenation. The oxygen-atom transfer is proposed to proceed through an electrophilic aromatic substitution mechanism based on slower reaction rate with electron-deficient phenolates with negative Hammett parameter ($\rho$ = -2.2) and inverse secondary kinetic isotope effect of 0.83(0.09) at the *ortho* position.[56] Oxygen-atom transfer to phenolate and rearomatization to form the catecholate requires the elimination of one proton from the substrate. Based on DFT geometry optimization, the lowest energy structure corresponds to **C**. Therefore, the eliminated proton is transferred to the second oxygen atom of the **A** intermediate. Any base (including counterion or a nearby uncoordinated nitrogen of DBED) present in the reaction mixture catalyzes the proton transfer, although direct deprotonation by the second oxygen atom has been proposed too. Addition of one equivalent of external acid (with respect to the phenolate) at -80 ºC protonates the bridging hydroxyl group that in turn causes the cleavage of the catecholato dimer into copper(II)-semiquinone (**SQ**) and another unknown copper species proposed to be $[(DBED)Cu(H_2O)]^+$. Addition of excess acid quenches the catecholate complex giving the free catechol and the free quinone in 1:1 ratio. Disproportionation of **SQ** into copper(I)-quinone and copper(II)-catecholate complex is proposed to be the reason for the formation of 1:1 catechol:quinone mixture upon acidic workup (Scheme 1-16).[7]

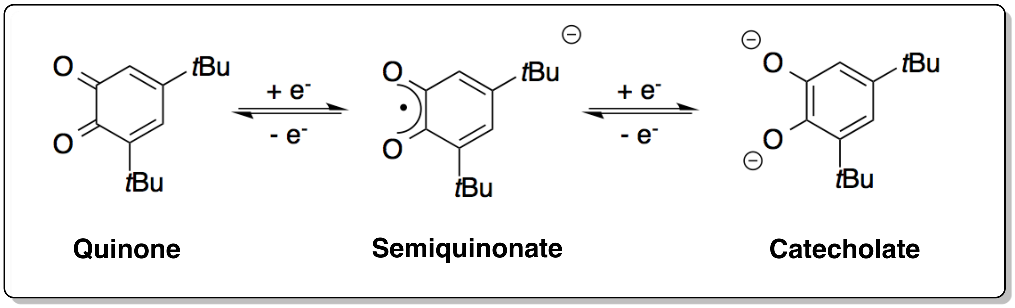

Scheme 1-16: Structures of quinone, semiquinonate, and catecholate.

Single turnover reactions employing phenolate salts eliminates all the complexities associated with catalytic reactions such as catalyst degradation, side reactions, and concentration dependence. However, for synthetic purposes catalytic reactions are desired. In order for catalytic turnover to occur, complex **C** must be protonated with an internal acid to release the semiquinone **SQ** that can further dissociate into free quinone and a copper(I) complex that re-enters the catalytic cycle. Therefore, the phenolates have to be generated in situ from phenol and an added base that by deprotonating the phenol provides the conjugate acid to protonate **C** and form the semiquinone.

### 1.4.3.2. Catalytic *ortho*-oxygenation of phenols

The transition from stoichiometric to catalytic *ortho*-oxygenation has been accompanied by several challenges including selectivity and substrate scope. As is usually done in metal-catalyzed reactions, most of the effort is spent on designing specially-tailored ligands to increase the yield and selectivity of the reaction under investigation. In the case of copper-catalyzed oxygenation of phenols, many ligands have been developed to favour the formation of $^{\mathbf{S}}\mathbf{P}$, and used to perform this reaction using the usual DTBP as the substrate. However, a mixture of products was always obtained (Scheme 1-17). The various products observed include the starting DTBP, bisphenol from C-C coupling, 3,5-di-*tert*-butylcatechol (DTBC), and the desired 3,5-di-*tert*-butylquinone (DTBQ). Typically, a large excess of triethylamine (two equivalents with respect to phenol is used and it is assumed that the highly basic medium is not detrimental to the Cu/$O_2$ intermediates. Réglier,[65] Casella,[66] and Tuczek[67] reported the bidentate ligands shown in Scheme 1-17 for the oxygenation of DTBP.

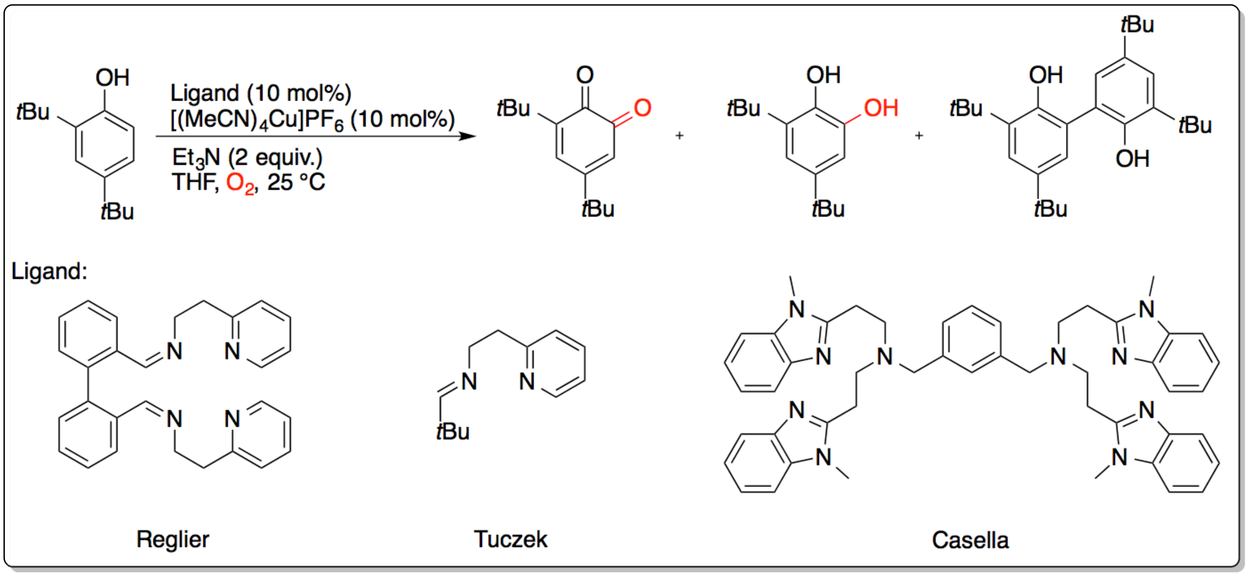

Scheme 1-17: Examples of aerobic *ortho*-oxygenation of DTBP in the presence of Reglier,[65] Tuczek,[67] and Casella[66] ligands with excess triethylamine.

In 2013 Herres-Pawlis and Stack reported the aerobic oxygenation of *para*-substituted phenols using copper(I) complex of a custom-designed ligand and two equivalents of triethylamine as the base (Scheme 1-18).[69] The intriguing property of the ligand is the formation of side-on peroxo complex that is stable at 25 ºC; typically these intermediates decay thermally by oxidizing the ligand or solvent. Even though formation of C-C coupled by-products and polymerization were not reported to occur, the difficulty of ligand synthesis, limited substrate scope, and low conversions render this method not practical for synthetic purposes. Furthermore, the large quantity of triethylamine needed for this reaction is impractical on larger scale reactions.

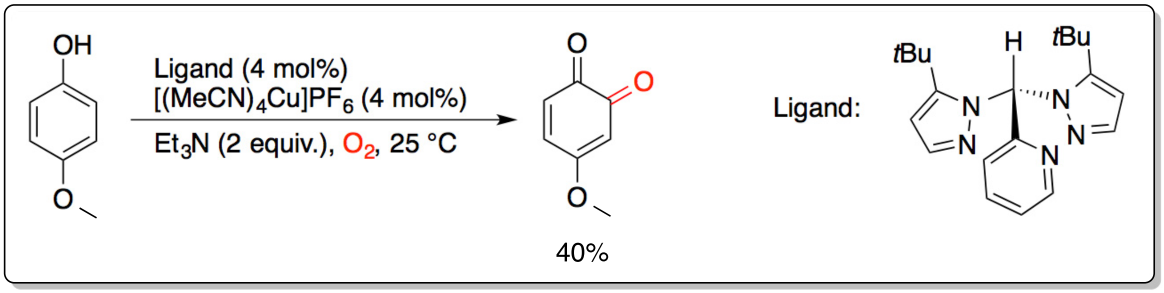

Scheme 1-18: The tridentate ligand reported by Herres-Pawlis and Stack with the general oxygenation reaction.[69]

In 2014 Jean-Philip Lumb at McGill University reported a catalytic aerobic reaction for the oxidation of phenols that provides quantitative yields and uses a copper(I) salt and triethylamine

(Scheme 1-19).[9] The reaction requires 50 mol% of triethylamine with respect to phenol, which is a significant improvement over previously reported methods. It is important to note that this reaction provides the oxidatively-coupled quinone as the final product as opposed to the uncoupled quinone. Molecular sieves were found to be important to achieve high conversions and yields, even though its exact role is not yet known. In the absence of molecular sieves, the yield drops drastically to 30-60% with the concomitant formation of intractable mixture of compounds. A possible explanation is the sensitivity of the product to hydrolysis by the water generated in the $O_2$-activation step. Such oxidatively-coupled quinones were previously reported to form in the aerobic oxidation of 4-methoxyphenol in the presence of CuCl and Cu(0) in methanol.[74] Even though the reported conditions provide significantly enhanced yields, scope, and selectivity when compared to previous methods, presence of molecular sieves in the reaction mixture causes complications in reproducibility and homogeneity of the reaction.

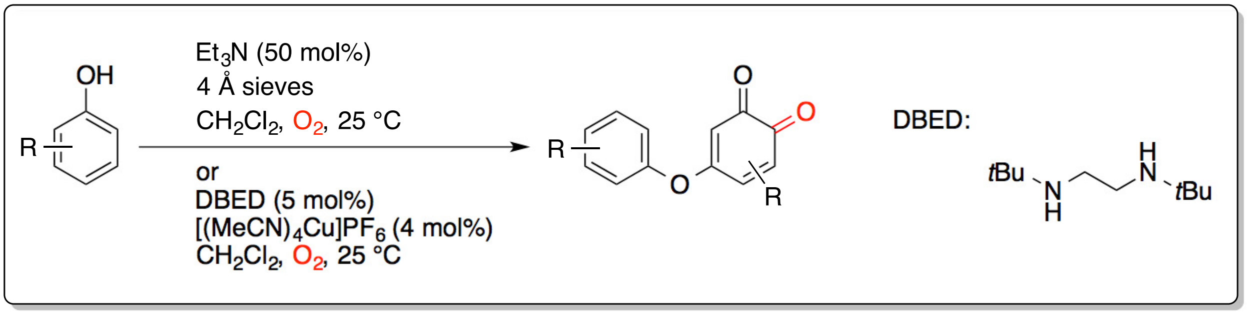

Scheme 1-19: Reaction conditions developed by Lumb for the oxygenation and oxidative coupling of phenols.[9]

Interestingly, using DBED as the ligand and base for this reaction eliminates the requirement for molecular sieves, providing homogenous reaction conditions and more reproducible results while still giving quantitative yield of the product (Scheme 1-19). The homogeneous nature of the reaction and its efficiency are ideal for mechanistic study of the oxygenation process by spectroscopic methods. The mechanism of the *ortho*-oxygenation in this reaction is the subject of chapter 2.

## 1.5. Nitrosoarenes as Mimics of $O_2$

Nitrosoarenes (ArNO) are aromatic compounds containing an -N=O functional group and are isoelectronic with dioxygen. ArNO species are singlet, but contrary to the unstable $^1O_2$, they can be prepared and stored indefinitely. Due to the similarity of $O_2$ and ArNO, it is expected that metal complexes of nitrosoarenes to be structural and electronic mimics of metal/$O_2$ complexes. Furthermore, they are expected to react with external substrates in similar way. Before introducing metal complexes of nitrosoarenes, the structure, preparation, and spectroscopy of nitrosoarenes will be described.

### 1.5.1. Structure and spectroscopy of nitrosoarenes

Compounds bearing the nitroso functional group (-N=O) are grouped into four main categories: C-nitroso (R-N=O, R = alkyl, aryl), N-nitroso ($R_2$N-N=O), O-nitroso (RO-N=O), and S-nitroso (RS-N=O). For the purpose of the research presented in this thesis, only C-nitrosoarenes (ArNO) will be further discussed. In the solid state, depending on the nature of the substituent on the aromatic ring, nitrosoarenes exist as monomers or diazoxy dimers (Scheme 1-20). In the arylnitroso series, the presence of electron-donating group on the aromatic ring favours the formation of the monomeric arylnitroso owing to the stabilization caused by the resonance structure. On the other hand, electron-withdrawing group on the aromatic ring favours the formation of diazoxy dimer. The dimers exist in either *cis*- or *trans*- configurations that depend on the substituents as well. Even though dimeric form is dominant in the solid state, the monomeric form predominates in solutions.[75]

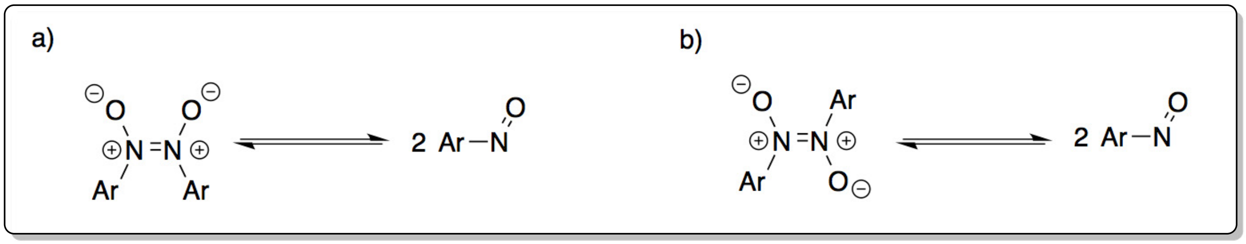

Scheme 1-20: Structures of a) *cis*- and b) *trans*-dimers of nitrosoarenes and the monomeric form.

The N=O bond length in structurally characterized nitrosoarenes monomers is in the range of 1.13-1.29 Å and in the dimers 1.25-1.28 Å (in PhNO 1.261(4) and 1.268(4) Å).[75] The UV-vis spectra of ArNO typically show two bands arising from the n→π* and π →π* at ca. 270 nm (strong) and 700 nm (weak), respectively.[75] The absorption in the visible region around 700 nm is the source of the light green colour of monomeric nitrosoarenes in solution. Infrared spectroscopy is often used in structural characterization of ArNO especially to probe the N=O stretch and hence the bond order. For monomeric nitrosoarenes, the N=O bond shows one band in the range 1488-1513 $cm^{-1}$ while in the *trans*-dimers the value is shifted to 1253-1299 $cm^{-1}$; the *cis*-dimers display two bands in the range of 1389-1397 cm$^{-1}$ and ca. 1409 cm$^{-1}$.[75] Due to presence of these bands in the C-C stretching and C-H bending frequencies of the infrared spectrum (1200-1600 cm$^{-1}$), definite assignment of the frequency usually requires the preparation of R-$^{15}$NO and determining the position by isotopic shift. Stretching frequencies reported for N=O bonds without isotope substitution are thus often misleading.

### 1.5.2. Preparation of nitrosoarenes

Nitrosoarenes are typically prepared through either oxidation of aromatic amines or electrophilic aromatic substitution with $NO^+$. For aniline and aromatic amines bearing electron-withdrawing substituents such as $-NO_2$, -X (X = halide), oxidation of the amine group under mild conditions provides the corresponding arylnitroso in good yields. The selective oxidation is usually performed using monopersulfate salts (Oxone®) or by employing hydrogen peroxide with molybdenate or tungstenate catalysts.[76] Recently, this method has been extended to solvent-free method by grinding the aromatic amine and Oxone® in the presence of sodium bicarbonate; the nitrosoarene is then separated from the mixture by sublimation.[77] Electron-rich aromatic amines, on the other hand, are not amenable to this selective oxidation as formation of the nitroamines will be favoured. Instead, electrophilic substitution reaction with $NO^+$ generated in situ from $NaNO_2$ in acidic conditions conveniently provides the arylnitroso.[78] Another source of the nitrosonium cation is $NOBF_4$ that has been used for the preparation of *p*-methoxy-nitrosobenzene.[79]

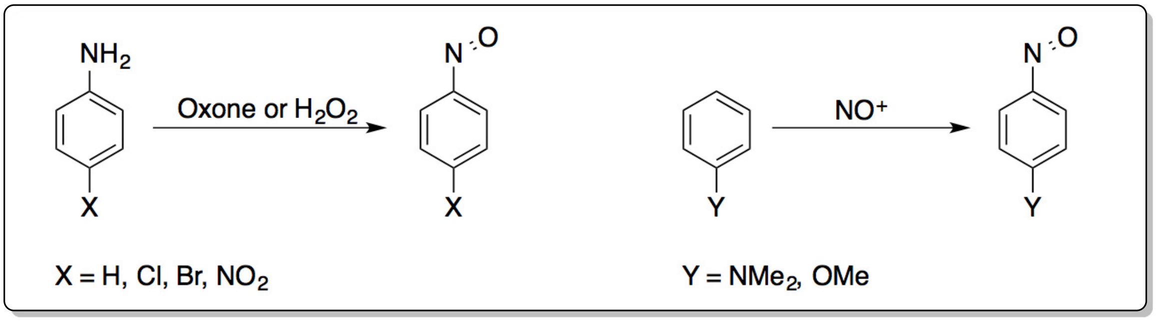

Scheme 1-21: Typical synthetic routes for the synthesis of nitrosoarenes.

### 1.5.3. Metal complexes of nitrosoarenes

The binding of ArNO to metal centres has initially attracted attention due to the possible presence of these compounds in the biological reduction of nitroarenes or oxidation of amines.[80-

82] Significant studies have been directed to understand the nature of binding of nitrosoarenes to metal-porphyrin complexes.[75] However, in non-biological systems, metal-ArNO adducts have shown interesting structural features and reactivities thus prompting more studies.

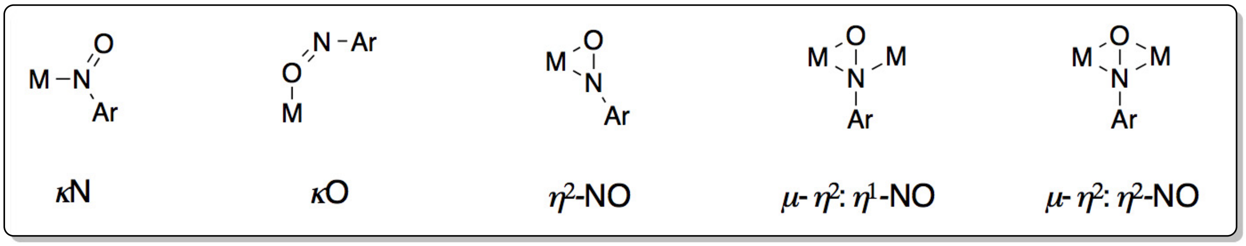

Scheme 1-22: Some of the binding modes observed in metal/nitrosoarene complexes.[75]

Owing to the asymmetric structure of ArNO in comparison to $O_2$, the structural variety of metal/nitrosoarene complexes exceeds that of metal/$O_2$ compounds. Some of the main binding modes of ArNO to metals are shown in Scheme 1-22.[75] In mononuclear adducts, the nitroso moiety can bind to metals through the nitrogen atom ($\kappa$N), the oxygen atom ($\kappa$O) or side-on to both nitrogen and oxygen atoms ($\eta^2$-NO). The most common binding mode of nitrosoarenes is through the nitrogen atom; $\kappa$O and the $\eta^2$-NO modes have been reported less often. The NO bond length in metal/ArNO complexes depends on the binding mode, the oxidation state of the metal, and the supporting ligands. In majority mononuclear $\kappa$N complexes of nitrosoarenes, the NO bond length is in the range of 1.209(3)-1.31(2) Å and compared to the NO bond lengths in free nitrosoarenes there is little or no elongation of the NO bond.[75] Figueroa *et al.* reported the Pd(0) complex with isocyanide supporting ligand $Pd(CNAr^{Dipp2})_2$, that upon treatment with PhNO formed square-planar complex by coordinating two nitrosobenzene molecules (Scheme 1-23). Based on the geometry of the Pd centre and the NO bond length of 1.291(2) Å, the authors proposed reduction of each nitrosobenzene by one electron to a nitrosobenzene radical anion and oxidation Pd(0) to Pd(II): $[(CNAr^{Dipp2})_2Pd^{II}(PhNO^{\bullet-})_2]$.[83] The one-electron reduction of nitrosobenzene by a transition metal is akin to the one electron reduction of $O_2$ to the superoxide ion ($O_2^{\bullet-}$).

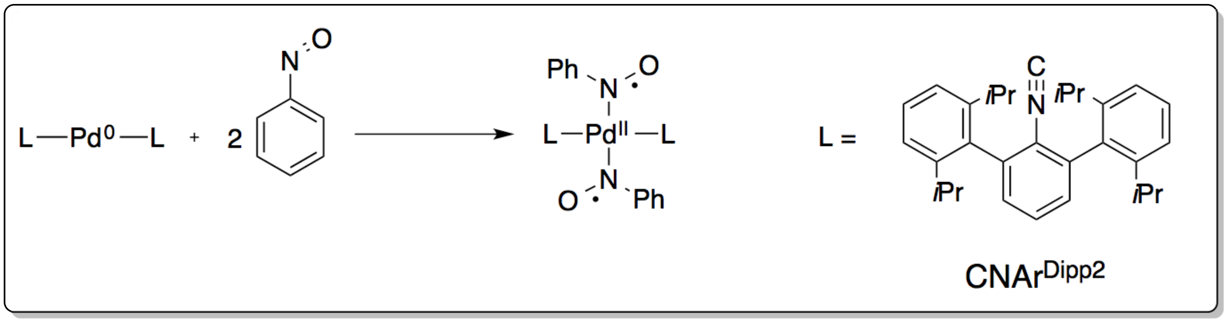

Scheme 1-23: One electron reduction of PhNO by Pd(0) complex.[83]

In mononuclear *κ*O complexes the NO bond length varies in the range of 1.057(10) – 1.33 Å.[75] The unusually short bond and the large variation is due to disordered X-ray structures frequently observed with O-bonded nitrosoarene complexes; thus, conclusive statements about the extent of back-donation and ArNO reduction cannot be made.[84-88] As will be discussed in chapter 4, the undisordered crystal structure of $[(Me_6tren)Cu(\kappa O\text{-}PhNO)]X$ (X = TfO, $SbF_6$, Scheme 1-24) shows significant NO bond elongation to 1.337(3) Å with $TfO^-$ and 1.320(4) Å with $SbF_6^-$ counter-ions. Magnetic moment measurement, vibrational studies on NO stretching frequency, and computational studies indicate that with the triflate (TfO) counterion nitrosobenzene is reduced by one electron from the copper centre giving formally copper(II) centres and nitrosobenzene radical anion (see chapter 4).[11]

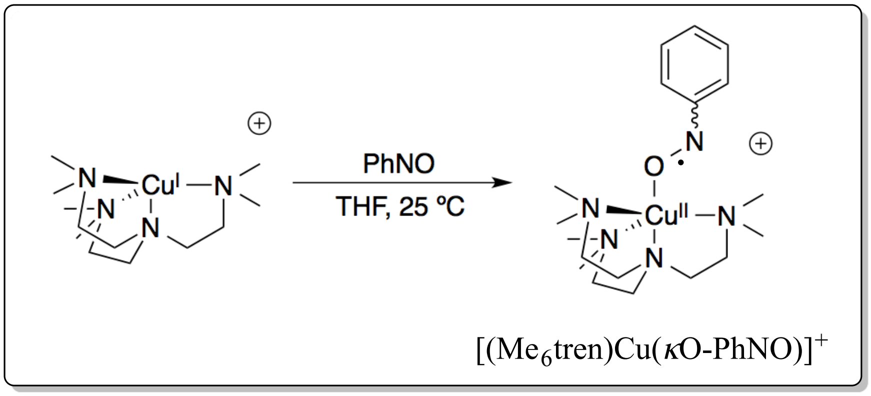

Scheme 1-24: Binding and reduction of PhNO by $[(Me_6tren)Cu]^+$ complex.

Monometallic complexes with side-on binding mode ($\eta^2$-NO) where both nitrogen and oxygen atoms coordinate to the metal centre are not frequently observed. Examples of such complexes with Mo,[89-91] W,[92] Ru,[93-94] and Pt[95] have been reported in the literature. The NO bond length in these complexes is in the range of 1.386(3) – 1.432(6) Å, significantly longer than in the free nitrosoarenes. More recently, Wieghardt reported the reaction of $Pd(CNAr^{Dipp2})_2$ with

TolNO.[96] The geometry of the resulting square planar complex where the nitrosarene binds in the side-on fashion, and the long NO bond length of 1.364(4) Å pointed to two electron reduction of the nitrosoarene by the Pd(0) centre forming the formally doubly deprotonated hydroxylamine and Pd(II). The two-electron reduction of nitrosoarene is similar to the reduction of $O_2$ to the peroxo ($O_2^{2-}$) by metal centres. Similarly, Warren *et al.* reported the β-diketiminate copper(I) complex that upon treatment with PhNO and then toluene gives the mononuclear [($Me_2$NN]Cu($\eta^2$-PhNO)] complex (Scheme 1-25).[97] The reported NO bond length of 1.336(6) Å is longer than in the free PhNO (1.261(4) and 1.268(4) Å) and the N-O vibrational stretch decreased to 1113 $cm^{-1}$ (1506 $cm^{-1}$ for PhNO). Dinuclear complexes with side-on binding of ArNO ($\mu$-$\eta^2$:$\eta^2$-NO) are even more rare and only few examples with Rh,[98] Zr,[99] Hf,[99] and Ni[97] are reported in the literature. The NO bond length in these complexes is in the range of 1.422(4) – 1.500(7) Å, markedly longer that NO double bonds. The NO stretching frequency in {[($Me_2$NN)Ni]$_2$($\mu$-$\eta^2$:$\eta^2$-PhNO)} (Scheme 1-25) is further shifted to 915 $cm^{-1}$, a clear indication of reduction in NO bond order.

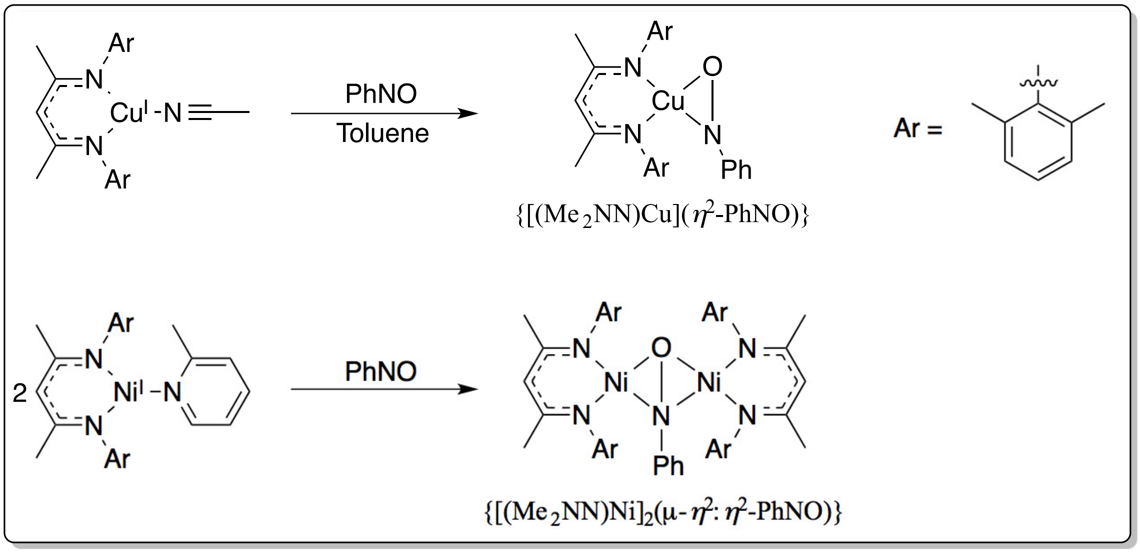

Scheme 1-25: Nitrosobenze adducts of β-dikitiminate copper(I) and nickel(I) complexex.[97]

The scarcity of $\mu$-$\eta^2$:$\eta^2$-NO complexes, in contrast to the abundance of $^{\mathbf{S}}\mathbf{P}$ complexes in Cu/$O_2$ adduct, is due to the lower oxidative power of nitrosoarenes in comparison to dioxygen. Thus, to enforce two-electron reduction of the NO bond in nitrosoarenes, either electron-rich metal complexes or electron-deficient nitrosoarenes must be used. The four-electron reduction of PhNO by the β-diketiminate Co(I) complex is the extreme case of PhNO activation using electron rich metal complexes.[100] Selective two-electron reduction of the electron-deficient *p*-$NO_2$-PhNO by a Cu(I) complex shown in Scheme 1-26 demonstrates the similarity between PhNO and $O_2$ activation by Cu(I) complexes. Detailed description of this complex and its reactivity is the subject of chapter 5.

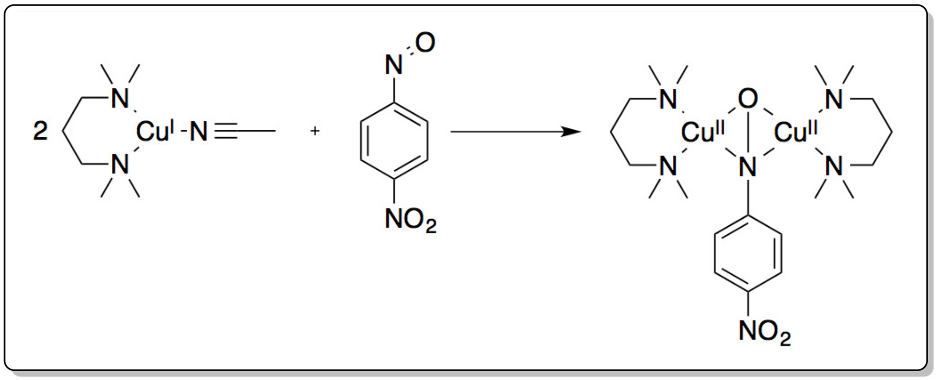

Scheme 1-26: Two-electron reduction of *p*-$NO_2$-PhNO with Cu(I) complex.

### 1.5.4. Reactivity of nitrosoarenes

Nitrosoarenes are of particular interest in organic synthesis as they are used to transfer nitrogen-containing functional groups to organic substrates; a transformation that is important in pharmaceuticals and materials industries. Examples of these reactions are shown in Scheme 1-27 and have been studied in the presence and absence of transition metals. Owing to the electrophilic nature of the nitrogen atom various nucleophiles such as enolates[101-103] and Grignard[104-105] reagents readily add to the -N=O functional group. In addition, nitrosarenes participate in percyclic reactions such as Diels-Alder[101-102] and nitroso-ene[106] reactions. All these reactions serve as a method for the inclusion of nitrogen, oxygen, or both functionalities into organic compounds.

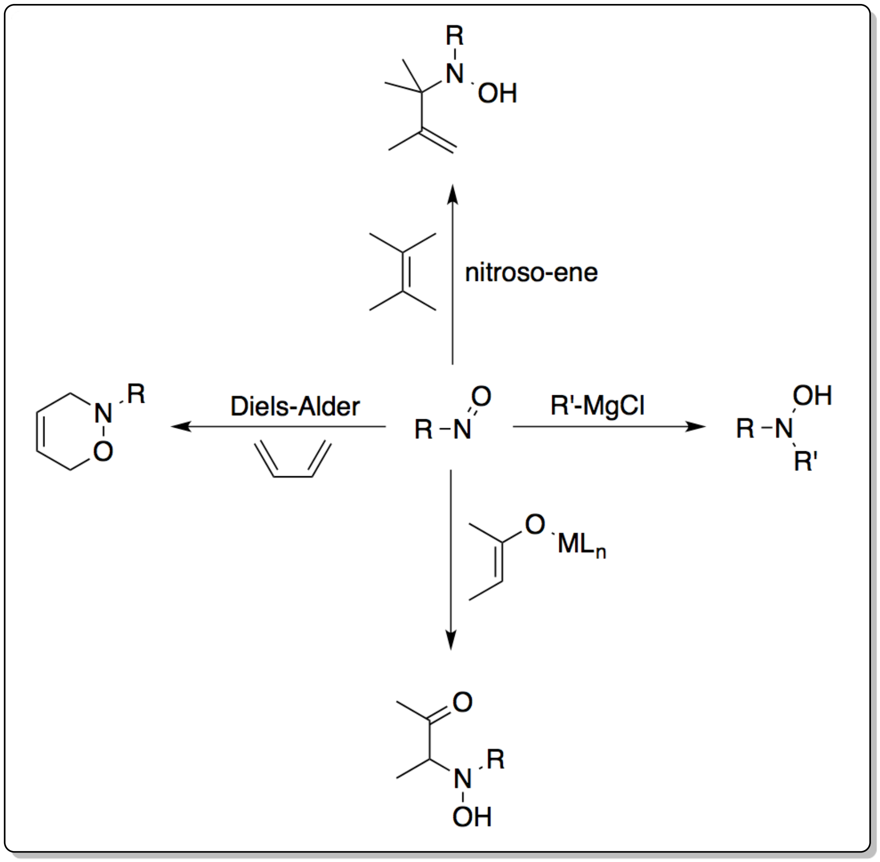

Scheme 1-27: Examples highlighting some reactions of nitroso compounds.[106]

The addition of enol ethers to nitrosoarenes and the hetero Diels-Alder reactions have been studied in detail and developed by Yamamoto.[101-102] As early as 1899, Ehrlich and Sachs reported the condensation of *para*-*N,N*-dimethylaminonitrosobenzene with phenylacetonitrile in the presence of base to give the imine (Scheme 1-28a).[107] Since then, methods have been developed for the functionalization of preformed or in situ generated enolates with nitrosoarene at the α-carbon. It was found that, depending on the structure of the enolate, solvent, catalyst and additive, the nucleophilic attack occurs on either the oxygen or the nitrogen atoms of the nitroso group allowing for either C-O or C-N bond formation (Scheme 1-28b).[101] The reactivity of nitrosoarenes with ketones is not limited to α-functionalization. More recently, nitrosoarenes were used for the synthesis of nitrones from ketones in good to excellent yields (Scheme 1-28c).[108] The nitroso Diels-Alder reaction provides a convenient route for the incorporation of both nitrogen and oxygen atoms in organic substrates however, it is of less synthetic importance with nitrosoarenes due to the difficulty of removing the aromatic group. In situ generated acylnitroso compounds and nitrosoalkanes have found more applications in the hetero Diels-Alder reactions.[101-102,109]

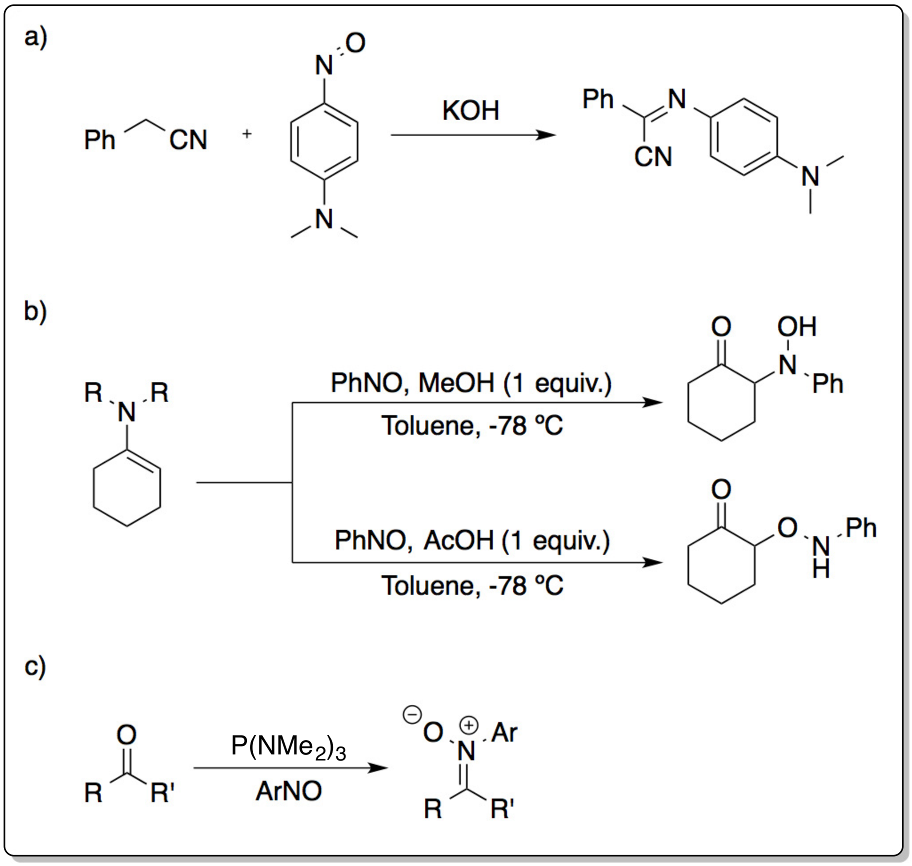

Scheme 1-28: Reaction of nitrosoarenes with enolates and ketones: a) the Ehrlich–Sachs reaction,[107] b) C-N vs. C-O bond formation between enamines and nitrosoarenes,[101] and c) Synthesis of nitrosnes from ketones and nitrosoarenes.[108]

Analogous to the ene reaction, substituted double bonds react with nitrosoarenes to give the ene product (Scheme 1-27).[106] The formation of various degradation products in the nitroso-ene reaction is one of the drawbacks of this reaction. Nitrosoarenes react cleanly with tetrasubstituted and trisubstituted alkenes, but with disubstituted and monosubstituted alkenes the ene product is not obtained and nitrosoarene decomposition prevails.[106] It has been observed that nitrosoarenes with electron-withdrawing substituents, such as 4-nitro-nitrosobenzene, significantly reduces the amount of side-products.[106] However, it severely limits the utility of this reaction in synthetic chemistry. The difficulty in removing the aromatic ring from arylamines limits the utility of nitrosoarenes in nitroso-ene reactions to cases where the aromatic ring is desired in the final product. A notable recent example is the intramolecular nitroso-ene reaction employed in the total synthesis of asmarines analogues (Scheme 1-29).[110] If the free amine is required acylnitroso compounds offer a better alternative as the product can be converted to the free amine through simple hydrolysis. Several mechanisms have been proposed for the nitroso-ene reaction, including concerted pericyclic pathway and step wise mechanism with the intermediacy of amine oxides or diradicals.[111] The metal-catalyzed nitroso-ene reaction involves the intermediacy of metal/nitrosoarene complexes and is further described in the next section.

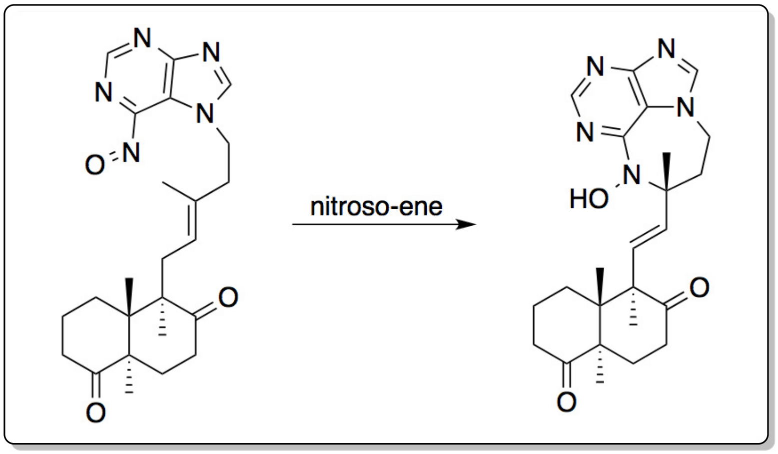

Scheme 1-29: An example of the utility of intramolecular nitroso-ene reaction in total synthesis.[110]

### 1.5.5. Reactivity of metal-nitrosoarene complexes

The coordinated nitrosoarene can undergo several reactions such as ligand displacement, reduction to the amine, oxygen-atom transfer, and nitrogen-group transfer. The most synthetically useful reaction is the nitrogen-group transfer and in metal-catalyzed variants, the intermediacy of metal/nitrosoarene complexes has been observed.[112-116] Of the reactions mentioned in section 1.5.4 the nitroso-aldol and the Diels-Alder reactions are usually performed without metal catalysts unless direct amination at α-carbon[117] or an enantioselective version is required.[101-102] The metal-catalyzed nitroso-ene reaction, however, has been studied in more detail. Typical catalysts for this reaction are molybdenum, iron, or copper complexes. Sharpless reported the stoichiometric amination of alkenes by a molybdenum arylnitroso complex to give the allylic amine[90] that was later developed by Srivatava into catalytic reaction employing phenylhydroxylamine (Ph-NHOH) as the nitrogen group source[112-113] and soon after, iron-[114] and copper[115-116]-catalyzed allylic amination reactions were reported.

The mechanism of the reaction is different from the metal-free variant and with the different metals used (Scheme 1-30). Based on control experiments, in the Mo-catalyzed reaction the active aminating species was found to be a side-on bound nitrosobenzene. When iron(II) was employed as the catalyst, the active species was found to be an iron(II) complex bonded to three nitrosobenze dimers. In this complex six nitrosoarenes bind to the iron centre through the oxygen atoms as three *cis*-dimers. Finally, in the copper-catalyzed reaction, the active aminating species was proposed to be $[(PhNO)_3Cu]^+$.

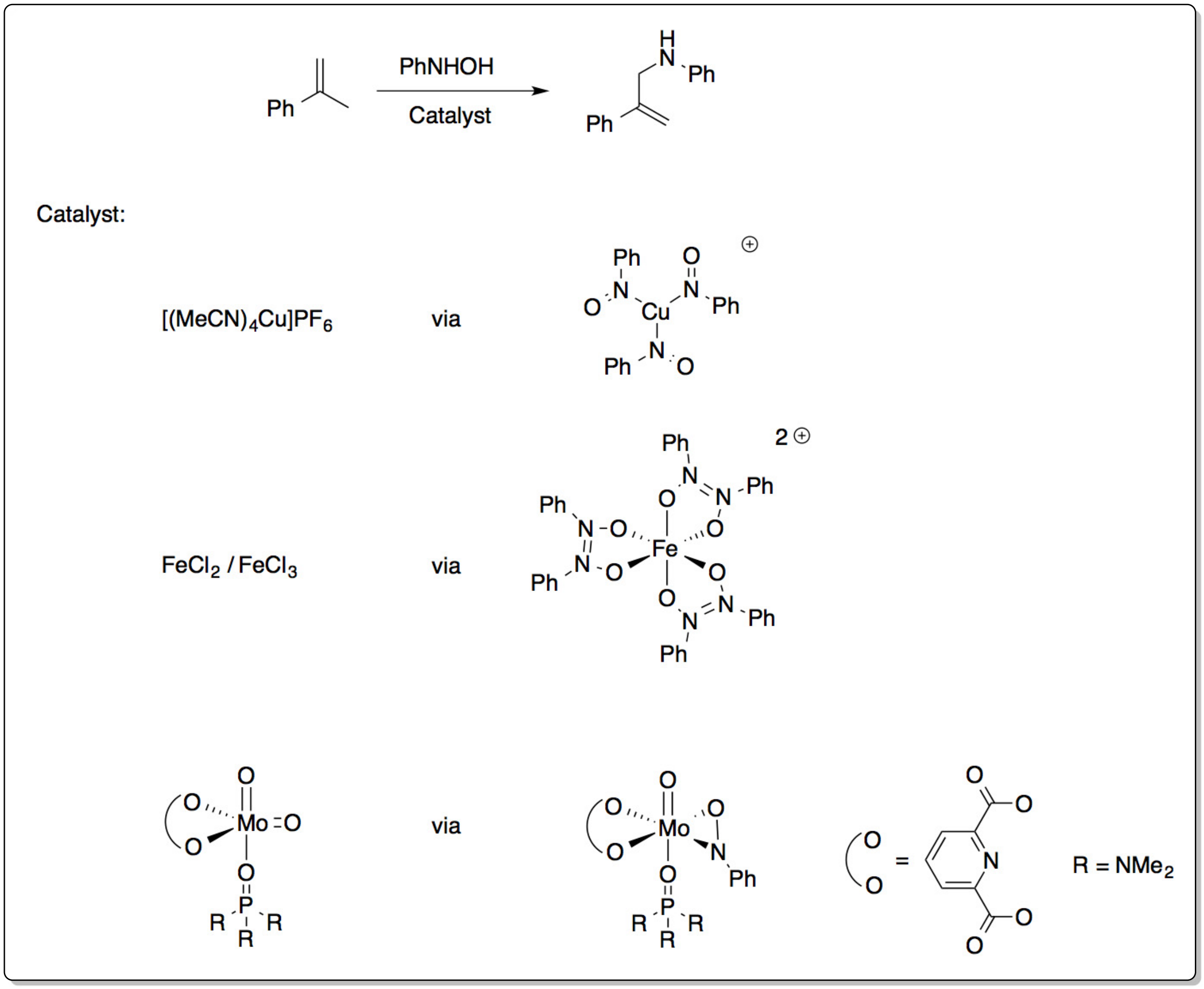

Scheme 1-30: Metal-catalyzed nitroso-ene reaction and the structure of the active catalyst.[112-116]

All the aforementioned reactions demonstrate the utility of nitrosoarene as a nitrogen-group source in the formation of C($sp^3$)-N bonds. C(aromatic)-N bond formation from nitrosoareneses has been less explored and requires pre-functionalization of the aromatic ring. An example of such reactions is the copper-mediated coupling of nitrosoarenes with arylboronic acids reported by Liebeskind.[118] It is speculated that a $\eta^2$-NO copper(III) intermediate performs the coupling reaction through a reductive elimination mechanism (Scheme 1-31).

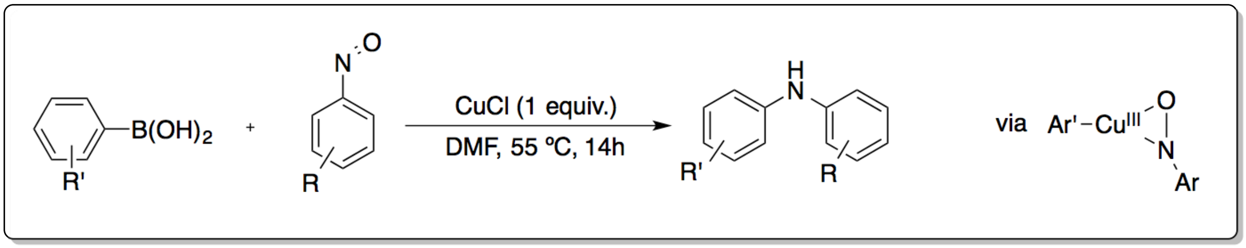

Scheme 1-31: Coupling of aromatic boronic acids with nitrosoarenes mediated by CuCl.[118]

Aromatic amination with a nitrosoarene without prefunctionalization is the subject of chapter 5 of this thesis. In conjunction with *ortho*-oxygenation of phenolates by Cu/$O_2$ species, the copper-mediated *ortho*-amination reaction is performed with a $\mu$-$\eta^2$:$\eta^2$-NO complex stoichiometrically, demonstrating the similarity in the reactivity of Cu/$O_2$ and Cu/nitrosoarene complexes.[12]

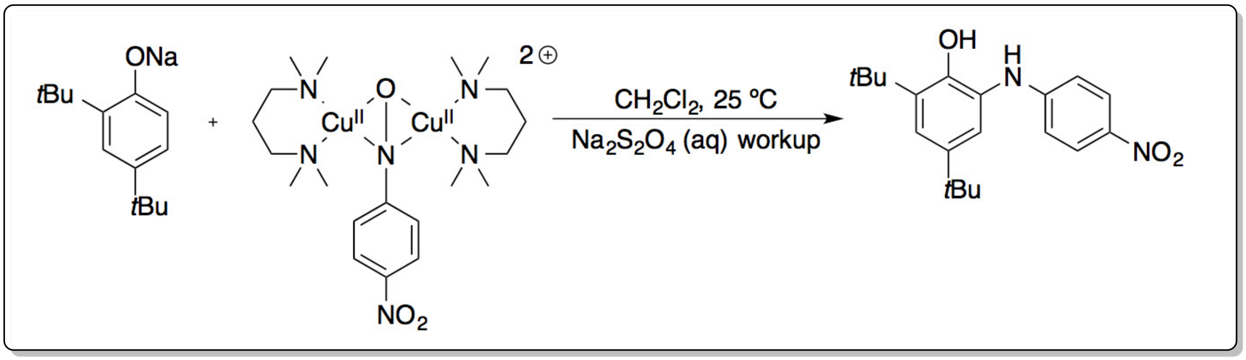

Scheme 1-32: Ortho-amination of phenolate by Cu(μ-$\eta^2$:$\eta^2$-ArNO) complex.

## 1.6. Thesis Organization

As seen above, Chapter 1 of this thesis provided an introduction to the Cu/$O_2$ and nitroso chemistry. The unifying theme of the two subjects is the inspiration from tyrosinase in the *ortho*-oxygenation of phenolic substrates. This chapter also provided a more detailed background than can be found in the subsequent manuscripts.

Chapter 2 describes the mechanistic study of the catalytic reaction reported by Lumb. The author performed all of the experimental work. At the time of thesis submission, the manuscript was submitted to *Inorganic Chemistry* for publication.

Chapter 3 presents an extension of the Lumb reaction by using air-stable copper(II)-precatalysts to perform the *ortho*-oxygenation of various phenols. The idea was developed based on observations made by the author during the mechanistic studies (chapter 1). The manuscript is published in *Dalton Transactions* (*Dalton Trans.* **2015**, *44*, 12094-12097). The author did the majority of the experimental work while two undergraduate students, Bryony McAllister and Andrew Proppe, and a Ph.D. student, Laura Andrea Rodríguez-Solano, assisted in performing some of the screening experiments.

Chapter 4 describes the synthesis and characterization of an copper-nitrosobenzene complex that is a structural and electronic mimic of end-on superoxocopper(II) ($^{\mathbf{E}}\mathbf{S}$) complexes. The work was published in *Chemical Communications* (*Chem. Commun.* **2011**, *47*, 8055-8057). An undergraduate student, Brigitte Girard, performed the initial crystallization of [($Me_6$tren)Cu(PhNO)](TfO) complex and the author performed the rest of the experimental and computational work presented in the paper.

Chapter 5 presents the first structural and electronic mimic of side-on peroxodicopper(II) ($^{\mathbf{S}}\mathbf{P}$) based on Cu/nitrosoarene chemistry. The ability of the complex to perform the *ortho*-amination of phenolates provides proof that the complex is also a reactive model. The author performed all the experimental work while our collaborator, Maylis Orio, performed the computational studies. The work is published in *Chemical Communication* (*Chem. Commun.* **2015**, *51*, 11206-11209).

Chapter 6 presents some concluding remarks encompassing the research presented in the previous sections and suggestions for future research work is provided in chapter 7.

# 2. Manuscript 1: A Biomimetic Mechanism for the Copper-Catalyzed Aerobic Oxygenation of 4-*tert*-Butylphenol

Mohammad S. Askari, Jean-Philip Lumb,* and Xavier Ottenwaelder*

The contents of this chapter is from the following article submitted to *Inorganic Chemistry*:

Mohammad S. Askari, Jean-Philip Lumb* and Xavier Ottenwaelder*, "A Biomimetic Mechanism for the Copper-Catalyzed Aerobic Oxygenation of 4-*tert*-Butylphenol". Manuscript ID: ic-2015-01297k

## 2.1. Abstract

Controlling product selectivity during the catalytic aerobic oxidation of phenols remains a significant challenge that hinders reaction development. This work provides a mechanistic picture of a copper (Cu)-catalyzed, aerobic functionalization of phenols that is selective for coupled *ortho*-quinones. The immediate product of *ortho*-oxygenation is a Cu(II)-semiquinone radical complex, which is the resting state of the Cu catalyst. A mechanistic study of the formation of this complex indicates that the oxygenation pathway mimics the dinuclear Cu enzyme tyrosinase by involving a dinuclear side-on peroxodicopper(II) oxidant, but unlike the enzyme, self-assembly of the oxidant has a significant influence on the overall rate of *ortho*-oxygenation. This is the first detailed mechanistic study of a catalytic phenol *ortho*-oxygenation reaction that does not involve an exogenous amine base. We provide details for all steps in the cycle and demonstrate that turnover is contingent upon proton-transfer events that are mediated by a slight excess of ligand. Finally, our knowledge of the reaction mechanism can be leveraged to diversify the reaction outcome. Thus, uncoupled *ortho*-quinones are favored in polar media, highlighting unusually high levels of chemoselectivity for a catalytic aerobic oxidation of a phenol.

## 2.2. Introduction

Selective aerobic oxidations are fundamentally important to the chemical industry due to the abundance of molecular oxygen ($O_2$) and the sustainable source of energy provided by its reduction.[1-2,119-121] Despite significant growth in this field, the application of aerobic oxidations to phenols, which are ubiquitous feedstock chemicals, remains underdeveloped due to issues of selectivity (Scheme 2-1a).[2,122-123] With few exceptions,[9,124-129] catalytic aerobic oxidations of phenols generate phenoxyl radicals, which undergo non-selective C−C dimerization or oxidation to the *para*-quinone, limiting their synthetic utility (Scheme 2-1a).[2,122-123] To avoid radical-based reactions, the overwhelming majority of phenolic oxidations used in synthesis employ stoichiometric amounts of a terminal oxidant other than $O_2$, but do so at the expense of atom- and step-efficiency.[13,15,130-132]

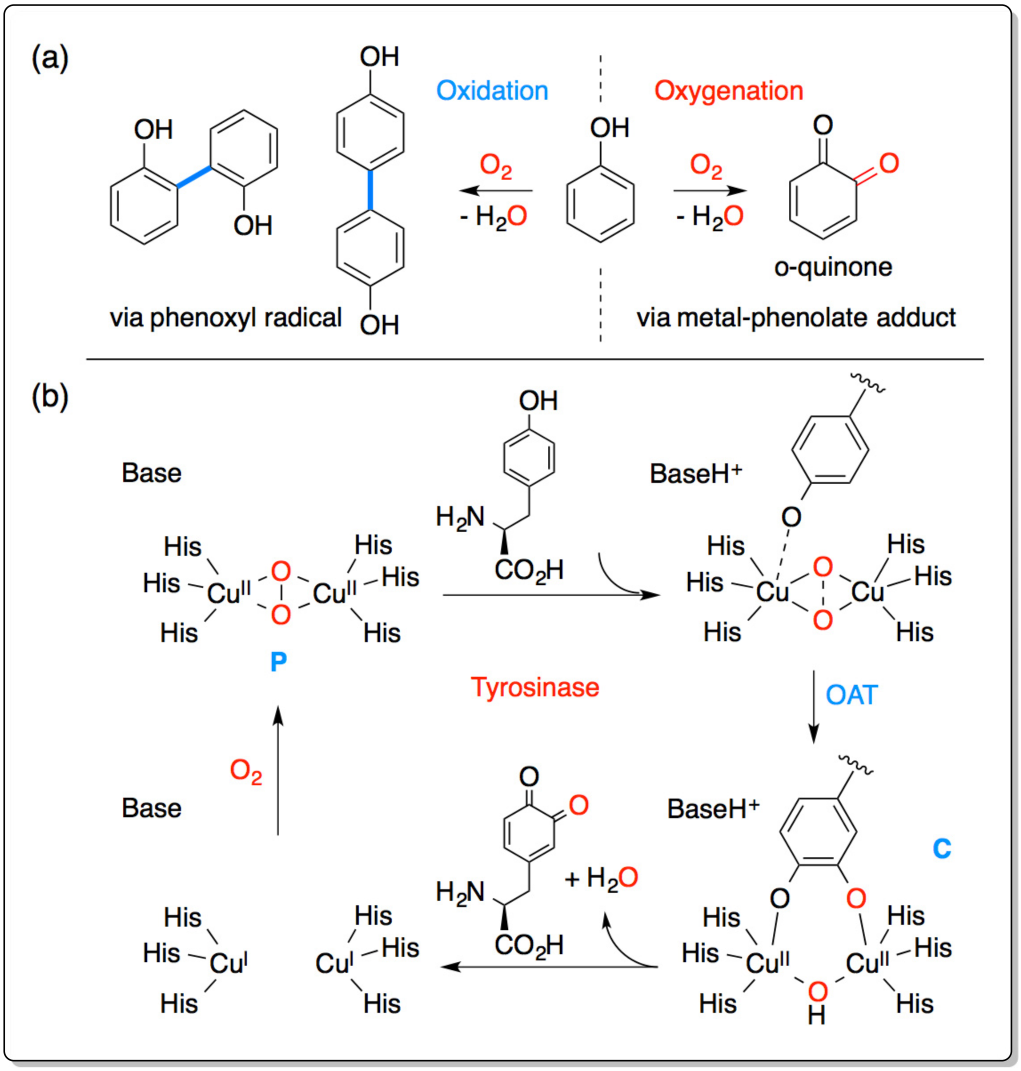

Scheme 2-1: (a) Selectivity issues upon oxidation/oxygenation of phenols (b) Simplified mechanism of the *o*-oxygenation of L-tyrosine by tyrosinase during melanogenesis, with the key $\mu$-$\eta^2$:$\eta^2$-peroxodicopper(II) (**P**) and $\mu$-catecholato-$\mu$-hydroxodicopper(II) (**C**) intermediates. The nature of the base in the active site is still debated.

A unique example of a selective catalytic aerobic oxygenation of phenols is mediated by the dinuclear Cu enzyme tyrosinase. This enzyme converts L-tyrosine into L-dopaquinone (Scheme 2-1b) in the first and rate-limiting step of the ubiquitous biosynthesis of melanin pigments.[6,27,133-134] Its fundamental importance for life and its unique reactivity have made tyrosinase the focal point of mechanistic investigations and bio-mimicry, which have provided considerable insight into factors that govern selectivity in the aerobic oxidation of phenols.[7,135] More generally, these studies have been fundamentally important in elucidating the speciation of

Cu(I) and $O_2$ in the presence of a vast array of amine ligands.[21,136] Of particular relevance to tyrosinase and melanogenesis are synthetic mimics of the enzyme's active site that recreate the characteristic $\mu$-$\eta^2$:$\eta^2$-peroxodicopper(II) oxidant (**P**, Scheme 1b). Upon stoichiometric exposure to sodium, lithium or tetrabutylammonium phenolate salts, these complexes achieve *ortho*-oxygenation, with the proposed catecholatodicopper(II) complex **C** as the reaction's end point. This leads to catechols or quinones after acidic work-up (Scheme 2-2).[56-57,66-67,69,137-148] If neutral phenols are used instead of phenolates, *ortho*-oxygenation is not observed, and products of C-C coupling reactions predominate,[10,149-153] except in one recent intramolecular case.[154] This has led to the generally accepted view that deprotonation of the phenol must precede the formation of a discrete Cu-phenolate complex, which ensures selective oxygen-atom transfer (OAT) via an inner-sphere mechanism (In this manuscript, we use the expression "*ortho*-oxygenation" for the bulk reaction and "OAT" for the specific mechanistic step where the oxygen atom is transferred to the substrate).[128,155] Likewise, deprotonation of the phenol substrate is believed to occur during the *ortho*-oxygenation by tyrosinase, where the suitable base is either a histidine residue or an activated water or hydroxide molecule near the enzyme's active site.[7-8,26,156]

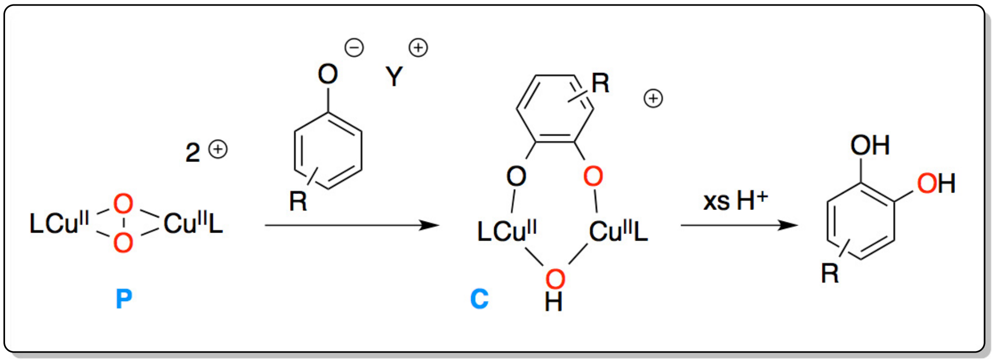

Scheme 2-2: Stoichiometric reaction of **P** species with phenolates.

The requirement of a phenolate in order to achieve selective OAT has impeded the development of conditions for *ortho*-oxygenation that are catalytic. In order to close a catalytic cycle, the hydroxide bridge of **C** must be protonated selectively (Scheme 2-1b), which is precluded in reactions employing a preformed phenolate. Characterization of the reactivity of **C** has received little attention, with the work of Tuczek,[67] Herres-Pawlis[69] and Mirica/Stack/Solomon[57] serving as important exceptions. The investigations of Mirica et al into the reactivity of the **P** species supported by the *N,N'*-di-*tert*-butylethylenediamine (DBED) ligand are particularly relevant to the current study (Scheme 2-3a).[54-57] Thus, the preformed DBED-supported **P** species reacts with 2.5 equivalents of 2,4-disubstituted phenolate salts at -120 ºC to afford bis(oxo)phenolatodicopper(III) species **A**, which converts to catecholate **C** via electrophilic aromatic substitution. Upon careful protonation at -80 ºC with 2.5 equiv of $H^+$ ($H_2SO_4$), this complex cleaves to a Cu(II)-semiquinone complex, **SQ**, whereas a 1:1 mixture of quinone and catechol is formed when a large excess of sulfuric acid is used (Scheme 2-3a). It is unclear whether the catechol/quinone mixture stems from disproportionation of the semiquinone or upon simultaneous protonation of both **C** and **SQ**.

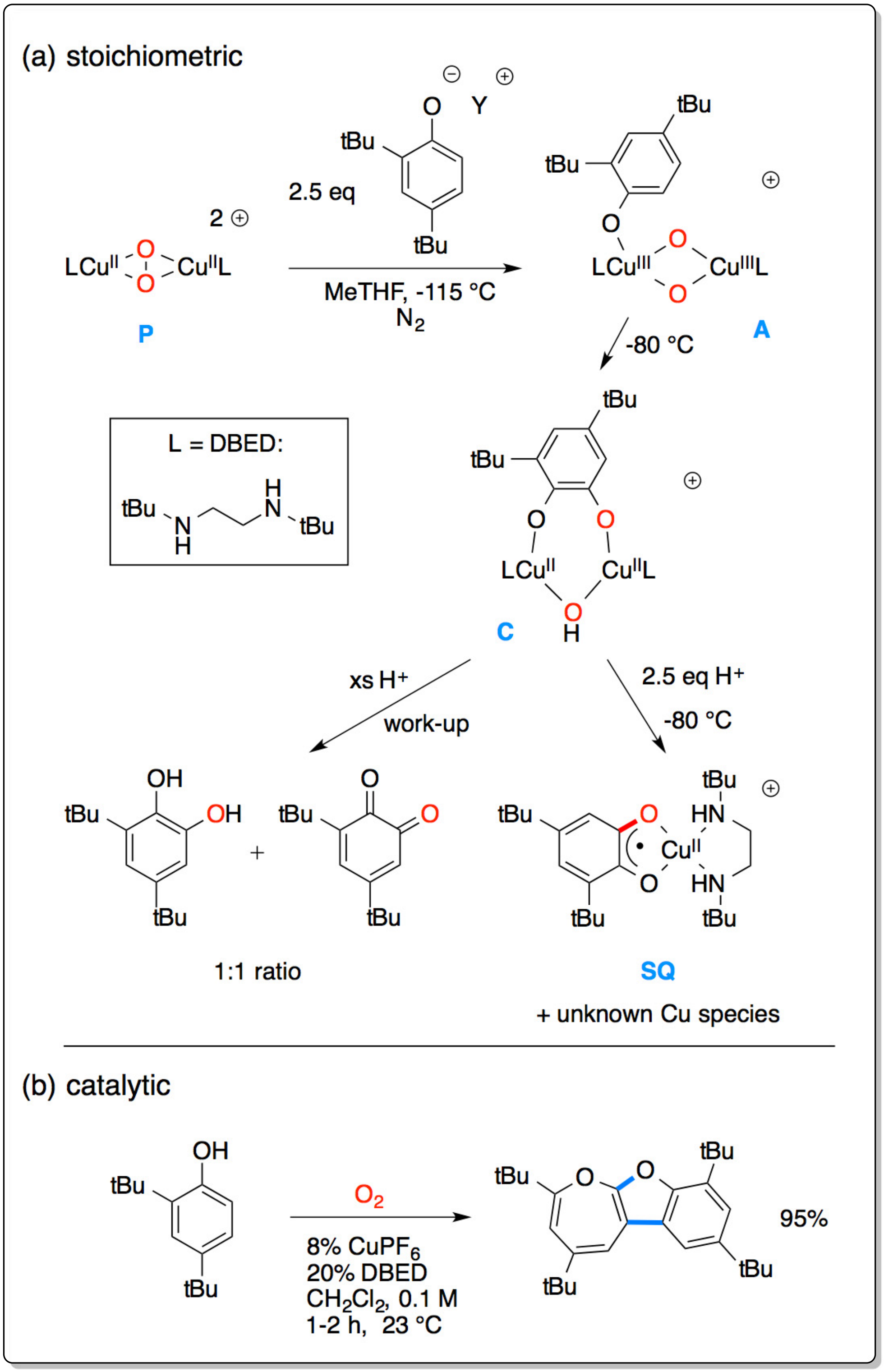

Scheme 2-3: Disconnect between (a) stochiometric and (b) catalytic oxidations of 2,4-di-*tert*-butylphenol(ate).

The recognition that **C** must be protonated in order to achieve turnover has prompted several groups to employ triethylamine ($Et_3N$, 2 equivalents per substrate) as a buffer for catalytic reactions starting from the phenol.[65-73] Deprotonation of the phenol in situ affords the necessary phenolate for oxygenation, along with the conjugate acid $Et_3NH^+$, which is thought to be suitably acidic to protonate **C**. Drawing mechanistic conclusions under these reaction conditions is complicated, however, because of a pronounced background oxygenation of the phenol with $Et_3N$, Cu and $O_2$ alone (i.e. catalytic oxygenation is observed in the absence of a biomimetic ligand).[9,128] Since these previous examples have not demonstrated that a **P** species can form in the presence of $Et_3N$ and a phenol, it is unclear to what extent independent characterization of **P**[69-71,139] relates to catalytic conditions in which **P** must self-assemble in the presence of all reaction components. Moreover, previous $Et_3N$-based catalytic systems produce more than one product or do not proceed to complete substrate conversion, indicating that competing pathways interfere with the mechanistic analysis. A recent report by Limberg presented another approach by using a catalytic amount of a phenolate base to initiate catalysis, but the system lacks selectivity for *ortho*-oxygenation and substrate scope is limited.[72] The one example of an *ortho*-oxygenation occurring in the absence of an exogenous base was reported recently by Tuczek, but so far this reaction is intramolecular and stoichiometric.[154]

In 2014, one of our groups reported a catalytic aerobic *ortho*-oxygenation of phenols that addresses many of these complications. It is catalytic in all components, uses a single amine to adjust the reaction pH and ligate Cu, and provides a single product at complete conversion. Thus, oxidation of 4-*tert*-butylphenol, **1**, in the presence of 4 mol% $[Cu(CH_3CN)_4](PF_6)$ ($CuPF_6$) and 5 mol% DBED affords coupled *ortho*-quinone **2** in isolated yields greater than 95% up to multi-gram scale (Scheme 2-4). This catalytic system provides a uniquely simple set of conditions for mechanistic investigations, wherein a single amine additive is used to mediate both $O_2$-activation and proton transfer. This catalytic system finds origin in the stoichiometric experiments of Mirica, Stack and Solomon (Scheme 2-3a), whose mechanistic investigations on the *ortho*-oxygenation of 2,4-di-*tert*-butylphenolate provide important spectroscopic signatures of the intermediates involved in $O_2$-activation and OAT when DBED is used as the ligand.[56-57] In spite of this precedent, the relevance of these intermediates to our catalytic conditions is unclear. For example, under our catalytic *ortho*-oxygenation conditions, 2,4-di-*tert*-butylphenol is oxidized to a benzoxepine along a radical-based pathway (Scheme 2-3b).[128] This radical-based oxidation was not observed by Mirica et al when they added 2,4-di-*tert*-butylphenolate salts to **P** at or below −80 °C, highlighting pronounced differences in the outcome of catalytic and stoichiometric reactions.

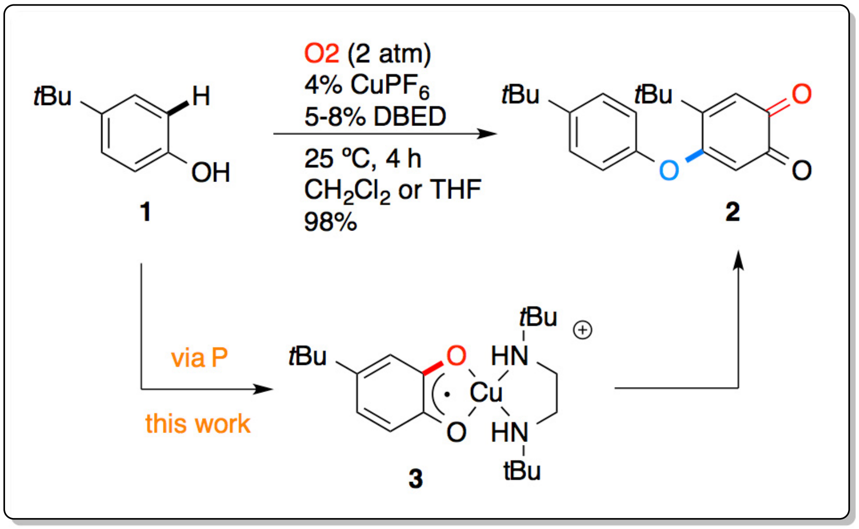

Scheme 2-4: This paper's study.

Herein, we bridge the gap between stoichiometric and catalytic conditions, and provide spectroscopic and kinetic support for a tyrosinase-like mechanism under conditions that are relevant to catalysis. In particular, we demonstrate that a **P** species is operative under turnover conditions at −80 °C and that selective protonation of **C** to a Cu(II)-semiquinone radical complex, **3**, is critical for selectivity and turnover. The existence of **3** creates an important distinction between our catalytic conditions and the chemistry of tyrosinase, which releases an uncoupled *ortho*-quinone from its active site following *ortho*-oxygenation. Using our mechanistic understanding, we can control the formation of **3** to divert the selectivity of the reaction towards uncoupled 4-*tert*-butyl-*ortho*-quinone **4**, representing a unique example of chemoselectivity among aerobic oxygenations of phenols.

## 2.3. Results and Discussion

### 2.3.1. Fast oxygenation to a Cu(II)-semiquinone

At the outset of our work, we monitored the conversion of **1** into **2** by in-situ UV-visible spectroscopy. Thus, introduction of $O_2$ into a $CH_2Cl_2$ mixture composed of **1**, 4% $CuPF_6$ and 8% DBED at 25 °C[9] results in the rapid formation of the purple DBED-$Cu^{II}$-semiquinone radical complex **3** ($\lambda_{max}$ = 545 nm) along with the product *ortho*-quinone **2** ($\lambda_{max}$ = 413 nm) (Figure 2-1). The structure of **3** was confirmed by an independent synthesis,[157] mass spectrometry and X-ray crystallography (Figure S 1-1 to Figure S 1-4, Supporting Information). Complex **3** remains at a near-steady-state concentration (>95% of the total [Cu]) as long as the reaction turns over to form **2** (Figure 2-1, inset).

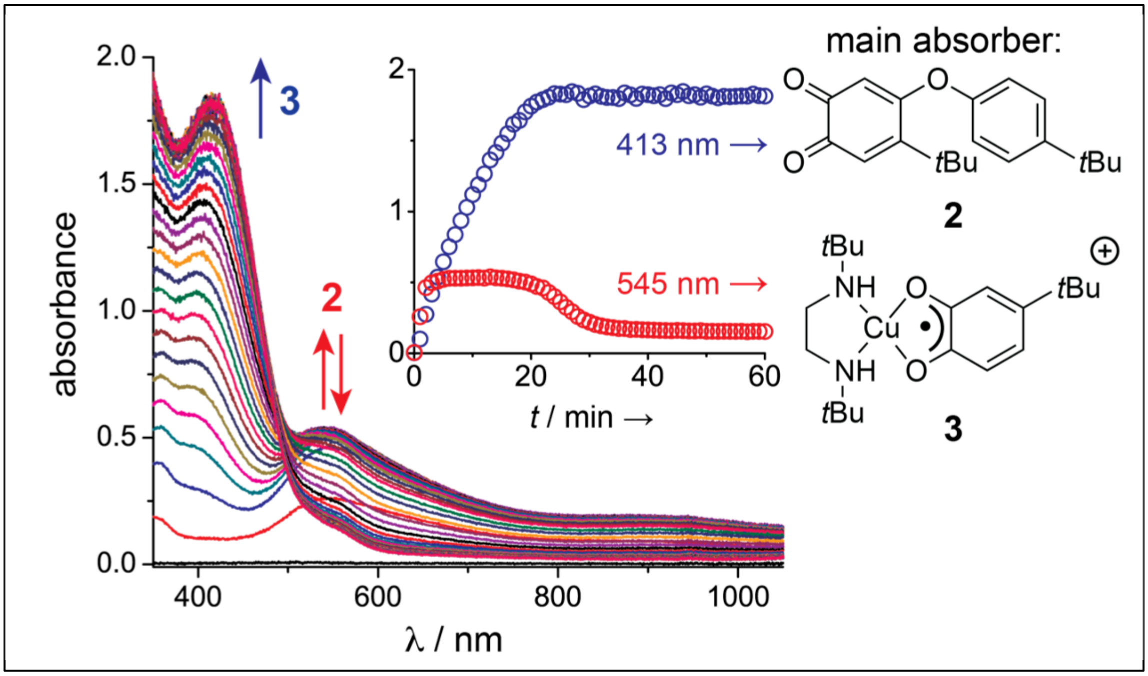

Figure 2-1: In-situ UV-vis spectroscopic monitoring under catalytic conditions: $CH_2Cl_2$, 25 °C, 30.7 mM **1**, 4% $CuPF_6$, 8% DBED, 1.0 mm pathlength. Inset: **3** (545 nm) remains an intermediate as long as **2** (413 nm) is being formed.

Time profiling of all species in solution during turnover reveals that the formation of complex **3** is the fastest observable process at room temperature (Figure 2-2). A small amount of uncoupled *ortho*-quinone **4** is observed along with **3** and remains at a concentration of ~9% of $[\mathbf{1}]_0$ throughout turnover (Figure 2-2) – **4** is not always obtained in bulk reactions that are carried out at higher concentrations than in these UV-vis experiments.[9,129] As the concentration of **2** increases, its corresponding Cu(II)-semiquinone complex **5** is observed. Quinones **2** and **4** are in equilibrium with their Cu(II)-semiquinone complexes, **3** and **5** respectively, with stronger binding observed between DBED-Cu(I) and the more electron-deficient quinone **4** (Scheme 2-5, Figure S 1-5 and Figure S 1-6). Complex **3** is the predominant Cu species until the concentration of **2** approaches 50%, at which point the concentration of complex **5** grows. Subsequent decay of **5** (and **3**) is consistent with its dissociation and subsequent oxidation of DBED-Cu(I) to the spectrally innocuous bis($\mu$-hydroxo)dicopper(II) complex,[158] which does not re-coordinate the quinones. We have previously demonstrated that this Cu(II)-hydroxide dimer can re-enter the catalytic cycle, such that its formation does not preclude catalysis.[129]

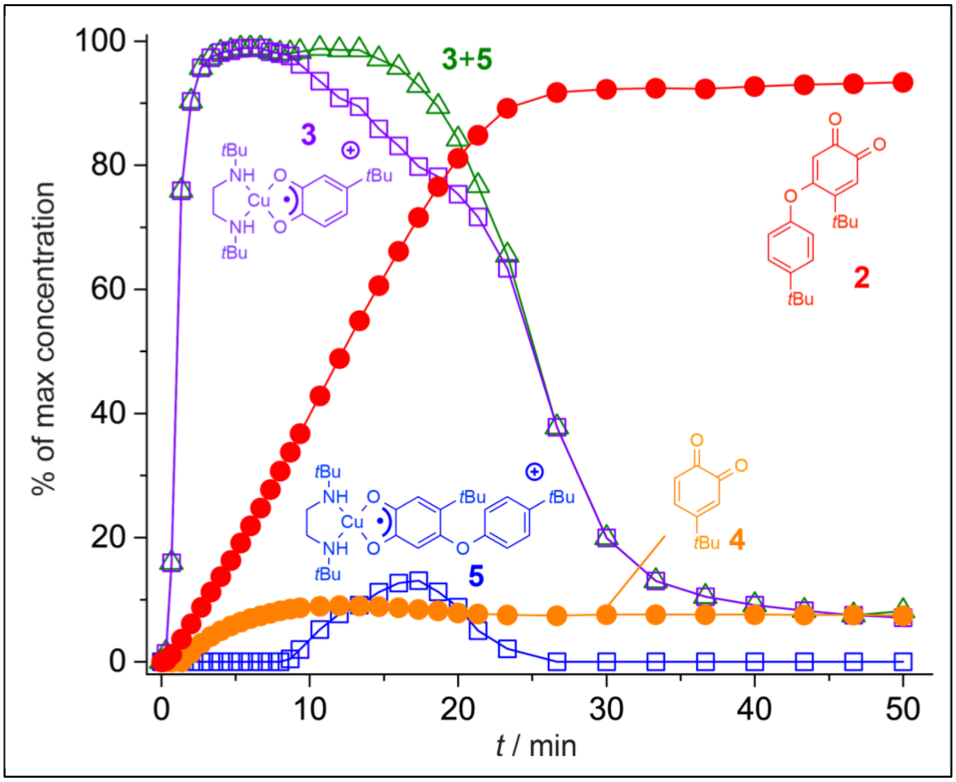

Figure 2-2: Concentrations of absorbing species during the reaction of Figure 2-1, deduced by fitting UV-vis spectra at various time points (e.g. Figure S 1-3). The y-axis is scaled to the maximum concentration of each species., i.e. $[\mathbf{3}]_{max}$ = $[\mathbf{5}]_{max}$ = $[CuPF_6]_0$, $[\mathbf{4}]_{max}$ = $[\mathbf{1}]_0$ and $[\mathbf{2}]_{max}$ = 0.5 $[\mathbf{1}]_0$. Thus each point in the graph gives the yield of each species.

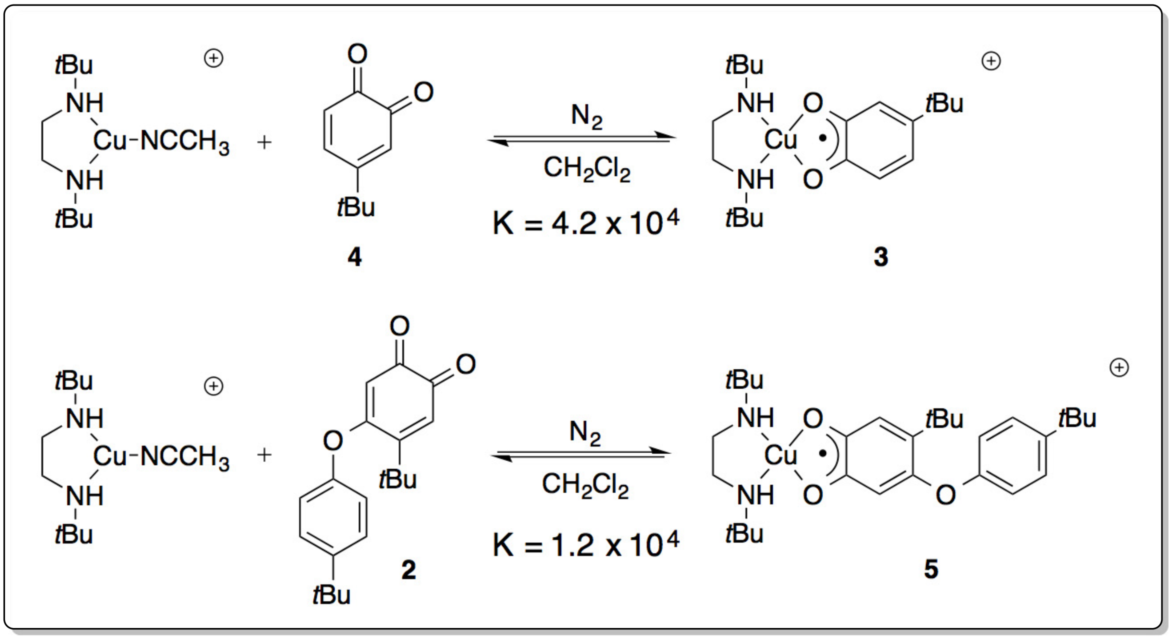

Scheme 2-5: DBEDCu(I)-quinone binding constants. The Cu(I) complex was prepared by mixing DBED and $[(MeCN)_4Cu]PF_6$ in a 1:1 ratio. Thus a total of 4 eq. $CH_3CN$ is present in solution.

The conversion of **3** into **2** is the rate-limiting sequence of the reaction at 25 °C and it does not proceed at −78 °C. When the reaction is run at −78 °C, **3** is the only visible species and it forms quantitatively with respect to the starting amount of Cu. Upon warming to 25 °C, turnover proceeds and **2** forms in 96% NMR yield, indicating that **3** is a competent intermediate. Complex **3** is also a suitable pre-catalyst to the reaction, as evidenced by the complete conversion of **1** to **2** when 5 mol% of **3** is used as the only source of Cu, along with an additional 5 mol% of DBED.

### 2.3.2. Low-temperature kinetic measurements

The selective formation of Cu(II)-semiquinone **3** from phenol **1** at low temperatures provides an opportunity to study the mechanism of *ortho*-oxygenation in the absence of the oxidative coupling (refer to Scheme 2-6 for the proposed mechanism). Thus, the formation of **3** was analyzed using stopped-flow kinetic experiments at −80 °C. The initial rate of the reaction shows a dependence on $[CuPF_6]$ (Figure 2-3 and Figure S 1-10) that is consistent with two-step formation of a dinuclear species, as expressed in eqns. 1-2.[159] This provides the first kinetic support for a dinuclear mechanism of $O_2$ activation under biomimetic *ortho*-oxygenation conditions.

$$\mathrm{DBEDCu^{+} + O_2 = DBEDCuO_2^{+}} \quad (1)$$

$$\mathrm{DBEDCuO_2^{+} + DBEDCu^{+} = DBED_2Cu_2O_2^{2+}} \quad (2)$$

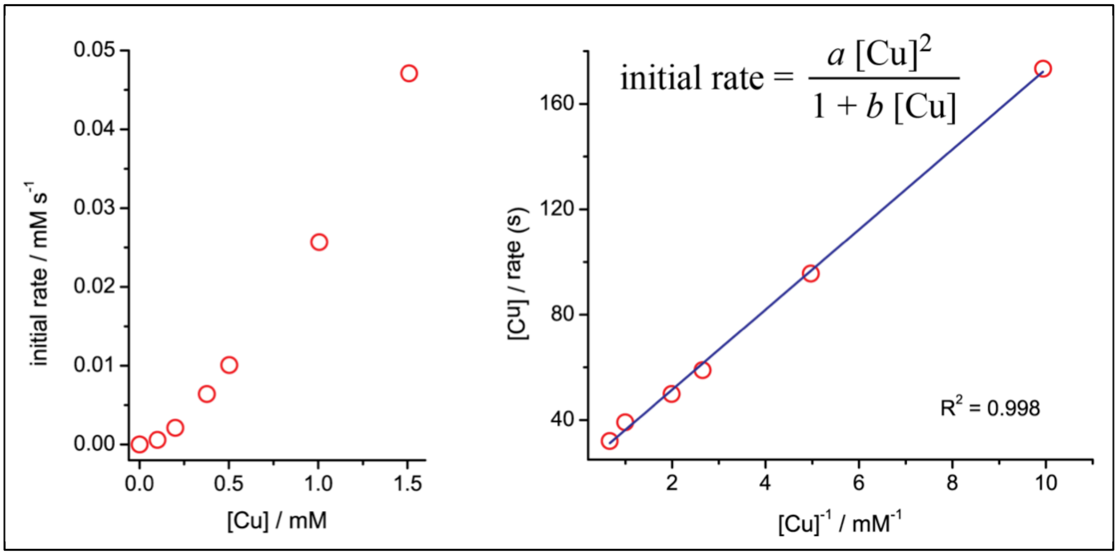

Figure 2-3: Dependence of the initial rate of formation of **3** on [$\mathrm{CuPF_6}$] = 0.1-1.5 mM, [**1**] = 2.5 mM, [DBED]/[$\mathrm{CuPF_6}$] = 1.1 in $\mathrm{CH_2Cl_2}$ at −80 °C.

The formation of a dinuclear complex ($\mathrm{O_2}$-activation) has more influence on the rate than substrate binding or the OAT. With a [DBED]/[$\mathrm{CuPF_6}$] ratio maintained at 1.1, no significant changes in the initial rate were observed upon varying [**1**] (Figure S 1-11), suggesting a zeroth order in [**1**]. This result is consistent with the absence of a kinetic isotope effect (KIE) when isotopically labeled 4-*tert*-butyl-2-deuterophenol ($\mathbf{1^{HD}}$) or 4-*tert*-butyl-2,6-dideuterophenol ($\mathbf{1^{DD}}$) is used instead of **1** (Figure S 1-12). These results create an important distinction with Mirica's stoichiometric experiments using a preformed **P** species, and suggest that the rate of self-assembly of a dinuclear Cu oxidant is rate-determining under catalytically relevant conditions at −78 °C. There is, however, an intramolecular KIE of 0.87(3) for the oxygenation of $\mathbf{1^{HD}}$ (Table S 1-2), which is consistent with previously reported values using tyrosinase[160-161] or synthetic[56-57] mimics.[6] Some tyrosinase enzymes[162-163] or synthetic models[138] do not exhibit a KIE, while the model system by Herres-Pawlis et al. surprisingly exhibits a non-inverse KIE of 1.2(2).[69] The one example of aromatic hydroxylation in a constrained **P** does not exhibit a KIE.[164]

### 2.3.3. Intermediates in the oxygenation

The second-order dependence in Cu supports a dinuclear mechanism for $O_2$-activation that is consistent with the mechanism of tyrosinase and previous work by Mirica, Stack and Solomon with the DBED ligand (Scheme 2-3a).[56-57] To gain insight into the structures of the key dinuclear intermediates, we monitored the oxygenation of a solution composed of **1**, 4% $CuPF_6$ and 5% DBED at −115 °C in 2-methyltetrahydrofuran (MeTHF). This generates a solution with an intense feature at 353 nm, possessing a small shoulder at 418 nm (Figure 2-4 i → ii, Figure S 1-7).[21] The same spectral features are observed upon the oxygenation of a 1:1 mixture of $CuPF_6$ and DBED in the absence of phenol (Figure S 1-8), indicating the formation of a ~5:1 mixture of rapidly interconverting[21] **P** and **O** species. Experiments conducted at −115 °C require MeTHF, creating an important difference with our experiments conducted in $CH_2Cl_2$ at −78 °C. The extent to which this solvent switch changes the details of *ortho*-oxygenation remains unclear, but we attribute our ability to visualize **P** at −115 °C to a decreased rate of OAT in a more coordinating and viscous solvent. Within minutes, the reaction, which contains phenol and a small excess of DBED per Cu, evolves to a 1:4 mixture of **3** and a species we tentatively assign as a catecholatohydroxodicopper(II) complex, **C** ($\lambda_{max}$ = 800 nm, Figure 2-4 iii, Figure S 1-9).[57] The assignment of **C** is supported by its independent synthesis from preformed **P** and 2.5 equivalents of 4-*tert*-butylphenolate.[57] The UV-visible spectrum of the obtained species is comparable to that reported by Mirica et al. with 2,4-di-*tert*-butylphenolate (Figure 2-5 iii, Figure S 1-9), and so is its reactivity (release of **3** upon addition of 2.5 equivalents of $H^+$ from $H_2SO_4$).[56-57] The flatness of the UV-visible spectrum of **C** prevented characterization by resonance Raman spectroscopy, as was the case in all other reports of similar species.[56-57,67,69,137-142]

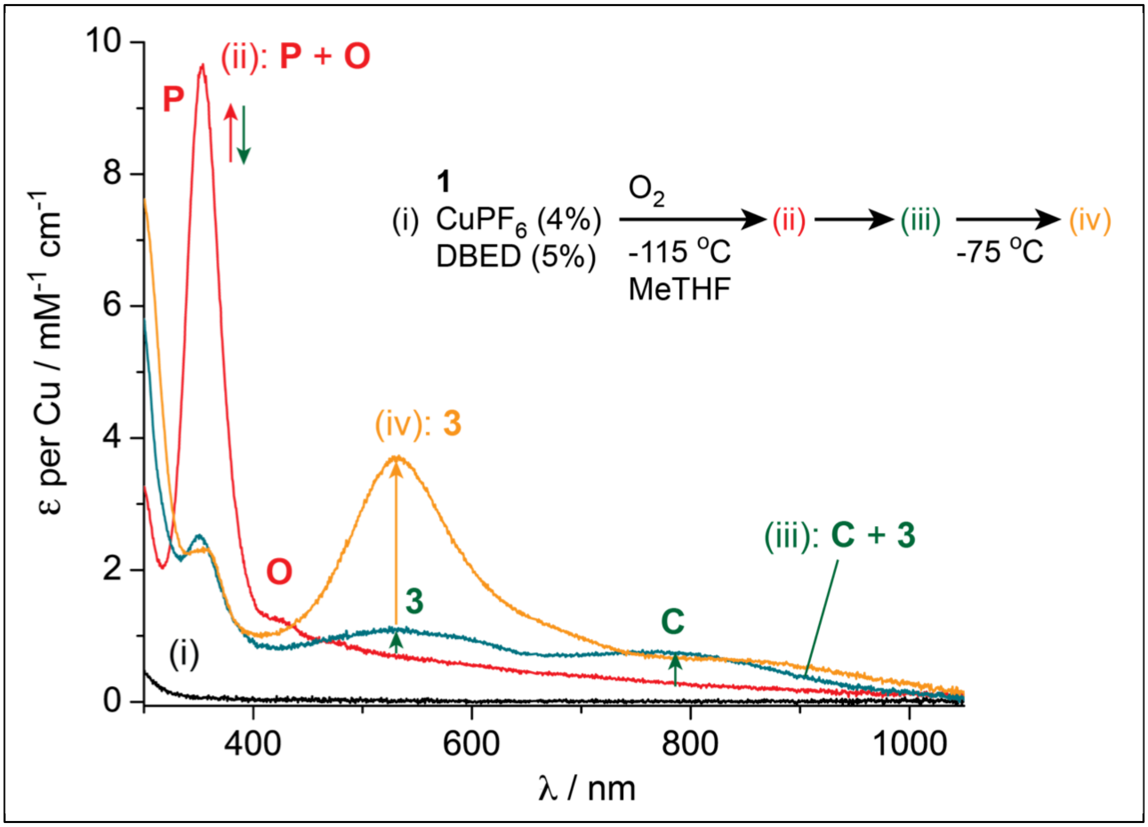

Figure 2-4: Intermediates in the oxygenation of **1** to **3**. Oxygenation at −115 °C of a MeTHF solution containing **1** (24.85 mM), 4% CuPF$_6$ and 5% DBED. (i, black): Solution before introducing O$_2$. (ii, red): Spectrum after oxygenating for 3 min, indicating the presence of **P** and **O**. (iii, green): Spectrum after 91 min under O$_2$, indicating a ~4:1 mixture of **C** (800 nm) and **3** (545 and 900 nm). (iv, orange): warming up to −78 °C under O$_2$ shows the conversion of **C** to >90% **3**.

Upon subsequent warming to −78 °C, the reaction mixture affords **3** in >90% with respect to the starting amount of CuPF$_6$ (Figure 2-4 iv). This percentage proves that the spectroscopically silent Cu species that forms upon cleavage of dinuclear **C** to mononuclear **3** can re-enter the oxygenation cycle to form additional **3** (details below). Since the dissociation of **C** occurs rapidly at −78 °C, **3** forms quantitatively relative to the total Cu concentration.

The **P**, **C** and **3** intermediates are analogous to those observed under Mirica's stoichiometric experiments, but the absence of a visible intermediate in-between **P** and **C** is an important distinction.[57] Whereas Mirica et al. observed a transient bis(oxo)phenolato complex **A** upon addition of 2,4-di-*tert*-butylphenolate to **P** at −115 °C (Scheme 2-3a),[57] we do not observe an **A** species under our catalytically relevant conditions (Figure 2-4 i → iii). An **A** species is also absent when the oxygenation of **1** is performed using its sodium phenolate under identical conditions to those reported by Mirica (Figure 2-5 ii → iii). We attribute this difference to a much faster OAT when the starting phenol lacks a 2-*tert*-butyl substituent.

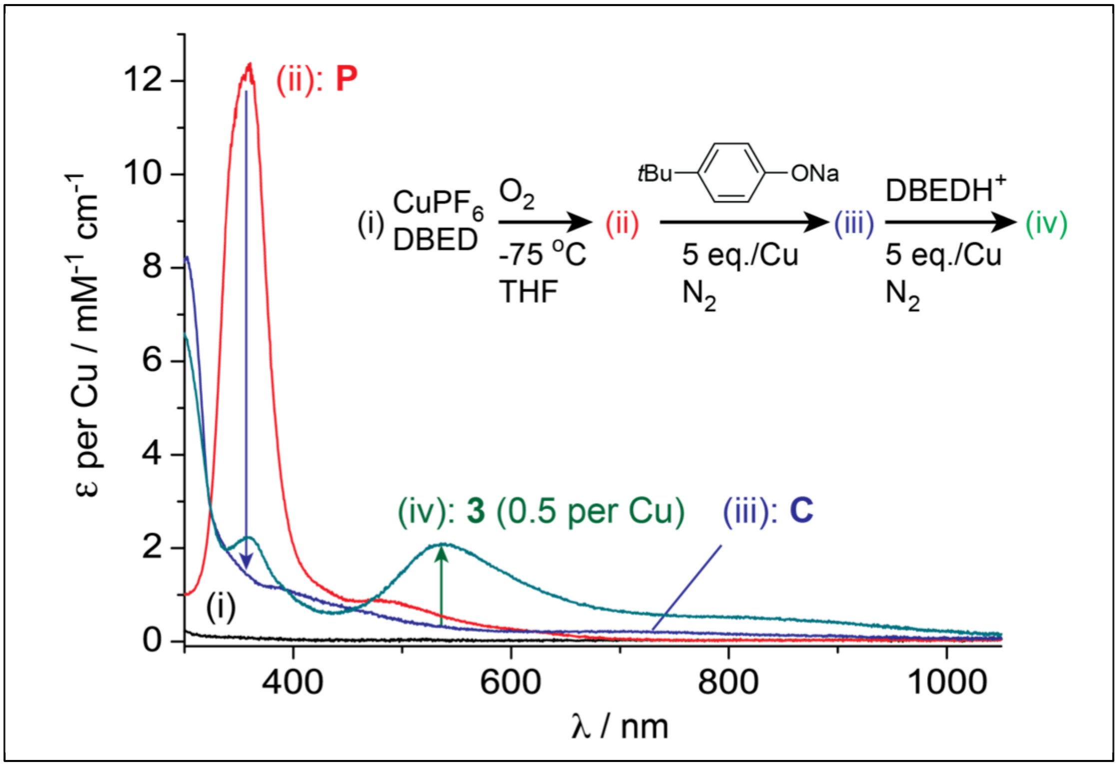

Figure 2-5: Closing the catalytic cycle: cleavage of **C**. **P** is formed by oxygenating a 1:1 solution of DBED:CuPF$_6$ in THF at −78 °C (i → ii). Addition 2.51 equivalents of sodium 4-*tert*-butylphenolate (per **P**) under N$_2$ leads to the formation of **C** (iii). Addition of 2.54 equivalents of DBEDH(PF$_6$) forms 1 equivalent of **3** with respect to **P** (iv). More details are provided in appendix 1 section 1.2.3.

### 2.3.4. Protonation of C and catalyst regeneration

The key step that enables catalyst turnover is the cleavage of **C** to **3** by redox tautomerization of the catecholate and the two Cu(II) centers of the dinuclear complex. Since this process is triggered by protonation of the hydroxide bridge (Scheme 2-3),[57] stoichiometric oxidations using phenolate salts cannot close the catalytic cycle of *ortho*-oxygenation. Under catalytic conditions, deprotonation of neutral phenol **1** by uncoordinated DBED (DBED is in excess of Cu) affords the mild acid DBEDH$^+$. DBEDH$^+$ is a suitably strong acid to protonate **C** and release **3** along with a colorless Cu(I) species that is capable of reentering the *ortho*-oxygenation cycle. We demonstrate this explicitly by the synthesis of **C** from **P** and the sodium phenolate of **1** at −78 °C (Figure 2-5 iii). Subsequent addition of DBEDH(PF$_6$) (prepared separately) affords one equivalent of mononuclear **3** per dinuclear **C** (Figure 2-5 iv), along with a Cu-containing species, **X**, which is spectroscopically silent. Species **X** can reenter the oxygenation cycle, as demonstrated in Figure 2-6. Thus, the reaction of **1** (2 equiv) with preformed **P** (1 equiv) under $N_2$ at −85 °C in the presence of a catalytic quantity of DBED (20% per Cu) rapidly forms one equivalent of **3** from every starting **P** (Figure 2-6 ii). If $O_2$ is introduced at this point, all remaining Cu present in solution is rapidly converted into **3** (Figure 2-6 iii), confirming that **X** is suitable for additional turnover to **3.** The demonstration that **X** promotes additional conversion of **1** into **3** closes the cycle of *ortho*-oxygenation and provides an explicit demonstration that the cleavage of **C** releases a catalytically competent Cu-species.[67]

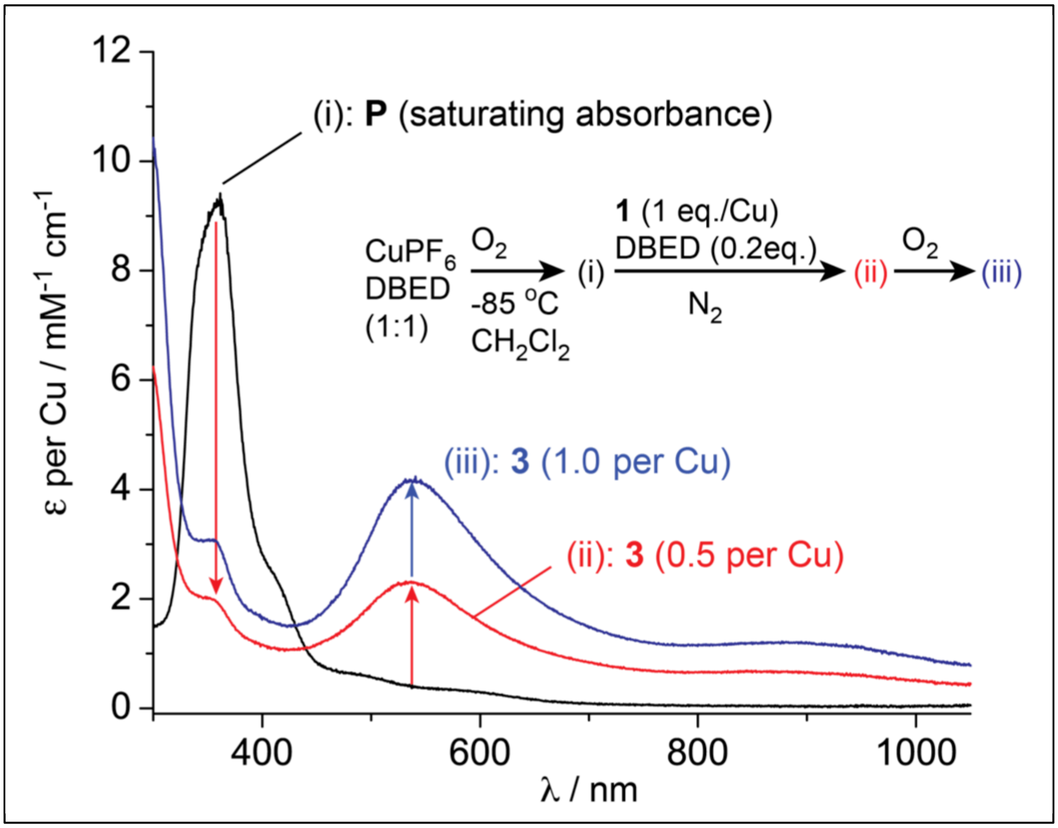

Figure 2-6: Closing the catalytic cycle: fate of the released Cu. (i) **P** species −85 °C in $CH_2Cl_2$ under $N_2$. (ii) Addition of **1** and a catalytic amount of DBED rapidly forms **3** (56% of the total [Cu]). (iii) After $O_2$ is reintroduced, **3** grows to 100% of the total [Cu]. More details are provided in appendix 1 section 1.2.3.

### 2.3.5. Mechanistic proposal

The visualization of **P** in the presence of a large excess of phenol under conditions that retain selectivity for *ortho*-oxygenation is noteworthy since **P** species are known to react with phenols via radical-based pathways.[10,149-153] In the absence of a small excess of DBED with respect to $CuPF_6$, preformed **P** does not react with **1** at −80°C, and **1** is recovered after work-up, as is the case with 2,4-di-*tert*-butylphenol.[54-55] This strongly suggests that the *ortho*-oxygenation must proceed through the phenolate and underscores the importance of a slight excess of DBED per Cu for turnover. Consistent with the second-order dependence of the rate on $[CuPF_6]$,[159] our mechanistic proposal at −80°C (Scheme 2-6) begins by assembling **P** from DBED-Cu(I) and $O_2$ (step 1), which then reacts with the in-situ-generated phenolate to make **C** (steps 2 and 3). Protonation of dicopper species **C** by $DBEDH^+$ releases **3** and Cu(I) complex **X**, which re-enters the oxygenation cycle (step 4). At −78 °C, complex **3** is kinetically inert, and requires higher temperatures before coupling with **1** affords **2**. Upon formation of the more electron-rich quinone **2**, DBED-Cu(I) is more easily released from the intermediate semiquinone **5** and can either re-enter the catalytic cycle or oxidize to the bis($\mu$-hydroxo)dicopper(II) species.

The absence of KIE between **1** and $\mathbf{1^{DD}}$ and the zeroth order dependence on [**1**] indicate that the OAT step is not rate-limiting at −80 °C. Instead, the rate of *ortho*-oxygenation is dependent on the formation of **P**, which requires the self-assembly of $O_2$ and two molecules of DBEDCu(I). This is distinct from the oxygenation of phenols catalyzed by tyrosinase, which rapidly forms **P** due to the colocalization of the two Cu(I) centers. The inverse intramolecular isotopic effect observed with $\mathbf{1^{HD}}$ (0.87) is consistent with an electrophilic aromatic substitution being a product-determining step. Whether OAT proceeds via a discrete Cu-phenolate species like **A** or by direct attack of the electron-rich aromatic ring onto the oxygen atom of **P** remains unclear, but efforts are underway to distinguish between these two possibilities.

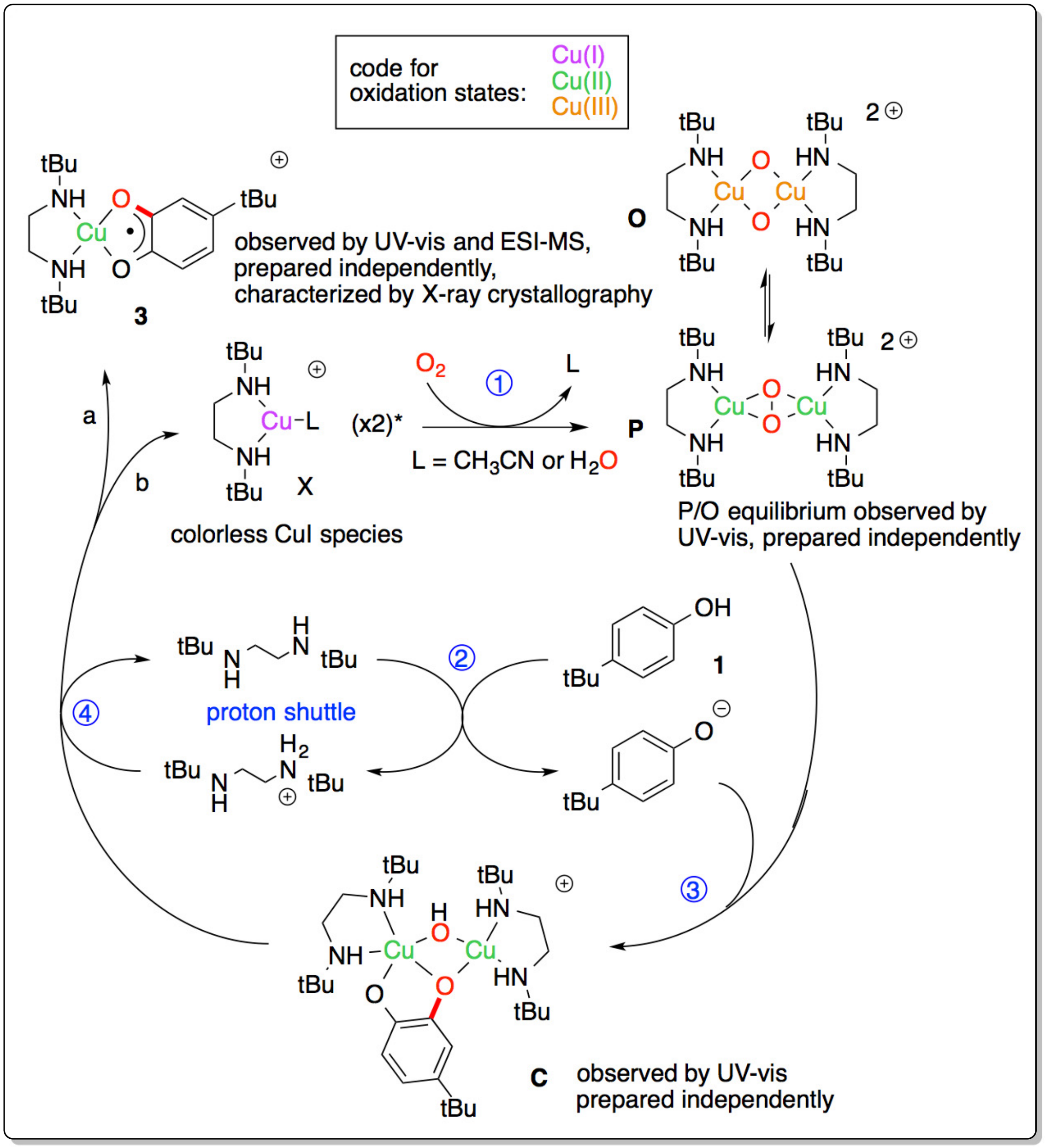

Scheme 2-6: Proposed mechanism for the *o*-oxygenation of phenol 1 to Cu(II)-semiquinone complex **3** at −80 °C. Step 4 produces one molecule of a Cu(I) complex, but two are required in step 1.

### 2.3.6. Diverting the course of the dearomatization reaction

The involvement of **3** in the formation of coupled *ortho*-quinone **2** at higher temperatures (25 °C) creates an opportunity to divert the course of the reaction to uncoupled *ortho*-quinone **4** by simply changing the solvent from $CH_2Cl_2$ to acetonitrile ($CH_3CN$). This affords a 1:1 mixture of quinones **2** and **4** at 25 °C (Table 2-1, entry 2), and a 1:4 mixture at −40 °C (entry 3). Under these conditions, we do not observe **3** by UV-visible spectroscopy, which suggests that $CH_3CN$ coordination to Cu(I) promotes the release of **4** faster than oxidative coupling with **1** to afford **2**. This scenario constitutes an important proof of principle that the *ortho*-oxygenation reaction can be performed in isolation of oxidative coupling, which is attractive for synthetic applications.

Table 2-1: Diversification of the reaction outcome [a]

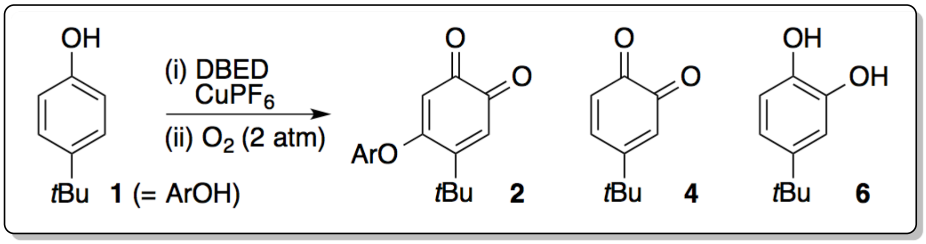

| Entry | $CuPF_6$ (mol%) | DBED (mol%) | Solvent | $T$ (°C) | Yields (%)[b] **2** | **4** | **6** |
|---|---|---|---|---|---|---|---|
| 1[c] | 4 | 8 | $CH_2Cl_2$ | 25 | 98 | 0 | 0 |
| 2[c] | 4 | 8 | $CH_3CN$ | 25 | 52 | 47 | 0 |
| 3[c] | 4 | 8 | $CH_3CN$ | –40 | 18 | 76 | 0 |
| 4[c] | 100 | 110 | $CH_2Cl_2$ | –78 | 0 | 82 | 0 |
| 5[d] | 100 | 110 | $CH_2Cl_2$ | –78 | 0 | 0 | 81 |

[a] Reactions performed on 1 mmol of phenol. [b] Isolated yields. [c] 10% $NaHSO_4$ work-up. [d] Saturated $Na_2S_2O_4$ work-up. See appendix 1 section 1.3 for experimental details.

If complete selectivity for **4** is desired, the oxygenation of **1** can be carried out at −78 °C in $CH_2Cl_2$ with 1 equivalent of $CuPF_6$ and 1.1 equivalents of DBED, which results in the quantitative formation of **3**. Subsequent exposure of **3** to either acidic or reductive conditions affords uncoupled *ortho*-quinone **4** (entry 4) or catechol **6** (entry 5), respectively. Semiquinones related to **3** have been popularized as non-innocent ligands for late transition metals,[165] but they have not been explored as strategic intermediates for synthesis. To our knowledge, this is the first synthesis of a semiquinone-metal complex directly from a phenol—these complexes are typically formed by inner-sphere reaction between a low-valent metal and an *ortho*-quinone.[165] This is also the first illustration that semiquinone-metal complexes are viable precursors to either free *ortho*-quinones or catechols, setting the stage for their development into strategic intermediates for synthesis.

## 2.4. Conclusions

Building upon the stoichiometric studies by Mirica, Solomon and Stack,[56-57] we establish that (1) the tyrosinase-like **P** species is indeed a viable oxidant under catalytic conditions and in the presence of excess phenol, (2) that *ortho*-oxygenation under catalytic conditions requires deprotonation of the phenol, and (3) that DBED is a suitable buffer to mediate proton transfer between **1** and **C**. In this sense, the *ortho*-oxygenation pathway under DBED/$CuPF_6$ conditions is very similar to that of tyrosinase, which proceeds through a **P** species, exhibits phenol deprotonation, and requires protonation of **C** for substrate release.[6-7,27,133-134] However, the formation of Cu(II)-semiquinone **3** marks an important point of divergence from tyrosinase. In the enzyme, both Cu atoms are retained in the protein-constrained active site following *ortho*-oxygenation.[6-7,133] This constraint enforces the release of the relatively unstable L-dopaquinone, which is prone to polymerization.[166-167] By contrast, our reaction attenuates the reactivity of the *ortho*-quinone by keeping it bound to Cu as a partially reduced semiquinone radical. Our work marks an important extension of mechanistic data acquired under stoichiometric conditions at cryogenic temperatures to a catalytic transformation that is conducted at room temperature on gram scale. This provides a mechanistic framework from which to explore the aerobic dearomatization of phenols, a reaction that holds significant promise for synthesis, but for which few selective catalytic aerobic systems have been developed.

## 2.5. Experimental Section

### 2.5.1. General procedures:

Chemicals and solvents were purchased from Sigma Aldrich, Alfa Aesar or Strem Chemicals. Inhibitor-free solvents were dried using a MBraun SPS 800, transferred to an inert-atmosphere glove box (MBraun Labmaster, <1 ppm $O_2$ and $H_2O$, filled with a dry $N_2$ atmosphere), further degassed under vacuum and stored over activated molecular sieves (4 Å). *tert*-Butylphenol **1** was purified by double recrystallization from $CH_2Cl_2$/hexanes. *N*,*N'*-di-*tert*-butylethylenediamine (DBED) was distilled over $CaH_2$ under $N_2$ and stored in the glovebox. The copper(I) salt $[Cu(CH_3CN)_4](PF_6)$, abbreviated $CuPF_6$, was purchased from commercial sources or made via a literature procedure.[168] $[Cu(CH_3CN)_4](SbF_6)$ was prepared via the same method, but using $HSbF_6$ instead of $HPF_6$. All copper(I) complexes were stored inside the glovebox.

Unless otherwise noted, reactions were performed in oven-dried glassware under a positive pressure of nitrogen using standard synthetic inert-atmosphere techniques. Bulk oxidation reactions were set-up in the glovebox in 25 mL, oven-dried Radley tubes equipped with a Teflon-coated stir bar. The reaction vessels were then connected to a cylinder of $O_2$, purged three times with $O_2$ and then over-pressurized to +1.0 atm.

UV-visible spectra were recorded on a B&W Tek iTrometer equipped with fiber-optic cables connected to a Hellma full-quartz dip-probe having a 1.0 mm pathlength. The probe was immersed in the solution inside a custom-made Schlenk flask. Temperature was maintained with external cooling baths: acetone/dry ice (−75 °C inside the solution), acetone/liquid nitrogen (−85 °C), pentane/liquid nitrogen (−115 °C). Spectra for mixtures or evolving solutions are reported in apparent $\varepsilon$, i.e. molar extinction coefficients with respect to the total Cu concentration.

Low-temperature stopped-flow experiments were carried out in the Département de Chimie at the Université de Montréal on a Hi-Tech CSF-61DX2 instrument (TgK Scientific) equipped with a diode-array detector over the 300-700 nm range. The UV-vis cuvette (pathlengths of 1.5 or 10 mm) was cooled by immersion in an ethanol bath cooled with liquid $N_2$. Syringe 1 was filled with a $CH_2Cl_2$ solution containing **1**, DBED and $CuPF_6$ in desired concentrations that was prepared in an MBraun Labmaster glovebox. Syringe 2 was filled with $CH_2Cl_2$ that was $O_2$-saturated at atmospheric pressure and room temperature. Concentrations were corrected for the 2-fold dilution upon mixing. Initial rates were calculated by measuring the tangent of the growth of the absorbance at 540 nm at the initial stage of the reaction (150 ms after mixing) and using $\varepsilon_{540}(\mathbf{3}) = 4{,}100\ M^{-1}\ cm^{-1}$.

Intramolecular competition experiments on $\mathbf{1^{HD}}$ were carried out on solutions containing 52 mM $\mathbf{1^{HD}}$, 52 mM $CuPF_6$ and 58 mM DBED in $CH_2Cl_2$ at −78 °C under 2 atm $O_2$ for 4h. Reductive work-up with $Na_2S_2O_4$ yielded the catechols. The ratios of **6** (major) to 5-*tert*-butyl-3-deuterocatechol ($\mathbf{6^{D}}$, minor) were measured by GC-MS on an Agilent 7890A GC with a HP 140915-433A column and an Agilent 5975C VL MSD (EI, 70 eV). Details in appendix 1 section 1.4.3.

### 2.5.2. Independent synthesis of 3:[157]

**3($PF_6$):** To a solution of DBED (51.8 mg, 0.30 mmol, 1.1 equiv.) and $CuPF_6$ (100 mg, 0.27 mmol, 1 equiv.) in 4 mL THF was added a solution of 4-*tert*-butylquinone (**4**, 48.5 mg, 0.30 mmol, 1.1 equiv.) in 1 mL THF with stirring. The color of the solution immediately changed from light pink to deep purple. The solution was stirred for two hours at 25 °C under $N_2$. The solution was then filtered through celite and added to 15 mL of stirring pentane pre-cooled to −35 °C upon which a purple solid precipitated. The solid was collected, washed with 2 mL $Et_2O$ and 2×2 mL pentane, and dried under vacuum for 24 hours. Yield: 110 mg, 75%. UV-vis, $CH_2Cl_2$, 25 °C, $\lambda$ / nm ($\varepsilon$ / $M^{-1}\cdot cm^{-1}$): 230 (6,380), 300 (9,000), 359 (1,910), 545 (3,500), 915 (1,300). Elemental analysis (mol%): expected for $C_{20}H_{36}N_2O_2F_6PCu \cdot 0.9\ CH_3CN \cdot 1.8\ H_2O$: C, 42.62; H, 6.94; N, 6.61; found: C, 42.75; H, 6.90; N, 6.61. Structural analysis of weakly diffracting crystals showed the same structure as for the **3**($SbF_6$) structure below, with the exception of smaller unit cell dimensions and a disordered $PF_6^-$ instead of $SbF_6^-$.

**3($SbF_6$):** was prepared similarly using $[Cu(MeCN)_4](SbF_6)$ as the copper source. Crystals suitable for X-ray diffraction studies were grown by slow layered diffusion of pentane into a $CH_2Cl_2$ solution of the complex at −30 °C in the glovebox. **3($SbF_6$)** was only used for structural characterization. For all solution experiments, the $PF_6^-$ salt was used.

## 2.6. Acknowledgments

We thank Kenneth V. N. Esguerra (McGill University) for experimental assistance. We are grateful to Prof. Hein Schaper and Prof. Garry Hanan (Université de Montréal) for access to their cryo-stopped-flow and glovebox equipment. MSA acknowledges NSERC for a PGS-D scholarship.

# 3. Manuscript 2: Catalytic Aerobic Oxidation of Phenols to *Ortho*-Quinones with Air-Stable Copper Precatalysts

Mohammad S. Askari, Laura Andrea Rodríguez-Solano, Andrew Proppe, Bryony McAllister, Jean-Philip Lumb and Xavier Ottenwaelder*

The contents of this chapter is from the following article published in Dalton Transactions:

Mohammad S. Askari, Laura Andrea Rodríguez-Solano, Andrew Proppe, Bryony McAllister, Jean-Philip Lumb and Xavier Ottenwaelder*, "Catalytic aerobic oxidation of phenols to *ortho*-quinones with air-stable copper precatalysts", *Dalton Trans.* **2015**, *44*, 12094-12097.

## 3.1. Abstract

A range of air-stable copper species was examined for catalytic activity in the catalytic aerobic transformation of phenols into *ortho*-quinones. Efficient catalysis was obtained with commercially available copper(II) acetate. The stability of all constituents before mixing makes for a practical process that advances previously reported copper(I)-based oxygenations.

## 3.2. Introduction

Due to their ability to activate oxygen ($O_2$), $Cu^I$ complexes are involved in a vast array of aerobic oxidations.[2] In particular, the Cu-catalyzed oxygenation of phenols into *ortho*-quinones has been extensively investigated because it is prevalent in biosynthesis and because it converts a readily available feedstock into a versatile, synthetically useful electrophile.[122-123,169] The quintessential example of such a reaction is the conversion of L-tyrosine into L-dopaquinone by the type-III Cu monooxygenase tyrosinase in the first step of melanin biosynthesis (Scheme 1a).[6] The resting (*met*) state of tyrosinase is a hydroxido $Cu^{II}_2$ dimer that requires reduction to the $O_2$-reactive $Cu^I_2$ (*deoxy*) state for phenol oxygenation to occur.[6] While replicating a tyrosinase-like oxygenation is synthetically desirable, the reactivity between $Cu^I$, $O_2$ and phenols outside a protein active site is plagued by competitive radical pathways that erode selectivity for *ortho*-oxygenation.[2] Progress has been made towards bio-inspired metal complexes that can emulate the reaction of tyrosinase,[7,21,136] although most reactions employ stoichiometric amounts of a Cu complex[55-57,137-139,141-148] or feature catalytic cycles that have poor turn-over, yield, or unfavourable reaction conditions.[65-67,69,71] Consistent throughout these studies has been the use of Cu in the +1 oxidation state together with non- or weakly coordinating anions,[58,170] which are thought to be requirements for selective $O_2$ activation and *ortho*-oxygenation.

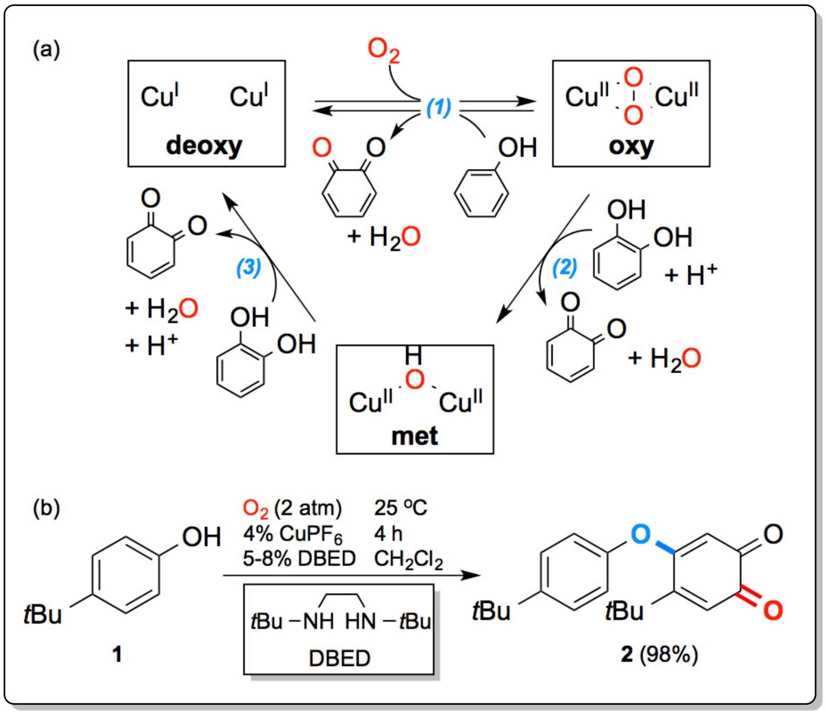

Scheme 3-1: (a) Mechanism of tyrosinase. The side chains of tyrosine (phenol), L-dopa (catechol) and dopaquinone (*o*-quinone) are omitted for clarity. (1): monophenolase activity, (2,3) diphenolase activity. (3) also represents an activation pathway from the *met* to the *deoxy* form. (b) Conversion of phenol **1** into *o*-quinone **2** under Lumb's conditions.[9] $CuPF_6$ is $[Cu^I(CH_3CN)_4](PF_6)$.

Recently, the Lumb group reported an efficient method for the aerobic conversion of phenols into functionalized *ortho*-quinones that is catalytic in all reaction components (Scheme 1b).[9] Typical conditions involve stirring a solution of phenol for 4 hours under 2 atm $O_2$ in the presence of 4 mol% of $[Cu^I(CH_3CN)_4](PF_6)$ and 5 mol% of *N*,*N'*-di-*tert*-butylethylenediamine (DBED). Under these conditions, DBED is thought to play the role of ligand to $Cu^I$, which promotes selective $O_2$ activation as a peroxo Cu dimer[55-57] similar to that in *oxy*-tyrosinase, as well as a base to generate a phenolate in situ.[171] The present work extends these conditions to a more practical and air-stable $Cu^{II}$ precatalyst. We reveal that catalytic *ortho*-oxygenation is possible from a range of Cu species, including those with oxidation states and coordinating counteranions that are not traditionally employed in biomimetic studies.

## 3.3. Results and Discussion

As a point of departure, we investigated the fate of Cu during the standard reaction of 4--*tert*-butylphenol **1**, which is converted into coupled *ortho*-quinone **2** in the presence of $O_2$, $[Cu^I(CH_3CN)_4](PF_6)$ and DBED. Recovered Cu at the end of this reaction is in the form of the well-known $[(DBED)Cu^{II}(\mu\text{-}OH)_2Cu^{II}(DBED)](PF_6)_2$ complex, **3**, as confirmed by IR spectroscopy and crystallization (see appendix 2 section 2.1 to 2.3). This air-stable product, which can be independently prepared by exposing a 1:1 mixture of DBED $[Cu^I(CH_3CN)](PF_6)$ to air or $O_2$,[158] is reminiscent of the $Cu^{II}$ dimer in *met*-tyrosinase. We were thus drawn by the prospect that **3** could re-enter the catalytic cycle in a manner that resembles the activation of *met*-tyrosinase, which must be reduced from $Cu^{II}$ to $Cu^I$ prior to *ortho*-oxygenation (Scheme 3-1a). Thus, using a 2.5 mol% of **3** (i.e. 5 mol% Cu) and an additional 5 mol% DBED (10 mol% total), phenol **1** is converted into **2** in 67% yield after 4 hours. This result is surprising since, to our knowledge, it represents the first example of a synthetic $Cu^{II}$ pre-catalyst that functions in an *ortho*-oxygenation.

Although **3** is not an ideal precatalyst due to its poor solubility and the necessity to synthesize it from a reactive $Cu^I$ precursor, this result demonstrates that phenol *o*-oxygenations can be carried out by air-stable $Cu^{II}$ precatalysts. This prompted us to investigate additional Cu salts with a range of oxidation states and counteranions using the **1** → **2** model reaction (Table 1). Several reactions were also tested in the presence of molecular sieves, as the inclusion of a desiccant was shown to improve conversion and yield.[9,128] In most cases, however, the effect of the molecular sieves was minimal.

Among the $Cu^I$ species that were probed (Table 3-1, entries 1-9), those with weakly coordinating anions such as $PF_6^-$ or sulfonates displayed varying levels of catalytic activity, whereas insoluble species (entries 4-9) were generally poor at initiating the reaction. Exceptions are $Cu^ICl$, $Cu^ICN$ and $Cu^I_2O$, but these precatalysts lead to low selectivity. Interestingly, insoluble $Cu^I_2O$ required an induction period of days during which no reaction was observed. Similarly, metallic $Cu^0$ (entries 10-11) is catalytically competent after an induction period of 3-4 days, at which point catalysis begins and complete conversion is reached within a few hours. This induction phenomenon with $Cu^0$ and $Cu^I{}_2O$ suggests that turnover requires a soluble catalyst (likely a $Cu^I$ species) formed by slow self-assembly under reaction conditions.

A survey of $Cu^{II}$ species (entries 12-25) revealed that commercially available $Cu(OAc)_2 \cdot H_2O$ is one of the most efficient precatalysts. Other caboxylates or hydrated sulfonates are also efficient, whereas non-hydrated $Cu^{II}(TfO)_2$ or $Cu^{II}(acac)_2$ are very poor at catalyzing the reaction. The discrepancy between $Cu^{II}(TfO)_2 \cdot 4\ H_2O$ (84% yield) and $Cu^{II}(TfO)_2$ (8% yield) is unexpected given the fact that water is a reaction by-product and is detrimental to the yield at long reaction times.[9] Poor catalysis is obtained with insoluble Cu salts such as $Cu^{II}(BF_4)_2 \cdot 6\ H_2O$ or $Cu^{II}(SO_4) \cdot 5\ H_2O$, while the completely insoluble $Cu^{II}O$ is inefficient even after several days. From the results included in Table 3-1, we conclude that good solubility of the Cu precursor leads to more efficient catalysis and that the coordinating ability / basicity of the counteranion is not a decisive factor.

Table 3-1: Screening of Cu precatalysts[a]

| Entry | Cu species | Time | Conversion (%) [yield(s) (%)][b] | |
|---|---|---|---|---|
| | | | no MS[c] | + MS[c] |
| **$Cu^I$ species** | | | | |
| 1 | $[Cu^I(CH_3CN)_4](PF_6)$ | 4h | 100 [89, 11][d] | 100 [95, 5][d] |
| 2 | $[Cu^I(CH_3CN)_4](TfO)$ | 4h | 100 [76, 7][d] | 100 [86, 7][d] |
| 3 | $[Cu^I(CH_3CN)_{3.5}](MsO)$ | 4h | 100 [92] | - |
| 4 | $Cu^I(AcO)$ | 4h | 25 [10] | 17 [7] |
| 5 | $Cu^ICl$ | 4h | 94 [58] | - |
| 6 | $Cu^IBr$ | 4h | [<30] [e] | - |
| 7 | $Cu^II$ | 4h | [<10] [e] | - |
| 8 | $Cu^ICN$ | 4h | 60 [33] | 43 [28] |
| 9 | $Cu^I{}_2O$ | 3d | 96 [74] | - |
| **$Cu^0$ species** | | | | |
| 10 | $Cu^0$, wire | 3d | 22 [22] | - |
| 11 | $Cu^0$, activated powder | 3d | 97 [88] | - |
| **$Cu^{II}$ species** | | | | |
| 12 | $[(DBED)Cu^{II}(\mu\text{-}OH)_2Cu^{II}(DBED)](PF_6)_2$, **3** [f] | 4h | 97 [67] | 100 [93] |
| 13 | $Cu^{II}(AcO)_2 \cdot H_2O$ | 4h | 98 [97] | 89 [89] |
| 14 | $Cu^{II}(AcO)_2 \cdot MeCN$ | 4h | 94 [75] | 92 [84] |
| 15 | $Cu^{II}(AcO)_2 \cdot MeCN$ | 8h | 98 [85] | - |
| 16 | $[Cu^{II}(DBED)(AcO)_2]$, **4** [f] | 4h | 98 [85] | 92 [72] |
| 17 | $Cu^{II}(HCO_2)_2 \cdot 4\ H_2O$ | 4h | 100 [91] | - |
| 18 | $Cu^{II}(TfO)_2$ | 4h | 43 [8] | - |
| 19 | $Cu^{II}(TfO)_2 \cdot 4\ H_2O$ | 4h | 100 [84, 3][d] | 100 [86, 3][d] |
| 20 | $Cu^{II}(BF_4)_2 \cdot 6\ H_2O$ | 4h | 7 [4] | 12 [12] |
| 21 | $Cu^{II}(acac)_2$ | 4h | 13 [7] | 2 [2] |
| 22 | $Cu^{II}Cl_2 \cdot 2\ H_2O$ | 4h | 77 [54] | - |
| 23 | $Cu^{II}Br_2$ | 4h | [e] | - |
| 24 | $Cu^{II}(SO_4) \cdot 5\ H_2O$ | 4h | 10 [1] | - |
| 25 | $Cu^{II}O$ | 3d | 0 | - |

[a] Conditions: 0.666 mmol **1**, 5% Cu, 10% DBED, 6 mL $CH_2Cl_2$ (0.1 M), 2 atm $O_2$, 25°C. Work-up: 10% $NaHSO_4$(aq) and extraction with $CH_2Cl_2$. [b] NMR conversion of **1** and yield of **2** calculated by NMR using hexamethylbenzene as internal standard. [c] MS = 4Å molecular sieves; 200 mg per mmol of **1** when used. [d] The first value is the yield of **2**, the second is the yield of 4-*tert*-butyl-*o*-quinone. [e] Reaction is not clean, noninterpretable NMR spectrum. [f] Only 5% extra DBED was added to adjust $[DBED]_{total}$ to 10% of [**1**].

The reactivity of $Cu^{II}(OAc)_2 \cdot H_2O$ as a precatalyst was explored in several solvents that ranged in polarity, hydrogen-bonding capability and miscibility with water (Table S 2-2).

Acetonitrile was found to promote the conversion of **1** to **2** in good yields, but the insolubility of **2** in this solvent led us to choose $CH_2Cl_2$ as the optimal solvent. While $Cu^{II}(OAc)_2 \cdot H_2O$ is itself insoluble in $CH_2Cl_2$, addition of DBED creates a clear blue solution within a few minutes, i.e. the active Cu species is in the same phase as the substrate for efficient initiation of catalysis. The soluble species is the discrete, neutral $[Cu^{II}(DBED)(AcO)_2]$ complex, **4**, which is also an efficient precatalyst when preformed outside the reaction mixture (Table 3-1, entry 16). The crystal structure of **4** (Figure 3-1) shows a distorted tetrahedral structure about the $Cu^{II}$ ion. The 49° angle between the $CuN_2$ and $CuO_2$ planes likely results from the large steric demands of the *tert*-butyl substituents, as is the case in **3** (Figure S 2-1) and other DBED–$Cu^{II}$ complexes.[157-158,171]

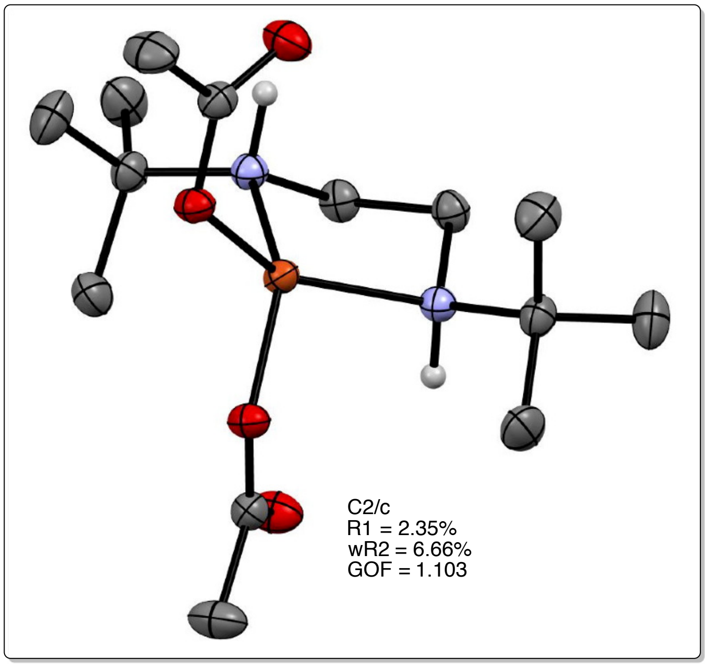

Figure 3-1: ORTEP representation at 50% ellipsoid probability of **4** at 293 K. Hydrogen atoms removed for clarity, except on N atoms. *i*: 1-*x*, *y*, ½−*z*. Selected bond lengths and angles: Cu1–O1 = 1.9272 Å, Cu1–N1 = 2.0281 Å. O1–Cu1–O1 = 87.19°, O1–Cu1–N1 = 146.61°, N1–Cu1–N1 = 87.18°.

The conversion of **1** into **2** was monitored by UV-vis spectroscopy to probe for reaction intermediates. With $Cu^{II}(OAc)_2 \cdot H_2O$, the spectra evolved from the initial light burgundy color of the $Cu^{II}$-**1**-DBED mixture to the orange color of **2** without detectable intermediacy of strongly colored species (Figure S 2-2). In contrast, $Cu^{II}(TfO)_2 \cdot 4H_2O$ led to the observation of ca. 80% (with respect to [Cu]) of $Cu^{II}$-semiquinone complex **5** (Figure 3-2), which is the same intermediate as in the reaction mediated by $[Cu^{I}(CH_3CN)_4](PF_6)$.[171] This suggests that the $Cu^{II}$-promoted reaction enters the same catalytic cycle as the $Cu^{I}$-promoted reaction, at least with non-coordinating counteranions. While more work is warranted to probe the conversion of the air-stable $Cu^{II}$ precatalyst into an $O_2$-reactive $Cu^{I}$ catalyst, several hypotheses can be proposed based on literature precedent. These include disproportionation of a $Cu^{II}$-phenolate into $Cu^{II}$-phenoxyl and $Cu^{I}$,[172] or in-situ reduction of $Cu^{II}$ by catechol impurities in the starting phenol (to the levels of detection of NMR and ESI-MS, we were unable to observe catechol as a contaminant in the phenol starting material), which is akin to the accepted activation of *met*-tyrosinase (Scheme 3-1a).

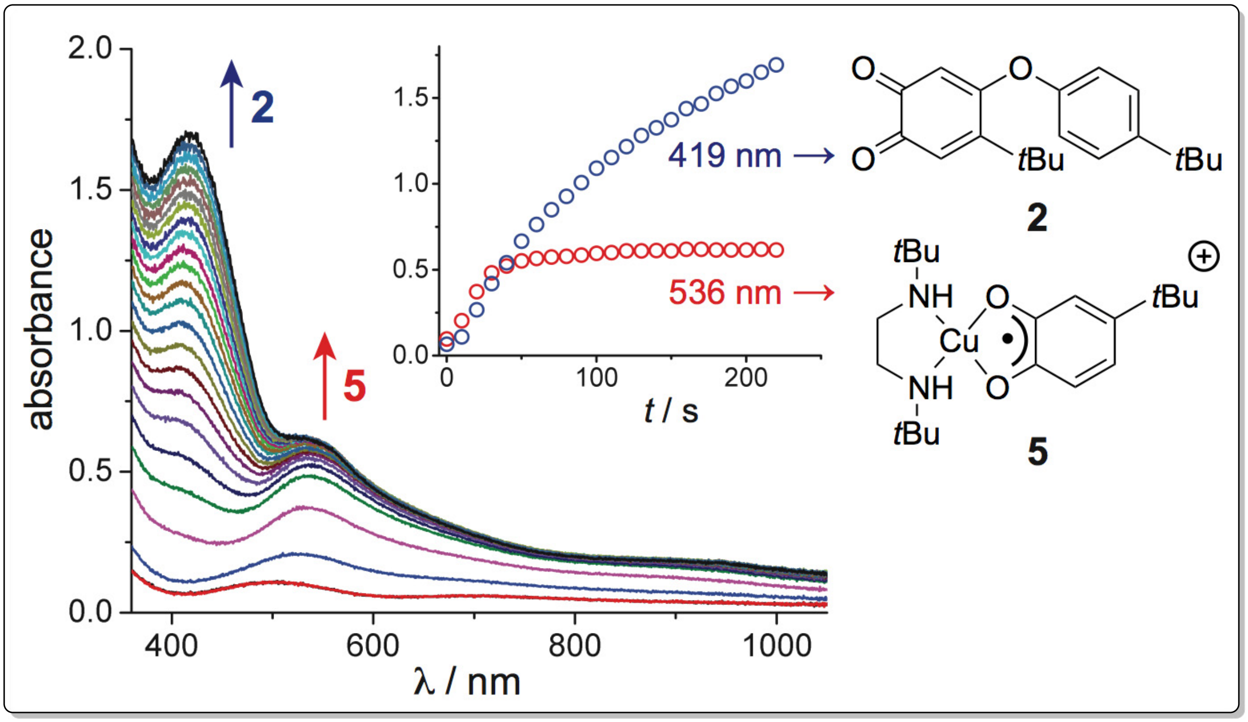

Figure 3-2: In-situ UV-visible monitoring of the reaction of **1** (50 mM) with 5% $Cu^{II}(OTf)_2 \cdot 4\ H_2O$ and 10% DBED, $CH_2Cl_2$ under 1.1 atm $O_2$ during the first 220s. Complete spectra in Figure S 2-3. Final yield of **2** was 98%.

The catalytic efficiency of the DBED:$Cu^{II}(OAc)_2{\cdot}H_2O$ system with various substrates (Scheme 3-2) is generally comparable to that of $Cu^{I}$,[9] and displays similar limitations. Thus, low yields are consistently observed for phenols that possess benzylic hydrogen atoms (**12-13**), presumably due to the ease with which the corresponding *ortho*-quinones undergo tautomerization. The reaction does not proceed for phenols possessing strongly electron-withdrawing substituents (**14**, 0% conversion). Electron-rich phenols and 2-naphthol produce intractable mixtures of products (**8**, **9**, **17**), in stark contrast to their $Cu^{I}$-mediated reactions. Based on the substantially lower oxidation potentials of these substrates compared with **1**,[149,173] we attribute this discrepancy to the ease of outer-sphere oxidations of these phenols into phenoxyl radicals by Cu$^{II}$ at the outset of the reaction.

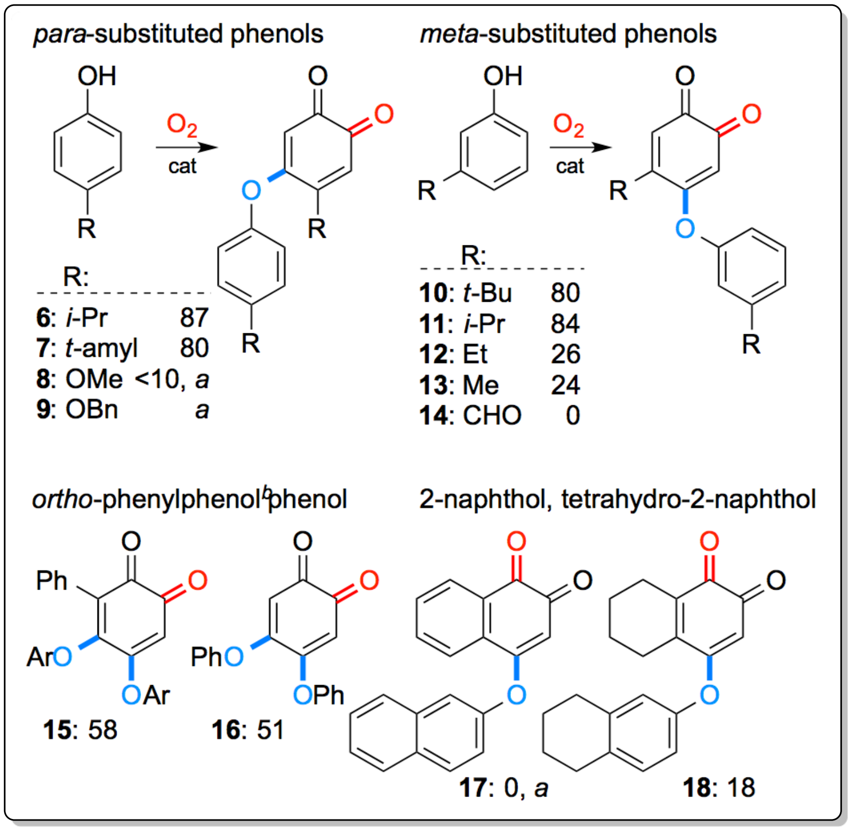

Scheme 3-2: Yields of coupled *ortho*-quinone for various substrates. Conditions: 1 mmol phenol, 5% Cu$^{II}$(OAc)$_2$ · H$_2$O, 10% DBED, 10 mL CH$_2$Cl$_2$ (0.1M), 2 atm O$_2$, 4h, 25°C. Work-up: 10% NaHSO$_4$(aq) or 0.1 M HCl and extraction with CH$_2$Cl$_2$. NMR yields calculated using hexamethylbenzene as internal standard. $^a$ Noninterpretable NMR spectrum. Reaction carried out with 200 mg of 4 Å molecular sieves (<5% yield without molecular sieves). $^b$ Ar = 2-phenylphenyl.

## 3.4. Conclusion

In summary, catalytic aerobic *ortho*-oxygenation of phenols is possible from a range of Cu precatalysts possessing 0, +1 or +2 oxidation states, as well as coordinating and non-coordinating counteranions. Solubility of the Cu precatalyst is essential for good reaction performance, as illustrated with the in-situ formation of the neutral [DBEDCu$^{II}$(OAc)$_2$] complex. This species provides an attractive starting point for additional reaction optimization and to probe the mechanism of Cu$^{II}$ reduction under the reaction conditions.

## 3.5. Acknowledgments

The authors belong to the CCVC-CGCC (Centre for Green Chemistry and Catalysis, Québec). We thank Andrew Dalton (Concordia) and Laurène Petitjean (McGill) for experimental help. Funding was provided by a team grant from FRQNT (Fonds de Recherche du Québec – Nature et Technologies) and individual Discovery grants from NSERC (Natural Sciences and Engineering Council of Canada) (XO and JPL). We are grateful to NSERC for graduate scholarships (MSA) and USRAs (AP, BMA). We acknowledge the CCVC-CGCC for awards (MSA, AP) and the Canadian Inorganic Chemistry Exchange program (BMA).

# 4. Manuscript 3: The Two Spin States of an End-on Copper(II)-Superoxide Mimic

Mohammad S. Askari, Brigitte Girard, Muralee Murugesu and Xavier Ottenwaelder*

The contents of this chapter is from the following article published in *Chemical Communications*:

Mohammad S. Askari, Brigitte Girard, Muralee Murugesu and Xavier Ottenwaelder*, “The two spin states of an end-on copper(II)-superoxide mimic”, *Chem. Commun.*, **2011**, *47*, 8055 – 8057.

## 4.1. Abstract

The reaction of nitrosobenzene with copper(I) complexes of a tetradentate ligand led to two novel species that are best described as copper(II) complexes of an O-bonded nitrosobenzyl radical anion, in either the singlet or the triplet spin-state. Both states were characterized by crystal structures, magnetic measurements and DFT calculations.

## 4.2. Introduction

The end-on copper(II)-superoxide motif, $[\mathrm{Cu^{II}}\text{-}(\eta^1\text{-}\mathrm{O_2}^{\bullet-})]$, is a proposed intermediate in the catalytic cycle of copper-dependent mononuclear monooxygenase enzymes such as peptidylglycine-α-hydroxylating monooxygenase and dopamine-$\beta$-hydroxylase.[8,174-177] Several synthetic end-on $\mathrm{Cu^{II}}$-superoxo complexes have been characterized as intermediates in the reaction of dioxygen ($O_2$) with electron-rich $\mathrm{Cu^I}$ complexes,[21,136] but the number of such species characterized extensively[178-179] or crystallographically[31,35] is small. This dearth stems from the high oxidative reactivity of these radical-type species, which are usually prepared and studied at low temperatures (typically -80°C).

The present study describes the reaction of nitrosobenzene (PhNO), an isoelectronic analogue of singlet $O_2$, with $\mathrm{Cu^I}$ complexes of the tetradentate ligand tris(2-dimethylaminoethyl)amine ($\mathrm{Me_6tren}$) (Scheme 4-1). $[\mathrm{Me_6trenCu^I}]^+$ complexes are known to yield very reactive end-on $\mathrm{Cu^{II}}$-superoxo intermediates that dimerize readily to $\mu$-1,2-

peroxodicopper(II) compounds even at -90°C.[180-181] Because PhNO has a lower oxidative potential than $O_2$, we hoped to stabilize analogues of intermediates that could occur in the $[Me_6trenCu^I]^+/O_2$ reaction but that are too transient to be studied in detail.[33,182] This reaction with PhNO was carried out from the $[Me_6trenCu^I](X)$ salts in which $X^-$ is the triflate ($TfO^-$) or hexafluoroantimonate ($SbF_6^-$) ion.

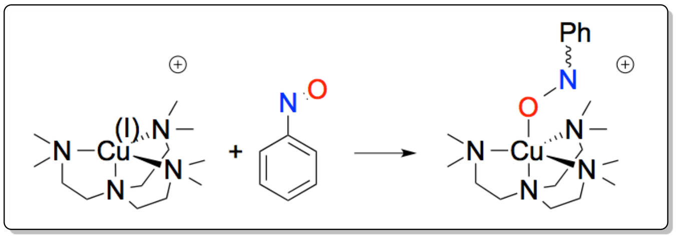

Scheme 4-1: Reaction of PhNO with $[(Me_6tren)Cu]^+$.

## 4.3. Results and Discussion

Two 1:1 $Me_6trenCu^I$:PhNO adducts, noted $[\mathbf{1}]^+$ hereafter, were isolated as solids, and crystallographically characterized as [**1**](TfO) and [**1**]($SbF_6$)•THF. The two crystal structures reveal an $[Me_6trenCu(PhNO\text{-}\kappa O)]^+$ complex in which the PhNO moiety is coordinated through its oxygen atom (Figure 4-1). While this bonding mode of a monomeric nitrosoaryl was already observed with other metal ions,[75,84-88] the present non-disordered structures are the first examples with Cu and the first with an O-bonded unsubstituted nitrosobenzene.[114-116] The $[\mathbf{1}]^+$ complexes in the two crystal structures differ mainly by the arrangement of the phenyl ring with respect to the Cu-O-N linkage. In [**1**](TfO), the Cu1-O1-N1-C1 torsion angle is -178.84(18)° and the Cu1-O1-N1 and phenyl planes are nearly coplanar. In stark contrast, this torsion angle is -124.2(3)° and the phenyl ring is significantly tilted away from the Cu1-O1-N1 plane in [**1**]($SbF_6$)•THF. In either structure, the phenyl ring experiences only two significant contacts: H3···F = 2.547 Å and H4···F = 2.624 Å in [**1**]($SbF_6$)•THF, and H2···O(TfO) = 2.589 Å and H5···O(TfO) = 2.613 Å in [**1**](TfO). Thus, the positioning of the phenyl ring with respect to the Cu1-O1-N1 plane may result from crystal packing.

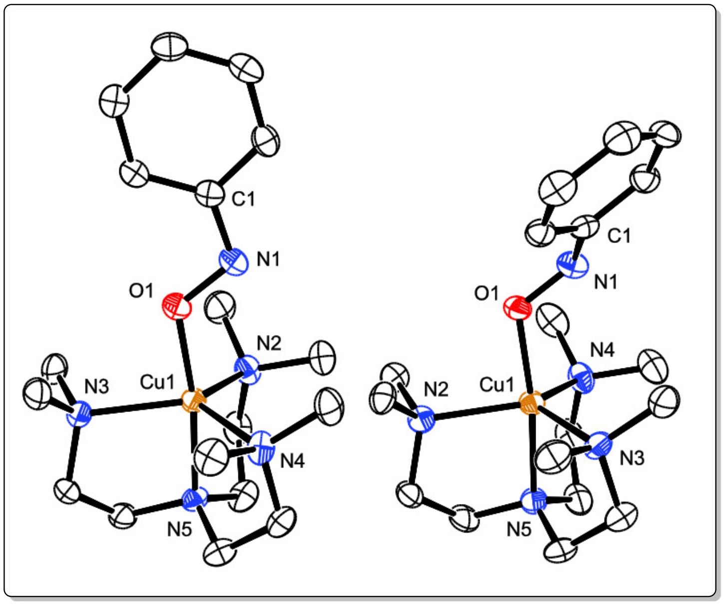

Figure 4-1: ORTEP representations at 50% probability of the $[\mathbf{1}]^+$ cations in the crystal structures of [**1**](TfO) (left) and [**1**]($SbF_6$)•THF (right). Hydrogen atoms, solvent molecules and counter-ions were omitted for clarity. Selected bond lengths (Å) and angles (°) in [**1**](TfO): Cu1-O1, 1.885(2); O1-N1, 1.337(3); N1-C1, 1.374(4); Cu1-N2, 2.150(2); Cu1-N3, 2.145(2); Cu1-N4, 2.158(2); Cu1-N5, 2.026(2); Cu1-O1-N1, 120.03(17); O1-N1-C1, 110.7(2); Cu1-O1-N1-C1, -178.84(18); in [**1**]($SbF_6$)•THF: Cu1-O1, 1.881(2); O1-N1, 1.320(4); N1-C1, 1.399(5); Cu1-N2, 2.136(3); Cu1-N3, 2.130(3); Cu1-N4, 2.201(3); Cu1-N5, 2.055(3); Cu1-O1-N1, 118.4(2); O1-N1-C1, 112.2(3); Cu1-O1-N1-C1, -124.2(3).

The molecular structures of the complexes provide information on the redox nature of the $[\mathbf{1}]^+$ adducts. The N1-O1 bonds, with lengths of 1.337(3) Å in [**1**](TfO) and 1.320(4) Å in [**1**]($SbF_6$)•THF, are longer than those measured in monomeric N-bonded nitrosoaryl molecules (1.209(3)-1.31(2) Å) and shorter than those in N,O-bonded metal C-nitroso compounds (1.358(2)-1.432(6)) Å.[75,97] They are also longer than the O-O bond length in the crystallographically characterized $Cu^{II}$-superoxo species: 1.280(3) Å.[31] Inasmuch as the trigonal-bipyramidal geometry of the Cu atom is suggestive of a $Cu^{II}$ oxidation state, the N-O bond lengths advocate for a PhNO moiety in a radical-anion state, $PhNO^{\bullet-}$, with a formal bond order of 1.5.[83,96] These crystal structures thus strongly suggest that the $[\mathbf{1}]^+$ adducts result from an inner-sphere electron transfer between PhNO and the $Cu^I$ precursor, as happens in the reaction between $[Me_6trenCu^I]^+$ and $O_2$. Alternatively, a $Cu^I$-(PhNO) hypothesis with strong backbonding into the $\pi_v$*(NO) is also plausible.

To substantiate the $Cu^{II}$-($PhNO^{\bullet-}$) formulation of the [**1**]$^+$ adducts, we carried out measurements of their magnetic properties on a SQUID magnetometer in the solid state. At 290 K, [**1**](TfO) exhibits the expected magnetic susceptibility of two unpaired S = 1/2 centres ($\chi_M T$ = 0.79 $cm^3$ K $mol^{-1}$), consistent with a $Cu^{II}$ oxidation state and a radical ($PhNO^{\bullet-}$) ligand (Figure S 3-2). Upon lowering the temperature, the increase in magnetic moment suggests a ferromagnetic coupling between the $Cu^{II}$ center and the $PhNO^{\bullet-}$ radical, but preliminary fitting of this behaviour was unsatisfactory. By contrast, no sample of [**1**]($SbF_6$)•THF had a measurable magnetic moment at room temperature, suggesting either a diamagnetic $Cu^{I}$-(PhNO) formulation or a very strongly antiferromagnetically coupled $Cu^{II}$-($PhNO^{\bullet-}$) species. For comparison, the side-on ($\eta^2$) $Cu^{II}$-superoxo complex with a crowded tris(pyrazolyl)borate, $Tp^{Ad}CuO_2$, exhibits an antiferromagnetic coupling constant of -1500 $cm^{-1}$, which was measurable by SQUID magnetometry.[183] While this is only preliminary data, these measurements strongly suggest that the two adducts have ground states of different spin: S = 1 for [**1**](TfO) and S = 0 for [**1**]($SbF_6$)•THF.

DFT calculations at the BP86/6-31G(d) level of theory confirmed the spin assignment of the two adducts. Optimization of a triplet state (S = 1) of an O-bonded adduct led to a geometry matching that of the cation in the crystal structure of [**1**](TfO) (rms deviation: 0.119 based on $CuN_4ONC_{ipso}$ and 0.266 on whole molecule), the main differences with the crystal structure being a small rotation of the phenyl ring about the N-$C_{ipso}$ bond. A single-point calculation in a geometry fixed to that of [**1**]$^+$ in the crystal structure of [**1**](TfO) identified the singlet state ~300 $cm^{-1}$ above the triplet state, consistent with the ferromagnetic coupling suggested experimentally. The two SOMOs of the triplet state are, in essence, the d($z^2$) of Cu and the $\pi_v$*(NO) perpendicular to the phenyl ring (Figure 4-2). These SOMOs are orthogonal to one another, a requirement for ferromagnetic coupling. Importantly, these orbitals are of the same nature as the SOMOs of the only crystallographically characterized $Cu^{II}$-superoxo complex.[35] The present electronic structure analysis thus supports the approach of using the Cu/PhNO reaction to mimic $Cu/O_2$ intermediates that cannot be observed easily, such as the transient $Cu^{II}$-superoxo species with the $Me_6$tren ligand.

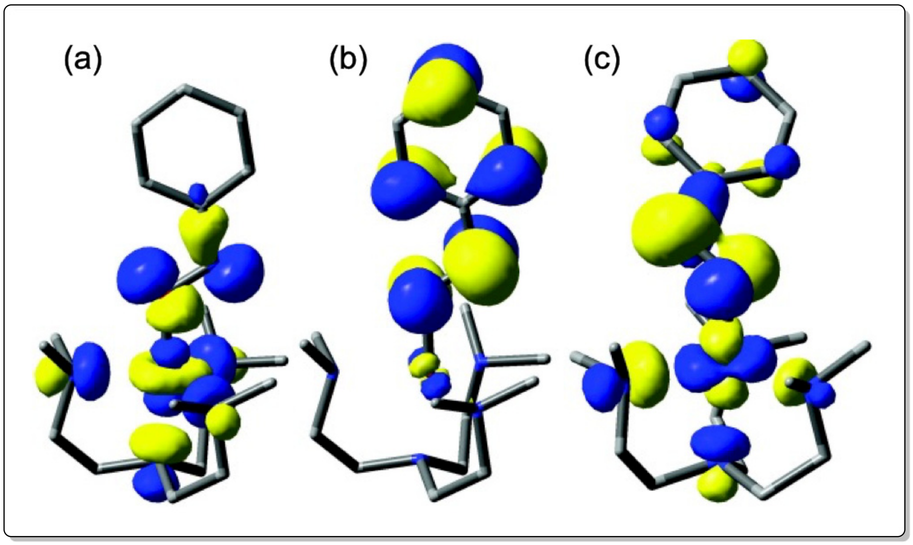

Figure 4-2: (a) and (b) SOMOs of [**1**]$^+$ in the triplet spin state (iso = 0.04). (c) HOMO of [**1**]$^+$ in the singlet spin state (iso = 0.04).

An unrestricted optimization of an O-bonded adduct in a singlet state (S = 0) refined to a geometry that matched that of [**1**]$^+$ in the crystal structure of [**1**]($SbF_6$)•THF (rms deviation: 0.044 based on $CuN_4ONC_{ipso}$ and 0.096 on whole molecule). A single-point electronic calculation based on the X-ray structure indicated a triplet state lying ~3000 cm$^{-1}$ above the singlet state, consistent with the diamagnetism observed experimentally. The twist of the phenyl ring out of the Cu1-O1-N1 plane imparts a lowering in symmetry and causes overlap between the d($z^2$) of Cu and the (formally) $\pi_v$*(NO) orbitals, leading to a strong stabilization of the singlet state (Figure 4-2). Although a broken-symmetry state could not be found using the BP86 functional, it is known that DFT cannot easily assess the true redox nature of complexes with non-innocent ligands. Further study is warranted.

## 4.4. Conclusion

In conclusion, the two adducts obtained in the solid state after reaction of [$Me_6$trenCu$^I$]$^+$ with PhNO reveal a yet-unknown PhNO-*κ*O bonding mode for an arylnitroso moiety to a Cu centre. The two complexes are distinct by a conformational change of the phenyl ring of the PhNO moiety, which in turn confers onto the complexes a different spin state, singlet or triplet. While the triplet molecule [**1**](TfO) is a Cu$^{II}$-(PhNO$^{\bullet-}$) species, indicating that electron transfer has occurred upon reaction, the nature of the singlet molecule [**1**]($SbF_6$)•THF is still under debate between a $Cu^I$-(PhNO) and a strongly antiferromagnetically coupled $Cu^{II}$-($PhNO^{\bullet-}$) formulation. Preliminary resonance Raman experiments recorded on solid samples indicated $^{14/15}N$ isotope-dependent peaks at 1119 (TfO) and 1160 ($SbF_6$) $cm^{-1}$, which are significantly lower than that of monomeric nitrosoaryl species (1506 $cm^{-1}$ for monomeric PhNO)[75] and support a $Cu^{II}$-($PhNO^{\bullet-}$) formulation.[96-97] Full vibrational studies are underway to decipher the nature of the N-O bond, hence the redox state of the PhNO moiety in both solid-state and solution. As mimics of the $Me_6trenCu^{II}$-superoxo species that has been observed only transiently, the two complexes provide the opportunity for further in-depth analysis of the influence of the spin-state on the bonding, electronic structure and reactivity of such exchange-coupled systems.

## 4.5. Acknowledgments

This work was supported by a Discovery Grant from the NSERC. Calculations were performed at Concordia's CERMM facilities and we are grateful to Dr. Guillaume Lamoureux for access to his cluster. We thank Po-Heng Li and Fatemah Habib (University of Ottawa) for the SQUID measurements and Alexandre Rodrigue-Witchel and Dr. Christian Reber (Université de Montréal) for preliminary resonance Raman data. M.S.A acknowledges NSERC for CGS-M and PGS-D scholarships.

## 4.6. Experimental

### 4.6.1. Synthesis of [1](X):

In an inert-atmosphere glovebox, a solution of $[Cu(MeCN)_4](X)$ (X = TfO or $SbF_6$, 0.11 mmol) in 2 mL of THF was added to a stirred solution of $Me_6tren$ (28 mg, 0.12 mmol) and PhNO (12 mg, 0.22 mmol) in 10 mL of ether. After stirring for one hour and decanting, the residual dark brown (TfO) or dark purple ($SbF_6$) solid was collected, triturated in ether (2 x 4 mL), and dried under vacuum for one hour (yields 72-77%). [**1**](TfO): Found: C, 41.2; H, 6.3; N, 12.45; S, 5.7. $C_{19}H_{35}N_5O_4F_3SCu$ requires C, 41.5; H, 6.4; N, 12.7; S, 5.8. [**1**]($SbF_6$)•0.2THF: Found: C, 34.4; H, 5.4; N, 10.35. $C_{18}H_{35}N_5OF_6CuSb$•0.2THF requires C, 34.7; H, 5.7; N, 10.75%. Single crystals of [**1**](TfO) and [**1**]($SbF_6$)•THF were grown by layered diffusion of pentane (TfO) or ether ($SbF_6$) into a THF solution of the complex at -30°C.

### 4.6.2. Crystal data for [1](TfO):

CCDC number: 815281; $C_{19}H_{35}CuF_3N_5O_4S$, $M$ = 550.12, orthorhombic, $a$ = 10.5615(11), $b$ = 13.7600(14), $c$ = 17.3141(18) Å, $U$ = 2516.2(5) Å$^3$, $T$ = 111 K space group $P2_12_12_1$ (no. 19), $Z$ = 4, 25370 reflections measured, 4632 unique ($R_{\text{int}}$ = 0.0484) which were used in all calculations. The final $wR(F^2)$ was 0.0751 (all data).

### 4.6.3. Crystal data for [1]($SbF_6$)•THF:

CCDC number: 815282; $C_{22}H_{43}CuF_6N_5O_2Sb$, $M$ = 708.90, monoclinic, $a$ = 12.4249(11), $b$ = 11.7456(10), $c$ = 20.7529(18) Å, $\beta$ = 105.8420(10)°, $U$ = 2913.6(4) Å$^3$, $T$ = 110 K space group $P2_1$/c (no. 14), $Z$ = 4, 32891 reflections measured, 6692 unique ($R_{\text{int}}$ = 0.0580) which were used in all calculations. The final $wR(F^2)$ was 0.0926 (all data).

# 5. Manuscript 4: Controlled Nitrene Transfer from a Tyrosinase-Like Arylnitroso-Copper Complex

Mohammad S. Askari, Maylis Orio, and Xavier Ottenwaelder*

The contents of this chapter is from the following article published in *Chemical Communications:*

Mohammad S. Askari, Maylis Orio, and Xavier Ottenwaelder*, "Controlled nitrene transfer from a tyrosinase-like arylnitroso-copper complex", *Chem. Commun.* **2015**, *51*, 11206-11209.

## 5.1. Abstract

The reaction between *p*-nitrosonitrobenzene and the tetramethylpropylenediamine-copper(I) complex yields a dinuclear complex that is structurally and electronically similar to side-on peroxo species known in Cu/$O_2$ chemistry. The complex reacts with di-*tert*-butylphenolate via nitrene transfer, as observed through an intermediate and the aminophenol product obtained upon reductive work-up.

## 5.2. Introduction

Transition metal complexes of non-innocent ligands have attracted much attention recently due to their application in catalysis and molecular switches.[184-185] In the case of the well-studied Cu/$O_2$ chemistry, the extent of dioxygen reduction by electron-rich $Cu^I$ species to the superoxo ($O_2^{\bullet-}$) or peroxo ($O_2^{2-}$) ligand, as well as the nuclearity of the ensuing Cu/$O_2$ complex, are controlled by the geometric and electronic properties of the supporting ligands (Scheme 5-1a).[6,21] One Cu/$O_2$ species of interest is the $\mu$-$\eta^2$:$\eta^2$-peroxodicopper(II), **P**, because it is the active oxidant in the ubiquitous enzyme tyrosinase, which promotes oxygen-atom transfer to convert a phenol into a versatile *ortho*-quinone (Scheme 5-1b).[6-7,21] But for a few exceptions,[44,69] the vast majority of Cu/$O_2$ species characterized outside a protein pocket are typically stable only at low temperatures (–80 °C), which makes them impractical to carry out oxygenation reactions.

Arylnitroso compounds can be used as surrogates for $O_2$ in reactions with $Cu^I$ and the adducts are stable at room temperature.[11,97,186] For example, the electron-rich $Cu^I$ complex with tetradentate ligand $Me_6tren$ reduces nitrosobenze by one electron to the radical anion, forming $[(Me_6tren)Cu^{II}(\kappa O\text{-}PhNO^{\bullet -})]^+$ complexes. These species are structural and electronic mimics of end-on $Cu^{II}$-superoxo species that are otherwise too transient to be isolated. In similar fashion, the one-electron reduction of nitrosobenzene upon binding to low-valent complexes further demonstrates the versatility of arylnitroso species for inner-sphere electron-transfer reactions.[96,187]

Here, we focus on the bidentate *N,N,N',N'*-tetramethylpropylenediamine (TMPD) ligand, which, in the case of Cu/$O_2$ chemistry, stabilizes the bis($\mu$-oxo)dicopper(III) **O** isomer (Scheme 5-1a).[188] The combination of the TMPD-$Cu^I$ complex and an electron-poor arylnitroso substrate yields a **P** mimic that displays tyrosinase-like reactivity (Scheme 5-1c).

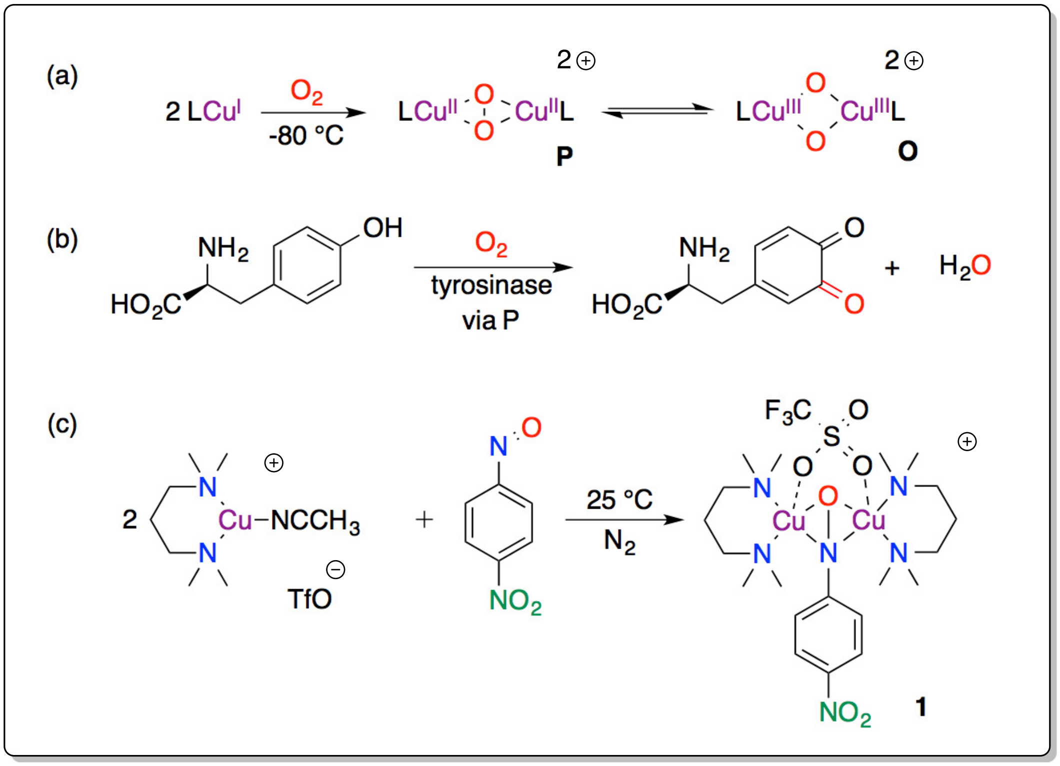

Scheme 5-1: (a) Typical $Cu^I/O_2$ reactivity with a bidentate ligand L. (b) Tyrosinase-catalyzed oxygenation of L-tyrosine during melanogenesis. (c) Synthesis of **1** via redox-controlled self-assembly.

## 5.3. Results and Discussion

Slow addition in THF at 25 °C of *p*-nitrosonitrobenzene (ArNO) to the TMPD-Cu(I) complex, formed from a 1:1 TMPD-[(MeCN)$_4$Cu](TfO) mixture,[188] results in the formation of a deep green complex, **1**, which remains stable for days under inert conditions. Clean samples of **1** are prepared via slow addition of a [(MeCN)$_4$Cu](TfO) solution to a solution of TMPD and ArNO in THF at 25 °C, then precipitated with pentane. $^1$H NMR spectra of **1** indicate a diamagnetic species with a 2:1 TMPD-ArNO stoichiometry. Crystallization of **1** by slow diffusion of pentane into the reaction mixture at –30 °C afforded crystals that were suitable for X-diffraction analysis. The solid-state structure of **1** (as its TfO$^-$ salt, Figure 5-1a) is consistent with the solution stoichiometry and shows a dinuclear species in which the NO moiety is bonded side-on to the two Cu centers ($\mu$-$\eta^2$:$\eta^2$), along with one of the two triflate ions bridging at axial positions. This coordination mode is reminiscent of the well-known side-on **P** species (Scheme 5-1).[6-7,21]

As with **P** species in which the $O_2$ molecule is reduced by two electrons to form the peroxide $O_2^{2-}$, we propose that the N=O bond of ArNO undergoes 2-electron reduction by the Cu$^I$ precursors to a hydroxylamine dianion in **1**. This proposal is based on the significantly lengthened N–O bond in **1** at 1.457(9) Å compared with 1.244(7)-1.253(7) Å in the organic ArNO dimer, ArN(O)N(O)Ar,[76] or other uncoordinated arylnitroso molecules (1.131(11)-1.343(47) Å).[75] This bond length matches well with N–O single bond in Diels-Alder adducts of ArNO (N–O = 1.463(5) and 1.4571(16) Å).[189] In addition, the square-pyramidal geometry of the Cu centers is consistent with a Cu$^{II}$ oxidation state. The overall Cu$_2$NO diamond core exhibits a butterfly distortion (38° angle between the two CuNO planes), and the Cu···Cu distance (3.416 Å) is between that for butterfly-distorted **P** dimers (3.2-3.4 Å)[190] and **P** species supported by mononucleating ligands (3.45-3.6 Å).[21] Quite remarkably, **1** is one of the few crystallographically characterized complexes exhibiting a $\mu$-$\eta^2$:$\eta^2$-bonded C-nitroso/hydroxylamine core.[97-99]

The degree of reduction of the ArNO moiety in **1** was further probed by vibrational analysis. Thus, IR spectra of solid **1** and its analogue with an Ar$^{15}$NO moiety reveal the presence of several isotope-sensitive bands (Figure S 4-6). Although the bands appear in the fingerprint region and many seem to undergo Fermi splitting, a clear feature is observed at ca. 875 ($\Delta\nu \approx 15$) cm$^{-1}$, which we assign to the N–O stretch based on computational investigation (Figure S 4-6 and

Figure S 4-7). This value is much lower than for the delocalized double N=O bond in the organic ArNO dimer, ArN(O)N(O)Ar (1238 (Δν = 20) $cm^{-1}$, Figure S 4-4),[75] and lower than in the mononuclear $Cu^{II}(\eta^2\text{-}PhNO^{\bullet-})$ species by Warren et al (1113 (Δν = 20) $cm^{-1}$).[97] This N−O stretch in **1** is comparable to that of the single N−O bond in primary hydroxylamines (910-920 $cm^{-1}$),[191] mononuclear $\eta^2\text{-}PhNO^{2-}$ complexes (900 $cm^{-1}$ range),[96] and the analogous $\mu\text{-}\eta^2\text{:}\eta^2\text{-}PhNO^{2-}$ $Ni^{II}$ dimer (915 (Δν = 14) $cm^{-1}$),[97] with the even lower wavenumber in **1** likely influenced by the *p*-$NO_2$ group. The vibrational analysis of **1** thus concurs with the structural analysis, confirming the 2-electron reduction of ArNO into a side-on hydroxylamine dianion that mimics the side-on peroxide in **P** species.

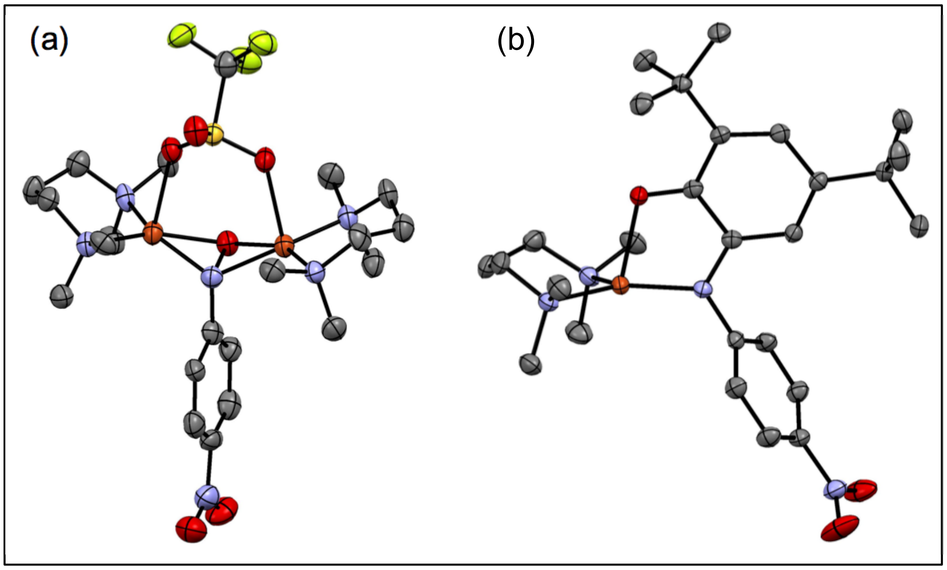

Figure 5-1: ORTEP representation of the solid-state structures of the monocations (a) **1** and (b) **2** at 50% ellipsoid probability (hydrogen atoms, non-coordinated $TfO^-$ anions and crystallization solvent molecules removed for clarity). Selected bond lengths (Å) and angles (°) for **1**: N1-O1, 1.457(9); Cu1-N1, 1.970(6); Cu1-O1, 1.926(6); Cu2-N1, 1.980(6); Cu2-O1, 1.916(6); Cu1-O2, 2.357(6); Cu2-O3, 2.359(6); Cu1-N2, 1.983(7); Cu1-N3, 1.991(7); Cu2-N4, 1.992(7); Cu2-N5, 2.006(8); N1-C1, 1.447(11); O1-N1-C1, 108.0(6); for **2**: Cu1-N1, 1.889(3); Cu1-O1, 2.165(2); Cu1-N3, 1.989(3); Cu1-N4, 2.018(3); O1-C12, 1.250(4); N1-C7, 1.333(4); C7-C8, 1.419(4); C8-C9, 1.363(5); C9-C10, 1.446(4); C10-C11, 1.360(5); C11-C12, 1.460(4); C7-C12, 1.486(5); N3-Cu1-N4, 102.94(12); N1 Cu1 N3, 139.86(12); N1-Cu1-N4, 115.88(11); N1-Cu1-O1, 79.95(10).

Complex **1** is also similar to **P** species in terms of electronic structure. Broken-symmetry DFT calculations indicate that **1** is a strongly antiferromagnetically coupled $Cu^{II}$ dimer (1798 $cm^{-1}$ between the ground singlet and excited triplet states), consistent with the experimentally observed diamagnetism. The calculated and experimental structures of **1** are within a 0.338 rms deviation (0.175 when only considering the first coordination sphere) and reveals a butterfly distorted $Cu_2NO$ core (59° angle between the two CuNO planes). The two UCOs (unrestricted corresponding orbitals) of **1** are each involving the $d(x^2\text{-}y^2)$ of one Cu atom in antibonding fashion with the in-plane $\pi_\sigma$* of the nitroso moiety (Figure S 4-10), which is reminiscent of the SOMOs of **P** species.[6,43,50-51] Likewise, the HOMO and LUMO of **1** are involving the out-of-plane $\pi_v$* and the in-plane $\pi_\sigma$* orbitals of the nitroso moiety, respectively (Figure 5-2d,e), as in known **P** species and the calculated peroxo analogue of **1** (Figure S 4-14 to Figure S 4-16). The UV-vis spectrum of **1** (Figure 5-2), with an intense band at 346 nm ($\varepsilon$ = 19.4 $mM^{-1}$ $cm^{-1}$) and several features in the visible region, resembles closely the spectra of **P** species,[21] particularly when a butterfly distortion is present.[190] TD-DFT calculations reproduce the spectrum accurately (Figure S 4-12). The 346 and 640 nm bands correspond to MLCT transitions involving the $\pi_\sigma$* of the nitroso moiety, consistent with the descent in symmetry from a $C_{2h}$ or $C_{2v}$ **P** to $C_s$ in **1**.[190]

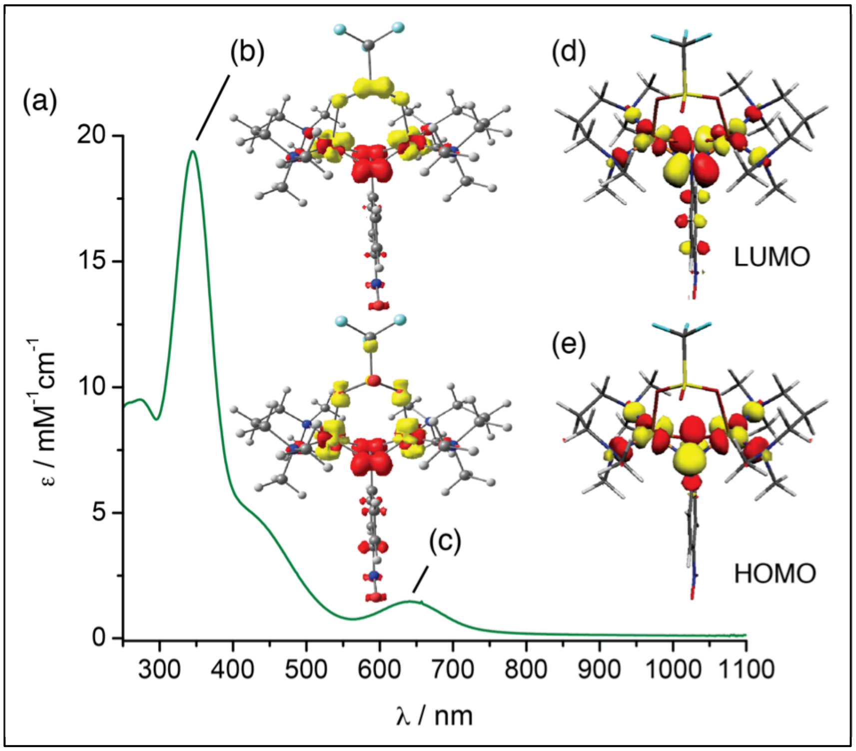

Figure 5-2: (a) UV-visible spectrum of **1** ($CH_2Cl_2$, 25 °C). (b,c) TD-DFT-calculated transitions as difference electron densities (yellow = negative, red = positive). (d) LUMO of **1**. (e) HOMO of **1**.

The electronic structure similarity between **1** and **P** species portends similar reactivities. Thus, reaction of **1** with 1.0 equivalent of sodium 2,4-di-*tert*-butylphenolate in $CH_2Cl_2$ at 25 °C leads to the fast formation of a deep blue solution, from which diamagnetic complex **2** can be isolated in 76% yield by slow diffusion of pentane at –30 °C (Scheme 5-2, top). The crystal structure of **2** reveals a TMPD-$Cu^I$-iminoquinone complex in which the nitrene of *p*-nitroaniline (*p*-$NO_2$-$C_6H_4$-N fragment) has formally replaced a hydrogen atom *ortho* to the phenol. The short C12–O1 (1.250(4) Å) and C7–N1 (1.333(4) Å) bonds and the quinoid C–C bond distribution on the chelating aromatic ring are strong indicators that the new ligand is an iminoquinone, in line with Wieghardt's comprehensive appraisal of such ligands (C–O of 1.24, 1.30, 1.35 and C–N of 1.30, 1.35, 1.37 Å for iminoquinone, iminosemiquinone and aminophenolate ligands, respectively).[192-199] In addition, the trigonal-monopyramidal coordination geometry of Cu in **2** is standard for a $Cu^I$ oxidation state. The dihedral angle between the $CuNN_{TMPD}$ and $CuNO_{iminoquinone}$ planes of 84° strongly contrasts with reported $Cu^{II}$-iminosemiquinone complexes for which minimal tetrahedral distortion (up to 26°) from square-planarity is consistent with a $Cu^{II}$ oxidation state.[199] The electronic assignment of **2** is further confirmed by DFT calculations conducted on both singlet ($Cu^I$-iminoquinone) and triplet ($Cu^{II}$-semiquinone) forms of **2**. Comparison of the optimized structures with X-ray data shows that **2** is compatible with a singlet $Cu^I$-iminoquinone species (Figure S 4-18). Energy analysis indicates that the singlet is stabilized by 11 kcal/mol over the triplet form (Figure S 4-12) and TD-DFT-predicted UV-vis parameters for the singlet do match the features of the experimental spectrum (Figure S 4-20).

Reductive work-up of the reaction mixture containing **2** with a saturated $Na_2S_2O_4$ aqueous solution under inert atmosphere provides novel 2-aminophenol **3** in 80% yield with respect to the phenolate (Scheme 5-2, top). Noteworthy, the corresponding iminoquinone was too reactive to be isolated, but its $Cu^I$ complex **2** was stable indefinitely in the glovebox. We assign this stability to $Cu^I$-to-iminoquinone backbonding (Figure S 4-21), which diminishes the electrophilicity of organic fragment.

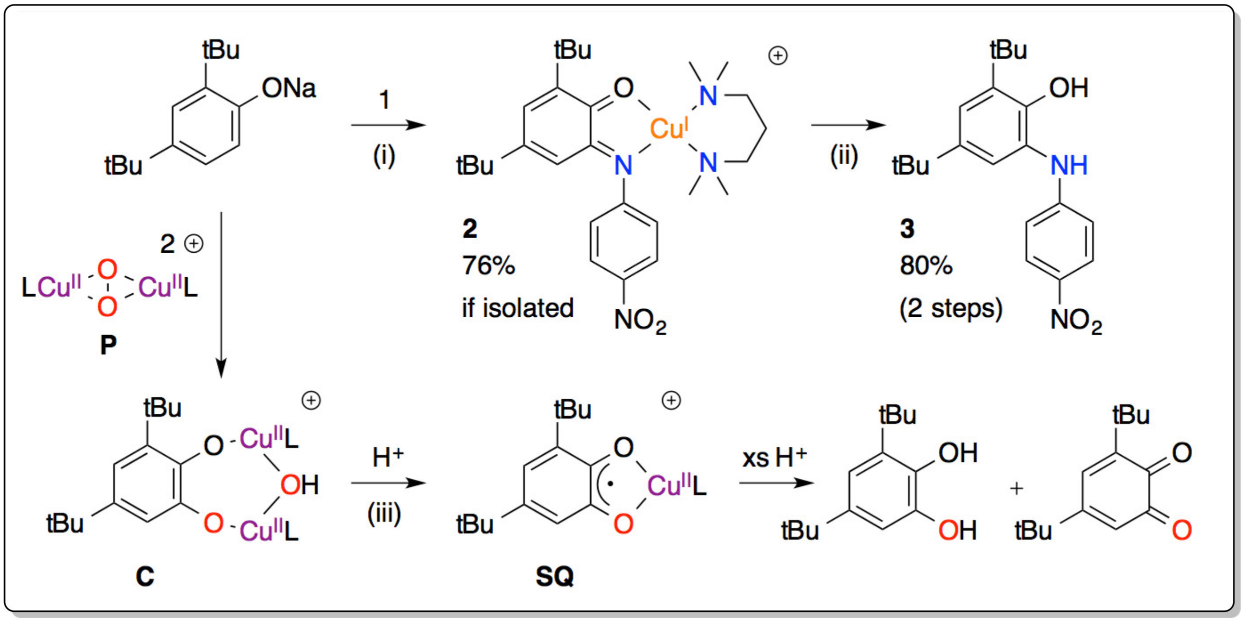

Scheme 5-2: Top: 1:1 reaction of **1** with 2,4-di-*tert*-butylphenolate and reductive work-up to **3**; L = TMPD; (i) $CH_2Cl_2$, $N_2$, 25°C; (ii) Saturated aqueous $Na_2S_2O_4$ work-up, $N_2$. Bottom: the comparable reaction with a **P** species requires careful protonation to release the **SQ** species; L' = *N,N'*-di-*tert*-butylethylenediamine; (iii) THF, –80 °C. 1 equiv $H^+$ per phenolate.

The C–H bond amination of the phenolate into **2** parallels the reaction carried by tyrosinase and its models whereby a **P** species transfers an oxygen atom to the phenolate via electrophilic aromatic substitution to yield a dinuclear catecholate species **C** (Scheme 5-2, bottom).[7,133] In stoichiometric models of tyrosinase, usually at –80 °C, this catecholate liberates the catechol upon acidic quench.[137-140,146] In one instance, **C** was shown to cleave into a mononuclear Cu$^{II}$-semiquinone species **SQ** upon careful acidification, which then liberates a mix of the corresponding catechol and *ortho*-quinone.[57] Complex **2** is similar to **SQ** except for the different valences of Cu and the ring, the iminoquinone being less electron-poor than the quinone. We propose that cleavage of a dimeric **C**-type intermediate into monomeric **2** does occur. This hypothesis is based on indirect evidence for the formation [TMPD-Cu$^{I}$-OH]$^{+}$ through the products of its disproportionation: the classic [TMPD-Cu$^{II}$(μ-OH)$_2$Cu$^{II}$TMPD]$^{2+}$ species as a precipitate and Cu$^{0}$ on the flask walls (while **2** is in solution). In our case, cleavage of the **C**-type dimer proceeds readily at 25 °C whereas it requires addition of an external acid in the case of Cu/$O_2$ reactions at –80 °C (Scheme 5-2). We were unable to observe any intermediate between **1** and **2** at temperatures ranging from 25 to –80 °C. The insolubility of the sodium phenolate in

$CH_2Cl_2$ seems to be important for the cleanliness of the reaction and, at the same time, prevents accumulation of intermediates. Performing the reaction in THF with a soluble phenolate led to intractable mixtures of products, highlighting the sensitivity of oxidant **1** to reaction conditions. Notwithstanding, **1** is selective for nitrogen transfer to the phenolate, and not its oxygen atom (only trace amounts of 3,5-di-*tert*-butyl-*o*-quinone were observed), a feature which will be the topic of a more in-depth study of **1** and analogous species.

## 5.4. Conclusions

Arylnitroso compounds have long been known to transiently generate nitrenes in their many unwanted side reactions leading to azoxy and azo compounds. Similarly, our control experiments for the phenolate reaction with *p*-nitrosonitrobenzene in the absence of Cu led to a intractable mixture of decomposition products. The clean reactivity of **1** with the phenolate is likely indicative of an inner-sphere mechanism similar to tyrosinase-like oxygenations.[56-57] Thus, phenolate would first bind to the Cu complex and then intramolecular nitrene transfer would occur. This reactivity contrasts with Cu-catalyzed allylic aminations (nitroso-ene reactions) in which C–N bond formation is thought to occur prior to N–O bond cleavage.[3,115-116] We are grateful to the Natural Sciences and Engineering Council of Canada (NSERC) for funding.

# 6. Conclusion

Tyrosinase catalyzes the *ortho*-oxygenation of tyrosine in the first step of the melanogenesis pathway. Despite 50 years of research in the field of Cu/$O_2$ chemistry, a fully catalytic and biomimetic method for the oxygenation of phenols has only been recently developed and reported. The difficulty has mainly been selectivity in the oxygenation reaction since formation of phenoxyl radicals through outer-sphere oxidation resulted in the formation of bisphenols even in the presence of a suitable base to confine the oxygen-atom transfer into the first coordination sphere of the metal centre. The interesting feature of the Lumb reaction is the use of a simple diamine ligand, DBED, as opposed to specially tailored ligands that have been the focus of most of the research in this field. The biomimetic nature of this reaction has been proven through mechanistic studies at low temperatures and by characterizing the intermediates involved. The high selectivity of this reaction is well explained by a mechanism in which in-situ generated phenolate first binds to the metal centre and is then oxygenated. This inner-sphere mechanism prevents generation of phenoxyl radicals. The side-on peroxo intermediate that is initially formed in this reaction is equivalent to the observed Cu/$O_2$ species in tyrosinase. In addition, kinetic studies indicate that the oxygen atom is transferred through an electrophilic aromatic substitution reaction. Interestingly, comparable efficiency and selectivity can be obtained using a DBED copper(II) precatalyst. This extension provides a more convenient method due to the inherent air-stability of copper(II) complexes.

Extending tyrosinase-like reactivity to *ortho*-amination of phenolates was achieved using copper complexes of nitrosoarenes that are isoelectronic with $O_2$. In the initial stages of the research, nitrosoarenes were shown to be redox labile thus undergoing one-electron reduction by metal centres and forming the radical-anion upon binding to electron-rich complexes. The one-electron reduced species is a structural and electronic mimic of the end-on superoxocopper(II) species, as evidenced by computational studies. By reducing the denticity of the ligand and using an electron-deficient nitrosoarene, two-electron reduction of the nitrosoarene was achieved. In this complex the nitroso group binds side-on to two copper centres and is reduced by one electron from each copper. Spectroscopic and computational studies indicate the similarity of electronic structure of this complex with side-on peroxodicopper(II) intermediates, thus providing a structural and electronic mimic of the peroxo oxidant observed in tyrosinase. The ability of this complex to transfer its nitrogen group to the *ortho*-position of a phenolate demonstrates that nitrosoarenes are suitable reagents for performing controlled C-H bond functionalization on phenols. Even though the reported reaction is still stoichiometric in metal and suffers from limited scope it provides a proof of concept in using nitrosoarenes as mimics of molecular oxygen.

# 7. Future work

The first two proposed future work directions concern the aerobic oxygenation of phenols and are summarized into 1) investigating the mechanism of oxidative coupling of quinones with phenols, and 2) studying the mechanism of aerobic oxidation of phenols when a copper(II)-precatalyst is employed. The third objective of the future work concerns the development of catalytic conditions for the *ortho*-amination of phenols using nitrosoarenes as the nitrogen-group source.

## 1. Mechanism of the oxidative C-O coupling

The mechanistic studies provided in chapter 2 of this thesis focused on the oxygen-atom transfer process at low temperature. The overall reaction at ambient temperature (25 ºC) comprises the oxygen-atom transfer followed by oxidative coupling of the generated quinone with another equivalent of phenol. Does this reaction occur on a free quinone or on a copper(II)-semiquinone complex? Are phenoxyl and carbon-centred radicals formed in this reaction? Kinetic studies and more thorough control experiments are required in order to understand the C-O bond formation step. Elucidation of the mechanism will be beneficial as it will allow for the functionalization of the generated quinone by other nucleophiles, such as amines, providing an efficient method for multiple functionalization of phenols.

## 2. Mechanism of aerobic phenol *ortho*-oxygenation by copper(II) precatalyst

The inability of copper(II) complexes to activate $O_2$ raises the question on the initiation of the oxidation reaction discussed in chapter 3. The reduction of the copper(II) complex to copper(I) must be the first step in the oxygen activation step. Two possible initiation pathways were proposed in chapter 3: 1) reduction of the copper(II) centres by catechol impurities present in the phenol, 2) disproportionation of copper(II)-phenolate complex to copper(I) and copper(II)-phenoxyl species. However, control experiments where a catechol was added to the reaction mixture did not improve catalysis, and preliminary studies did not provide evidence for the disproportionation of a copper(II)-phenolate species. Future work in this project will focus on kinetic studies of the reaction in order to determine the order with respect to each species and propose a plausible mechanism for the initiation step.

## 3. Development of Cu-catalyzed *ortho*-amination of phenols

Contrary to Cu/$O_2$ chemistry that have seen significant development over the past 50 years, metal/nitrosoarene chemistry has received less attention, in part because nitrosoarenes are inherently reactive molecules that decompose readily. The stoichiometric phenolate *ortho*-amination presented in chapter 5 is the first step towards developing a selective and catalytic system that follows a biomimetic pathway. The short-term objective is to find suitable conditions for the stoichiometric *ortho*-amination of a variety of phenolates using nitrosoarenes as nitrogen-group donors. For this purpose, the reaction will be optimized through substrate, solvent, copper source, and ligand screening. In addition, the effect of temperature and reaction time will be investigated. Mechanistic studies will then be required to explain the observed selectivity, where only the nitrogen moiety is transferred to the substrate. In the long term, the aim is to render the *ortho*-amination of phenols catalytic in a manner that parallels the development of the *ortho*-oxygenation chemistry, i.e. from structural characterization of reactive intermediates into a practical synthetic method.

# 8. Reference

[1] L. Que, W. B. Tolman, *Nature* **2008**, *455*, 333-340.

[2] S. E. Allen, R. R. Walvoord, R. Padilla-Salinas, M. C. Kozlowski, *Chem. Rev.* **2013**, *113*, 6234-6458.

[3] R. T. Gephart, T. H. Warren, *Organometallics* **2012**, *31*, 7728-7752.

[4] R. M. Mariarty, O. M. Prakash, *Organic Reactions*, Wiley, Hoboken, **2004**.

[5] S. C. Mitchell, P. Carmichael, R. Waring, in *Kirk-Othmer Encyclopedia of Chemical Technology*, John Wiley & Sons, Inc., **2000**.

[6] E. I. Solomon, D. E. Heppner, E. M. Johnston, J. W. Ginsbach, J. Cirera, M. Qayyum, M. T. Kieber-Emmons, C. H. Kjaergaard, R. G. Hadt, L. Tian, *Chem. Rev.* **2014**, *114*, 3659-3853.

[7] M. Rolff, J. Schottenheim, H. Decker, F. Tuczek, *Chem. Soc. Rev.* **2011**, *40*, 4077-4098.

[8] E. I. Solomon, J. W. Ginsbach, D. E. Heppner, M. T. Kieber-Emmons, C. H. Kjaergaard, P. J. Smeets, L. Tian, J. S. Woertink, *Faraday Discuss.* **2011**, *148*, 11-39.

[9] K. V. N. Esguerra, Y. Fall, J.-P. Lumb, *Angew. Chem., Int. Ed.* **2014**, *53*, 5877-5881.

[10] S. Itoh, S. Fukuzumi, *Acc. Chem. Res.* **2007**, *40*, 592-600.

[11] M. S. Askari, B. Girard, M. Murugesu, X. Ottenwaelder, *Chem. Commun.* **2011**, *47*, 8055-8057.

[12] M. S. Askari, M. Orio, X. Ottenwaelder, *Chem. Commun.* **2015**, *51*, 11206-11209.

[13] D. Magdziak, A. A. Rodriguez, R. W. Van De Water, T. R. R. Pettus, *Org. Lett.* **2002**, *4*, 285-288.

[14] L. Pouységu, T. Sylla, T. Garnier, L. B. Rojas, J. Charris, D. Deffieux, S. Quideau, *Tetrahedron* **2010**, *66*, 5908-5917.

[15] M. Uyanik, T. Mutsuga, K. Ishihara, *Molecules* **2012**, *17*, 8604-8616.

[16] D. J. C. Constable, P. J. Dunn, J. D. Hayler, G. R. Humphrey, J. J. L. Leazer, R. J. Linderman, K. Lorenz, J. Manley, B. A. Pearlman, A. Wells, A. Zaks, T. Y. Zhang, *Green Chem.* **2007**, *9*, 411-420.

[17] E. Roduner, W. Kaim, B. Sarkar, V. B. Urlacher, J. Pleiss, R. Gläser, W.-D. Einicke, G. A. Sprenger, U. Beifuß, E. Klemm, C. Liebner, H. Hieronymus, S.-F. Hsu, B. Plietker, S. Laschat, *ChemCatChem* **2013**, *5*, 82-112.

[18] S. V. Kryatov, E. V. Rybak-Akimova, S. Schindler, *Chem. Rev.* **2005**, *105*, 2175-2226.

[19] T. L. Poulos, *Chem. Rev.* **2014**, *114*, 3919-3962.

[20] D. S. Surry, S. L. Buchwald, *Chem. Sci.* **2011**, *2*, 27-50.

[21] L. M. Mirica, X. Ottenwaelder, T. D. P. Stack, *Chem. Rev.* **2004**, *104*, 1013-1046.

[22] J. P. Klinman, *Chem. Rev.* **1996**, *96*, 2541-2562.

[23] S. T. Prigge, B. A. Eipper, R. E. Mains, L. M. Amzel, *Science* **2004**, *304*, 864-867.

[24] S. T. Prigge, A. S. Kolhekar, B. A. Eipper, R. E. Mains, L. M. Amzel, *Nat. Struct. Mol. Biol.* **1999**, *6*, 976-983.

[25] P. Chen, E. I. Solomon, *J. Am. Chem. Soc.* **2004**, *126*, 4991-5000.

[26] Y. Matoba, T. Kumagai, A. Yamamoto, H. Yoshitsu, M. Sugiyama, *J. Biol. Chem.* **2006**, *281*, 8981-8990.

[27] H. Decker, T. Schweikardt, F. Tuczek, *Angew. Chem., Int. Ed.* **2006**, *45*, 4546-4550.

[28] M. E. Winkler, K. Lerch, E. I. Solomon, *J. Am. Chem. Soc.* **1981**, *103*, 7001-7003.

[29] S.-i. Yamazaki, S. Itoh, *J. Am. Chem. Soc.* **2003**, *125*, 13034-13035.

[30] C. J. Cramer, W. B. Tolman, *Acc. Chem. Res.* **2007**, *40*, 601-608.

[31] C. Würtele, E. Gaoutchenova, K. Harms, M. C. Holthausen, J. Sundermeyer, S. Schindler, *Angew. Chem., Int. Ed.* **2006**, *45*, 3867-3869.

[32] K. Fujisawa, M. Tanaka, Y. Moro-oka, N. Kitajima, *J. Am. Chem. Soc.* **1994**, *116*, 12079-12080.

[33] M. Weitzer, S. Schindler, G. Brehm, S. Schneider, E. Hörmann, B. Jung, S. Kaderli, A. D. Zuberbühler, *Inorg. Chem.* **2003**, *42*, 1800-1806.

[34] R. R. Jacobson, Z. Tyeklar, A. Farooq, K. D. Karlin, S. Liu, J. Zubieta, *J. Am. Chem. Soc.* **1988**, *110*, 3690-3692.

[35] J. S. Woertink, L. Tian, D. Maiti, H. R. Lucas, R. A. Himes, K. D. Karlin, F. Neese, C. Würtele, M. C. Holthausen, E. Bill, J. r. Sundermeyer, S. Schindler, E. I. Solomon, *Inorg. Chem.* **2010**, *49*, 9450-9459.

[36] S. Trofimenko, *Chem. Rev.* **1993**, *93*, 943-980.

[37] M. E. Cuff, K. I. Miller, K. E. van Holde, W. A. Hendrickson, *J. Mol. Biol.* **1998**, *278*, 855-870.

[38] K. A. Magnus, H. Ton-That, J. E. Carpenter, *Chem. Rev.* **1994**, *94*, 727-735.

[39] K. Magnus, H. Ton-That, *J. Inorg. Biochem.* **1992**, *47*, 20.

[40] H. Decker, T. Schweikardt, D. Nillius, U. Salzbrunn, E. Jaenicke, F. Tuczek, *Gene* **2007**, *398*, 183-191.

[41] H. Decker, F. Tuczek, *Trends Biochem. Sci.* **2000**, *25*, 392-397.

[42] M. J. Baldwin, P. K. Ross, J. E. Pate, Z. Tyeklar, K. D. Karlin, E. I. Solomon, *J. Am. Chem. Soc.* **1991**, *113*, 8671-8679.

[43] E. I. Solomon, F. Tuczek, D. E. Root, C. A. Brown, *Chem. Rev.* **1994**, *94*, 827-856.

[44] C. Würtele, O. Sander, V. Lutz, T. Waitz, F. Tuczek, S. Schindler, *J. Am. Chem. Soc.* **2009**, *131*, 7544-7545.

[45] N. Kitajima, T. Koda, S. Hashimoto, T. Kitagawa, Y. Moro-oka, *Chem. Commun.* **1988**, 151-152.

[46] N. Kitajima, K. Fujisawa, Y. Morooka, K. Toriumi, *J. Am. Chem. Soc.* **1989**, *111*, 8975-8976.

[47] N. Kitajima, T. Koda, S. Hashimoto, T. Kitagawa, Y. Morooka, *J. Am. Chem. Soc.* **1991**, *113*, 5664-5671.

[48] N. Kitajima, K. Fujisawa, C. Fujimoto, Y. Morooka, S. Hashimoto, T. Kitagawa, K. Toriumi, K. Tatsumi, A. Nakamura, *J. Am. Chem. Soc.* **1992**, *114*, 1277-1291.

[49] K. A. Magnus, B. Hazes, H. Ton-That, C. Bonaventura, J. Bonaventura, W. G. J. Hol, *Proteins: Struct., Funct., Bioinf.* **1994**, *19*, 302-309.

[50] P. K. Ross, E. I. Solomon, *J. Am. Chem. Soc.* **1990**, *112*, 5871-5872.

[51] P. K. Ross, E. I. Solomon, *J. Am. Chem. Soc.* **1991**, *113*, 3246-3259.

[52] E. I. Solomon, P. Chen, M. Metz, S.-K. Lee, A. E. Palmer, *Angew. Chem., Int. Ed.* **2001**, *40*, 4570-4590.

[53] M. J. Baldwin, D. E. Root, J. E. Pate, K. Fujisawa, N. Kitajima, E. I. Solomon, *J. Am. Chem. Soc.* **1992**, *114*, 10421-10431.

[54] L. M. Mirica, M. Vance, D. J. Rudd, B. Hedman, K. O. Hodgson, E. I. Solomon, T. D. P. Stack, *J. Am. Chem. Soc.* **2002**, *124*, 9332-9333.

[55] L. M. Mirica, D. J. Rudd, M. A. Vance, E. I. Solomon, K. O. Hodgson, B. Hedman, T. D. P. Stack, *J. Am. Chem. Soc.* **2006**, *128*, 2654-2665.

[56] L. M. Mirica, M. Vance, D. J. Rudd, B. Hedman, K. O. Hodgson, E. I. Solomon, T. D. P. Stack, *Science* **2005**, *308*, 1890-1892.

[57] B. T. Op't Holt, M. A. Vance, L. M. Mirica, D. E. Heppner, T. D. P. Stack, E. I. Solomon, *J. Am. Chem. Soc.* **2009**, *131*, 6421-6438.

[58] X. Ottenwaelder, D. J. Rudd, M. C. Corbett, K. O. Hodgson, B. Hedman, T. D. P. Stack, *J. Am. Chem. Soc.* **2006**, *128*, 9268-9269.

[59] T. D. P. Stack, *Dalton Trans.* **2003**, 1881-1889.

[60] J. Cahoy, P. L. Holland, W. B. Tolman, *Inorg. Chem.* **1999**, *38*, 2161-2168.

[61] M. J. Henson, P. Mukherjee, D. E. Root, T. D. P. Stack, E. I. Solomon, *J. Am. Chem. Soc.* **1999**, *121*, 10332-10345.

[62] J. L. Que, W. B. Tolman, *Angew. Chem., Int. Ed.* **2002**, *41*, 1114-1137.

[63] M. C. Kozlowski, B. J. Morgan, E. C. Linton, *Chem. Soc. Rev.* **2009**, *38*, 3193-3207.

[64] M. M. Pereira, M. J. F. Calvete, R. M. B. Carrilho, A. R. Abreu, *Chem. Soc. Rev.* **2013**, *42*, 6990-7027.

[65] M. Réglier, C. Jorand, B. Waegell, *Chem. Commun.* **1990**, 1752-1755.

[66] L. Casella, M. Gullotti, R. Radaelli, P. Di Gennaro, *Chem. Commun.* **1991**, 1611-1612.

[67] M. Rolff, J. Schottenheim, G. Peters, F. Tuczek, *Angew. Chem., Int. Ed.* **2010**, *49*, 6438-6442.

[68] J. Schottenheim, N. Fateeva, W. Thimm, J. Krahmer, F. Tuczek, *Z. Anorg. Allg. Chem.* **2013**, *639*, 1491-1497.

[69] A. Hoffmann, C. Citek, S. Binder, A. Goos, M. Rübhausen, O. Troeppner, I. Ivanović-Burmazović, E. C. Wasinger, T. D. P. Stack, S. Herres-Pawlis, *Angew. Chem., Int. Ed.* **2013**, *52*, 5398-5401.

[70] J. N. Hamann, F. Tuczek, *Chem. Commun.* **2014**, *50*, 2298-2300.

[71] C. Wilfer, P. Liebhäuser, H. Erdmann, A. Hoffmann, S. Herres-Pawlis, *Eur. J. Inorg. Chem.* **2015**, *2015*, 494-502.

[72] A. Arnold, R. Metzinger, C. Limberg, *Chem.--Eur. J.* **2015**, *21*, 1198-1207.

[73] J. Schottenheim, C. Gernert, B. Herzigkeit, J. Krahmer, F. Tuczek, *Eur. J. Inorg. Chem.* **2015**, DOI: 10.1002/ejic.201500029.

[74] O. Reinaud, P. Capdevielle, M. Maumy, *Tetrahedron Lett.* **1985**, *26*, 3993-3996.

[75] J. Lee, L. Chen, A. H. West, G. B. Richter-Addo, *Chem. Rev.* **2002**, *102*, 1019-1066.

[76] I. Halasz, I. Biljan, P. Novak, E. Meštrović, J. Plavec, G. Mali, V. Smrečki, H. Vančik, *J. Mol. Struct.* **2009**, *918*, 19-25.

[77] I. Huskic, I. Halasz, T. Friscic, H. Vancik, *Green Chem.* **2012**, *14*, 1597-1600.

[78] R. S. Heying, L. G. Nandi, A. J. Bortoluzzi, V. G. Machado, *Spectrochim. Acta. A* **2015**, *136, Part C*, 1491-1499.

[79] E. Bosch, J. K. Kochi, *J. Org. Chem.* **1994**, *59*, 5573-5586.

[80] M. KIESE, *Pharmacol. Rev.* **1966**, *18*, 1091-1161.

[81] P. Eyer, *Xenobiotica* **1988**, *18*, 1327-1333.

[82] P. J. O'brien, W. C. Wong, J. Silva, S. Khan, *Xenobiotica* **1990**, *20*, 945-955.

[83] L. A. Labios, M. D. Millard, A. L. Rheingold, J. S. Figueroa, *J. Am. Chem. Soc.* **2009**, *131*, 11318-11319.

[84] G.-e. Matsubayashi, K. Nakatsu, *Inorg. Chim. Acta* **1982**, *64*, L163-L164.

[85] S. Hu, D. M. Thompson, P. O. Ikekwere, R. J. Barton, K. E. Johnson, B. E. Robertson, *Inorg. Chem.* **1989**, *28*, 4552-4554.

[86] N. G. Bokii, A. I. Udel'nov, Y. T. Struchkov, D. N. Kravtsov, V. M. Pachevskaya, *J. Struct. Chem.* **1977**, *18*, 814-819.

[87] S. J. Fox, L. Chen, M. A. Khan, G. B. Richter-Addo, *Inorg. Chem.* **1997**, *36*, 6465-6467.

[88] L.-S. Wang, L. Chen, M. A. Khan, G. B. Richter-Addo, *Chem. Commun.* **1996**, 323-324.

[89] S. K. Dutta, D. B. McConville, W. J. Youngs, M. Chaudhury, *Inorg. Chem.* **1997**, *36*, 2517-2522.

[90] L. S. Liebeskind, K. B. Sharpless, R. D. Wilson, J. A. Ibers, *J. Am. Chem. Soc.* **1978**, *100*, 7061-7063.

[91] F. Ridouane, J. Sanchez, H. Arzoumanian, M. Pierrot, *Acta. Crystallogr. C* **1990**, *46*, 1407-1410.

[92] E. B. Brouwer, P. Legzdins, S. J. Rettig, K. J. Ross, *Organometallics* **1994**, *13*, 2088-2091.

[93] S. J. Skoog, W. L. Gladfelter, *J. Am. Chem. Soc.* **1997**, *119*, 11049-11060.

[94] S. J. Skoog, J. P. Campbell, W. L. Gladfelter, *Organometallics* **1994**, *13*, 4137-4139.

[95] M. Pizzotti, F. Porta, S. Cenini, F. Demartin, N. Masciocchi, *J. Organomet. Chem.* **1987**, *330*, 265-278.

[96] N. C. Tomson, L. A. Labios, T. Weyhermüller, J. S. Figueroa, K. Wieghardt, *Inorg. Chem.* **2011**, *50*, 5763-5776.

[97] S. Wiese, P. Kapoor, K. D. Williams, T. H. Warren, *J. Am. Chem. Soc.* **2009**, *131*, 18105-18111.

[98] D. W. Hoard, P. R. Sharp, *Inorg. Chem.* **1993**, *32*, 612-620.

[99] M. J. Scott, S. J. Lippard, *Organometallics* **1998**, *17*, 466-474.

[100] X. Dai, P. Kapoor, T. H. Warren, *J. Am. Chem. Soc.* **2004**, *126*, 4798-4799.

[101] H. Yamamoto, N. Momiyama, *Chem. Commun.* **2005**, 3514-3525.

[102] H. Yamamoto, M. Kawasaki, *Bull. Chem. Soc. Jpn.* **2007**, *80*, 595-607.

[103] N. Momiyama, H. Yamamoto, *Org. Lett.* **2002**, *4*, 3579-3582.

[104] J. G. Aston, D. F. Menard, *J. Am. Chem. Soc.* **1935**, *57*, 1920-1924.

[105] A. R. Forrester, S. P. Hepburn, *J. Chem. Soc. C* **1971**, 3322-3328.

[106] W. Adam, O. Krebs, *Chem. Rev.* **2003**, *103*, 4131-4146.

[107] P. Ehrlich, F. Sachs, *Ber. Dtsch. Chem. Ges.* **1899**, *32*, 2341-2346.

[108] A. P. Chavannavar, A. G. Oliver, B. L. Ashfeld, *Chem. Commun.* **2014**, *50*, 10853-10856.

[109] S. Carosso, M. J. Miller, *Org. Biomol. Chem.* **2014**, *12*, 7445-7468.

[110] K. K. Wan, K. Iwasaki, J. C. Umotoy, D. W. Wolan, R. A. Shenvi, *Angew. Chem., Int. Ed.* **2015**, *54*, 2410-2415.

[111] X. Lu, *Org. Lett.* **2004**, *6*, 2813-2815.

[112] A. Srivastava, Y.-A. Ma, R. Pankayatselvan, W. Dinges, K. M. Nicholas, *Chem. Commun.* **1992**, 853-854.

[113] R. S. Srivastava, K. M. Nicholas, *J. Org. Chem.* **1994**, *59*, 5365-5371.

[114] R. S. Srivastava, M. A. Khan, K. M. Nicholas, *J. Am. Chem. Soc.* **1996**, *118*, 3311-3312.

[115] R. S. Srivastava, M. A. Khan, K. M. Nicholas, *J. Am. Chem. Soc.* **2005**, *127*, 7278-7279.

[116] R. S. Srivastava, N. R. Tarver, K. M. Nicholas, *J. Am. Chem. Soc.* **2007**, *129*, 15250-15258.

[117] S. Murru, C. S. Lott, F. R. Fronczek, R. S. Srivastava, *Org. Lett.* **2015**, *17*, 2122-2125.

[118] Y. Yu, J. Srogl, L. S. Liebeskind, *Org. Lett.* **2004**, *6*, 2631-2634.

[119] T. Punniyamurthy, S. Velusamy, J. Iqbal, *Chem. Rev.* **2005**, *105*, 2329-2364.

[120] A. E. Wendlandt, A. M. Suess, S. S. Stahl, *Angew. Chem., Int. Ed.* **2011**, *50*, 11062-11087.

[121] J. Piera, J.-E. Bäckvall, *Angew. Chem., Int. Ed.* **2008**, *47*, 3506-3523.

[122] S. Yamamura, *The Chemistry of Phenols*, John Wiley & Sons, Ltd., West Sussex, UK., **2003**.

[123] S. Quideau, D. Deffieux, L. Pouységu, *Comprehensive Organic Synthesis II*, Second ed., Elsevier, Amsterdam, **2014**.

[124] A. S. Hay, H. S. Blanchard, G. F. Endres, J. W. Eustance, *J. Am. Chem. Soc.* **1959**, *81*, 6335-6336.

[125] G. F. Endres, A. S. Hay, J. W. Eustance, *J. Org. Chem.* **1963**, *28*, 1300-1305.

[126] A. S. Hay, *Polym. Eng. Sci.* **1976**, *16*, 1-10.

[127] Y. E. Lee, T. Cao, C. Torruellas, M. C. Kozlowski, *J. Am. Chem. Soc.* **2014**, *136*, 6782-6785.

[128] K. V. N. Esguerra, Y. Fall, L. Petitjean, J.-P. Lumb, *J. Am. Chem. Soc.* **2014**, *136*, 7662-7668.

[129] M. S. Askari, L. A. Rodriguez-Solano, A. Proppe, B. McAllister, J. P. Lumb, X. Ottenwaelder, *Dalton Trans.* **2015**, *44*, 12094-12097.

[130] L. Pouységu, D. Deffieux, S. Quideau, *Tetrahedron* **2010**, *66*, 2235-2261.

[131] S. Quideau, D. Deffieux, C. Douat-Casassus, L. Pouységu, *Angew. Chem., Int. Ed.* **2011**, *50*, 586-621.

[132] S. P. Roche, J. A. Porco, *Angew. Chem., Int. Ed.* **2011**, *50*, 4068-4093.

[133] E. I. Solomon, U. M. Sundaram, T. E. Machonkin, *Chem. Rev.* **1996**, *96*, 2563-2606.

[134] M. Fairhead, L. Thöny-Meyer, *New Biotechnol.* **2012**, *29*, 183-191.

[135] L. Q. Hatcher, K. D. Karlin, in *Adv. Inorg. Chem., Vol. 58* (Eds.: R. v. Eldik, J. Reedijk), Academic Press, **2006**, pp. 131-184.

[136] E. A. Lewis, W. B. Tolman, *Chem. Rev.* **2004**, *104*, 1047-1076.

[137] L. Santagostini, M. Gullotti, E. Monzani, L. Casella, R. Dillinger, F. Tuczek, *Chem.--Eur. J.* **2000**, *6*, 519-522.

[138] S. Itoh, H. Kumei, M. Taki, S. Nagatomo, T. Kitagawa, S. Fukuzumi, *J. Am. Chem. Soc.* **2001**, *123*, 6708-6709.

[139] G. Battaini, M. D. Carolis, E. Monzani, F. Tuczek, L. Casella, *Chem. Commun.* **2003**, 726-727.

[140] S. Palavicini, A. Granata, E. Monzani, L. Casella, *J. Am. Chem. Soc.* **2005**, *127*, 18031-18036.

[141] C. Citek, C. T. Lyons, E. C. Wasinger, T. D. P. Stack, *Nat. Chem.* **2012**, *4*, 317-322.

[142] J. Matsumoto, Y. Kajita, H. Masuda, *Eur. J. Inorg. Chem.* **2012**, *2012*, 4149-4158.

[143] S. Herres-Pawlis, P. Verma, R. Haase, P. Kang, C. T. Lyons, E. C. Wasinger, U. Flörke, G. Henkel, T. D. P. Stack, *J. Am. Chem. Soc.* **2009**, *131*, 1154-1169.

[144] S. Mandal, J. Mukherjee, F. Lloret, R. Mukherjee, *Inorg. Chem.* **2012**, *51*, 13148-13161.

[145] P. Capdevielle, M. Maumy, *Tetrahedron Lett.* **1982**, *23*, 1577-1580.

[146] L. Casella, E. Monzani, M. Gullotti, D. Cavagnino, G. Cerina, L. Santagostini, R. Ugo, *Inorg. Chem.* **1996**, *35*, 7516-7525.

[147] E. Monzani, L. Quinti, A. Perotti, L. Casella, M. Gullotti, L. Randaccio, S. Geremia, G. Nardin, P. Faleschini, G. Tabbì, *Inorg. Chem.* **1998**, *37*, 553-562.

[148] Y.-T. Cheng, H.-L. Chen, S.-Y. Tsai, C.-C. Su, H.-S. Tsang, T.-S. Kuo, Y.-C. Tsai, F.-L. Liao, S.-L. Wang, *Eur. J. Inorg. Chem.* **2004**, *2004*, 2180-2188.

[149] T. Osako, K. Ohkubo, M. Taki, Y. Tachi, S. Fukuzumi, S. Itoh, *J. Am. Chem. Soc.* **2003**, *125*, 11027-11033.

[150] P. P. Paul, Z. Tyeklar, R. R. Jacobson, K. D. Karlin, *J. Am. Chem. Soc.* **1991**, *113*, 5322-5332.

[151] N. Kitajima, T. Koda, Y. Iwata, Y. Morooka, *J. Am. Chem. Soc.* **1990**, *112*, 8833-8839.

[152] H. V. Obias, Y. Lin, N. N. Murthy, E. Pidcock, E. I. Solomon, M. Ralle, N. J. Blackburn, Y.-M. Neuhold, A. D. Zuberbühler, K. D. Karlin, *J. Am. Chem. Soc.* **1998**, *120*, 12960-12961.

[153] J. A. Halfen, V. G. Young, W. B. Tolman, *Inorg. Chem.* **1998**, *37*, 2102-2103.

[154] J. N. Hamann, M. Rolff, F. Tuczek, *Dalton Trans.* **2015**, *44*, 3251-3258.

[155] S. Kobayashi, H. Higashimura, *Prog. Polym. Sci.* **2003**, *28*, 1015-1048.

[156] M. Goldfeder, M. Kanteev, S. Isaschar-Ovdat, N. Adir, A. Fishman, *Nat. Commun.* **2014**, *5*, 4505.

[157] P. Verma, J. Weir, L. Mirica, T. D. P. Stack, *Inorg. Chem.* **2011**, *50*, 9816-9825.

[158] L. M. Mirica, T. D. P. Stack, *Inorg. Chem.* **2005**, *44*, 2131-2133.

[159] J. M. Hoover, B. L. Ryland, S. S. Stahl, *J. Am. Chem. Soc.* **2013**, *135*, 2357-2367.

[160] N. Fujieda, M. Murata, S. Yabuta, T. Ikeda, C. Shimokawa, Y. Nakamura, Y. Hata, S. Itoh, *J. Biol. Inorg. Chem.* **2013**, *18*, 19-26.

[161] K. Suzuki, C. Shimokawa, C. Morioka, S. Itoh, *Biochemistry* **2008**, *47*, 7108-7115.

[162] J. L. Muñoz-Muñoz, J. Berna, M. d. M. García-Molina, F. Garcia-Molina, P. A. Garcia-Ruiz, R. Varon, J. N. Rodriguez-Lopez, F. Garcia-Canovas, *Biochem. Biophys. Res. Commun.* **2012**, *424*, 228-233.

[163] C. Morioka, Y. Tachi, S. Suzuki, S. Itoh, *J. Am. Chem. Soc.* **2006**, *128*, 6788-6789.

[164] M. F. Qayyum, R. Sarangi, K. Fujisawa, T. D. P. Stack, K. D. Karlin, K. O. Hodgson, B. Hedman, E. I. Solomon, *J. Am. Chem. Soc.* **2013**, *135*, 17417-17431.

[165] C. G. Pierpont, C. W. Lange, in *Prog. Inorg. Chem., Vol. 41*, John Wiley & Sons, Inc., **2007**, pp. 331-442.

[166] M. E. Marín-Zamora, F. Rojas-Melgarejo, F. García-Cánovas, P. A. García-Ruiz, *J. Biotechnol.* **2009**, *139*, 163-168.

[167] M. Guazzaroni, C. Crestini, R. Saladino, *Bioorg. Med. Chem.* **2012**, *20*, 157-166.

[168] G. J. Kubas, *Inorg. Synth.* **1990**, *28*, 68-70.

[169] J. Zakzeski, P. C. A. Bruijnincx, A. L. Jongerius, B. M. Weckhuysen, *Chem. Rev.* **2010**, *110*, 3552-3599.

[170] Y. Funahashi, T. Nishikawa, Y. Wasada-Tsutsui, Y. Kajita, S. Yamaguchi, H. Arii, T. Ozawa, K. Jitsukawa, T. Tosha, S. Hirota, T. Kitagawa, H. Masuda, *J. Am. Chem. Soc.* **2008**, *130*, 16444-16445.

[171] M. S. Askari, J.-P. Lumb, X. Ottenwaelder, *Inorg. Chem.*, *submitted.*

[172] Y. Shimazaki, S. Huth, A. Odani, O. Yamauchi, *Angew. Chem., Int. Ed.* **2000**, *39*, 1666-1669.

[173] F. G. Bordwell, J. Cheng, *J. Am. Chem. Soc.* **1991**, *113*, 1736-1743.

[174] J. P. Klinman, *J. Biol. Chem.* **2006**, *281*, 3013-3016.

[175] S. Itoh, *Curr. Opin. Chem. Biol.* **2006**, *10*, 115-122.

[176] M. Rolff, F. Tuczek, *Angew. Chem., Int. Ed.* **2008**, *47*, 2344-2347.

[177] R. A. Himes, K. D. Karlin, *Curr. Opin. Chem. Biol.* **2009**, *13*, 119-131.

[178] D. Maiti, H. C. Fry, J. S. Woertink, M. A. Vance, E. I. Solomon, K. D. Karlin, *J. Am. Chem. Soc.* **2007**, *129*, 264-265.

[179] P. J. Donoghue, A. K. Gupta, D. W. Boyce, C. J. Cramer, W. B. Tolman, *J. Am. Chem. Soc.* **2010**, *132*, 15869-15871.

[180] M. Becker, F. W. Heinemann, S. Schindler, *Chem.--Eur. J.* **1999**, *5*, 3124-3129.

[181] S. Schindler, *Eur. J. Inorg. Chem.* **2000**, *2000*, 2311-2326.

[182] K. Komiyama, H. Furutachi, S. Nagatomo, A. Hashimoto, H. Hayashi, S. Fujinami, M. Suzuki, T. Kitagawa, *Bull. Chem. Soc. Jpn.* **2004**, *77*, 59-72.

[183] P. Chen, D. E. Root, C. Campochiaro, K. Fujisawa, E. I. Solomon, *J. Am. Chem. Soc.* **2003**, *125*, 466-474.

[184] P. J. Chirik, K. Wieghardt, *Science* **2010**, *327*, 794-795.

[185] V. Lyaskovskyy, B. de Bruin, *ACS Catal.* **2012**, *2*, 270-279.

[186] K. D. Williams, A. J. P. Cardenas, J. D. Oliva, T. H. Warren, *Eur. J. Inorg. Chem.* **2013**, *2013*, 3812-3816.

[187] N. C. Tomson, K. D. Williams, X. Dai, S. Sproules, S. DeBeer, T. H. Warren, K. Wieghardt, *Chem. Sci.* **2015**, *6*, 2474-2487.

[188] V. Mahadevan, J. L. DuBois, B. Hedman, K. O. Hodgson, T. D. P. Stack, *J. Am. Chem. Soc.* **1999**, *121*, 5583-5584.

[189] G. R. Stephenson, A. M. Balfe, D. L. Hughes, R. D. Kelsey, *Tetrahedron Lett.* **2010**, *51*, 6806-6809.

[190] E. Pidcock, H. V. Obias, M. Abe, H.-C. Liang, K. D. Karlin, E. I. Solomon, *J. Am. Chem. Soc.* **1999**, *121*, 1299-1308.

[191] A. Muñoz, F. Mathis, R. Mathis-Noël, *C. R. Acad. Sci.* **1957**, *244*, 1751-1754.

[192] S. Kokatam, T. Weyhermüller, E. Bothe, P. Chaudhuri, K. Wieghardt, *Inorg. Chem.* **2005**, *44*, 3709-3717.

[193] P. Chaudhuri, C. N. Verani, E. Bill, E. Bothe, T. Weyhermüller, K. Wieghardt, *J. Am. Chem. Soc.* **2001**, *123*, 2213-2223.

[194] H. Chun, C. N. Verani, P. Chaudhuri, E. Bothe, E. Bill, T. Weyhermüller, K. Wieghardt, *Inorg. Chem.* **2001**, *40*, 4157-4166.

[195] H. Chun, P. Chaudhuri, T. Weyhermüller, K. Wieghardt, *Inorg. Chem.* **2002**, *41*, 790-795.

[196] X. Sun, H. Chun, K. Hildenbrand, E. Bothe, T. Weyhermüller, F. Neese, K. Wieghardt, *Inorg. Chem.* **2002**, *41*, 4295-4303.

[197] V. Bachler, G. Olbrich, F. Neese, K. Wieghardt, *Inorg. Chem.* **2002**, *41*, 4179-4193.

[198] P. Ghosh, A. Begum, D. Herebian, E. Bothe, K. Hildenbrand, T. Weyhermüller, K. Wieghardt, *Angew. Chem., Int. Ed.* **2003**, *42*, 563-567.

[199] C. Mukherjee, U. Pieper, E. Bothe, V. Bachler, E. Bill, T. Weyhermüller, P. Chaudhuri, *Inorg. Chem.* **2008**, *47*, 8943-8956.

[200] J. Irangu, M. J. Ferguson, R. B. Jordan, *Inorg. Chem.* **2005**, *44*, 1619-1625.

[201] G. J. P. Britovsek, J. England, A. J. P. White, *Inorg. Chem.* **2005**, *44*, 8125-8134.

[202] A. D. Becke, *J. Chem. Phys.* **1986**, *84*, 4524-4529.

[203] J. P. Perdew, *Phys. Rev. B: Condens. Matter Mater. Phys.* **1986**, *33*, 8822.

[204] J. P. Perdew, *Phys. Rev. B: Condens. Matter Mater. Phys.* **1986**, *34*, 7406.

[205] M. J. Frisch, G. W. Trucks, H. B. Schlegel, G. E. Scuseria, M. A. Robb, J. R. Cheeseman, G. Scalmani, V. Barone, B. Mennucci, G. A. Petersson, H. Nakatsuji, M. Caricato, X. Li, H. P. Hratchian, A. F. Izmaylov, J. Bloino, G. Zheng, J. L. Sonnenberg, M. Hada, M. Ehara, K. Toyota, R. Fukuda, J. Hasegawa, M. Ishida, T. Nakajima, Y. Honda, O. Kitao, H. Nakai, T. Vreven, J. J. A. Montgomery, J. E. Peralta, F. Ogliaro, M. Bearpark, J. J. Heyd, E. Brothers, K. N. Kudin, V. N. Staroverov, T. Keith, R. Kobayashi, J. Normand, K. Raghavachari, A. Rendell, J. C. Burant, S. S. Iyengar, J. Tomasi, M. Cossi, N. Rega, J. M. Millam, M. Klene, J. E. Knox, J. B. Cross, V. Bakken, C. Adamo, J. Jaramillo, R. Gomperts, R. E. Stratmann, O. Yazyev, A. J. Austin, R. Cammi, C. Pomelli, J. W. Ochterski, R. L. Martin, K. Morokuma, V. G. Zakrzewski, G. A. Voth, P. Salvador, J. J. Dannenberg, S. Dapprich, A. D. Daniels, O. Farkas, J. B. Foresman, J. V. Ortiz, J. Cioslowski, D. J. Fox, *Gaussian 09, Revision B.01*,

[206] J. Rosevear, J. Wilshire, *Aust. J. Chem.* **1985**, *38*, 723-733.

[207] F. Neese, *Wiley Interdiscip. Rev. Comput. Mol. Sci.* **2012**, *2*, 73-78.

[208] A. D. Becke, *Phys. Rev. A* **1988**, *38*, 3098-3100.

[209] A. Schafer, C. Huber, R. Ahlrichs, *J. Chem. Phys.* **1994**, *100*, 5829-5835.

[210] F. Neese, *J. Comput. Chem.* **2003**, *24*, 1740-1747.

[211] F. Weigend, *Phys. Chem. Chem. Phys.* **2006**, *8*, 1057-1065.

[212] A. Klamt, G. Schuurmann, *J. Chem. Soc., Perkin Trans. 2* **1993**, 799-805.

[213] A. D. Becke, *J. Chem. Phys.* **1993**, *98*, 1372-1377.

[214] C. Lee, W. Yang, R. G. Parr, *Phys. Rev. B: Condens. Matter Mater. Phys.* **1988**, *37*, 785-789.

[215] L. Noodleman, *J. Chem. Phys.* **1981**, *74*, 5737-5743.

[216] L. Noodleman, D. A. Case, in *Adv. Inorg. Chem., Vol. 38* (Ed.: C. Richard), Academic Press, **1992**, pp. 423-470.

[217] L. Noodleman, E. R. Davidson, *Chem. Phys.* **1986**, *109*, 131-143.

[218] T. Soda, Y. Kitagawa, T. Onishi, Y. Takano, Y. Shigeta, H. Nagao, Y. Yoshioka, K. Yamaguchi, *Chem. Phys. Lett.* **2000**, *319*, 223-230.

[219] K. Yamaguchi, Y. Takahara, T. Fueno, in *Applied Quantum Chemistry* (Eds.: V. Smith, Jr., H. Schaefer, III, K. Morokuma), Springer Netherlands, **1986**, pp. 155-184.

[220] W. Heisenberg, *Z. Physik* **1926**, *38*, 411.

[221] W. Heisenberg, *Z. Physik* **1928**, *49*, 619.

[222] P. A. M. Dirac, *Proc. Roy. Soc.* **1929**, *A123*, 714.

[223] J. H. Van Vleck, *The Theory of Electronic and Magnetic Susceptibilities*, Oxford University, London, **1932**.

[224] M. E. Casida, in *Recent Advances in Density Functional Methods, Vol. 1* (Ed.: D. P. Chong), World Scientific, Singapore, **1995**.

[225] R. E. Stratmann, G. E. Scuseria, M. J. Frisch, *J. Chem. Phys.* **1998**, *109*, 8218-8224.

[226] R. Bauernschmitt, R. Ahlrichs, *Chem. Phys. Lett.* **1996**, *256*, 454-464.

[227] S. Hirata, M. Head-Gordon, *Chem. Phys. Lett.* **1999**, *314*, 291-299.

[228] S. Hirata, M. Head-Gordon, *Chem. Phys. Lett.* **1999**, *302*, 375-382.

[229] F. Neese, *J. Chem. Phys.* **2001**, *115*, 11080-11096.

[230] G. A. Andrienko, *Chemcraft*, http://www.chemcraftprog.com.

# 9. Appendices

# 1. Supplementary Information for Chapter 2

### A Biomimetic Mechanism for the Copper-Catalyzed Aerobic Oxygenation of 4-*tert*-Butylphenol

Mohammad S. Askari, Jean-Philip Lumb,* and Xavier Ottenwaelder*

## 1.1. Characterization of 3

### 1.1.1. X-ray structure and crystallographic data of 3(SbF$_6$) · 0.5 CH$_2$Cl$_2$

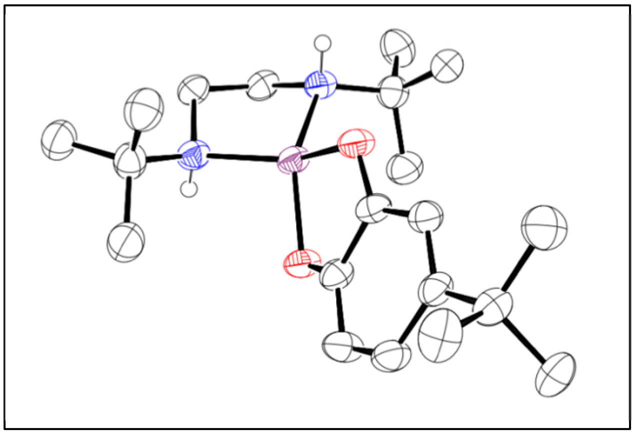

Figure S 1-1: Crystal structure of the cationic part of **3**(SbF$_6$) · 0.5 CH$_2$Cl$_2$ at 50% ellipsoid probability. Hydrogen atoms on carbons were omitted for clarity.

A dark purple block-like specimen of $C_{20.50}H_{37}ClCuF_6N_2O_2Sb$, approximate dimensions 0.070 mm x 0.129 mm x 0.200 mm, was used for the X-ray crystallographic analysis. The X-ray intensity data were measured on a Bruker SMART APEX II CCD system equipped with a Cu IμS microfocus source with QUAZAR optics ($\lambda = 1.54178$ Å). A total of 5856 frames were collected. The total exposure time was 16.27 hours. The frames were integrated with the Bruker SAINT software package using a narrow-frame algorithm. The integration of the data using a monoclinic unit cell yielded a total of 36357 reflections to a maximum θ angle of 65.08° (0.85 Å resolution), of which 4656 were independent (average redundancy 7.809, completeness = 99.6%, $R_{int}$ =

10.44%, $R_{sig}$ = 5.98%) and 3604 (77.41%) were greater than $2\sigma(F^2)$. The final cell constants of a = 14.6057(7) Å, b = 12.7363(5) Å, c = 17.9897(9) Å, β = 124.907(3)°, volume = 2744.4(2) $Å^3$, are based upon the refinement of the XYZ-centroids of 4494 reflections above 20 σ(I) with 7.380° < 2θ < 106.9°. Data were corrected for absorption effects using the multi-scan method (SADABS). The ratio of minimum to maximum apparent transmission was 0.669. The calculated minimum and maximum transmission coefficients (based on crystal size) are 0.2346 and 0.5350. The structure was solved and refined using the Bruker SHELXTL Software Package, using the space group P 1 21/c 1, with Z = 4 for the formula unit, $C_{20.50}H_{37}ClCuF_6N_2O_2Sb$. The final anisotropic full-matrix least-squares refinement on F2 with 316 variables converged at $R_1$ = 4.62%, for the observed data and $wR_2$ = 12.52% for all data. The goodness-of-fit was 1.019. The largest peak in the final difference electron density synthesis was 1.157 $e^-/Å^3$ and the largest hole was −0.918 $e^-/Å^3$ with an RMS deviation of 0.100 $e^-/Å^3$. On the basis of the final model, the calculated density was 1.642 $g/cm^3$ and F(000), 1364 $e^-$.

Table S 1-1: Crystal data and structure refinement for **3**($SbF_6$).

| CCDC deposition number | 950162 |
|---|---|
| Empirical formula | $C_{20}H_{36}N_2O_2Cu \cdot SbF_6 \cdot 0.5\ CH_2Cl_2$ |
| Formula weight | 678.26 |
| Temperature | 110(2) K |
| Wavelength | 1.54178 Å |
| Crystal system | Monoclinic |
| Space group | $P2_1/c$ |
| Unit cell dimensions | $a$ = 14.6057(7) Å<br>$b$ = 12.7363(5) Å<br>$c$ = 17.9897(9) Å<br>$\alpha$ = 90.00°<br>$\beta$ = 124.907(3)°<br>$\gamma$ = 90.00° |
| Volume | 2744.4(2) $Å^3$ |
| Z | 4 |
| Density (calculated) | 1.642 $g/cm^3$ |
| Absorption coefficient | 10.205 $mm^{-1}$ |
| F(000) | 1364 |
| Crystal size | 0.20 × 0.13 × 0.07 mm |
| Theta range for data collection | 3.69 – 65.08° |
| Index ranges | $h = -17 \rightarrow 17$<br>$k = -14 \rightarrow 14$<br>$l = -21 \rightarrow 20$ |
| Reflections collected | 36357 |
| Independent reflections | 4656 ($R_{int}$ = 10.44%) |
| Completeness to theta = 65.08° | 99.6% |
| Absorption correction | Multiscan |
| Refinement method | Full-matrix least-squares on $F^2$ |
| Data / restraints / parameters | 4656 / 0 / 316 |
| Goodness of fit on $F^2$ | 1.019 |
| Final R indices [$I > 2\sigma(I)$] | $R_1$ = 4.62%, $wR_2$ = 11.36% |
| R indices (all data) | $R_1$ = 6.53%, $wR_2$ = 12.52% |
| Largest diff. peak and hole | 1.157 and –0.918 e $Å^{-3}$ |

### 1.1.2. Characterization of 3($PF_6$) and the catalytic reaction at 25 °C

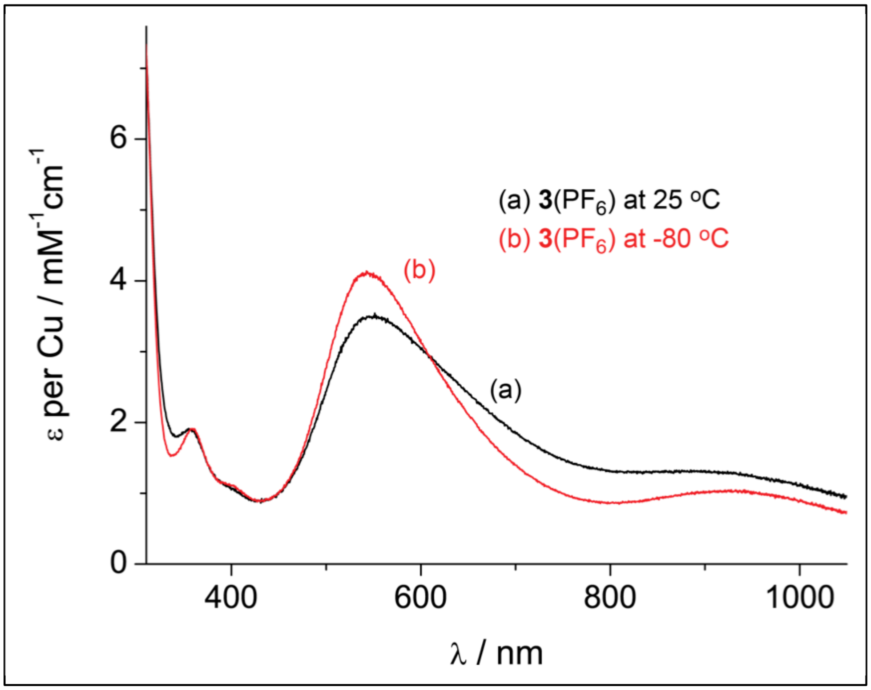

Figure S 1-2: UV-visible spectra of **3**($PF_6$) in $CH_2Cl_2$ at 25 °C and −80 °C.

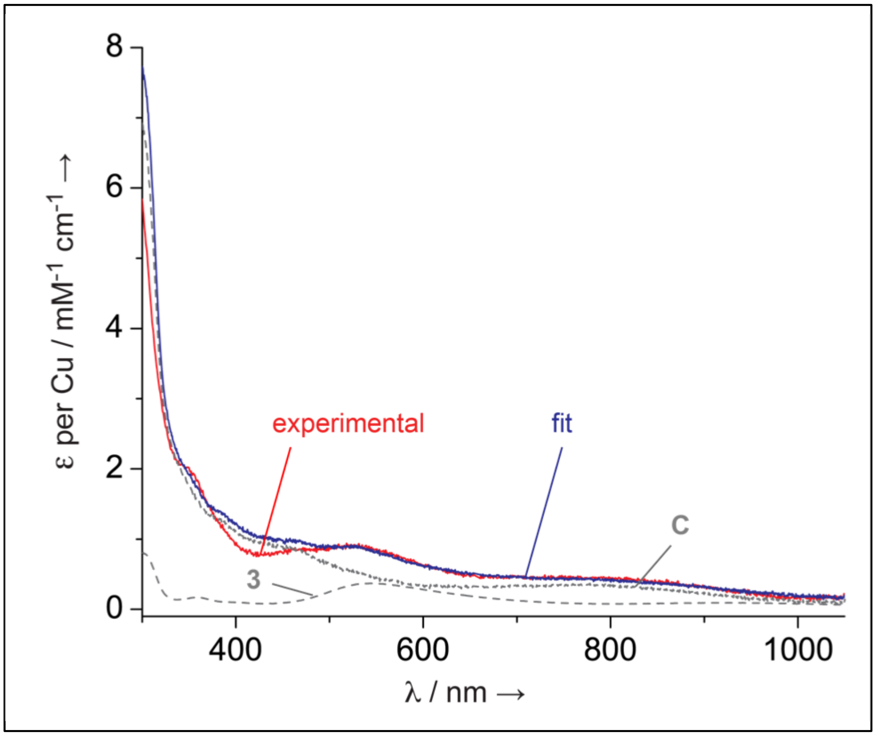

Figure S 1-3: Deconvolution of the spectrum obtained in Figure 2-1 after 8 min of reaction. Red: experimental trace, blue: fit via linear combination of known spectra of **2**, **3** and **4** (grey) with appropriate ratios. At this stage, the quantity of **3** corresponds to 100% of the Cu present in solution. As a note, the overlap of **4** ($\lambda_{max}$ = 389 nm) and its progressive conversion to **2** ($\lambda_{max}$ = 426 nm) are responsible for the shift of the 400-413 nm band upon reaction, as observed in Figure 2-1.

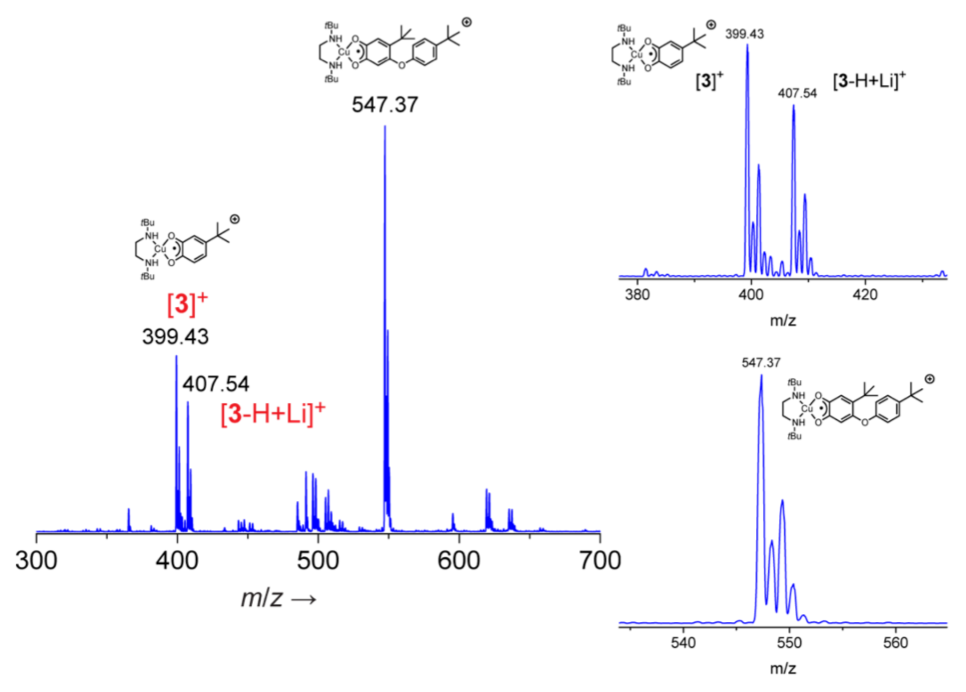

Figure S 1-4: A $CH_2Cl_2$ solution of 30.7 mm **1**, 4% $CuPF_6$, 8% DBED was oxygenated at 25 °C for 5 seconds, then purged with Ar, diluted with degassed $CH_3CN$ and injected in an ESI-MS. The spectrogram mainly shows the semiquinone complexes of **4** (complex **3**) and of **2** (complex **5**).

### 1.1.3. Formation constants for Cu(II)-semiquinone complexes 3 and 5

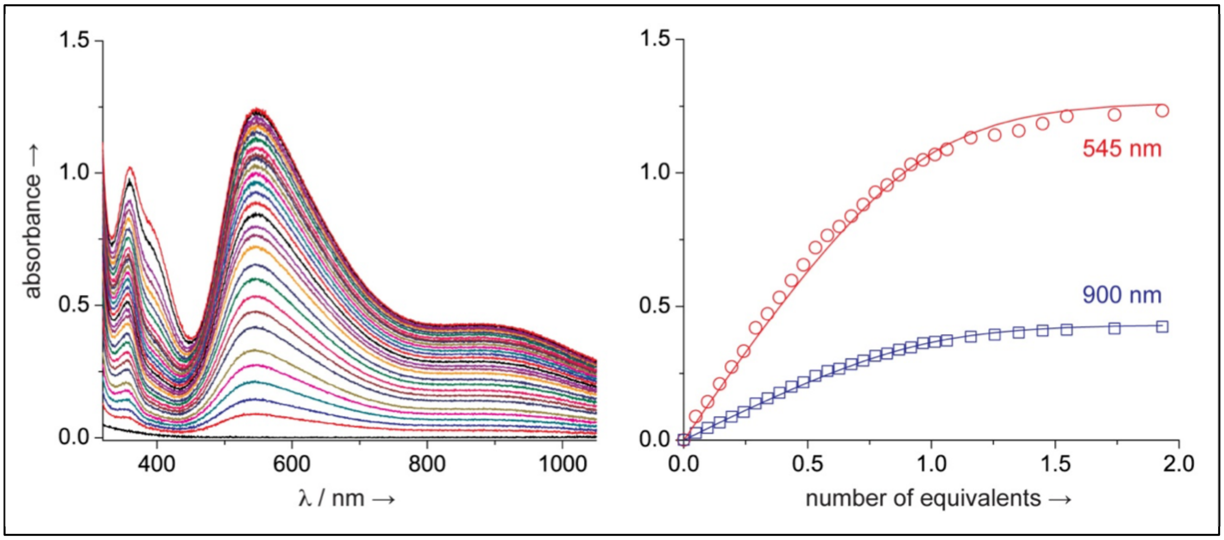

Figure S 1-5: Titration of a 0.36 mM solution of DBED:CuPF$_6$ (1:1) in CH$_2$Cl$_2$ with a 7.06 mM solution of **4** in CH$_2$Cl$_2$ at 23 °C in 5 μL increments. Pathlength = 1.0 cm. Multivariate fitting yielded a binding constant log$_{10}$ $K$ = 4.623 ±0.003 for a 1:1 model.

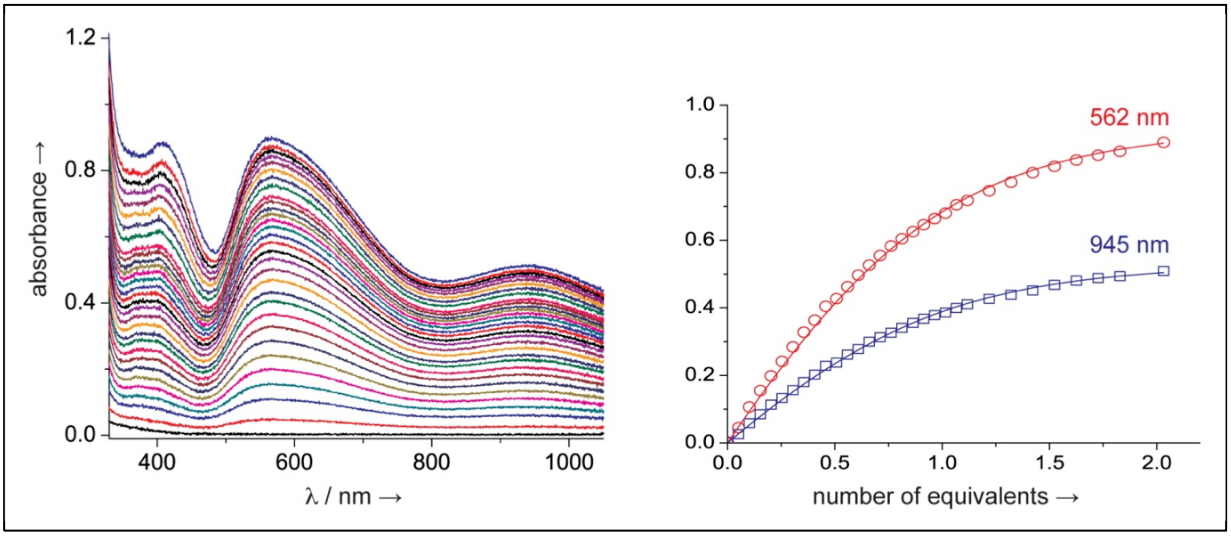

Figure S 1-6: Titration of a 0.36 mM solution of DBED:CuPF$_6$ (1:1) in CH$_2$Cl$_2$ with a 7.43 mM solution of **2** in CH$_2$Cl$_2$ at 23 °C in 5 μl increments. Pathlength = 1.0 cm. Multivariate fitting yielded a binding constant log$_{10}$ $K$ = 4.066 ±0.002 for a 1:1 model.

## 1.2. Low temperature experiments

### 1.2.1. Experiments at –115 °C

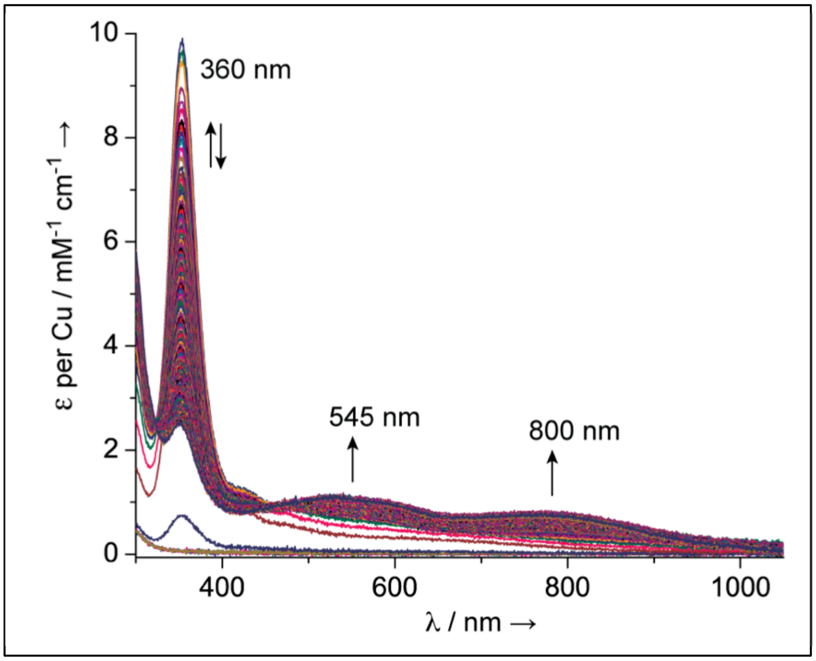

Figure S 1-7: Monitoring the catalytic reaction at −115 °C. Oxygenation at −115 °C of a solution with [$CuPF_6$] = 0.993 mM (4 mol%), [DBED] = 1.243 mM (8 mol%), [**1**] = 24.85 mM; one spectrum every 20 s. The features at 360 and 418 nm grow together, then decay to the spectrum of a brown solution with less intense features at 545 and 800 nm.

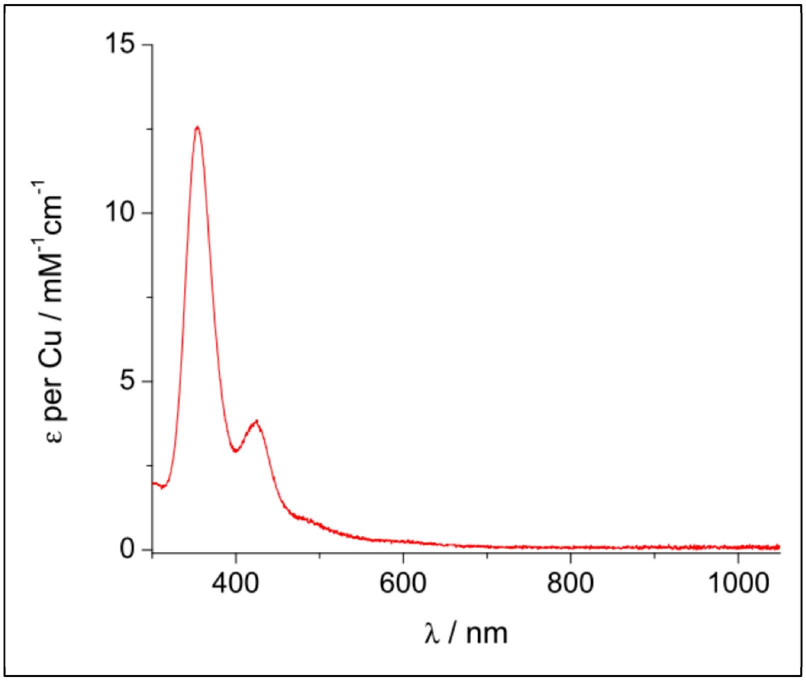

Figure S 1-8: Formation of the **P**/**O** mixture in 2-MeTHF at −115 °C by oxygenation of a 1:1 DBED-$CuPF_6$ mixture. **P** absorbs at 354 nm and **O** at 423 nm.

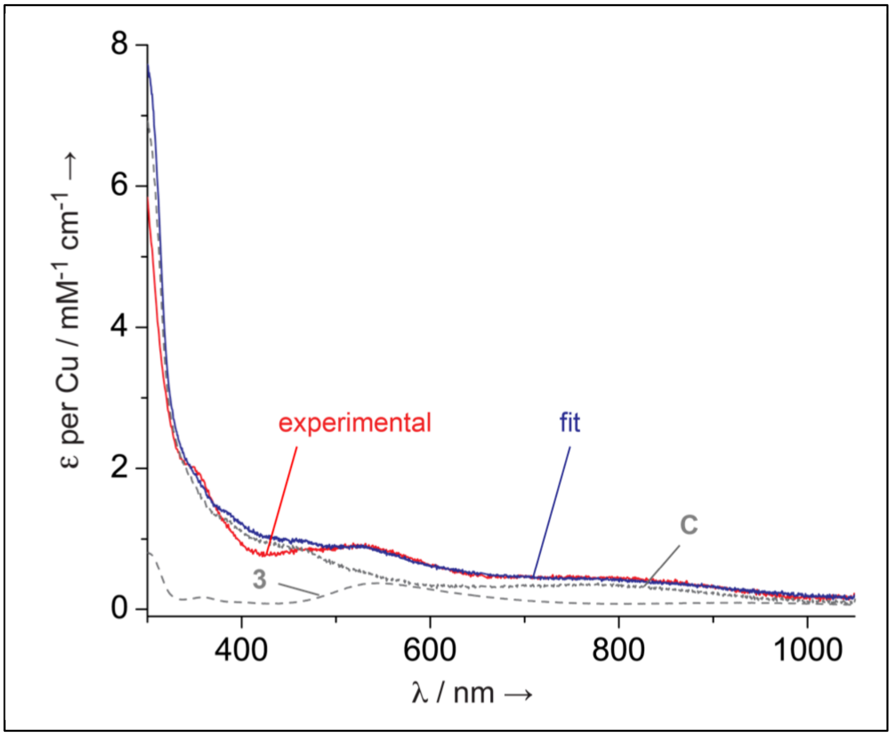

Figure S 1-9: Deconvolution of final spectrum after adding $O_2$ at −115 °C to a MeTHF solution containing **1** (6.8 mM), 14% $CuPF_6$ (1.0 mM), 18% DBED (1.2 mM). Red: experimental trace, blue: fit via linear combination of known spectra of **C** and **3** (grey).

### 1.2.2. Formation and protonation of C

**Sodium 4-*tert*-butylphenolate** was prepared by adding NaH (20 mg, 0.80 mmol, 1.5 equiv.) to 4-*tert*-butylphenol (80 mg, 0.53 mmol, 1 equiv.) in 5 mL of THF under $N_2$ in the glovebox. Once evolution of hydrogen ceased, the solution was filtered through a syringe microfilter (0.45 μm) and was used as is.

**DBEDH($PF_6$)** was prepared by adding $HPF_6$ (65% solution in water, 0.12 mL, 0.85 mmol) onto a solution of DBED (270 mg, 1.6 mmol, 1.9 equiv.) in 5 mL of MeOH. Subsequent evaporation to dryness in vacuo and trituration with diethyl ether yielded the compound as a white solid which was then stored inside the $N_2$-filled glovebox.

### 1.2.3. Closing the cycle

**Procedure for** Figure 2-5**.** A 1:1 solution of DBED: $CuPF_6$ (7.90 μmol each, 1.49 mM) in THF was cooled to −75 °C (i, black) and oxygenated to form the side-on peroxo species **P** (ii, red, in equilibrium with a small amount of its **O** isomer visible at ca. 400 nm). $O_2$ was then removed from the solution by bubbling Ar for 20 min. Addition of a THF solution containing 9.91 μmol of sodium 4-*tert*-butylphenolate ([Cu] = 1.44 mM, [DBED] = 1.44 mM, [ArONa] = 1.81 mM) leads to the formation of **C** (iii, blue). To this solution was added a THF solution containing 10.05 μmol of DBEDH($PF_6$) ([Cu] = 1.26 mM, [DBED] = 1.26 mM, [ArONa] = 1.58 mM, [DBEDH$PF_6$] = 1.60 mM). The solution rapidly forms **3** (iv, green) in concentration [**3**] = 0.64 mM based on $\varepsilon_{545}$(**3**) = 4,000 $M^{-1}$ $cm^{-1}$ at −75 °C. This corresponds to 50% of the total [Cu].

**Procedure for** Figure 2-6**.** A 1:1 solution of DBED:$CuPF_6$ (11.67 μmol each, 2.23 mM) in $CH_2Cl_2$ was cooled to −85 °C and oxygenated to form **P** (i, black). $O_2$ was then removed by bubbling $N_2$ and a $CH_2Cl_2$ solution containing 12 μmol **1** and 2.3 μmol DBED was added ([Cu] = 2.15 mM, [DBED] = 2.58 mM, [**1**] = 2.22 mM). The solution rapidly forms **3** (i, red) in concentration [**3**] = 1.20 mM based on $\varepsilon_{545}$(**3**) = 4,100 $M^{-1}$ $cm^{-1}$ at −85 °C. This corresponds to 56% of the total [Cu]. After $O_2$ is reintroduced, the quantity of **3** grows to [**3**] = 2.15 mM (iii, blue), *i.e.* 100% of the total [Cu].

## 1.3. Synthetic procedures for Table 2-1

### 1.3.1. Procedure for entry 3:

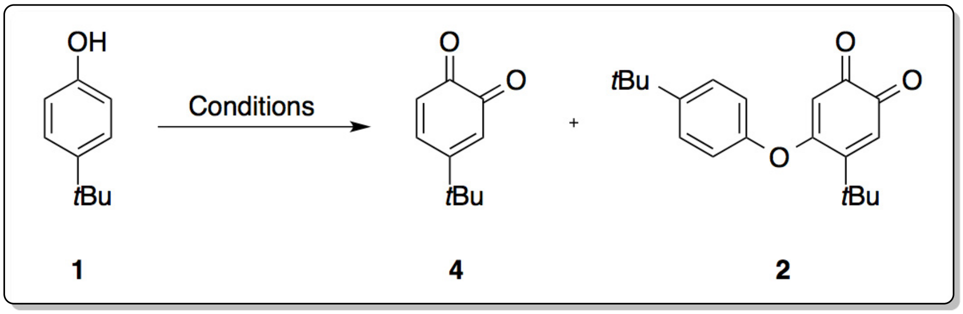

Scheme S 1-1: Catalytic oxidation of **1** in $CH_3CN$ at -40 ºC.

In a glovebox, DBED (10.9 μL, 8.61 mg, 0.05 mmol, 0.05 equiv.) was dissolved in 5 mL of $CH_3CN$ and was added solid $CuPF_6$ (14.9 mg, 0.04 mmol, 0.04 equiv.) and **1** (0.150 g, 1.0 mmol, 1.0 equiv) to give a homogeneous solution after stirring. The solution was then transferred to a 25-mL Radley tube, equipped with a Teflon-coated stir bar, and diluted to 10mL with $CH_3CN$ to give final phenol concentration of 0.1M. The reaction vessel was sealed with a Radley cap, removed from the glovebox, cooled to −40 °C, and stirred for 20 minutes. The Radley cap was then connected to a tank of $O_2$ and pressurized to 1 atm. Under a constant pressure of $O_2$ (1 atm), the reaction was vented 3 times for 10 s to remove $N_2$. The reaction mixture was then stirred at −40 °C for 4 h, depressurized by opening to the atmosphere and quenched by the addition of $NaHSO_4$ (10 mL, 10% by weight aqueous solution). The phases were then separated and the aqueous phase was extracted with $CH_2Cl_2$ (3 x 20 mL). The combined organic fractions were then dried over $MgSO_4$, filtered and concentrated *in vacuo* to afford a red solid. The resulting crude material was purified by flash column chromatography using a gradient column (5% EtOAc in hexanes to isolate **4**, and 10% EtOAc in hexanes to isolate **2**, 25 g Snap Ultra column) to afford **2** (26.5 mg, 0.09 mmol, 18%) and **4** (124.8 mg, 0.76 mmol, 76%) as a red solids.

### 1.3.2. Procedure for entry 4

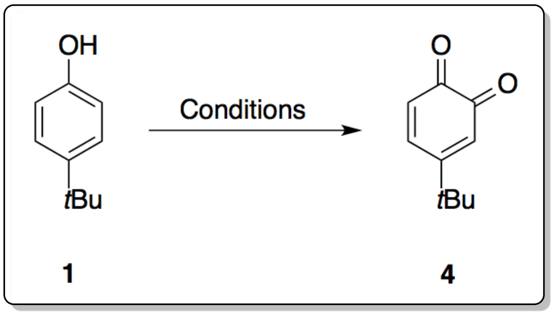

Scheme S 1-2: Stoichiometric oxygenation of **1** in $CH_2Cl_2$ at -78 ºC.

Using a glovebox, a 25-mL Radley tube, equipped with a Teflon-coated stir bar was charged with **1** (0.150 g, 1.0 mmol, 1.0 equiv), and $CH_2Cl_2$ (5 mL). In a separate, 10-mL round bottom flask $CuPF_6$ (372.6 mg, 1.0 mmol, 1.0 equiv.) and DBED (237 µL, 189.5 mg, 1.1 mmol, 1.1 equiv.) were dissolved in $CH_2Cl_2$ (5.0 mL) to afford a homogeneous pink solution. This solution was then added to the Radley tube via syringe to afford a final volume of 10 mL and a phenol concentration of 0.1M. The reaction vessel was sealed with a Radley cap, removed from the glovebox, cooled to −78 °C using a dry ice/acetone bath, and stirred at this temperature for 15 minutes. The Radley cap was then connected to a tank of $O_2$ and pressurized to 1 atm. Under a constant pressure of $O_2$ (1 atm), the reaction was vented 3 times for 10 s to remove $N_2$. The reaction mixture was then stirred at −78 °C for 4 h, depressurized by opening to the atmosphere and quenched by the addition of aq. 10% $NaHSO_4$ (10 mL). The reaction mixture was allowed to warm to rt, and diluted with $CH_2Cl_2$. The phases were then separated and the aqueous phase was extracted with $CH_2Cl_2$ (3 x 20 mL). The combined organic fractions were then dried over $MgSO_4$, filtered and concentrated *in vacuo* to afford a red solid. The resulting crude material was purified by flash column chromatography (7% EtOAc in hexanes, 25 g Snap Ultra column) to afford **4** (134.6 mg, 0.82 mmol, 82%) as a red solid.

### 1.3.3. Procedure for entry 5

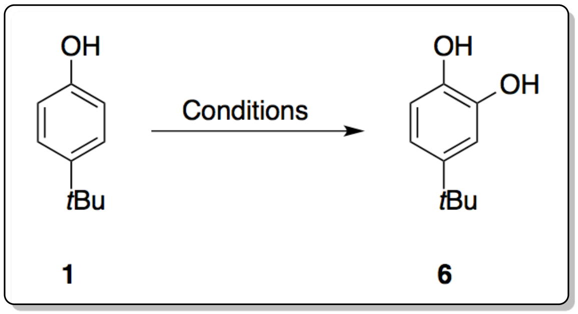

Scheme S 1-3: Stoichiometric oxygenation of **1** in $CH_2Cl_2$ at -78 ºC followed by reductive work-up.

Using a glovebox, a 25-mL Radley tube, equipped with a Teflon-coated stir bar was charged with **1** (0.150 g, 1.0 mmol, 1.0 equiv), and $CH_2Cl_2$ (5 mL). In a separate, 10-mL round bottom flask $CuPF_6$ (372.6 mg, 1.0 mmol, 1.0 equiv.) and DBED (237 µL, 189.5 mg, 1.1 mmol, 1.1 equiv.) were dissolved in $CH_2Cl_2$ (5.0 mL) to afford a homogeneous pink solution. This solution was then added to the Radley tube via syringe to afford a final volume of 10 mL and a phenol concentration of 0.1M. The reaction vessel was sealed with a Radley cap, removed from the glovebox, cooled to −78 °C using a dry ice/acetone bath, and stirred at this temperature for 15 minutes. The Radley cap was connected to a tank of $O_2$ and pressurized to 1 atm. Under a constant pressure of $O_2$ (1 atm), the reaction was vented 3 times for 10 s to remove $N_2$. The reaction mixture was then stirred at −78 °C for 4 h, depressurized by opening to the atmosphere and quenched by the addition of a saturated aqueous solution of $Na_2S_2O_4$ (6.0 mL). The reaction mixture was allowed to warm to rt and was stirred for 1h at rt. The reaction mixture was transferred to a 250-mL separatory flask and diluted with $CH_2Cl_2$ (20 mL). The phases were then separated and the aqueous phase was extracted with $CH_2Cl_2$ (3 x 20 mL). The combined organic fractions were then dried over $MgSO_4$, filtered and concentrated *in vacuo* to afford a brown residue. The resulting crude material was purified by flash column chromatography (20% EtOAc in hexanes, 25 g Snap Ultra column) to afford **6** (134.6 mg, 0.81 mmol, 81%) as a brown solid.

**Compound 6: $^1$H-NMR** (400 MHz, $CDCl_3$): δ = 6.92 (d, *J* = 1.9 Hz, 1H), 6.81 (d, *J* = 1.9 Hz, 1H), 6.80 (s, 1H), 5.16 (brs, 1H), 5.06 (brs, 1H), 1.27 (s, 9H) ppm.

*Compound **6** is a commercially available reagent [CAS: 98-29-3].*

## 1.4. Kinetic analysis and isotopic effects

### 1.4.1. Kinetic profiles

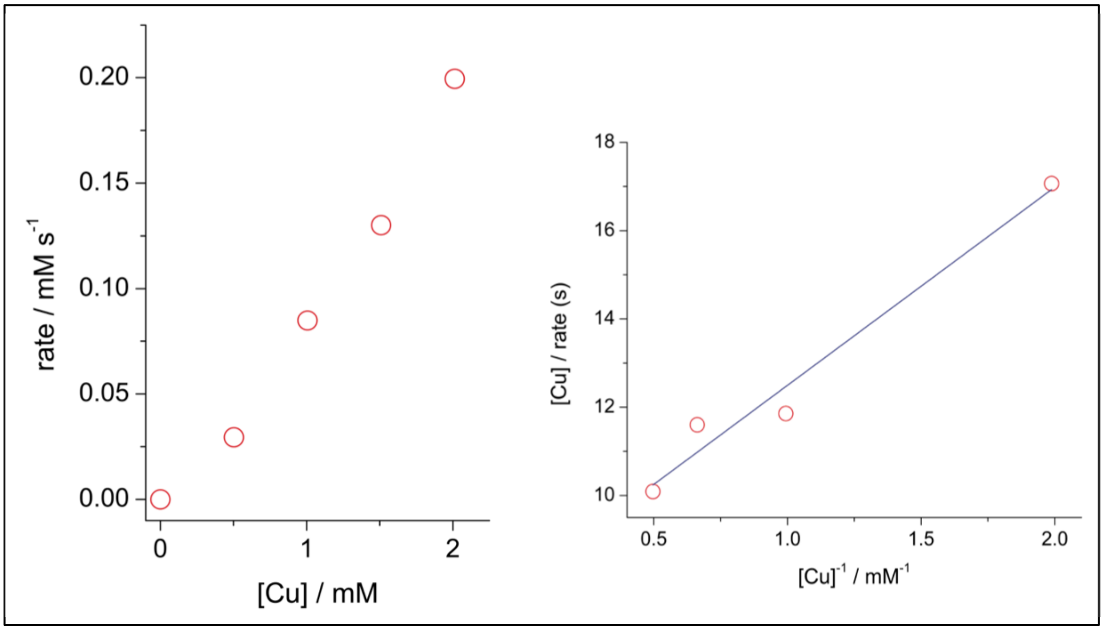

Figure S 1-10: Dependence of the initial rate of formation of **3** on: [$CuPF_6$] = 0.50-2.01 mM while [**1**] = 9.99 mM, and [DBED] = 10.33 mM. $CH_2Cl_2$, −80 °C.

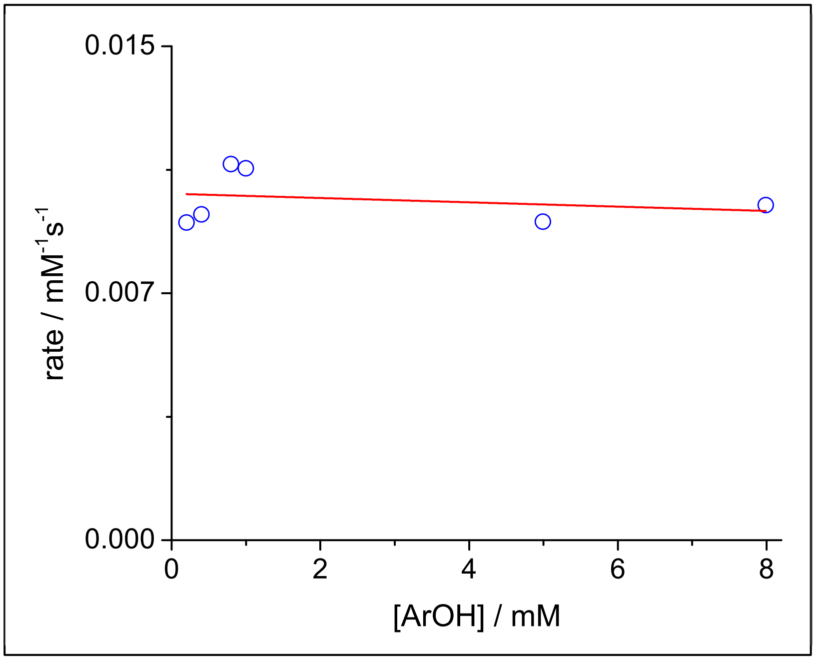

Figure S 1-11: Dependence of the initial rate of formation of **3** on [**1**] = 0.20, 0.40, 0.80, 1.0, 5.0 and 8.0 mM while [$CuPF_6$] = 0.50 mM and [DBED] = 0.55 mM. $CH_2Cl_2$, −80 °C.

### 1.4.2. Isotopic effects: comparison of 1, $1^{HD}$ and $1^{DD}$

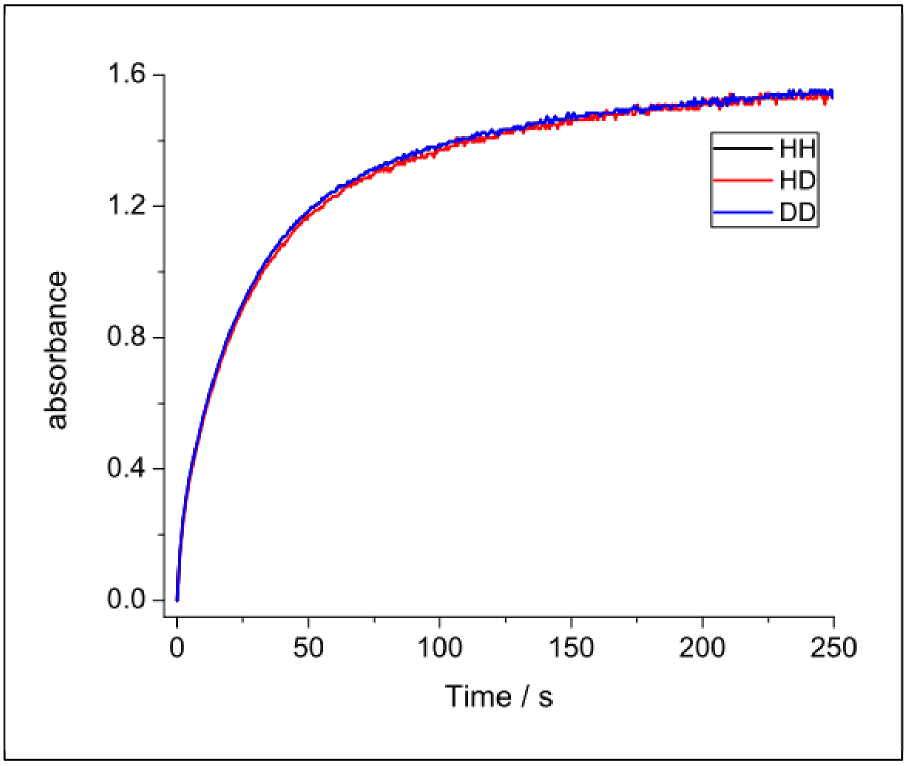

Figure S 1-12: Growth profile for the formation of **3** using **1** (HH), 2-D-4-*tert*-butylphenol $\mathbf{1}^{HD}$ (HD), and 2,6-di-D-4-*tert*-butylphenol $\mathbf{1}^{DD}$ (DD) in stopped-flow experiments at –80 °C. [$CuPF_6$] = 0.74 mM, [DBED] = 0.93 mM, [phenol] = 18.57 mM.

### 1.4.3. Isotopic effects: intramolecular competition experiment with $1^{HD}$

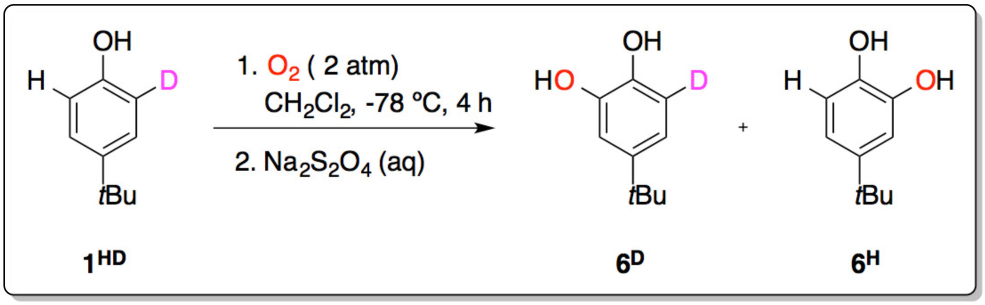

Scheme S 1-4: Intramolecular competition experiment.

Table S 1-2: Measurement of the intramolecular KIE with $\mathbf{1^{HD}}$.[a]

| Experiment [b] | Ion counts at $m/z$ = 166 for $\mathbf{6^{H}}$ | Ion counts at $m/z$ = 167 for $\mathbf{6^{D}}$ | Ratio $\mathbf{6^{D}}/\mathbf{6^{H}}$ |
|---|---|---|---|
| 174-1 [c] | 504527.692 | 433806.877 [d] | 0.860 |
| 174-2 [c] | 477748.907 | 411798.873 [d] | 0.862 |
| 175-1 [c] | 494012.557 | 419903.682 [d] | 0.850 |
| 175-2 [c] | 406583.595 | 349998.235 [d] | 0.861 |
| 176-1 | 428979.342 | 377105.335 [d] | 0.879 |
| 176-2 | 396571.342 | 347507.380 [d] | 0.876 |
| 177-1 | 533717.468 | 468447.535 [d] | 0.878 |
| 177-2 | 490272.81 | 429136.320 [d] | 0.875 |
| | | **Average:** | **0.868** |
| | | Standard deviation: | 0.011 |

[a] Conditions: DBED (53 mg, 0.31 mmol, 1.2 equiv.) and $CuPF_6$ (98 mg, 0.26 mmol, 1 equiv.) were combined in 2 mL $CH_2Cl_2$ under nitrogen. Solid $\mathbf{1^{HD}}$ (40 mg, 0.26 mmol, 1 equiv.) was added and the solution transferred to a Radley tube and diluted to 5 mL, giving final concentrations: $[CuPF_6]$ = 52 mM, [DBED] = 58 mM, $[\mathbf{1^{HD}}]$ = 52 mM. The solution was cooled to −78 °C and oxygenated ($O_2$ pressure = 2 bar) for 4 hours, after which a saturated aqueous $Na_2S_2O_4$ solution was added and the mixture warmed up to 25 °C. The organic layer was separated and washed with water (20 mL) then brine (20 mL), dried over $Na_2SO_4$, filtered, and the solvent was removed under reduced pressure to give a white solid. The product was dissolved in diethyl ether and analyzed by GC-MS. [b] Each solution was measured twice on the GC-MS. [c] These experiments were carried out in the presence of 100 mg of 4Å molecular sieves, with no observable difference from the other experiments. [d] These values were corrected from the 11% signal arising from the isotopic pattern of $\mathbf{6^{H}}$.

# 2. Supplementary Information for Chapter 3

## Catalytic Aerobic Oxidation of Phenols to *Ortho*-Quinones with Air-Stable Copper Precatalysts

M.S. Askari, L.A. Rodríguez-Solano, A. Proppe, B. McAllister, J.-P. Lumb and X. Ottenwaelder*

## 2.1. General Experimental

Chemicals and solvents were purchased from Sigma Aldrich, Alfa Aesar or Strem Chemicals. Inhibitor-free solvents were dried using a MBraun SPS 800, transferred to an inert-atmosphere glove box (MBraun Labmaster, <1 ppm $O_2$ and $H_2O$, filled with a dry $N_2$ atmosphere), further degassed under vacuum and stored over activated molecular sieves (4 Å). *tert*-Butylphenol **1** was purified by double recrystallization from $CH_2Cl_2$/hexanes. *N*,*N'*-di-*tert*-butylethylenediamine (DBED) was distilled over $CaH_2$ under $N_2$ and stored in an inert atmosphere glove box. The copper(I) salt $[Cu(CH_3CN)_4](PF_6)$, abbreviated $CuPF_6$, was made via a literature procedure.[168] $Cu^{II}(TfO)_2\cdot 4H_2O$,[200] anhydrous $Cu^{II}(TfO)_2$,[200] and $[Cu(MeCN)_{3.5}](MsO)$[58] were prepared according to literature procedures. $Cu^{II}(OAc)_2\cdot MeCN$ was prepared by reacting $Cu^{II}O$ with acetic acid and acetic anhydride (1:1) in dry acetonitrile then extracted by Soxhlet (48h). All copper(I) complexes were stored inside the glovebox.

Unless otherwise noted, reactions were performed in oven-dried glassware under a positive pressure of nitrogen using standard synthetic inert-atmosphere techniques. Bulk oxidation reactions were set-up in the glovebox in 25 mL, oven-dried Radley tubes equipped with a Teflon-coated stir bar. The reaction vessels were then connected to a cylinder of $O_2$, purged three times with $O_2$ and then overpressurized to +1.0 atm.

UV-visible spectra were recorded on a B&W Tek iTrometer equipped with fiber-optic cables connected to a Hellma full-quartz dip-probe having a 1.0 mm pathlength. The probe was immersed in the solution inside a custom-made Schlenk flask.

## 2.2. Syntheses and Characterizations

### 2.2.1. Synthesis of 3

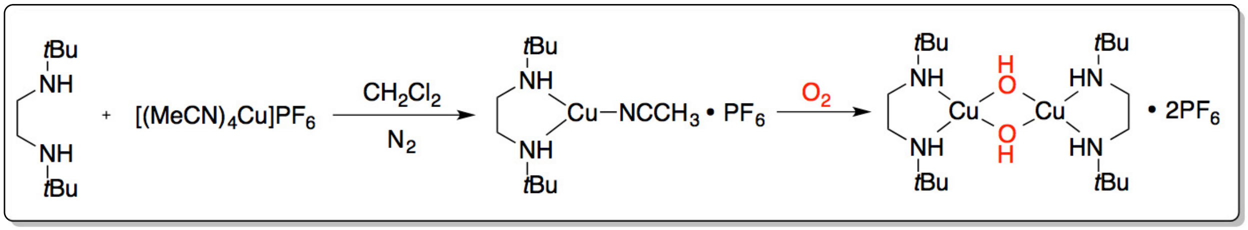

Scheme S 2-1: Synthesis of $[(DBED)Cu(OH)]_2 \cdot (2PF_6)$.

**3:**[158] In the glovebox, solid $[Cu(MeCN)_4]PF_6$ (370 mg, 0.99 mmol) was added to a solution of DBED (172 mg, 1.0 mmol) in 5 mL of $CH_2Cl_2$. The resulting pink solution was stirred until all the copper dissolved. The solution was then exposed to oxygen or air upon which the color changed to deep green. Diethyl ether was added to the mixture to precipitate the complex. The solid was filtered off, washed with $Et_2O$, and dried in vacuo. Crystals suitable for x-ray diffraction were grown by slow evaporation of a concentrated solution in $CH_2Cl_2$.

### 2.2.2. Synthesis of 4

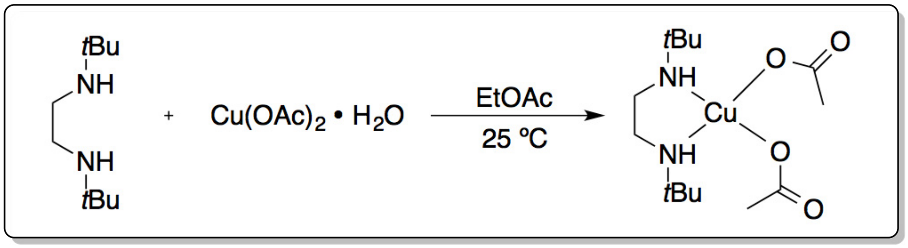

Scheme S 2-2: Synthesis of $[(DBED)Cu(OAc)_2]$.

**4:** To a solution of DBED (1.9 g, 11 mmol) in 10 mL ethyl acetate was added solid $Cu^{II}(OAc)_2 \cdot H_2O$ (2.0 g, 10 mmol). The blue solution was left stirring until all the copper was dissolved. The solution was then filtered and solvent was removed in vacuo to give a blue solid residue. The solid was triturated in $Et_2O$, filtered off, and dried in vacuo to give a blue powder. Yield: 82%. Elemental analysis (mol%): expected for $C_{14}H_{30}N_2O_4Cu$: C, 47.51; H, 8.54; N, 7.81; found: C, 47.67; H, 8.58; N, 7.85. Crystals suitable for X-ray diffraction were grown by slow evaporation of a concentrated solution of **4** in ethyl acetate.

## 2.3. Crystallographic details

**3:** A rhomb-like specimen of $C_{20}H_{50}Cu_2F_6N_4O_2P_2$, approximate dimensions 0.367 mm x 0.469 mm x 0.503 mm, was used for the X-ray crystallographic analysis. The integration of the data using a monoclinic unit cell yielded a total of 12237 reflections to a maximum θ angle of 27.55° (0.77 Å resolution), of which 12237 were independent (average redundancy 1.000, completeness = 94.9%, $R_{sig}$ = 3.62%) and 8327 (68.05%) were greater than $2\sigma(F^2)$. Unit cell The final cell constants of a = 24.870(3) Å, b = 16.8713(18) Å, c = 18.708(2) Å, β = 120.7840(10)°, volume = 6743.7(13) $Å^3$, are based upon the refinement of the XYZ-centroids of reflections above 20 σ(I). Scaling The calculated minimum and maximum transmission coefficients (based on crystal size) are 0.6216 and 0.7456. The structure was solved and refined using the Bruker SHELXTL Software Package, using the space group C 1 2/c 1, with Z = 8 for the formula unit, $C_{20}H_{50}Cu_2F_6N_4O_2P_2$. Structure refinement The final anisotropic full-matrix least-squares refinement on $F^2$ with 393 variables converged at R1 = 6.33%, for the observed data and wR2 = 16.59% for all data. The goodness-of-fit was 1.115. The largest peak in the final difference electron density synthesis was 0.895 $e^-/Å^3$ and the largest hole was -0.651 $e^-/Å^3$ with an RMS deviation of 0.112 $e^-/Å^3$. On the basis of the final model, the calculated density was 1.567 $g/cm^3$ and F(000), 3280 $e^-$.

**4:** A light blue rhomb-like specimen of $C_{14}H_{30}CuN_2O_4$, approximate dimensions 0.422 mm x 0.558 mm x 1.140 mm, was used for the X-ray crystallographic analysis. The X-ray intensity data were measured on measured on Mo Kα radiation (λ = 0.71073 Å) of Bruker APEX DUO. A total of 1464 frames were collected. The total exposure time was 4.07 hours. Integration The frames were integrated with the Bruker SAINT software package using a narrow-frame algorithm. The integration of the data using a monoclinic unit cell yielded a total of 9419 reflections to a maximum θ angle of 27.98° (0.76 Å resolution), of which 2002 were independent (average redundancy 4.705, completeness = 93.9%, $R_{int}$ = 2.07%, $R_{sig}$ = 1.52%) and 1867 (93.26%) were greater than $2\sigma(F^2)$. Unit cell The final cell constants of a = 15.876(4) Å, b = 11.938(3) Å, c = 12.088(6) Å, β = 129.534(3)°, volume = 1766.9(11) $Å^3$, are based upon the refinement of the XYZ-centroids of 6748 reflections above 20 σ(I) with $4.765° < 2\theta < 55.95°$. Scaling Data were corrected for absorption effects using the multi-scan method (SADABS). The ratio of minimum to maximum apparent transmission was 0.697. The calculated minimum and maximum transmission coefficients (based on crystal size) are 0.3295 and 0.6202. The structure was solved and refined using the Bruker SHELXTL Software Package, using the space group C 1 2/c 1, with Z = 4 for the formula unit, $C_{14}H_{30}CuN_2O_4$. Structure refinement The final anisotropic full-matrix least-squares refinement on $F^2$ with 100 variables converged at R1 = 2.35%, for the observed data and wR2 = 6.66% for all data. The goodness-of-fit was 1.103. The largest peak in the final difference electron density synthesis was 0.283 $e^-/Å^3$ and the largest hole was -0.440 $e^-/Å^3$ with an RMS deviation of 0.065 $e^-/Å^3$. On the basis of the final model, the calculated density was 1.331 g/cm$^3$ and F(000), 756 $e^-$.

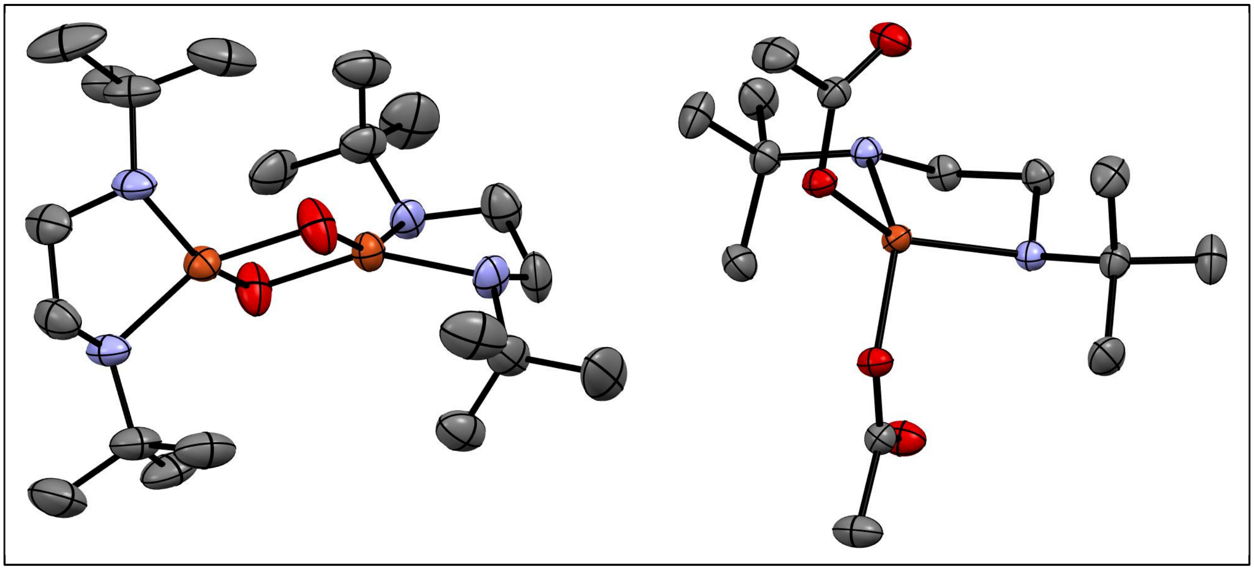

Figure S 2-1: ORTEP representation at 50% ellipsoid probability of **3** (left, one cation only) and **4** (right). Hydrogen atoms removed for clarity. Selected bond lengths and angles for **4**: Cu–O = 1.9272(11) Å, Cu–N = 2.0282(13) Å. O1–Cu1–O1 = 87.19(6)°, O1–Cu1–N1 = 146.62(5)°, N1–Cu1–N1 = 87.18(8)°.

Table S 2-1: Crystal data and structure refinement for **3** and **4**.

| | | |
|---|---|---|
| CCDC deposition number | 1051251 | 1051252 |
| Empirical formula | $C_{20}H_{50}N_4O_2F_6P_2Cu_2$ | $C_{14}H_{30}N_2O_4Cu$ |
| Formula weight | 795.66 | 353.94 |
| Temperature | 150(2) | 293(2) K |
| Wavelength | 0.71073 Å | 0.71073 Å |
| Crystal system | Monoclinic | Monoclinic |
| Space group | C2/c | C2/c |
| Unit cell dimensions | *a* = 24.870(3) Å<br>*b* = 16.8713(18) Å<br>*c* = 18.708(2) Å<br>α = 90.00°<br>β = 120.7840(10)°<br>γ = 90.00° | *a* = 15.876(4) Å<br>*b* = 11.938(3) Å<br>*c* = 12.088(6) Å<br>α = 90.00°<br>β = 129.534(3)°<br>γ = 90.00° |
| Volume | 6743.8(13) | 1766.9(11) $Å^3$ |
| Z | 8 | 4 |
| Density (calculated) | 1.567 $g/cm^3$ | 1.331 $g/cm^3$ |
| Absorption coefficient | 1.448 $mm^{-1}$ | 1.252 $mm^{-1}$ |
| F(000) | 3280 | 756 |
| Crystal size | 0.503 × 0.469 × 0.367 mm | 1.14 × 0.558 × 0.422 mm |
| Theta range for data collection | 2.26 – 27.44° | 2.38 – 27.98° |
| Index ranges | *h* = −32→27<br>*k* = 0→21<br>*l* = 0→24 | *h* = −19→20<br>*k* = −15→14<br>*l* = −15→15 |
| Reflections collected | 12237 | 9419 |
| Independent reflections | 12237 | 2002 ($R_{int}$ = 2.07%) |
| Completeness | 94.9% | 93.9% |
| Absorption correction | Multiscan | Multiscan |
| Refinement method | Full-matrix least-squares on $F^2$ | Full-matrix least-squares on $F^2$ |
| Data / restraints / parameters | 12237 / 0 / 393 | 2002 / 0 / 100 |
| Goodness of fit on $F^2$ | 1.115 | 1.103 |
| Final R indices [$I > 2\sigma(I)$] | $R_1$ = 6.33%, $wR_2$ = 14.17% | $R_1$ = 2.35%, $wR_2$ = 6.49% |
| R indices (all data) | $R_1$ = 10.43%, $wR_2$ = 16.59% | $R_1$ = 2.62%, $wR_2$ = 6.66% |
| Largest diff. peak and hole | 0.895 and −0.651 e $Å^{-3}$ | 0.283 and −0.440 e $Å^{-3}$ |

## 2.4. Typical Reaction Procedure

For reproducibility of the yield measurements, solutions were prepared in the glovebox prior to oxygenation. A solution containing DBED (0.1 mol), $Cu^{II}(OAc)_2{\cdot}H_2O$ (0.05 mol), and phenol (1 mmol) in 10 mL $CH_2Cl_2$ was placed in a Radley tube equipped with a stir bar, then sealed with a Radley cap. Outside the glovebox, the tube was then pressurized with 2 atmospheres of dry $O_2$ (after 5 purges) and left stirring for 4 hours. The reaction mixture was then transferred to a separatory funnel and hexamethylbenzene (0.15 equiv.) was added. The organic layer was washed twice with aqueous 10% $NaHSO_4$, dried over $Na_2SO_4$, and filtered. Evaporation of the solvent under reduced pressure afforded the quinone which was analyzed by NMR in $CDCl_3$.

Alternatively, the reaction can be set up in the air as follow: the 1:1 mixture of DBED and $Cu^{II}(OAc)_2{\cdot}H_2O$ in 5 mL $CH_2Cl_2$ was placed in the Radley tube and solubilized. Then a solution of the phenol in 5 mL $CH_2Cl_2$ was added and the vessel was closed, purged and pressurized with $O_2$.

## 2.5. Solvent Screening

Table S 2-2: Solvent screening of the $Cu^{II}(OAc)_2 \cdot H_2O$-precatalyzed reaction [a]

| Entry | Solvent | Yield (%) [b] |
|---|---|---|
| 1 | Dichloromethane | 98 |
| 2 | Chloroform | <30 |
| 3 | Tetrahydrofuran | 31 |
| 4 | Acetone | 31 |
| 5 | Ethyl acetate | 65 |
| 6 | Toluene | 60 |
| 7 | Hexanes | 3 |
| 8 | Dimethylsulfoxide | 32 |
| 9 | Acetonitrile | 93 |
| 10 | Methanol | 17 |
| 11 | Ethanol | 0 |

[a] Conditions: 0.666 mmol **1**, 5% Cu, 10% DBED, 6 mL solvent (0.1 M), 2 atm $O_2$, 4 h, 25°C. [b] NMR yield calculated based on relative peak areas of **1** and **2**.

## 2.6. UV-Visible Spectroscopic Monitoring of the Reactions

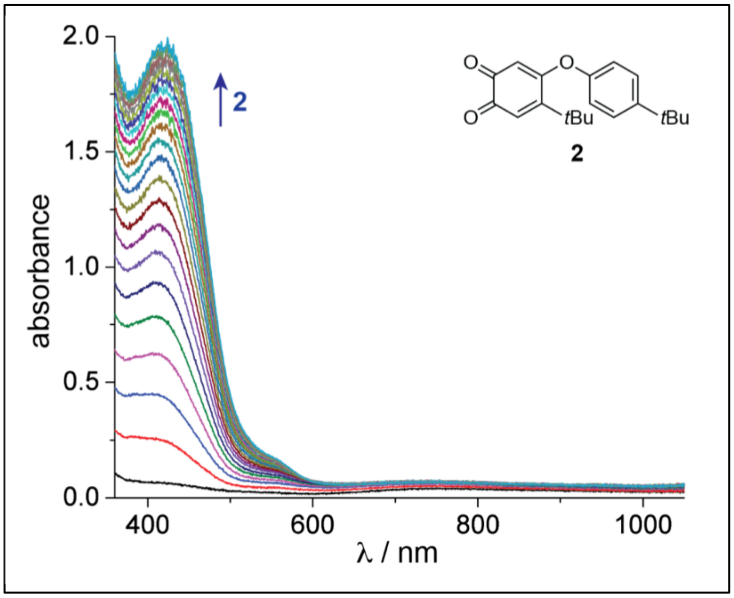

Figure S 2-2: In-situ UV-visible monitoring of the reaction of **1** (50 mM) with 5% $Cu^{II}(OAc)_2 \cdot H_2O$ and 10% DBED, $CH_2Cl_2$ under 1.1 atm $O_2$ at 25°C. One spectrum every 2 min. The reaction was stopped after 4h, at which time, the final yield of **2** was 82% (reaction was not complete at this Cu concentration and under this lower $O_2$ pressure than in the bulk).

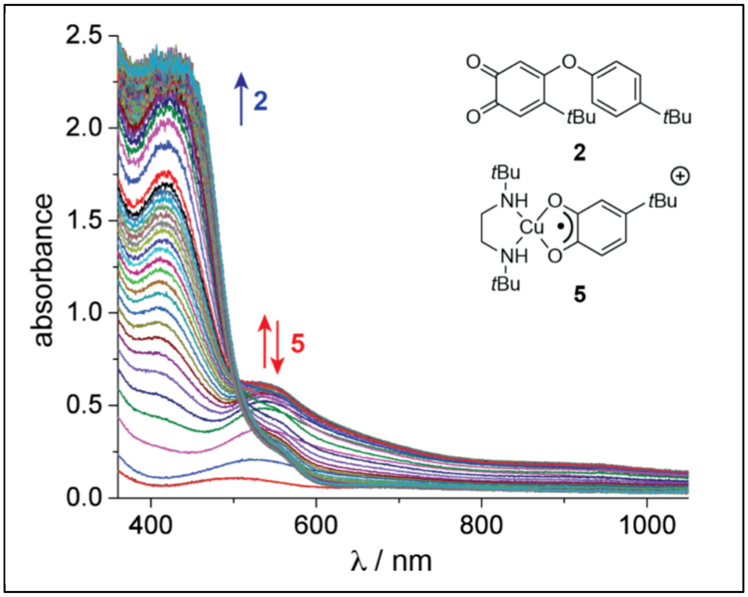

Figure S 2-3: In-situ UV-visible monitoring of the reaction of **1** (50 mM) with 5% $Cu^{II}(OTf)_2 \cdot 4\ H_2O$ and 10% DBED, $CH_2Cl_2$ under 1.1 atm $O_2$ at 25°C. First part of the growth (until $A_{416} \approx 1.75$): one spectrum every 10s, then one spectrum every 1 min, at which point the absorbance of **2** saturates. Final yield of **2** was 98%.

# 3. Supplementary Information for Chapter 4

**The Two Spin States of an End-On Copper(II)-Superoxide Mimic**

Mohammad S. Askari, Brigitte Girard, Muralee Murugesu and Xavier Ottenwaelder*

## 3.1. Experimental procedures

All the syntheses of the copper complexes were performed in a dry nitrogen filled glove-box ($O_2 < 0.1$ ppm, $H_2O < 0.1$ ppm). Solvents were dried by standard procedures, degassed, and stored over activated molecular sieves (4 Å) in the glove-box. The ligand $Me_6$tren was prepared following a literature procedure,[201] distilled over $CaH_2$ under vacuum, and stored under the inert atmosphere of the glove-box. The copper salts $[Cu(MeCN)_4](TfO)$ and $[Cu(MeCN)_4](SbF_6)$ were prepared according to the standard literature procedure using TfOH or $HSbF_6$ (Sigma-Aldrich).[168] Nitrosobenzene (Sigma-Aldrich) was stored in the glove-box at -30 °C.

### 3.2. Solid State UV-vis

UV-visible spectra were recorded on an Agilent 8453 spectrophotometer. The samples were prepared by grinding the compounds in Nujol and placing the suspension between two quartz disks.

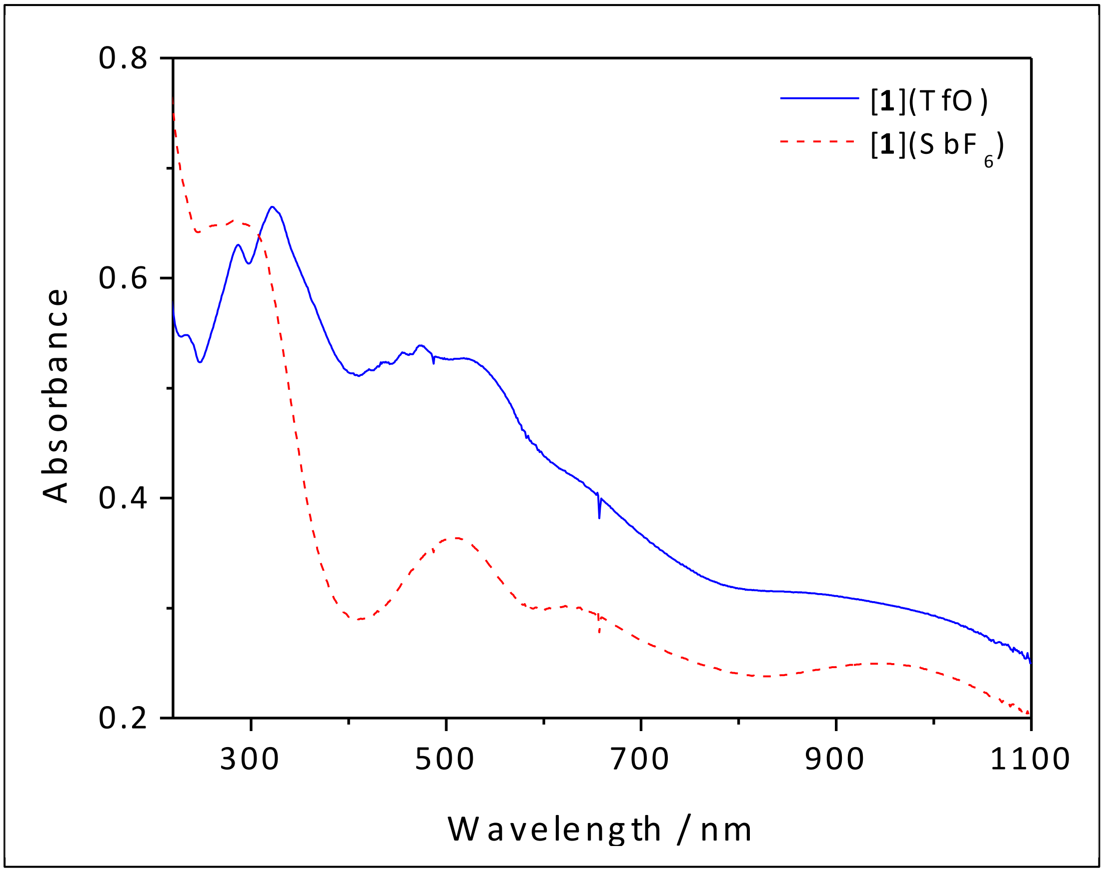

Figure S 3-1: Solid-state UV-vis spectra of [**1**](TfO) and [**1**]SbF$_6$.

## 3.3. Magnetic Behaviour of [1](TfO):

Variable temperature dc magnetic susceptibility measurements were performed on a 50 mg crushed crystalline sample in the temperature range of 2.5–300K and an applied dc field of 1000 Oe. The $\chi T$ *vs*. $T$ plot shown below indicates a room temperature value of 0.79 $cm^3 \cdot K \cdot mol^{-1}$ which is in good agreement with the value for two non-interacting S=1/2 spins (0.75 $cm^3 \cdot K \cdot mol^{-1}$). The $\chi T$ product increases immediately upon decreasing the temperature indicating strong ferromagnetic coupling within the molecule.

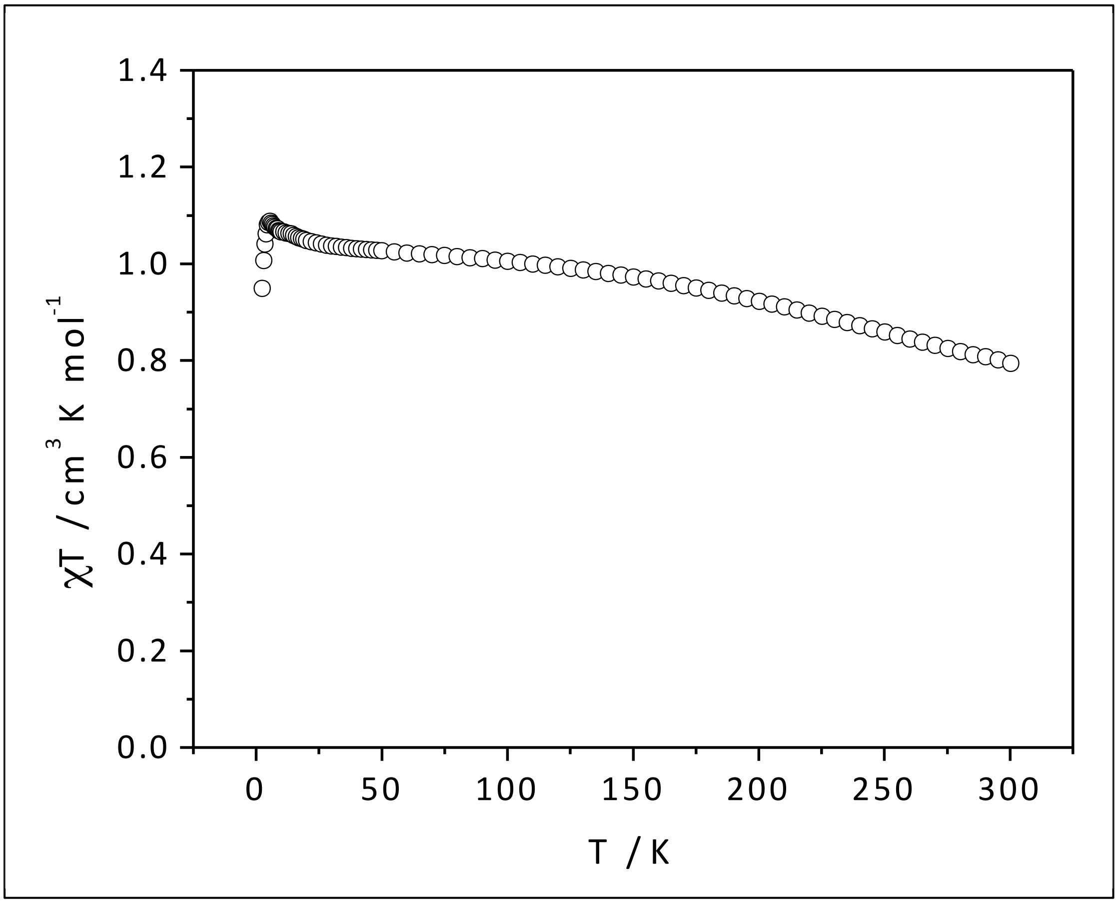

Figure S 3-2: Variable temperature dc magnetic susceptibility measurement on [**1**](TfO).

## 3.4. Computational Details

The calculations were performed using the 6-31G(d) basis set and the BP86 functional[202-204] with the Gaussian-09 quantum chemistry package.[205] The crystal structure geometries were used as the initial coordinates for optimization. Atomic coordinates of the optimized geometries:

### 1. [(Me$_6$tren)Cu(PhNO)]$^+$, S=0

| Atom | X | Y | Z |
|---|---|---|---|
| Cu | 0.7142660 | -0.0470230 | -0.0764740 |
| O | -0.9281390 | -0.0755350 | -1.0260120 |
| N | -1.8375040 | 0.8438600 | -0.8109080 |
| N | 1.3759630 | -1.6342900 | -1.3573900 |
| N | 0.1147930 | -0.4457450 | 1.9089430 |
| N | 1.1565150 | 2.0746190 | -0.6159380 |
| N | 2.6750100 | -0.0424070 | 0.6324210 |
| C | -3.1037080 | 0.3368950 | -0.4704680 |
| C | -4.0999330 | 1.3183380 | -0.2230490 |
| H | -3.8155530 | 2.3744690 | -0.2838930 |
| C | -5.4093280 | 0.9328210 | 0.0767460 |
| H | -6.1735030 | 1.6943120 | 0.2648740 |
| C | -5.7463520 | -0.4323580 | 0.1322210 |
| H | -6.7732210 | -0.7348260 | 0.3624920 |
| C | -4.7636480 | -1.4127030 | -0.1194550 |
| H | -5.0356070 | -2.4738040 | -0.0891460 |
| C | -3.4521770 | -1.0404070 | -0.4208660 |
| H | -2.6869800 | -1.7900810 | -0.6424520 |
| C | 3.4919160 | -0.9139710 | -0.2626360 |
| H | 4.4016940 | -1.2792290 | 0.2560320 |
| H | 3.8370660 | -0.2985740 | -1.1099830 |
| C | 2.6626010 | -2.0975680 | -0.7741060 |
| H | 3.2569610 | -2.6853750 | -1.5051620 |
| H | 2.4213970 | -2.7814160 | 0.0598890 |
| C | 0.4219650 | -2.7668730 | -1.4693030 |
| H | 0.7929470 | -3.5413300 | -2.1719790 |
| H | -0.5404680 | -2.3743230 | -1.8322430 |
| H | 0.2663500 | -3.2273470 | -0.4806310 |

| | | | |
|---|---|---|---|
| C | 1.5752710 | -1.0872730 | -2.7242280 |
| H | 1.9080850 | -1.8767540 | -3.4299690 |
| H | 2.3303900 | -0.2852500 | -2.7124820 |
| H | 0.6206420 | -0.6630970 | -3.0727600 |
| C | 3.1880490 | 1.3616210 | 0.6348470 |
| H | 4.2968850 | 1.3785750 | 0.6317440 |
| H | 2.8673400 | 1.8386860 | 1.5762210 |
| C | 2.6378770 | 2.1425050 | -0.5627450 |
| H | 3.0011690 | 3.1919920 | -0.5230100 |
| H | 3.0250300 | 1.7112890 | -1.5037990 |
| C | 0.6792380 | 2.4506900 | -1.9725470 |
| H | 0.9926650 | 3.4828230 | -2.2364430 |
| H | -0.4184950 | 2.3820430 | -1.9852720 |
| H | 1.0879470 | 1.7536720 | -2.7202800 |
| C | 0.5495580 | 3.0269450 | 0.3465440 |
| H | 0.7988440 | 4.0788940 | 0.0889990 |
| H | 0.9078280 | 2.8296220 | 1.3708440 |
| H | -0.5436790 | 2.8946000 | 0.3170980 |
| C | 2.6085500 | -0.5981720 | 2.0165120 |
| H | 3.4986160 | -0.3053800 | 2.6099910 |
| H | 2.6263880 | -1.6988020 | 1.9450750 |
| C | 1.3297080 | -0.1336360 | 2.7191870 |
| H | 1.2643840 | -0.5896740 | 3.7293840 |
| H | 1.3546520 | 0.9608070 | 2.8630830 |
| C | -1.0264320 | 0.3668930 | 2.4110340 |
| H | -1.2326690 | 0.1458840 | 3.4785050 |
| H | -1.9222580 | 0.1396650 | 1.8162030 |
| H | -0.8000430 | 1.4381230 | 2.3016330 |
| C | -0.2517310 | -1.8800370 | 2.0691460 |
| H | -0.4946060 | -2.1156620 | 3.1264040 |
| H | 0.5787180 | -2.5268280 | 1.7453350 |
| H | -1.1295000 | -2.0942650 | 1.4406400 |

### 2. [(Me$_6$tren)Cu(PhNO)]$^+$, S=1

| Atom | X | Y | Z |
|---|---|---|---|
| Cu | -0.7601130 | 0.0479100 | -0.0253180 |
| N | 1.9015050 | -0.4961240 | -0.0769300 |

| | | | |
|---|---|---|---|
| N | -0.7529120 | -1.5453350 | -1.4583200 |
| N | -1.2373150 | 2.0870510 | -0.6036500 |
| N | -0.7952110 | -0.5027720 | 2.0843930 |
| N | -2.8035330 | -0.2164060 | 0.0426530 |
| O | 1.0553200 | 0.5467850 | -0.0540050 |
| C | 3.2420350 | -0.1428690 | -0.0464620 |
| C | 4.1761900 | -1.2190870 | -0.0794380 |
| H | 3.7936330 | -2.2446540 | -0.1275500 |
| C | 5.5470340 | -0.9631940 | -0.0511310 |
| H | 6.2550420 | -1.7986200 | -0.0776150 |
| C | 6.0233720 | 0.3618350 | 0.0111280 |
| H | 7.0999260 | 0.5593530 | 0.0332380 |
| C | 5.1066850 | 1.4312530 | 0.0448820 |
| H | 5.4758680 | 2.4620440 | 0.0935650 |
| C | 3.7309200 | 1.1944290 | 0.0171400 |
| H | 3.0182960 | 2.0230730 | 0.0443760 |
| C | -3.4495880 | 0.9594780 | -0.6211680 |
| H | -3.4501770 | 0.7740400 | -1.7081900 |
| H | -4.5099580 | 1.0522000 | -0.3117790 |
| C | -2.6848640 | 2.2486470 | -0.3065350 |
| H | -3.1287980 | 3.0967050 | -0.8690240 |
| H | -2.7797610 | 2.4961200 | 0.7655560 |
| C | -0.4427790 | 3.1211620 | 0.1072770 |
| H | -0.6881630 | 4.1392230 | -0.2582720 |
| H | 0.6250910 | 2.9155030 | -0.0592380 |
| H | -0.6428050 | 3.0716260 | 1.1886520 |
| C | -0.9725220 | 2.2387350 | -2.0582300 |
| H | -1.2036180 | 3.2679840 | -2.4035170 |
| H | -1.5846010 | 1.5298270 | -2.6386240 |
| H | 0.0901650 | 2.0214890 | -2.2469570 |
| C | -3.2056700 | -0.3058580 | 1.4818900 |
| H | -4.1980420 | -0.7893090 | 1.5836760 |
| H | -3.3115190 | 0.7225330 | 1.8647450 |
| C | -2.1559710 | -1.0653450 | 2.3003060 |
| H | -2.4397140 | -1.0524860 | 3.3738410 |
| H | -2.1288740 | -2.1260600 | 1.9941240 |
| C | 0.2378140 | -1.4885160 | 2.4983430 |
| H | 0.1949780 | -1.6777800 | 3.5906770 |

| | | | |
|---|---|---|---|
| H | 1.2316590 | -1.1037280 | 2.2251710 |
| H | 0.0830940 | -2.4380680 | 1.9642890 |
| C | -0.5937860 | 0.7244090 | 2.8976290 |
| H | -0.6155730 | 0.4952440 | 3.9834210 |
| H | -1.3804510 | 1.4650160 | 2.6813490 |
| H | 0.3822520 | 1.1624290 | 2.6377530 |
| C | -3.1188190 | -1.4815850 | -0.6929340 |
| H | -4.1755070 | -1.4906670 | -1.0268630 |
| H | -2.9991940 | -2.3220150 | 0.0107770 |
| C | -2.1746190 | -1.6540000 | -1.8874500 |
| H | -2.3748180 | -2.6226240 | -2.3911980 |
| H | -2.3588420 | -0.8634690 | -2.6371540 |
| C | -0.2870190 | -2.8213210 | -0.8504390 |
| H | -0.2703400 | -3.6360770 | -1.6037190 |
| H | -0.9532940 | -3.1221200 | -0.0257400 |
| H | 0.7265800 | -2.6541750 | -0.4531540 |
| C | 0.1208350 | -1.2677900 | -2.6300890 |
| H | 0.0693830 | -2.0930240 | -3.3691150 |
| H | 1.1558440 | -1.1601250 | -2.2703160 |
| H | -0.1902540 | -0.3302810 | -3.1162630 |

# 4. Supplementary Information for Chapter 5

**Controlled nitrene transfer from a tyrosinase-like arylnitroso-copper complex**

Mohammad S. Askari, Maylis Orio, and Xavier Ottenwaelder*

## 4.1. Experimental Procedures

Chemicals were obtained from Sigma-Aldrich and Alfa Aesar, except acetanilide-$^{15}N$ from Cambridge Isotope Laboratories. Air-sensitive compounds were handled under inert atmosphere ($N_2$) in a dry nitrogen glove-box ($O_2$ < 0.1 ppm, $H_2O$ < 0.1 ppm) or using standard Schlenk techniques. Solvents were dried by standard procedures, degassed, and stored over 4 Å molecular sieves in the glove-box. *N,N,N',N'*-tetramethyl-1,3-propanediamine (TMPD) was distilled over $CaH_2$ under nitrogen, and stored in the glove-box. The copper salt $[(MeCN)_4Cu](TfO)$ was prepared by adapting the Kubas procedure using TfOH.[168] 4-nitrosonitrobenzene was prepared via a literature procedure.[76] Sodium 2,4-di-*tert*-butylphenolate was prepared in the glove-box by treating recrystallized 2,4-di-*tert*-butylphenol with NaH in THF followed by filtering off the solids and precipitating with diethyl ether. NMR spectra were recorded on Varian Innova-500 MHz instrument. IR spectra were recorded on a Nicolet iS5 (Thermo Scientific) ATR. UV-vis spectra were recorded on Agilent 8453 spectrophotometer.

## 4.2. Synthetic procedures

### 4.2.1. Preparation of *p*-$NO_2$-$C_6H_4{}^{15}NO$:

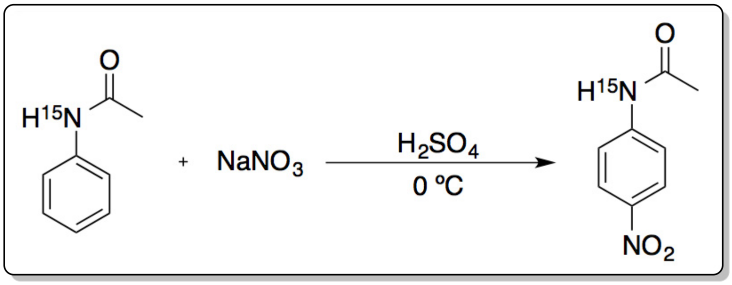

Scheme S 4-1: *Para*-nitration of acetanilide-$^{15}N$.[206]

(a) *p*-nitroacetanilide-$^{15}$N. Acetanilide-$^{15}$N was nitrated by adapting a literature procedure.[206] To a solution of acetanilide-$^{15}$N (500 mg, 3.7 mmol) in 6 mL of concentrated $H_2SO_4$ at 0 °C, a solution of $NaNO_3$ (313 mg, 3.7 mmol, 1 equiv.) in 4 mL concentrated $H_2SO_4$ was added dropwise over 20 minutes. The mixture was left stirring for 5 hours at 0 °C and then poured onto ice-water mixture. The yellow precipitated solid was filtered off and washed with water and used for next step without further purification. Yield: 563 mg, 85%. $^1$H-NMR (acetone-d$_6$): δ (ppm) 9.80-9.62 (d, 1H, -C$^{15}$N*H*-, $^1J_{H\text{-}^{15}N}$ = 90 Hz), 8.22-8.21 (d, 2H, Ar-*H*), 7.91-7.89 (d, 2H, Ar-*H*), 2.17 (s, 3H, -C(O)C$H_3$).

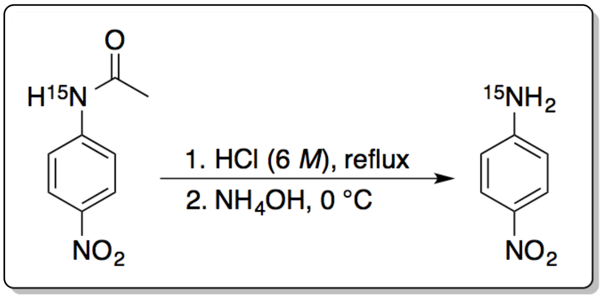

Scheme S 4-2: Deprotection of the acetanilide.

(b) *p*-nitroaniline-$^{15}$N. *p*-nitroacetanilide-$^{15}$N (563 mg, 3.1 mmol) was dissolved in 20 mL of 6 M HCl and the solution refluxed for 24 hours. The solution was then cooled to 0 °C and basified by adding $NH_4OH$ upon which yellow crystals formed which were filtered off and washed with cold water. Yield: 416 mg, 96%. $^1$H-NMR ($CDCl_3$): δ (ppm) 8.08-8.06 (m, 2H, Ar-*H*), 6.63-6.62 (m, 2H, Ar-*H*), 4.39 (d, 2H, $^{15}$N$H_2$, $^1J_{H\text{-}^{15}N}$ = 86Hz).

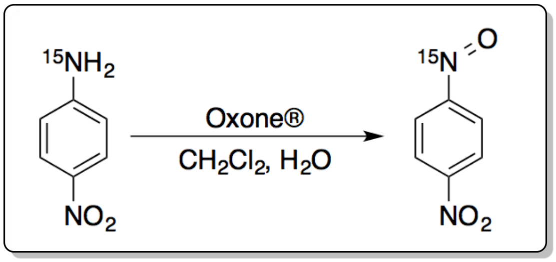

Scheme S 4-3: Oxidation of the *p*-nitroaniline-$^{15}$N with Oxone®.[76]

(c) *p*-($^{15}$N-nitroso)nitrobenzene. Oxidation of *p*-nitroaniline-$^{15}$N was carried out following a literature procedure.[76] To a solution of *p*-nitroaniline-$^{15}$N (400 mg, 2.9 mmol) in 20 mL of $CH_2Cl_2$ at 25 °C a solution of Oxone® ($2KHSO_5 \bullet KHSO_4 \bullet K_2SO_4$, 3.9g, 6.3 mmol, 2.2 equiv.) in 10 mL of water was added and the mixture stirred vigorously. The progress of the reaction was monitored by TLC until all the starting material was consumed. The organic phase was separated and the aqueous layer was extracted twice with $CH_2Cl_2$. The combined organic layer was washed once with 1 M aqueous HCl, dried over $Na_2SO_4$, filtered, and solvent removed under reduced pressure to give brown solid. The crude product was purified by sublimation under vacuum to afford green crystals of the nitrosoarene that dimerized at 25 °C over few hours. Yield: 220 mg, 50%. $^{1}$H-NMR ($CDCl_3$): δ (ppm) 8.52-8.51 (m, 2H, Ar-*H*), 8.06-8.04 (m, 2H, Ar-*H*). $^{13}C\{^{1}H\}$-NMR (125 MHz, $CDCl_3$): 162.43 (d, $^{1}J_{^{13}C\text{-}^{15}N}$ = 13.3Hz), 125.5, 124.9, 121.3 (d, $^{2}J_{^{13}C\text{-}^{15}N}$ = 4.3Hz). $^{15}N\{^{1}H\}$-NMR (50 MHz, $CDCl_3$): 913.8

### 4.2.2. Preparation of {[(TMPD)Cu]$_2$(TfO)($\mu$-$\eta^2$:$\eta^2$-*p*-NO$_2$-C$_6$H$_4$NO)}(TfO), 1:

To a stirring solution of TMPD (40 mg, 0.31 mmol, 1.2 equiv.) and 4-nitrosonitrobenzene (46 mg , 0.30 mmol, 0.7 equiv.) in 5 mL THF, a solution of $[(MeCN)_4Cu](TfO)$ (100 mg, 0.26 mmol, 1 equiv.) in 2 mL THF was added dropwise at 25 °C. The color changed immediately to deep green. The solution was stirred for 15 minutes and then cooled down to –30 °C. Dropwise addition of the solution to 15 mL of swirling pentane previously cooled to –30 °C resulted in the precipitation of a green solid. The solid was isolated and washed with $Et_2O$, pentane and dried in vacuo. Yield: 80%. $^{1}$H-NMR (acetone-d$_6$): δ (ppm) 8.26-8.17 (m, 4H, aromatic), 2.82 (bs, 4H, N–C*H$_2$*), 2.72 (bs, 24H, N(C*H$_3$*)$_2$), 1.93 (bs, 4H, CH$_2$–C*H$_2$*–CH$_2$). UV-vis $\lambda_{max}$ / nm (ε / $M^{-1}cm^{-1}$): 346 (19 400), 445 (4 400, shoulder), 643 (1 500). Elemental analysis: calculated for $C_{22}H_{40}N_6O_9F_6S_2Cu_2$, C 31.54, H 4.81, N 10.03, S 7.65; found C 31.60, H 2.03*, N 9.81, S 7.81. * The presence of fluorine in the sample interfered with the normal integration peak for hydrogen. The value for H is not trustworthy.

Crystals suitable for X-ray structure determination were grown through slow layered diffusion of pentane into a concentrated solution of the complex in THF at –30 °C.

### 4.2.3. Preparation of complex 2 (reaction of 1 with phenolate):

To a solution of **1** (86.7 mg, 0.1 mmol, 1 equiv.) in 10 mL $CH_2Cl_2$, solid sodium 2,4-di-*tert*-butylphenolate (25.6 mg, 0.1 mmol, 1 equiv.) was added at 25 °C. Within a few minutes the color of the solution changed from green to deep blue. After stirring for 1 h, the solution was filtered through a 0.45 μM PTFE syringe filter. Fast precipitation through dropwise addition of the solution into stirring pentane precooled to –30 °C gave blue microcrystalline solid of **2**, which was collected and dried under vacuum. Yield: 76%. $^1$H-NMR ($CDCl_3$): δ 8.47 (d, 2H), 7.67 (s, 1H), 7.64 (d, 2H), 6.40 (s, 1H), 3.09 (t, 4H), 2.59 (bs, 12H), 1.87 (bs, 2H), 1.51 (s, 9H), 1.13 (s, 9H). UV-vis $\lambda_{max}$ / nm ($\varepsilon$ / $M^{-1}cm^{-1}$): 328 (8 100), 556 (2 800, shoulder), 713 (7 500). Elemental analysis: calculated for $C_{28}H_{42}N_4O_6F_3SCu \cdot 0.2CH_2Cl_2$,* C 48.37, H 6.10, N 8.00, S 4.58; found C 48.03, H 6.33, N 8.14, S 5.08. * 80% of the crystallization solvent evaporated when drying the sample.

X-ray quality crystals were grown by layered diffusion of pentane into a concentrated solution of the complex in $CH_2Cl_2$ at –30 °C.

### 4.2.4. *N*-(2-hydroxyphenyl)-4-nitroaniline, 3:

To a solution of **1** (86.7 mg, 0.1 mmol, 1 equiv.) in 10 mL $CH_2Cl_2$, solid sodium 2,4-di-*tert*-butylphenolate (25.6 mg, 0.1 mmol, 1 equiv.) was added at 25 °C. Within a few minutes the colour of the solution changed from green to deep blue. To this solution a saturated solution of $Na_2S_2O_4$ was added under Ar upon which the color changed to light yellow, at which stage the solutions were handled in the air. The aqueous phase was then extracted twice more with $CH_2Cl_2$, organics combined, dried over $Na_2SO_4$, filtered, and solvent removed under reduced pressure to give a yellow oil. Purification by silica gel column (hexanes/ethyl acetate) provided the pure title compound as pale yellow solid. Yield: 80%. $^1$H-NMR (CDCl3): δ (ppm) 8.10-8.08 (d, 2H), 7.30 (s, 1H), 7.03 (s, 1H), 6.68-6.66 (d, 2H), 5.86 (bs, 1H), 5.74 (bs, 1H), 1.44 (s, 9H), 1.28 (s, 9H). $^{13}C\{^1H\}$-NMR (125 MHz, $CDCl_3$): δ (ppm) 152.5, 148.8, 143.0, 140.2, 136.4, 126.2, 125.3, 123.3, 121.6, 113.7, 35.1, 34.4, 31.5, 29.5. IR (ATR, $cm^{-1}$): 3466, 3327, 2954, 1589, 1481, 1420, 1362, 1297, 1216, 1181, 1110, 974, 839, 751, 697, 652. HRMS: m/z calculated for $[M+H]^+$, 343.20217; found, 343.20135.

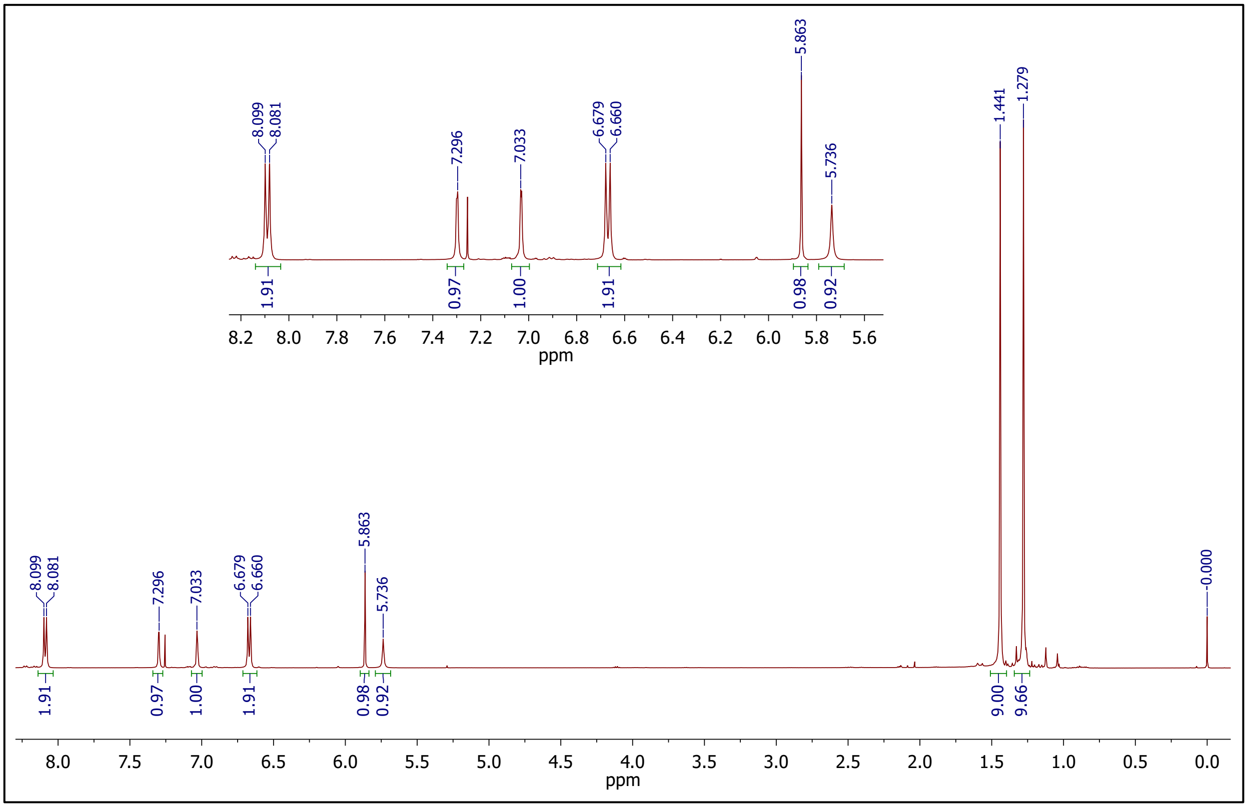

Figure S 4-1: $^{1}$H NMR spectrum of **3** ($CDCl_3$, 25 °C)

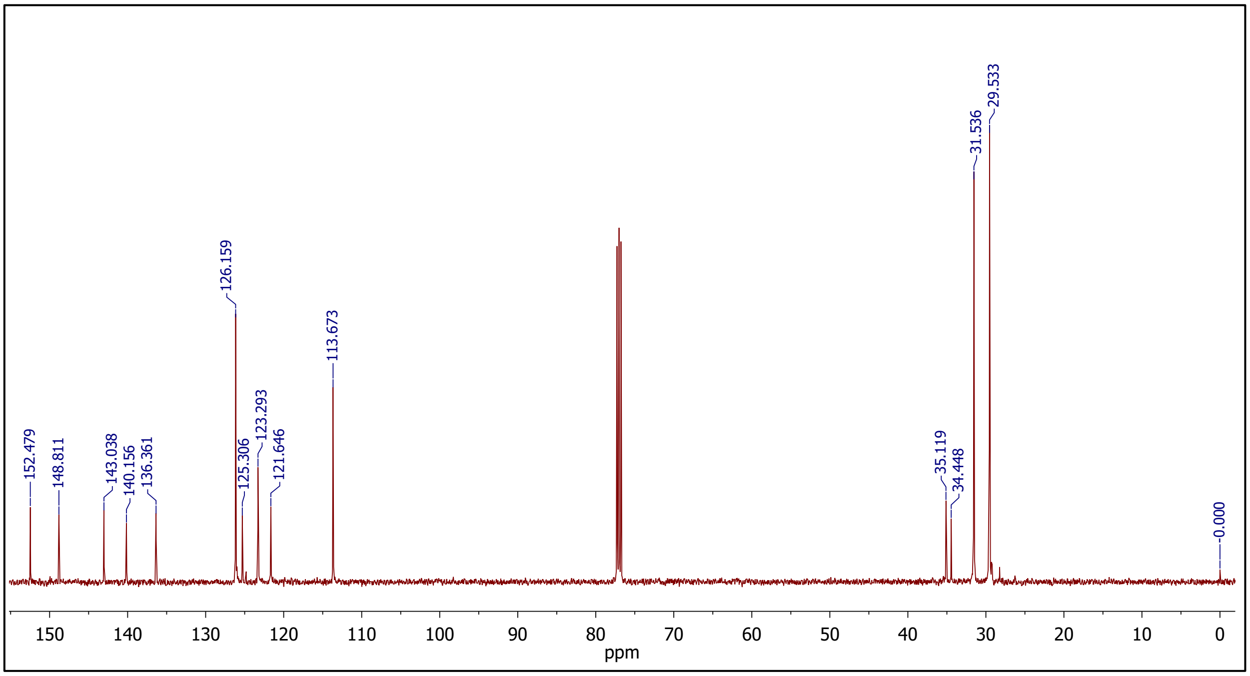

Figure S 4-2: $^{13}C\{^{1}H\}$ NMR spectrum of **3** ($CDCl_3$, 25 °C).

## 4.3. X-ray Crystallography

X-ray diffraction data were collected on a Bruker APEX DUO used micro-focused copper source. The frames were integrated with the Bruker SAINT software package using a narrow-frame algorithm. The Data were corrected for absorption effects using the multi-scan method (SADABS). The structure was solved and refined using the Bruker SHELXTL Software Package. The final anisotropic full-matrix least-squares refinement is on $F^2$.

Table S 4-1: Crystallographic data for [**1**](TfO) and [**2**](TfO)·$CH_2Cl_2$.

| | [**1**](TfO) | [**2**](TfO)·$CH_2Cl_2$ |
|---|---|---|
| CCDC deposition number | 1029423 | 1029424 |
| Empirical formula | $C_{22}H_{40}Cu_2F_6N_6O_9S_2$ | $C_{29}H_{44}Cl_2CuF_3N_4O_6S$ |
| Formula weight | 837.80 | 768.18 |
| *T* (K) | 110(2) | 113(2) |
| Wavelength (Å) | 1.54178 | 1.54178 |
| Crystal system | orthorhombic | orthorhombic |
| Space group | $P2_12_12_1$ | *P*bcn |
| *Unit cell dimensions* | | |
| a (Å) | 12.6647(4) | 34.9331(5) |
| b (Å) | 15.6022(7) | 10.1199(2) |
| c (Å) | 17.2534(8) | 20.5135(3) |
| α (°) | 90.00 | 90.00 |
| β (°) | 90.00 | 90.00 |
| γ (°) | 90.00 | 90.00 |
| *V* (Å$^3$) | 3409.2(2) | 7251.9(2) |
| *Z* | 4 | 8 |
| $D_{calc}$ | 1.632 | 1.407 |
| Absorption coefficient | 3.478 | 3.262 |
| F(000) | 1720 | 3200 |
| Crystal size (mm) | 0.073 x 0.107 x 0.124 | 0.07 x 0.30 x 0.38 |
| *θ* (°) | 3.820 – 62.746 | 2.53 – 68.16 |
| Index ranges | *h* = -14 – 14 | *h* = -41 – 41 |
| | *k* = -17 – 17 | *k* = -12 – 12 |
| | *l* = -19 – 19 | *l* = -24 – 23 |
| Reflections collected | 45388 | 99756 |
| Independent reflections | 5454 | 6605 |
| Completeness (*θ*) | 99.4% | 99.6% |
| Data/restraints/parameters | 5454/0/433 | 6605/19/453 |
| Goodness of fit (GOF) on $F^2$ | 1.021 | 1.049 |
| Final R indices [$I > 2\sigma(I)$] (%) | $R_1$=5.02, $wR_2$=10.43 | $R$ = 5.27, $wR_2$ = 14.23 |
| R indices (all data) (%) | $R_1$ = 8.67<br>$wR_2$ = 12.04 | $R_1$ = 7.21<br>$wR_2$ = 15.61 |
| Largest difference in peak and hole (e Å$^{-3}$) | 0.552 and -0.493 | 1.214 and -1.148 |

## 4.4. UV-Vis Spectra

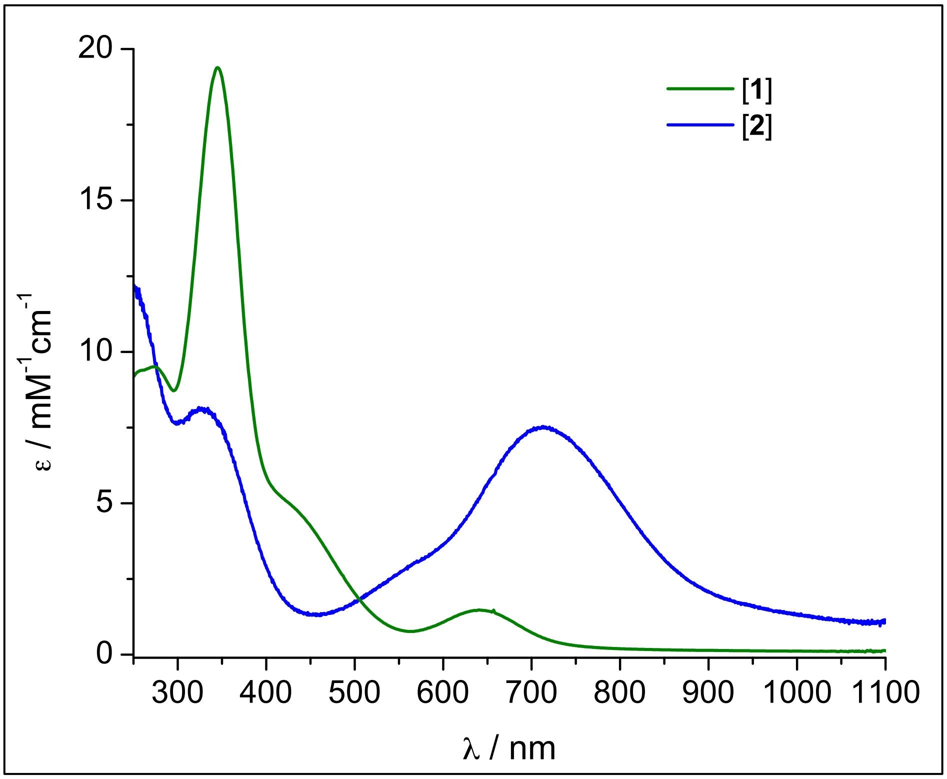

Figure S 4-3: UV-vis spectra of **1** and **2** in $CH_2Cl_2$ at 25 °C.

## 4.5. IR Spectra and Vibrational Analysis

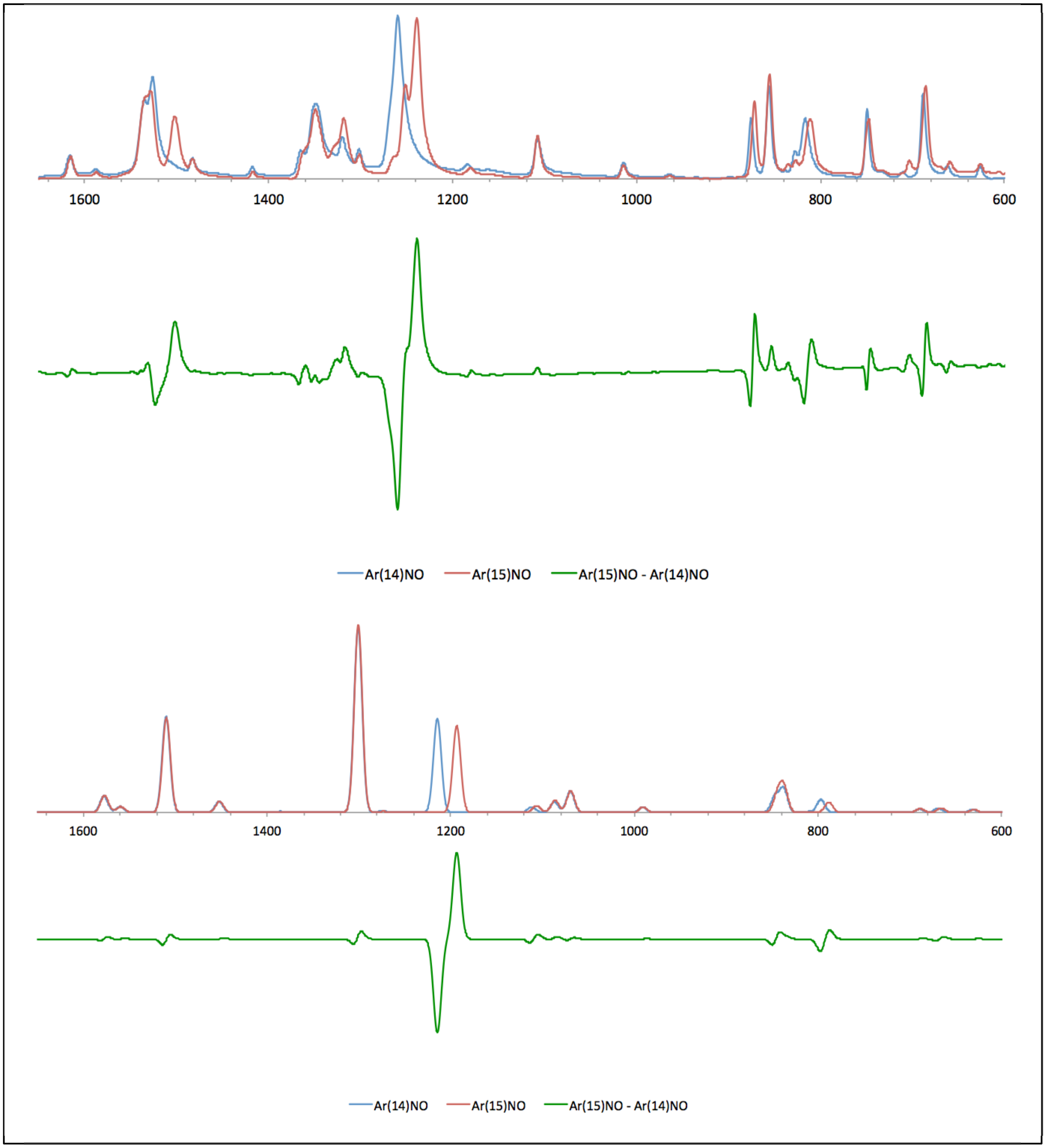

Figure S 4-4: Experimental (top) and computational (bottom, see below for details) IR spectra for solid *p*-($^{14}$N-nitroso)nitrobenzene (blue), *p*-($^{15}$N-nitroso)nitrobenzene (red), and difference spectra (green).

Table S 4-2: Selected calculated IR parameters for Ar$^{14/15}$NO (dimer form).

| **Ar$^{14}$NO** | | **Ar$^{15}$NO** | | Assignment |
|---|---|---|---|---|
| Freq. (cm$^{-1}$) | Intensity (a.u.) | Freq. (cm$^{-1}$) | Intensity (a.u.) | |
| 796.9 | 62.6 | 788.2 | 49.1 | $\delta_r$ NN + $\delta_r$ CH$_{Ar}$ |
| 1214.5 | 443.9 | 1193.4 | 409.7 | $\nu_s$ NO + $\nu_s$ CH$_{Ar}$ |

Computational details below. $\nu_s$: streching, $\delta_b$: bending, $\delta_r$: rocking, $\delta_w$: wagging, $\delta_t$: twisting

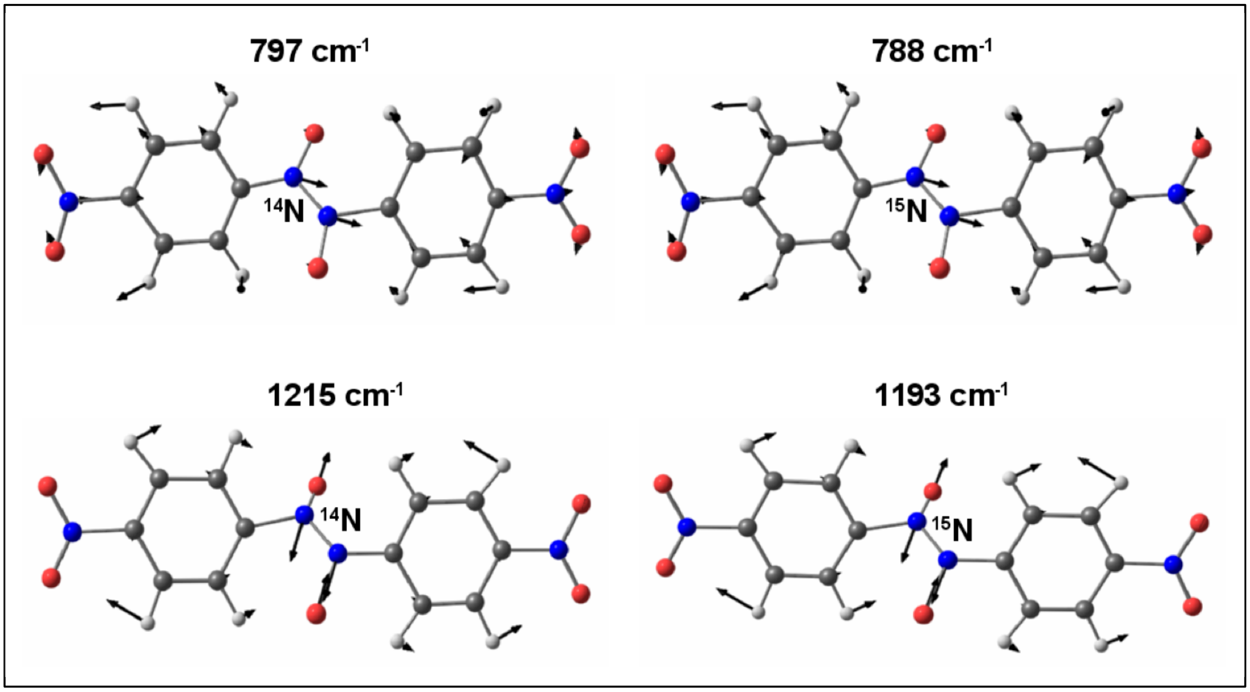

Figure S 4-5: Relevant vibrational normal modes of Ar$^{14/15}$NO, a dimer in the solid-state structure.

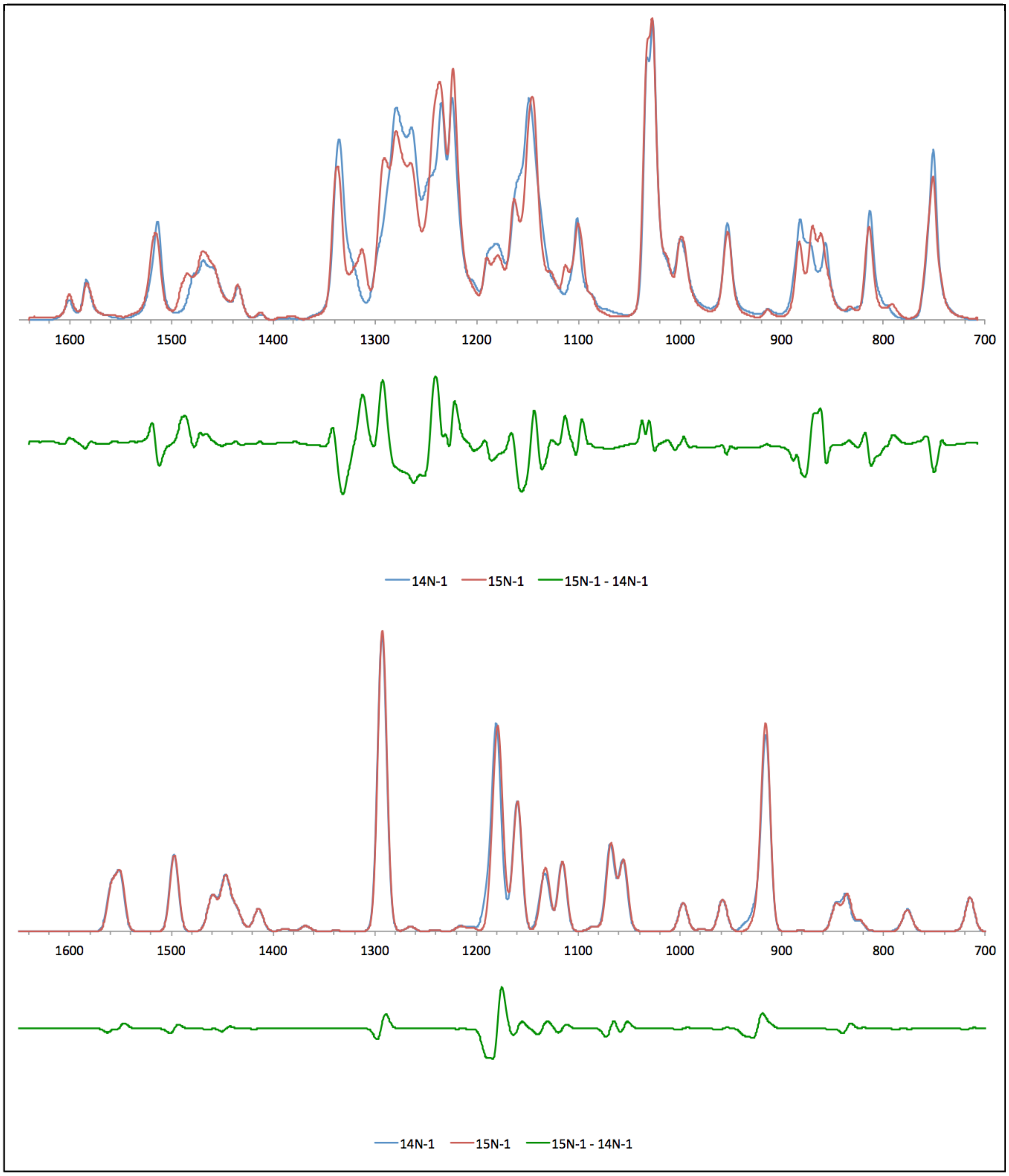

Figure S 4-6: Experimental (top) and computational (bottom, see below for details) IR spectra for **1**-$^{14}$N (blue), **1**-$^{15}$N (red), and difference spectra (green).

Table S 4-3: Selected calculated IR parameters for **1**.

| **$^{14}$N-1** | | **$^{15}$N-1** | | Assignment |
|---|---|---|---|---|
| Freq. (cm$^{-1}$) | Intensity (a.u.) | Freq. (cm$^{-1}$) | Intensity (a.u.) | |
| 935.9 | 60.3 | 918.8 | 87.8 | $\nu_s$ NO |
| 1189.7 | 71.1 | 1183.7 | 109.0 | $\nu_s$ $N_{NO}$-$C_{Ar}$ + $\nu_s$ $CH_{Ar}$ |

Computational details below. $\nu_s$: streching, $\delta_b$: bending, $\delta_r$: rocking, $\delta_w$: wagging, $\delta_t$: twisting

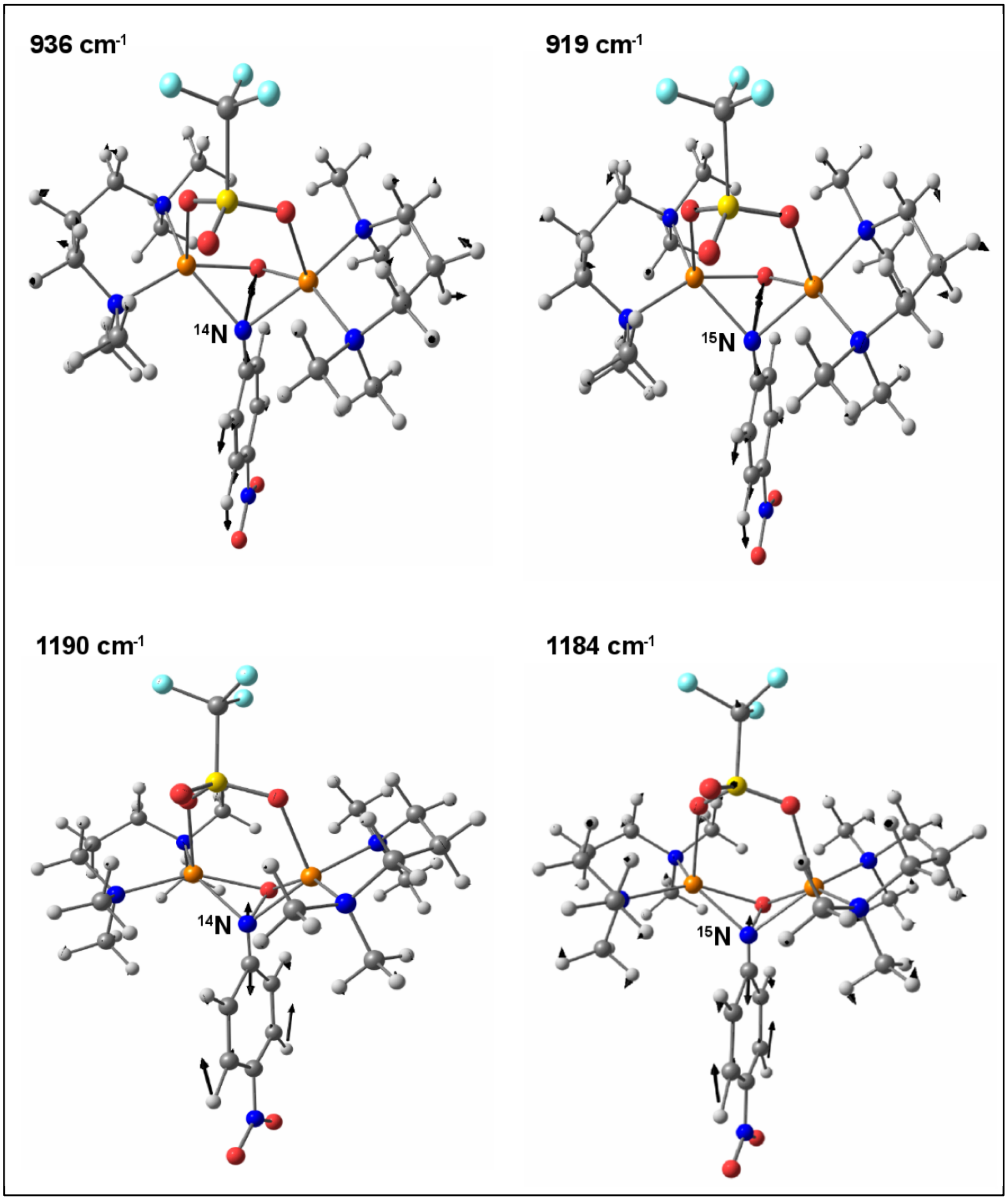

Figure S 4-7: Relevant vibrational normal modes of $^{14}$N- and $^{15}$N-labeled **1**.

## 4.6. DFT calculations

All theoretical calculations were performed with the ORCA program package.[207] Full geometry optimizations were carried out for all complexes using the GGA functional BP86[203-204,208] in combination with the TZV/P[209] basis set for all atoms and by taking advantage of the resolution of the identity (RI) approximation in the Split-RI-J variant[210] with the appropriate Coulomb fitting sets.[211] Increased integration grids (Grid4 in ORCA convention) and tight SCF convergence criteria were used. Solvent effects were accounted for according to the experimental conditions. For that purpose, we used the $CH_2Cl_2$ ($\varepsilon = 9.08$) solvent within the framework of the conductor like screening (COSMO) dielectric continuum approach.[212] The relative energies were obtained from single-point calculations using the B3LYP[213-214] functional together with the TZV/P basis set. They were computed from the gas-phase optimized structures as a sum of electronic energy, thermal corrections to free energy, and free energy of solvation. The Heisenberg isotropic exchange coupling constants $J$ were evaluated from single point calculations based on the Broken Symmetry (BS) approach[215-217] using the B3LYP functional and the TZV/P basis set. The Yamaguchi formula[218-219] was used to estimate the exchange coupling constants $J$ based on the Heisenberg–Dirac–van Vleck Hamiltonian[220-223] Optical properties were predicted from additional single-point calculations using the same functional/basis set as employed before. Electronic transition energies and dipole moments for all models were calculated using time-dependent DFT (TD-DFT)[224-226] within the Tamm-Dancoff approximation.[227-228] To increase computational efficiency, the RI approximation[229] was used in calculating the Coulomb term. At least 40 excited states were calculated in each case and difference transition density plots were generated for each transition. IR spectra were obtained from numerical frequency calculations performed on optimized structures using the B3LYP functional together with the TZV/P basis set. Isotope shift effects ($^{14}N/^{15}N$) were taken into account using the orca_vib utility program. Vibrational normal modes were visualized with Chemcraft[230] software and differential spectra were plotted using the orca_maspc utility program.

### 4.6.1. DFT calculations for 1:

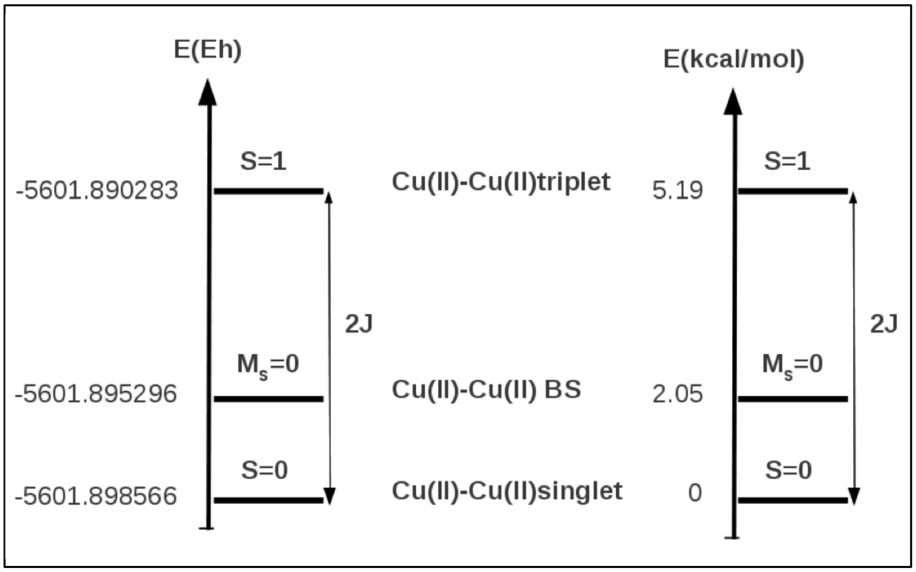

Figure S 4-8: Energetic analysis of the DFT calculations for **1**.

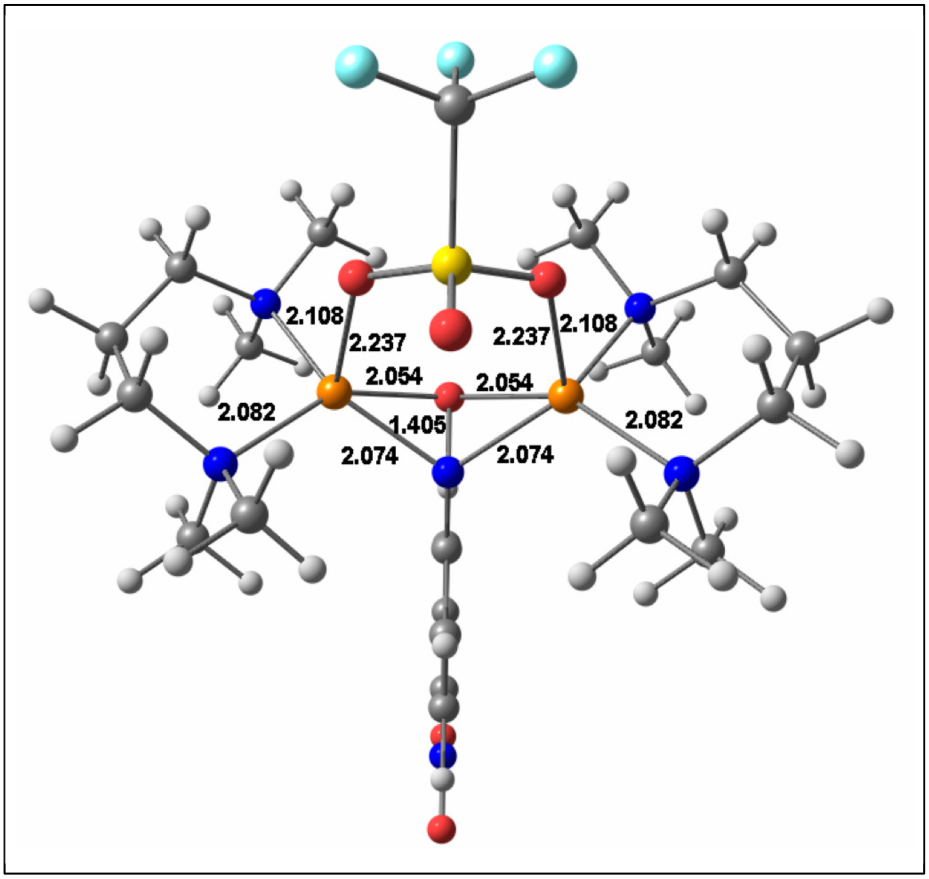

Figure S 4-9: Optimized structure of cation **1** together with interatomic distances.

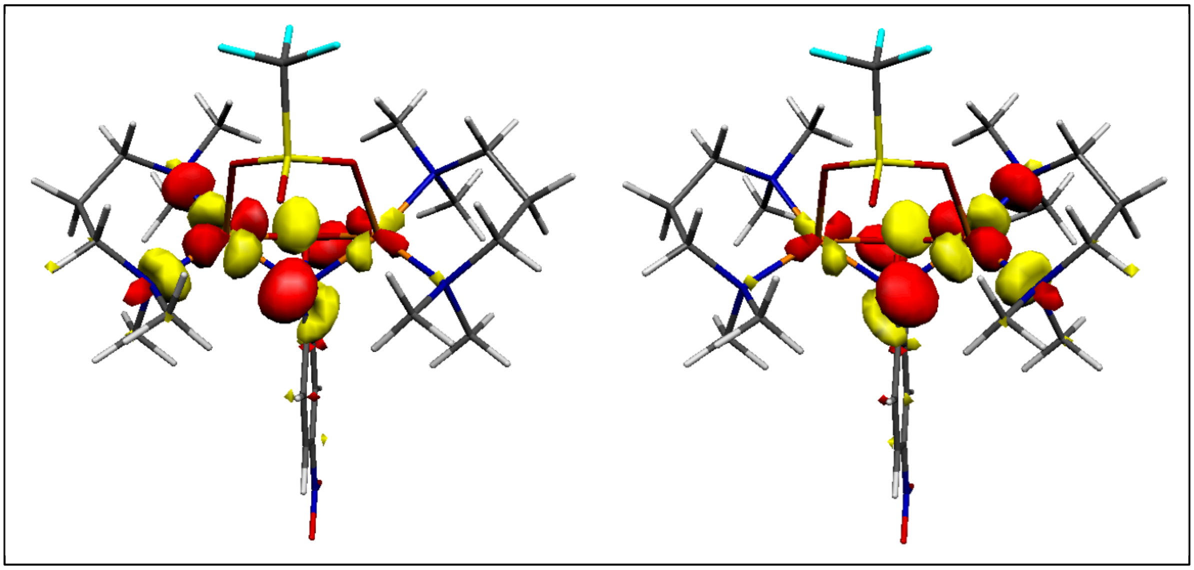

Figure S 4-10: Unrestricted corresponding orbitals of **1**.

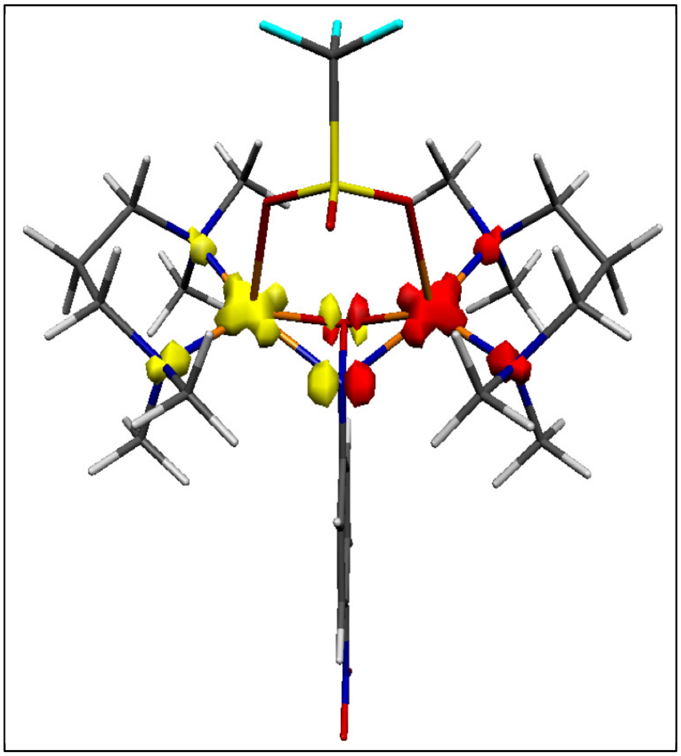

Figure S 4-11: Spin population distribution in **1**.

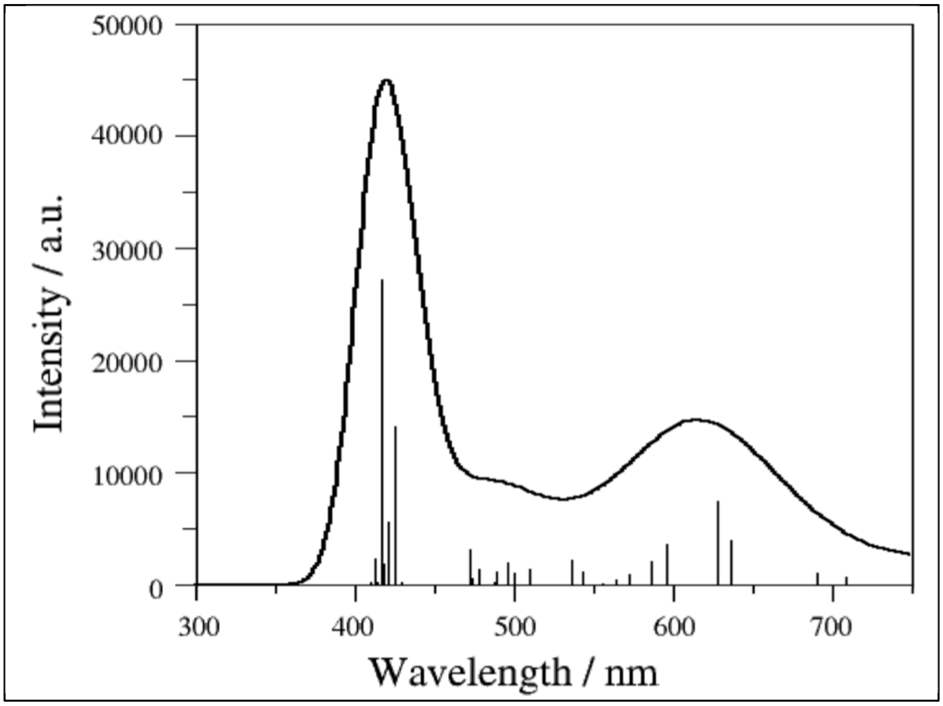

Figure S 4-12: Theoretical fit of the UV-vis spectrum of **1**.

Table S 4-4: Calculated electronic transitions of **1**.

| Transition | $\lambda^{calc}$ (nm) | $f^{calc}$ | Assignment | $\lambda^{expt}$ (nm) | $\varepsilon$ ($M^{-1}$ $cm^{-1}$) |
|---|---|---|---|---|---|
| 1 | 664 | 0.126 | MLCT | 643 | 1500 |
| 2 | 454 | 0.095 | LLCT | 445 | 4400 |
| 3 | 418 | 0.272 | MLCT | 346 | 19400 |

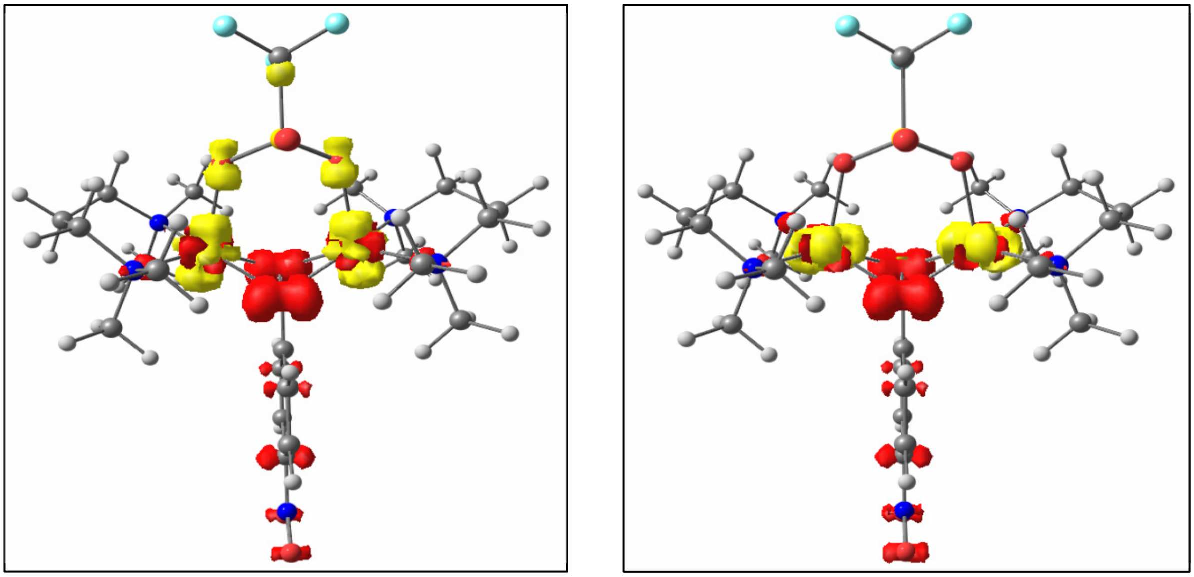

Transition 1

Transition 2

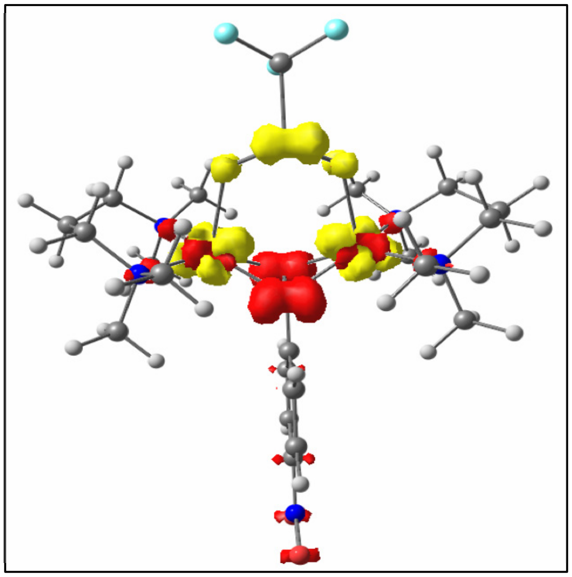

Transition 3

Figure S 4-13: Difference electron densities sketch of transitions 1-3 for **1** (yellow = negative, red = positive).

### 4.6.2. Peroxo analogue of 1

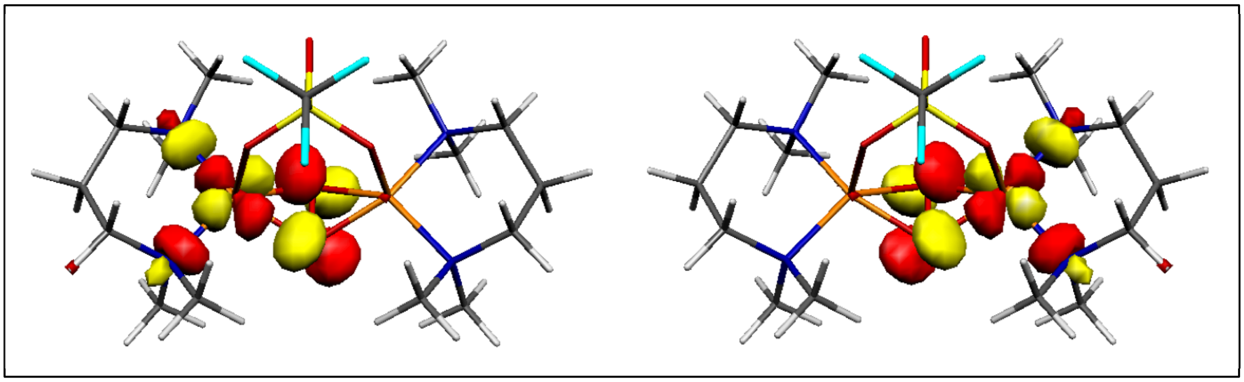

Figure S 4-14: Unrestricted corresponding orbitals for peroxo analogue of **1**.

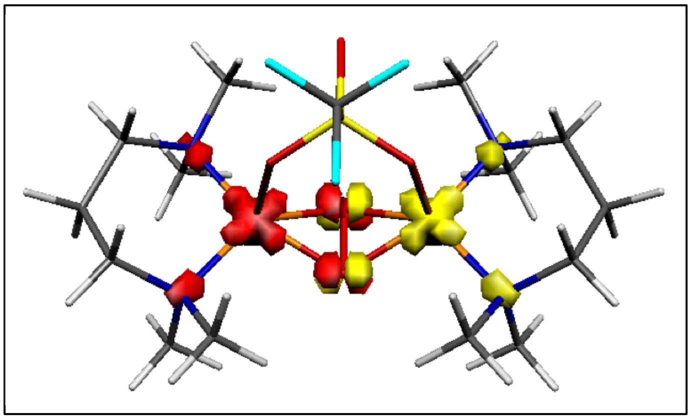

Figure S 4-15: Spin population distribution for peroxo analogue of **1**.

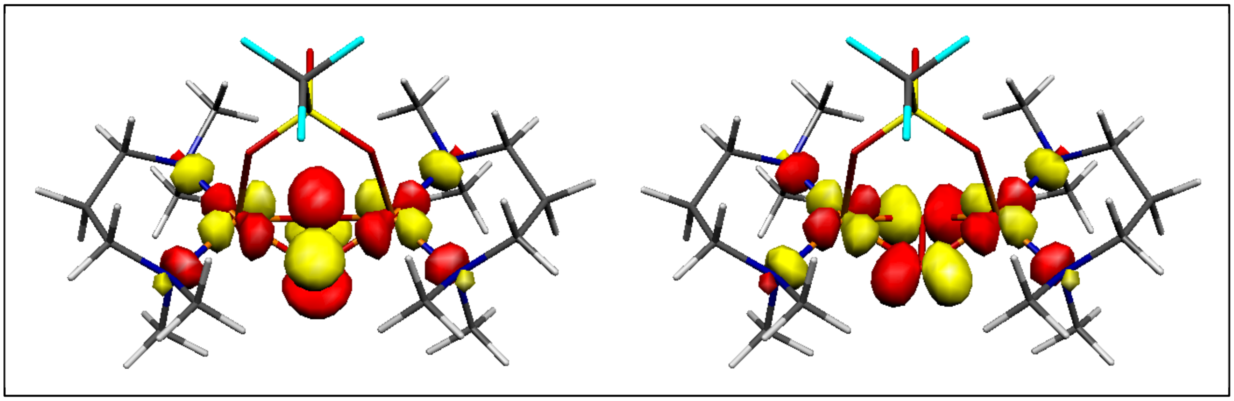

Figure S 4-16: HOMO (left) and LUMO (right) for peroxo analogue of **1**.

### 4.6.3. DFT calculations for 2

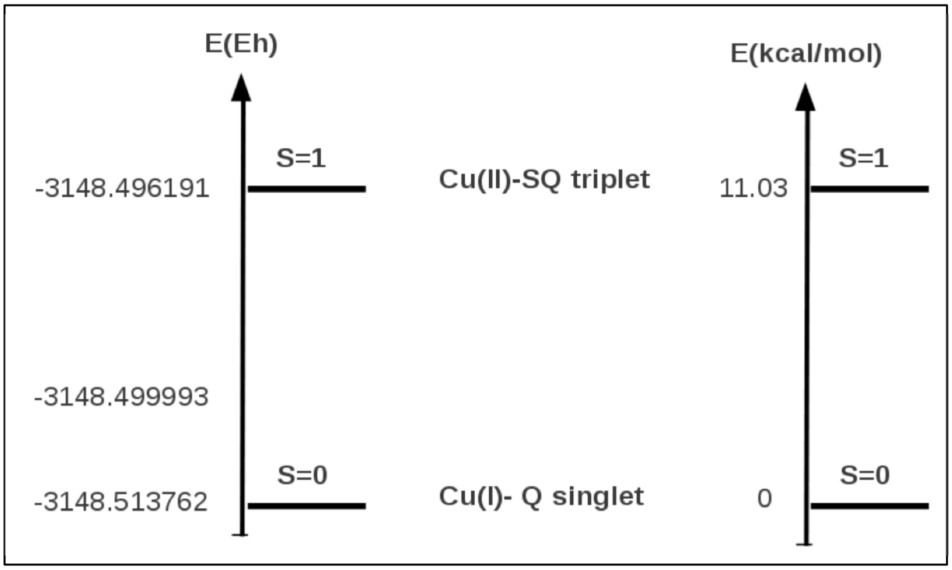

Figure S 4-17: Energetic analysis of the DFT calculations for **2**.

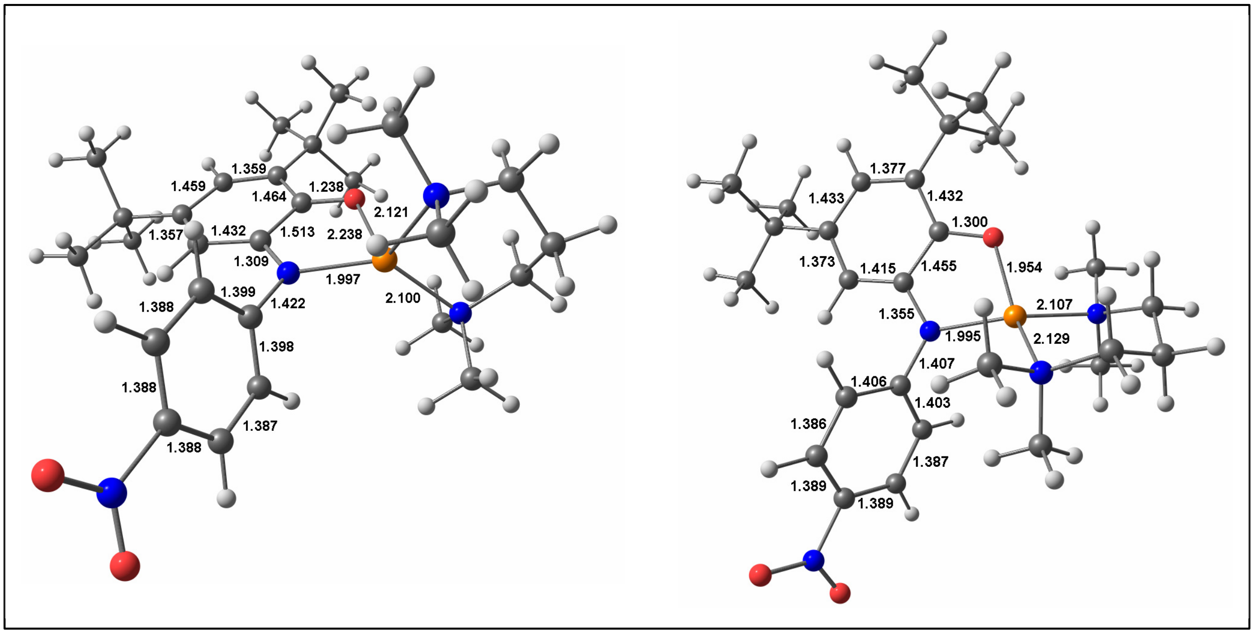

Figure S 4-18: Optimized structures of singlet cation **2** (left) and triplet cation **2** (right) together with interatomic distances.

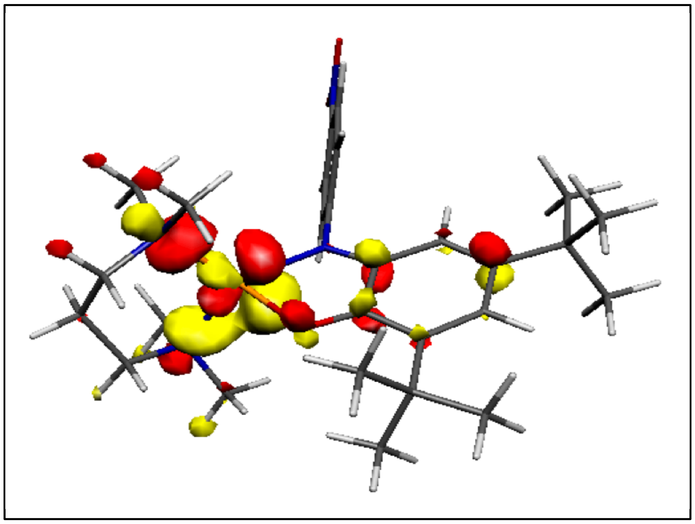

Figure S 4-19: HOMO of singlet cation **2**.

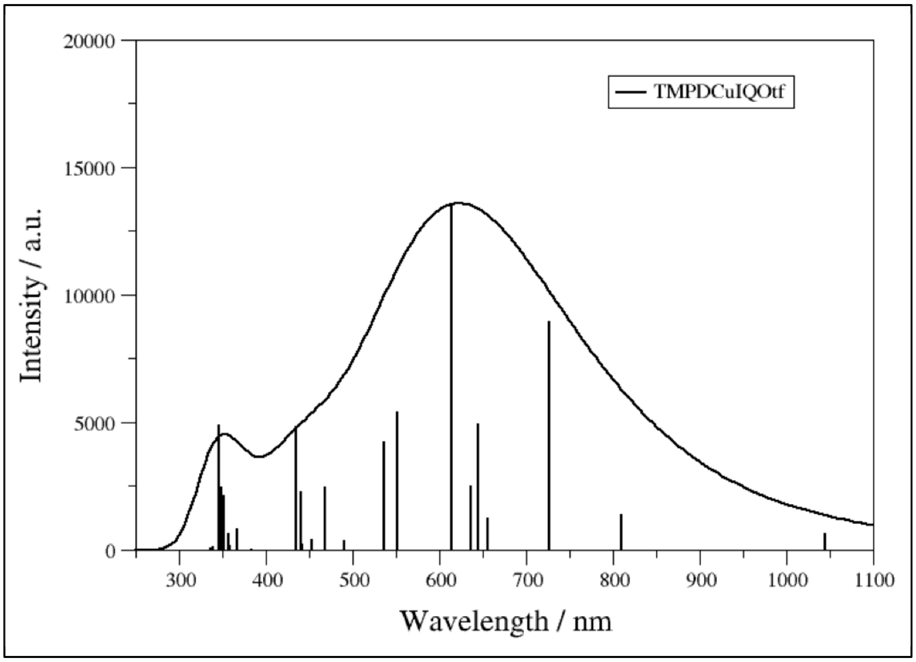

Figure S 4-20: Theoretical fit of the UV-vis spectrum of singlet cation **2**.

Table S 4-5: Calculated electronic transtisions of singlet cation **2**.

| Transition | $\lambda^{calc}$ (nm) | $f^{calc}$ | Assignment | $\lambda^{expt}$ (nm) | $\varepsilon$ ($M^{-1}$ $cm^{-1}$) |
|---|---|---|---|---|---|
| 1 | 720 | 0.112 | MLCT | 713 | 7500 |
| 2 | 613 | 0.129 | MLCT | 556 | 2800 |
| 3 | 351 | 0.082 | LLCT | 328 | 8100 |

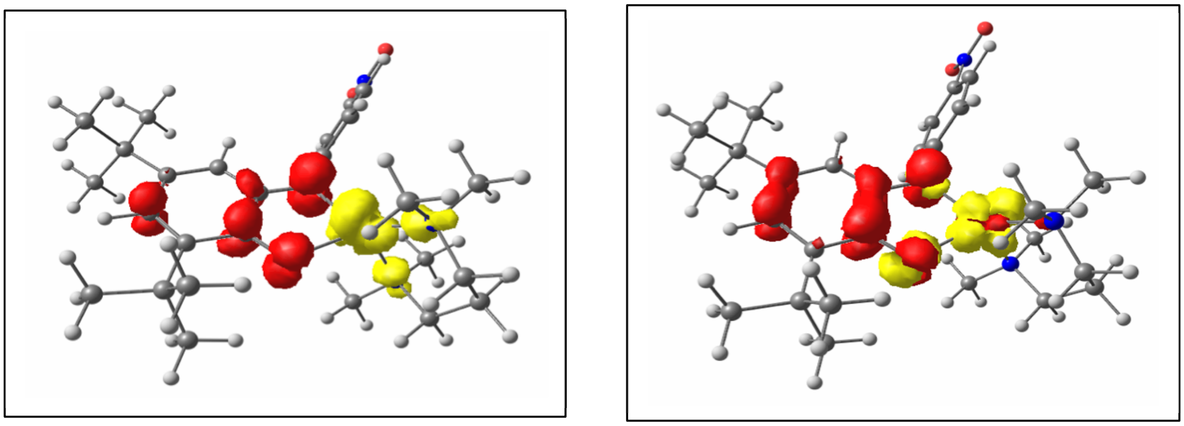

Transition 1

Transition 2

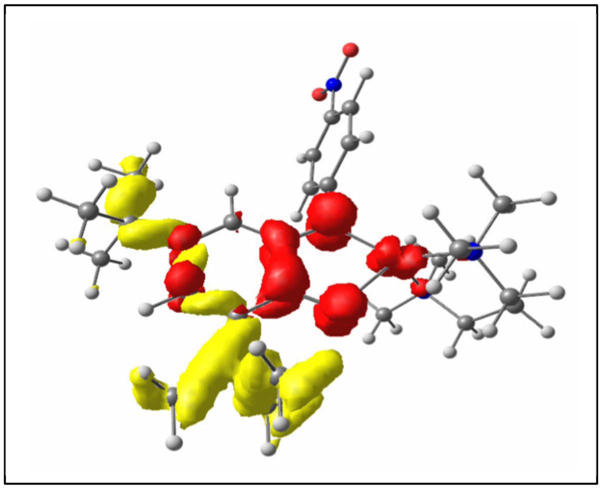

Transition 3

Figure S 4-21: Difference electron densities sketch of transitions 1-3 for singlet cation **2** (yellow = negative, red = positive).